# High Pressure Rheology: A Probe for Formulation Development

Katie Jayne Pepper

Thesis submitted to the University of Nottingham

for the degree of Doctor of Philosophy

September 2018



University of Nottingham

UK | CHINA | MALAYSIA

# Declaration

All work presented in this Thesis is the original work of the author, with the exception of results referenced to other sources. It has not been submitted as part of any other degree or professional qualification.

Signed:……

Date: ……

Katie Jayne Pepper

# Acknowledgements

I would like to thank Professor Steve Howdle, not only for giving me the opportunity to undertake this PhD, but also for taking a chance on me back on my undergraduate results day in 2013. Without that conversation, I would not have got the job at Critical Pharmaceuticals Ltd which led to this PhD. Which leads me on to thank Andrew Naylor and Anjumn Shabir-Ahmed (formerly of Critical Pharmaceuticals Ltd) for their continued help, advice and support throughout this project.

I would also like to thank all the members of the B10 lab group, past and present. I have had an amazing time being a member of such a supportive group and I have made many life-long friends. In particular, I would like to acknowledge Simon Bassett for his scientific knowledge and advice and for those 7 am ranting sessions. I'm not sure I would have made it past second year without them! I would also like to acknowledge Alice Haddleton, for producing the SEM images in this thesis, and whose friendship has made this whole process bearable. I would also like to mention Timothé Masson, who produced the block copolymers used in Chapter 4. Many thanks also go to Andrea Hufendiek for her help, support and friendship throughout the writing up period.

Of course, none of this would have been possible without the support of the technical staff here at the School of Chemistry. My thanks go to Mark Guyler, Martin Dellar, Pete Fields, Rich Wilson, Dave Litchfield and their colleagues. Thanks also goes to Graham Rance for performing the micro Raman spectroscopy.

I would like to thank my friends and family outside of B10 for all their love, help and support, especially in the final months of writing. They have believed in me when I did not and they have kept me going on my lowest days. Finally, my thanks go to Jay, for his love, support and encouragement.

# Abstract

The development of new routes for therapeutic delivery such as controlled or sustained delivery systems, is time and cost consuming. This is because it is necessary to perform multiple *in vitro* dissolution studies to investigate the release profiles of all the formulations in the early stages of development. This thesis aims to investigate the potential use of rheology as a pre-screening tool to aid formulation development by reducing the number of *in vitro* studies that need to be performed. The hypothesis being that rheology could be used to assess the homogeneity and processability of a formulation, with the expectation that a homogeneous formulation would exhibit consistent release profiles on a batch-to-batch basis.

Recent advances in pharmaceutical research have identified supercritical carbon dioxide ($scCO_2$) as a potential green solvent alternative for the production of microparticles that promote the sustained release of APIs (active pharmaceutical ingredients) from a polymer matrix. Mild conditions are necessary to preserve the integrity of the API and carbon dioxide ($CO_2$) is well documented to be able to reduce the viscosity of polymers at low temperatures. In order to quantify this, a robust and reliable rheology method was established to measure the polymer melt viscosity in the presence of $CO_2$. First, the viscosity of the single polymers: polycaprolactone ($PCL_{112}$) and poly($_{D,L}$-lactide) ($PLA_{11}$), in their molten states was measured at ambient pressure and in the presence of $CO_2$. For simplicity these measurements were made at elevated temperature (80-90 °C), where the samples were already molten at ambient pressure. However, this method was not suitable for formulations containing thermosensitive APIs, such as proteins or peptides, because they degrade at temperatures above physiological conditions (> 40 °C). Therefore, the method was adapted for use at lower temperatures by exposing the polymers to 140 bar of $CO_2$ at 40 °C, without preheating.

Although $CO_2$ is known to reduce the viscosity of polymers it has been shown that the polymer melt viscosity remains relatively high, hindering the incorporation and even distribution of the drug. Additives such as plasticisers can be used to optimise the viscosity and processing parameters of a pharmaceutical formulation.

Poly(ethylene glycol) (PEG) has been employed extensively as a polymeric plasticiser for Poly(lactic acid) (PLA) and as an excipient in pharmaceutical formulations. It was thought that by combining both the plasticising effects of $CO_2$ and PEG it would be possible to further reduce the viscosity of PLA. This was not the case; however, a reduction in the time taken for the samples to reach their saturation viscosity was observed. The effect of the mode of PEG incorporation was also investigated, where PEG as a blended excipient was compared to PEG as a covalently linked entity in a block copolymer. The plasticising effect was found to have similar efficiency regardless of the incorporation method.

Finally, a series of formulations containing a model protein drug, bovine serum albumin (BSA) encased in a polymer matrix were produced using a $CO_2$ mixing procedure. The influence of the composition of the polymer matrix was investigated and a mix of $P_{D,L}LA$ and PLGA was found to be the most suitable. The effect of BSA content, BSA particle size and polymer ratio on the rheological properties and the release profiles was evaluated. A content assay and micro Raman spectroscopy were performed to assess the API content and the homogeneity of the formulations. It was expected that a formulation that can be readily processed will have a homogenous distribution of API and would exhibit consistent release profiles on a batch-to-batch basis. An *in vitro* dissolution study was performed on the formulations and the results were compared to the rheological data. It was found that if the rheology of a formulation could be measured and analysed and the viscosity was sufficiently low, then this formulation should exhibit consistent release profiles across different batches.

Overall, this thesis aims to determine whether high pressure rheology can be used as an aid for formulation development. The data show that it is possible to measure the viscosity of complex formulations in a robust and reliable manner. These preliminary data suggest there is a general correlation between the rheological properties of a formulation and the consistency of its *in vitro* release.

# Publications

1. **K.J. Pepper**, T.O. Masson, D. De Focatiis, S.M. Howdle, Can a combination of poly(ethylene glycol) and dense phase carbon dioxide improve processing of polylactide? A high pressure rheology investigation, Journal of Supercritical Fluids (2018), 133, 343. doi:10.1016/j.supflu.2017.10.014.

2. Q.-Y. Meng, **K.J. Pepper**, R.-H. Cheng, S.M. Howdle, B.-P. Liu, Effect of supercritical $CO_2$ on the copolymerization behaviour of cyclohexene oxide/$CO_2$ and copolymer properties with DMC/Salen-Co(III) catalyst system, Journal of Polymer Science Part A: Polymer Chemistry, (2016), 54, 2785. doi:10.1002/pola.28162.

# Abbreviations

| | |
|---|---|
| $^1$H NMR | Proton Nuclear Magnetic Resonance |
| API | Active Pharmaceutical Ingredient |
| BSA | Bovine Serum Albumin |
| *c* | Carreau Constant |
| $CDCl_3$ | Deuterated Chloroform |
| CLS | Classic Least Square Regression Fitting |
| $CO_2$ | Carbon Dioxide |
| *Đ* | Dispersity |
| dn/dc | Differential Index Of Refraction |
| DPBS | Dulbecco's Phosphate Buffer Saline |
| DSC | Differential Scanning Calorimetry |
| EPDM | Ethylene Propylene Diene Monomer Rubber |
| EtOH | Ethanol |
| FDA | U.S. Food And Drug Administration |
| FTIR | Fourier Transform Infra Red Spectroscopy |
| *G'* | Storage Modulus |
| *G''* | Loss Modulus |
| *G** | Complex Modulus |
| GPC | Gel Permeation Chromatography |
| HME | Hot Melt Extrusion |
| LVE | Linear Viscoelastic |
| $M_n$ | Number Average Molecular Weight |
| $M_w$ | Weight Average Molecular Weight |
| $P_c$ | Critical Pressure |
| PCL | Polycaprolactone |
| $P_{DL}LA$ | Poly($_{D,L}$-lactide) |

| | |
|---|---|
| PDMS | Polydimethylsiloxane |
| PE | Polyethylene |
| PEG | Poly(ethylene glycol) |
| PEO | Poly(ethylene oxide) |
| PGA | Polyglycolide |
| PGSS | Particles From Gas Saturated Solutions |
| PLA | Poly(lactic acid) |
| PLGA | Poly($_{D,L}$-lactide-co-glycolide) |
| $P_LLA$ | Poly($_L$-lactide) |
| PP | Polypropylene |
| PS | Polystyrene |
| RESS | Rapid Expansion Of Supercritical Solutions |
| RI | Refractive Index |
| ROP | Ring Opening Polymerisation |
| RSD | Relative Standard Deviation |
| $scCO_2$ | Supercritical Carbon Dioxide |
| SCF | Supercritical Fluid |
| SEC | Size Exclusion Chromatography |
| SEM | Scanning Electron Microscopy |
| $Sn(oct)_2$ | Tin (II) 2-Ethylhexanoate |
| $t$ | Time |
| $T$ | Temperature |
| tan($\delta$) | Loss Tangent, ratio of loss modulus to storage modulus |
| $T_c$ | Critical Temperature |
| $T_g$ | Glass Transition Temperature |
| THF | Tetrahydrofuran |
| $T_m$ | Melting Temperature |
| $t_{sat}$ | Time To Saturation |

| | |
|---|---|
| USP | United States Pharmacopeia |
| VOC | Volatile Organic Solvent |
| $\gamma$ | Shear Strain |
| $\dot{\gamma}$ | Shear Rate |
| $\delta$ | Phase Shift |
| $\eta$ | Viscosity |
| $\eta_0$ | Zero Shear Viscosity |
| $\eta_0(p_{amb})$ | Ambient Pressure Zero Shear Viscosity |
| $\eta_\infty$ | Infinite Shear Viscosity |
| $\eta_{sat}$ | Saturation Viscosity |
| $\lambda$ | Relaxation Time |
| $\sigma$ | Shear Stress |
| $\tau$ | Stress |

# Contents

Declaration ..... ii

Acknowledgements ..... iii

Abstract ..... iv

Publications ..... vi

Abbreviations ..... vii

Contents ..... x

Chapter 1 ..... 1-1

1.1 Contents ..... 1-2

1.2 Biodegradable Polymers ..... 1-3

1.3 Biodegradable Polymers for Drug Delivery ..... 1-4

1.4 Processing Polymers for Drug Delivery ..... 1-7

1.4.1 Double Emulsion Techniques ..... 1-7

1.4.2 Spray Drying ..... 1-9

1.4.3 Extrusion Techniques ..... 1-11

1.5 Supercritical Carbon Dioxide (scCO2) ..... 1-14

1.5.1 $scCO_2$ for Polymer Processing ..... 1-17

1.6 Rheology ..... 1-21

1.6.1 Rheology of Polymers ..... 1-24

1.6.2 High Pressure Rheology ..... 1-26

1.6.3 Effect of APIs on Polymer Melt Viscosity ..... 1-26

1.7 Aims and Objectives ..... 1-29

Chapter 2 ..... 2-31

2.1 Overview ..... 2-32

2.2 Contents ..... 2-33

2.3 Sample Naming System ..... 2-34
2.3.1 Purchased Polymers Naming System ..... 2-34
2.3.2 Synthesised Polymers Naming System ..... 2-34
2.3.3 Polymer Blends Naming System ..... 2-35
2.3.4 Formulation Naming System ..... 2-37
2.4 Rheology ..... 2-38
2.4.1 Oscillatory Measurement Mode ..... 2-38
2.4.2 Rotational Measurement Mode ..... 2-41
2.5 High Pressure Equipment ..... 2-45
2.5.1 High Pressure Rheometer ..... 2-47
2.5.2 View Cell ..... 2-51
2.5.3 MKIII Clamp Sealed Autoclave ..... 2-53
2.6 Characterisation Methods ..... 2-55
2.6.1 Differential Scanning Calorimetry ..... 2-55
2.6.2 Gel Permeation Chromatography ..... 2-55
2.6.3 $^{1}$H Nuclear Magnetic Resonance Spectroscopy ..... 2-56
2.6.4 SEM ..... 2-56
2.6.5 Micro Raman Spectroscopy ..... 2-56
Chapter 3 ..... 3-59
3.1 Abstract ..... 3-60
3.2 Contents ..... 3-61
3.3 Introduction ..... 3-62
3.4 Materials ..... 3-68
3.5 Methods ..... 3-69
3.5.1 Rheology Measurements ..... 3-69
3.5.2 Characterisation of the Polymers ..... 3-74

3.6 Results ..... 3-76
3.6.1 Rheology of $PCL_{112}$ ..... 3-76
3.6.2 Rheology of $PLA_{11}$ ..... 3-81
3.6.3 Rheology at 140 bar and 40 °C ..... 3-87
3.6.4 Characterisation of the Polymers Before and After Rheology ..... 3-93
3.7 Summary ..... 3-97
3.8 Conclusions ..... 3-99
Chapter 4 ..... 4-101
4.1 Abstract ..... 4-102
4.2 Contents ..... 4-103
4.3 Introduction ..... 4-104
4.4 Materials ..... 4-106
4.5 Methods ..... 4-107
4.5.1 Polymer Synthesis ..... 4-107
4.5.2 Polymer Characterisation ..... 4-109
4.5.3 Rheological Measurements ..... 4-110
4.6 Results and Discussion ..... 4-112
4.6.1 Polymer Synthesis ..... 4-112
4.6.2 Viscosity Analysis ..... 4-118
4.7 Summary ..... 4-129
4.8 Conclusions ..... 4-130
Chapter 5 ..... 5-131
5.1 Abstract ..... 5-132
5.2 Contents ..... 5-134
5.3 Introduction ..... 5-135
5.4 Materials ..... 5-141

5.5 Methods ..... 5-142
5.5.1 Jet Milling of the BSA ..... 5-142
5.5.2 Rheology ..... 5-143
5.5.3 BSA Content Assay ..... 5-143
5.5.4 *In Vitro* Dissolution Study ..... 5-145
5.6 Results ..... 5-145
5.6.1 Polymer Matrix Selection ..... 5-146
5.6.2 Formulations Containing BSA ..... 5-153
5.7 Summary ..... 5-180
5.8 Conclusions ..... 5-182
Chapter 6 ..... 6-183
6.1 Overview ..... 6-184
6.2 Summary ..... 6-184
6.1 Conclusions ..... 6-187
6.2 Future Work ..... 6-187
6.3 References ..... 6-190

# Chapter 1

Introduction

# 1.1 Contents

Chapter 1 ..... 1-1

1.1 Contents ..... 1-2

1.2 Biodegradable Polymers ..... 1-3

1.3 Biodegradable Polymers for Drug Delivery ..... 1-4

1.4 Processing Polymers for Drug Delivery ..... 1-7

1.4.1 Double Emulsion Techniques ..... 1-7

1.4.2 Spray Drying ..... 1-9

1.4.3 Extrusion Techniques ..... 1-11

1.5 Supercritical Carbon Dioxide (scCO2) ..... 1-14

1.5.1 $scCO_2$ for Polymer Processing ..... 1-17

1.6 Rheology ..... 1-21

1.6.1 Rheology of Polymers ..... 1-24

1.6.2 High Pressure Rheology ..... 1-26

1.6.3 Effect of APIs on Polymer Melt Viscosity ..... 1-26

1.7 Aims and Objectives ..... 1-29

## 1.2 Biodegradable Polymers

For more than a century, synthetic polymers have reigned as one of the greatest innovations of the human race. These relatively simple molecules, made up from repeating units of covalently linked monomers, are extremely versatile with a wide range of properties that can be determined from the starting materials and synthetic conditions.[1] Around 400 million tonnes of plastic is produced from polymers worldwide every year and it remains in the environment for hundreds of years, unless it is incinerated.[2] On top of this, over 90% of all polymers are produced from fossil fuel feedstocks, with the polymer industry accounting for 6-8% of the total global oil consumption.[3,4] Conventional polymers derived from the petrochemical industry are not biodegradable and if they do break down they remain in the environment as microscopic particles.[5,6] Therefore, it is imperative that the polymer industry makes an effort to move towards a closed-loop economy where these polymer products are 100% recyclable and reusable.[6]

One solution is the development of environmentally benign bioplastics from bio-based and/or biodegradable polymers to replace conventional plastics. Bio-based polymers are non-biodegradable polymers derived from plants, which have the same properties as conventional polymers and can be recycled in the same way. Although they do not biodegrade, their development will reduce the global dependency on fossil fuels and greenhouse gas emissions. Biodegradable polymers can be produced using fossil fuels or derived from plant-based resources.[7] These polymers are broken down into small molecules such as carbon dioxide ($CO_2$), methane ($CH_4$) and water by microorganisms or by other processes such as photodegradation, oxidation and hydrolysis.[6]

To date the production of bioplastics equates to less than 1% of the global annual plastic production, with biobased polyethylene (PE) and Poly(ethylene terephthalate (PET) being the most widely produced.[7] Examples of biodegradable polymers include polyglycolide (PGA), polycaprolactone (PCL), polyhydroxyalkanoates (PHA), poly(butylene succinate) (PBS) and poly(butylene adipate terephthalate) (PBAT).[6–8] However, their use in society is restricted by costly manufacturing processes and

sub-optimal mechanical properties in addition to the fact that the degradation processes can only occur at certain conditions.[3]

Poly(lactic acid) (PLA) is another example of a biodegradable polymer and it is predicted to be one of the biggest growth drivers for biodegradable polymers in the near future. Not only can PLA be produced from sustainable resources, it has good mechanical strength and low toxicity making it suitable for packaging and biomedical applications.[9] In comparison to conventional polymers and bio-based polymers, it has a relatively fast degradation time, decomposing in years as opposed to decades or centuries.[6] However, its implementation in society has thus far been limited by its poor thermal properties and the need for specific conditions for degradation. Fortunately, these drawbacks do not impede its use in biomedical applications.

## 1.3 Biodegradable Polymers for Drug Delivery

There are three main conventional methods for the administration of medication.[10] Oral administration is most preferred by patients but poor absorption and fast degradation is prolific and leads to low efficacy and the need for frequent dosing.[11] Injection dosing has better efficacy but is invasive and often requires clinicians, also the short term effects mean that frequent dosing is necessary.[12] The third method of dosing includes creams and ointments that are largely used for topical effects, not systemic. Although these methods are still used today, there is a wealth of research focusing on their development to overcome their limitations. Conventional methods tend to release faster requiring frequent dosing and the concentration of the drug in the blood plasma often exceeds the therapeutic level resulting in toxic side effects (Figure 1.1). This has prompted recent research to be directed towards developing alternative delivery routes to oral and parenteral administration.[13,14] An ideal drug delivery system will enhance and facilitate the action of the drug and deliver the correct amount to the correct place at the correct rate in order to optimize the therapeutic response.[10,12] In the 1950s the first sustained release therapy was developed to achieve a consistent release of the drug within the therapeutic region, with no peaks or troughs (Figure 1.1).[15,16] This reduced the need for multiple dosing occasions and the occurrence of toxic side effects.

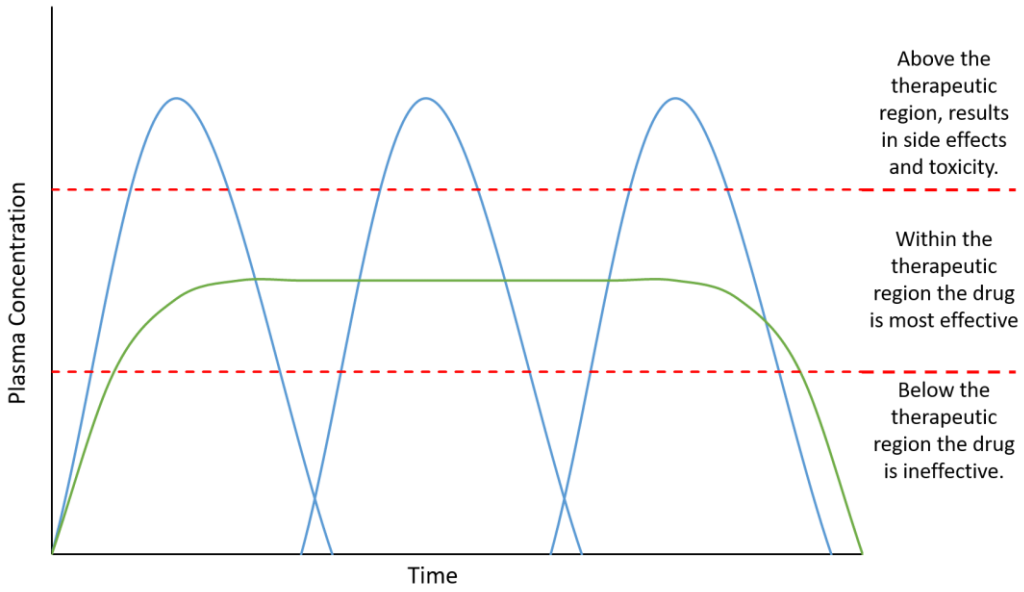



Figure 1.1. Comparison of conventional release profiles (blue) and a sustained release profile (green). Conventional release profiles not only release faster requiring frequent dosing, the plasma concentration often exceeds the therapeutic level and becomes toxic. For sustained release, more of the dose remains within the therapeutic region making it more effective.

These advanced delivery systems promote controlled release and specific targeting of the drug molecules. One system that has received much attention is the encapsulation of drug molecules in biodegradable polymers.[17,18] These systems also offer some protection for the drug as it travels through the body. This is particularly beneficial for protein and peptide based active pharmaceutical ingredients (API) that suffer from short half-lives, low stability and poor absorption.[19]

Biodegradable polymers are a popular choice for biomedical applications because they are generally biocompatible and insoluble in the body.[20] Examples include polyurethanes which are investigated for use as long term medical implants, poly(ester amides) for suture materials and site specific delivery of hydrophobic drugs (CAMEO®), poly(ortho esters) for pH sensitive drug delivery and polyanhydrides.[21] Aliphatic polyesters such as PLA, PGA, their copolymer derivatives poly(lactide-*co*-glycolide) (PLGA) and PCL remain the most widely studied polymers for use in medical devices and drug delivery systems.[18,22–25] These polymers are preferred because they breakdown into non-toxic water soluble molecules during natural metabolic processes, thus circumventing the need for surgical removal.[22] Their ease of synthesis and the ease with which their properties can be tailored

during synthesis makes them highly versatile and allows for application specific design.[26,27]

Different polymers are preferred for different applications depending on their properties. For example their rate of degradation can be controlled by their physical and chemical properties including molecular weight, porosity and ratio of co-monomers (Table 1.1).[25,28]

Table 1.1. Properties of some common biodegradable polymers used for medical devices.[22,29]

| Polymer | Crystallinity[a] | $T_g$ (°C) | Degradation Rate[b] | Typical Applications |
|---|---|---|---|---|
| PGA | Highly crystalline ($T_m$ = 225-230 °C) | 35-40 | 2-3 months | Sutures |
| $P_LLA$ | Semi-crystalline ($T_m$ = 173-178 °C) | 60-65 | >2 years | Fracture fixation, ligament augmentation |
| $P_{D,L}LA$ | Amorphous | 55-60 | 12-16 months | Drug delivery systems |
| PLGA | Amorphous | 45-55 | 1-6 months[c] | Suture, fracture fixation, oral implant, drug delivery |
| PCL | Semi-crystalline ($T_m$ = 60 °C) | -60 | >4 years | Contraceptive delivery implants, tissue scaffolds |

a) $T_m$ is the melting temperature. b) Degradation rates depend on molecular weight. c) Degradation rate depends on the monomer ratio of lactide:glycolide.

Another example of exploiting polymers for drug delivery is the use of poly(ethylene glycol) (PEG) as a processing aid or release enhancer.[24,30] Despite not being classified as biodegradable, PEG is approved for use in the body by the U.S. Food and Drug Administration (FDA). Combining PEG with other polymers to produce a block copolymer yields other interesting properties that can be utilised for drug delivery. For example, Jeong et al. synthesised a thermoresponsive block copolymer of PEG and Poly($_L$-lactide) ($P_LLA$) that could be injected as an aqueous solution at elevated temperatures, before cooling to form a gel at body temperature.[18] Zentner et al. report on the use of a biodegradable triblock copolymer which exhibits reverse thermal gelation properties for the delivery of water insoluble drugs.[31]

The first advanced drug delivery system made commercially available in the U.S was the Lupron Depot®, in 1989.[32] Designed for treatment of prostate and breast cancer, luteinising hormone releasing hormone (LH-RH) super agonist was encased in PLGA or PLA microspheres. A high encapsulation efficiency and sustained release (1-3 months) were achieved using a water-oil-water emulsion.[33] Before this, LH-RH was administered by daily injection because it is a large water soluble peptide with a short half-life.[32] Today, research is focusing on even more advanced systems such as the targeted delivery of doxorubicin to cancerous cells, responsive delivery devices such as glucose-sensitive insulin with on-off switching capability and even longer sustained release ranging from 6 months to a year.[34]

As mentioned previously these systems are particularly beneficial for the delivery of biopharmaceuticals derived from proteins, peptides and oligonucleotides. However, the challenges associated with their delivery are also a problem for their incorporation into these advanced polymer delivery systems.

## 1.4 Processing Polymers for Drug Delivery

Conventional methods of preparing polymer based drug delivery systems include emulsion, spray drying and extrusion techniques.[14,24,35,36] These will each be discussed in detail in the following sections.

### 1.4.1 Double Emulsion Techniques

The emulsion technique is primarily utilised to encapsulate water-soluble drugs in hydrophobic polymer microspheres.[37] Typically, the drugs are protein or peptide based which are unstable in bodily fluids and rapidly excreted.[32] The microspheres are produced by first dissolving the hydrophilic drug in an aqueous solution to give a “uniform first water phase” while the polymer is dissolved in an organic solvent. These two phases are then mixed at high shear (ultrasonification or homogenisation) to give a primary water-in-oil emulsion (W/O). The primary emulsion is then dispersed in a secondary external aqueous phase containing a stabiliser, again at high shear, to produce the double water-in-oil-in-water emulsion (W/O/W). The protein loaded microspheres are then obtained by removing the organic solvent and drying

(Figure 1.2).[14,32,37–40] Although this process is relatively complex, it is favoured because it produces uniform, spherical particles with a high encapsulation efficiency at high yields.[24] Control of particle size is possible by adjusting the various parameters, including the volume and viscosity of the phases, polymer concentration and molecular weight, surfactant type and stirring speed.[41–43]

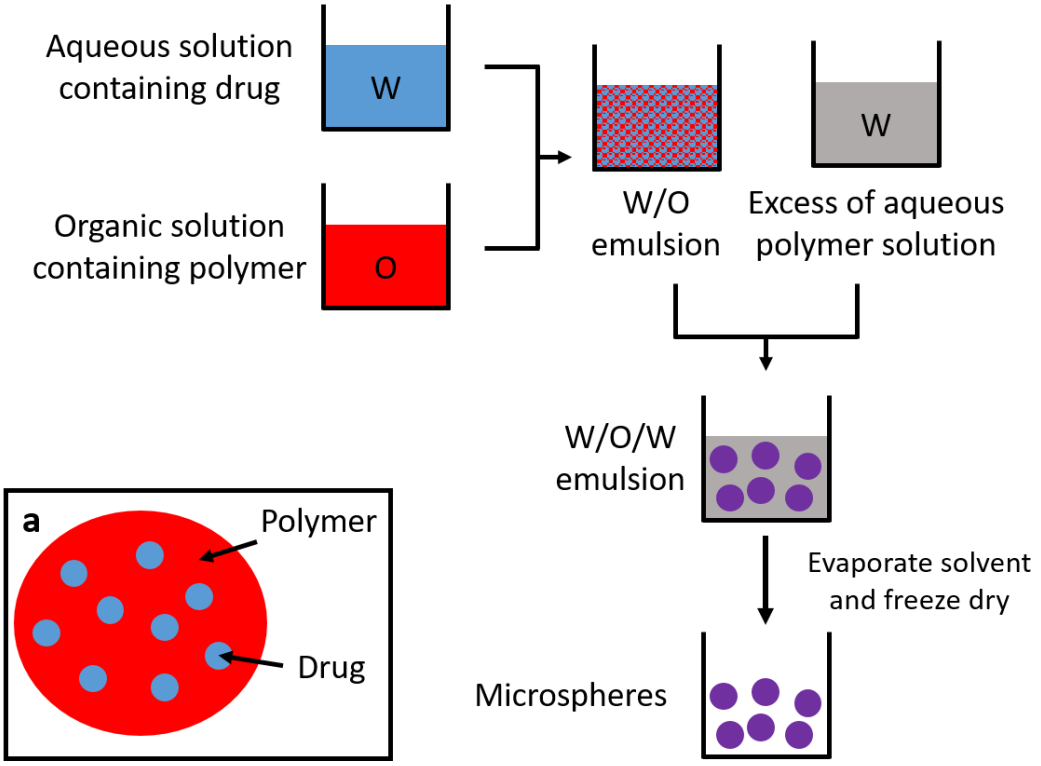



Figure 1.2. Double emulsion technique for the encapsulation of hydrophilic drug in polymeric microspheres. a) Cross section of a microsphere, where the drug is dispersed throughout the polymer matrix. Adapted from Okada et al.[32]

Despite using organic solvents to produce the oil phase, Okada et al. demonstrated that only 100 ppm of residual solvent remains in the final product, which is well below the limit defined by the United States Pharmacopeia (600 ppm).[32,44] Hydrophobic drugs can also be encapsulated using a modified version of this technique in which the drug and polymer are dissolved in an organic solvent before being added to an excess of a dilute polymer solution (aqueous). The resultant oil-in-water emulsion is then exposed to a vacuum to remove the solvent and produce the dry microspheres.[38] Wang et al. showed that this technique could be modified to allow for the simultaneous encapsulation of hydrophilic and hydrophobic drug

molecules.[38] They follow a similar procedure as described, but during the mixing of the first emulsion with the second aqueous phase, a solution of the hydrophobic drug in organic solvent is added slowly, before the whole mixture is emulsified again.

As previously mentioned, the first advanced drug delivery system was prepared via a double emulsion technique,[32] some other examples include the encapsulation of BSA, doxorubicin and paclitaxel and insulin.[37–40] However, there are limitations to this technique regarding the stability of the protein during the various stages of the process particularly lyophilisation and exposure to harsh organic solvents, heat and surface tension.[24,40,45,46]

### 1.4.2 Spray Drying

Spray drying techniques are simple, fast and reproducible methods for the encapsulation of drugs in polymer matrices though the conversion of a liquid formulation into a solid powder.[24,47,48] By selecting an appropriate formulation with optimised processing conditions, it is possible to produce stable pharmaceutical powders.[49] This process comprises of four stages:[47] first, the polymer and drug are dissolved in a suitable solvent, which is then fed through a nozzle and atomised into a stream of hot gas. Reduction of the droplet size results in a sudden increase in surface area leading to the rapid evaporation of the solvent. The droplets then solidify to form uniform, spherical particles, which are separated from the gas stream and collected as a dry powder product (Figure 1.3).[14,47] Typically, organic solvents are used because they have low boiling points that are below the glass transition temperatures ($T_g$) of the polymers. This means that the temperature required to remove the solvent will be lower than that of the polymer $T_g$, preventing aggregation of the particles.[48] Usually, air is used as the gas stream because it is less costly than other inert gases. If necessary it is possible to employ a closed loop system and use other gases such as nitrogen.[50]

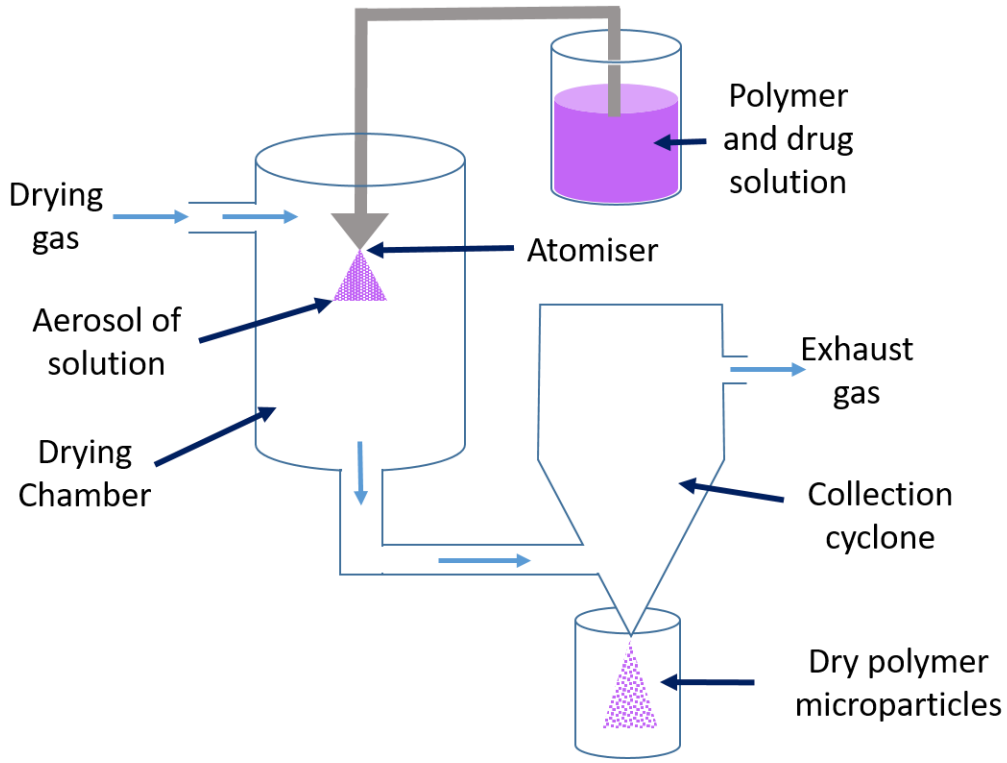



Figure 1.3. Diagram of the spray drying equipment used for the encapsulation of drug in polymer microparticles.

One key advantage of this technique is the combination of particle formation and drying in a single step.[35] It also boasts short processing times (hours), ease of scale up and mild operating conditions, specifically the use of atmospheric pressures.[47,49] On top of this, it is a continuous process that can convert a variety of liquid forms; such as solutions, emulsions, slurries or pastes, to solid particles with adjustable size, shape, porosity, density and chemical composition.[47] Altering the processing conditions allows for well-defined control of particle size, shape, morphology, which can lead to the production of microparticles with controlled release properties.[24,49–51] For example, a high feed flow rate, large nozzle aperture and high solution concentration will result in larger particle sizes (x$10^2$ µm). Alternatively, low surface tension, high atomisation pressure and a small nozzle aperture will produce smaller particles.[48]

These powders have increased stability in comparison with liquid formulations due to the lack of moisture and can also be re-dispersed prior to administration.[47,48] The process can also cause the drug molecules to transition from a crystalline to a more amorphous state, which can result in improved solubility.[48,52] Hence, there have

been numerous studies into the application of spray drying for the encapsulation of drugs including Exubera®, the first inhaled therapeutic to be manufactured by spray drying.[47,49] Other examples include ketotifen encapsulated in PLA and PLGA,[53] ibuprofen in soy proteins[54] and vancomycin in PLGA.[55]

The major downsides to this approach are the need for organic solvents and that high temperatures can be detrimental to certain bioactive drugs, resulting in their degradation or loss of activity.[14] This technique also suffers from low yields at low processing scales (50-70%). Much of the product is lost on the chamber walls and small particles can pass into the exhaust stream. This is less of an issue at large scales, because the fraction of lost material accounts for a smaller portion of the total product.[48]

### 1.4.3 Extrusion Techniques

Extrusion techniques are gaining ground in the pharmaceutical industry as a method for enhancing the solubility and bioavailability of poorly soluble APIs by producing amorphous solid dispersions.[56–59] A conventional extruder is comprised of a feed hopper, a heated barrel with rotating screws, a die and heating/cooling systems (Figure 1.4).[57,58] The formulation components, including the API and the carrier materials, are physically mixed before being introduced to the extruder via a hopper.[60] The materials are then conveyed through a heated barrel using one or more screws and forced through a small nozzle called a die.[56,61] The heat melts the polymer, reducing its viscosity; while the combination of heat and shear disperses the drug particles throughout the matrix.[36] The final extrudate has a uniform shape that can be determined by altering the shape of the die making it possible to produce a range of pharmaceutical products including tablets, films, implants and scaffolds.[36,56,60] The extruder is typically connected to a computer to control and monitor the torque, screw speed, melt viscosity, pressure, and die and barrel temperatures.[56,57]

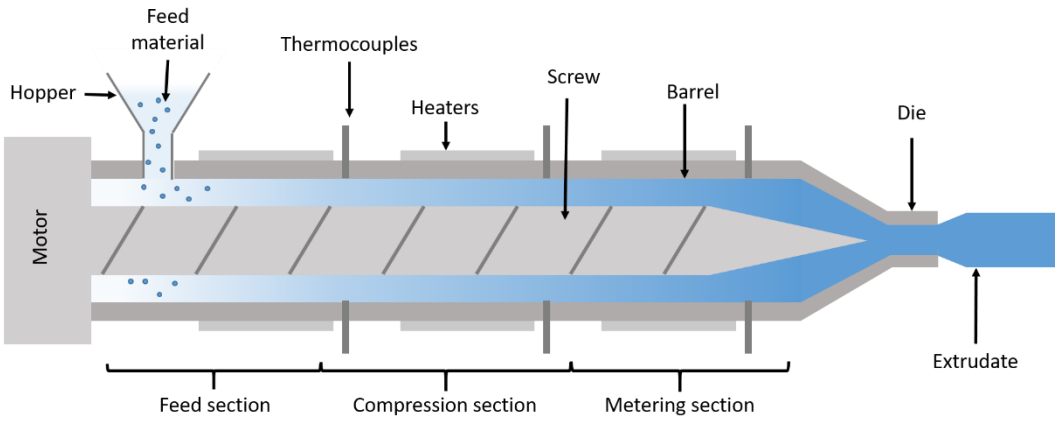



Figure 1.4. Diagram of a single screw extruder.

In addition to short manufacturing process times and high throughput capabilities, there is also the potential for Process Analytical Technology (PAT) allowing for continuous optimisation of the process. Consequently, the drug development process can be significantly shortened, making hot melt extrusion one of the most widely used processing techniques for drug delivery systems.[56] The intense mixing imparted by the screws results in a uniform distribution of the drug throughout the polymer matrix.[57,61] To ensure complete homogenisation of the extrudate, the process is optimised by altering parameters such as the screw design.[61] As a result of direct mixing it is possible to achieve high drug loading efficiencies (>90 %) because no drug is lost during the removal of solvents.[60,62] This versatile and robust technique also offers the advantage of being solvent free and economical, with the option of being a continuous or bulk process.[36,56,57,60,61] Current research is now investigating the potential for a hot melt extrusion-additive manufacturing processing method to develop personalised medications.[63] This method sees the components of a pharmaceutical device mixed via hot melt extrusion to produce a filament that can be fed directly into a 3D printer.[64]

Due to its versatility there are a number of examples of pharmaceutical delivery systems that have been produced using hot melt extrusion techniques.[61] Since its introduction to the pharmaceutical industry in 1971, hot melt extrusion techniques have been modified to produce products for a range of delivery routes.[56] Examples include gastroretentive drug delivery systems with bioadhesive properties,[65] fast

release oral films for anti-allergy applications,[66] PLGA-based implants for sustained protein release[67] and bioadhesive films for buccal and transdermal delivery.[68,69]

However, the requirement for high temperatures limits its use to thermally stable materials and inhibits the use of protein and peptide based pharmaceuticals.[58,60] By selecting polymers with low melting temperatures, it is possible to process some thermally sensitive materials.[57] This also makes it an energy intensive manufacturing process. Also there are strict quality control measures in place to ensure the integrity of the APIs, because processing could have a direct impact on the physiochemical properties of the product and its efficacy.[60] Additionally, many polymers have extremely high melt viscosities which can cause the instrument torque to exceed its working limits.[70] In order to process such materials, plasticisers can be employed to reduce the viscosity. However, this can lead to an increase mobility in the final composition, which can enable the drug molecules to recrystallise during storage.[61]

In all these techniques the polymer must be in a liquefied state in order for the polymer and drug to mix homogeneously. As stated previously, this is usually achieved by heating above the $T_g$ or $T_m$ of the polymer or by dissolving the components in an organic solvent. Both of these methods can be detrimental to the integrity of the API, especially those derived from proteins and peptides.[14,71]

At elevated temperatures, the polymer chains have more mobility and increased free volume resulting in a transition to a liquid state with reduced viscosity. The temperature at which this transition occurs ($T_g$ or $T_m$) is dependent on the molecular weight and intermolecular structure of the polymer. Therefore, it can be altered by the addition of side chains, which would increase steric hindrance and free volume therefore lowering the $T_g/T_m$.[72] Small molecules, called plasticisers, can also be added to reduce $T_g$. By penetrating into the free volume between the polymer chains and interacting with the polymer backbone, they reduce the number of polymer chain interactions resulting in increased chain mobility.[73] Since any plasticisers used will remain in the final product and will eventually be released into the body during degradation they are unsuitable for pharmaceutical applications. However, inactive additives such as poloxamers can be incorporated to improve processability.[71,74] As well as improving processability they can act as binding agents, dyes, preservatives,

flavourings and facilitate the transport of drug through the body.[75] These excipients have to be approved by the U.S Food and Drug Administration (FDA) before use, to confirm they do not affect the therapeutic action of the active component.[76] Reducing the $T_g$ or $T_m$ of the polymer means that its viscosity will be reduced at lower temperatures, negating the need for elevated processing temperatures. This has positive implications for energy usage and production costs. However, there is still a requirement for temperatures that are above the degradation temperatures of most thermally sensitive APIs.

Although the use of solvents is often less detrimental to the drug and avoids the use of high temperatures there is an environmental impact. Intensive purification steps are required to remove any excess solvent and disposal of the waste solvent can be expensive and environmentally harmful. Thus, green solvents, in particular supercritical carbon dioxide ($scCO_2$), are being investigated as possible alternatives.

## 1.5 Supercritical Carbon Dioxide (scCO2)

A supercritical fluid (SCF) is the defined state of a compound, mixture or element above its critical temperature and pressure, $T_c$ and $P_c$,[77] which has a density close to or above its critical density (Figure 1.5).[78]

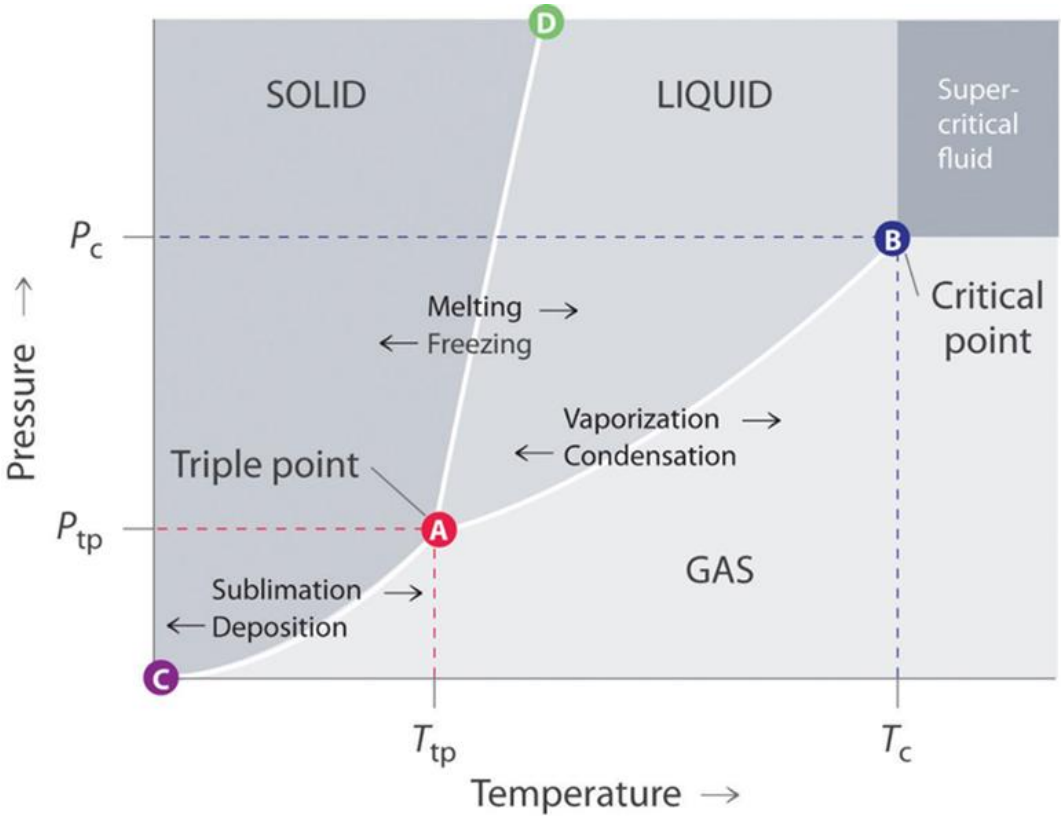



Figure 1.5. Typical phase diagram showing the triple point (A) and the critical point (B).[80]

This transition can be visualised using a view cell (Figure 1.6).[79] Initially two phases, liquid and gas, can be seen clearly separated by the meniscus at the phase boundary. As the temperature is increased the liquid begins to boil and expand as its density decreases, until it reaches a point above the critical temperature and pressure in which only a single supercritical phase is observed. The temperature and pressure at which a substance becomes supercritical is called the critical point.[80]

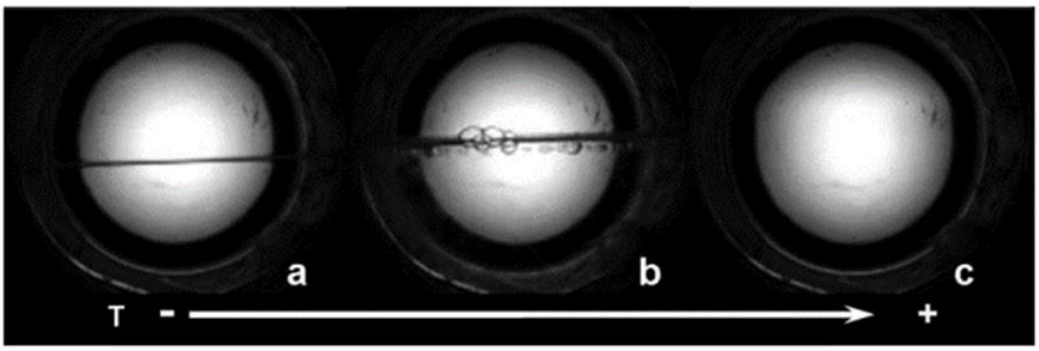



Figure 1.6. Still images capturing the phase change of a liquid as temperature is increased (from left to right). **a**) The phase boundary between the liquid and gas can clearly be seen. **b**) As the temperature is increased, the liquid begins to boil and the meniscus is elevated as the liquid density decreases resulting in expansion. **c**) Once the temperature is above the $T_c$, a single supercritical phase is observed. Reprinted with permission of Royal Society of Chemistry, from "Supercriticality"; a dramatic but safe demonstration of the critical point, P. Licence, D. Litchfield, M. P. Dellar, M. Poliakoff, Copyright (2004) Green Chemistry.[79]

Supercritical fluids have properties similar to both liquids and gases. Liquid-like density results in good solvating powers while gas-like behaviour allows for better solute diffusivity.[81] Another unique attribute is the 'tunability' of the density from liquid- to gas-like values; hence, by altering the pressure, the solvent power can be manipulated.[82] These properties make SCFs attractive alternatives to harmful and environmentally unfriendly solvents such as benzene or hexane, which are commonly used in the chemical industry.[83]

Supercritical carbon dioxide ($scCO_2$) is cheap, non-toxic and non-flammable with an accessible critical point ($P_c$ = 73.8 bar, $T_c$ = 31.1 °C),[78] making it the most widely used supercritical fluid. It is also considered a green solvent because it is recovered as a by-product from other processes including fermentation, combustion and ammonia synthesis, therefore producing no net contribution to the greenhouse effect.[84] $ScCO_2$ has been commercialised for use in extraction processes[85,86] and it has been utilised as a solvent for chemical reactions including the hydrogenation of isophorone and Friedel Crafts alkylations.[87] Other applications include polymer synthesis and polymer processing.[88–90]

### 1.5.1 $scCO_2$ for Polymer Processing

The solvent properties of $scCO_2$ can be exploited for use in polymer processing where its low viscosity and high diffusivity enable it to behave as a plasticiser.[91] Examples include the production of foams or scaffolds, particle formation, polymer impregnation and drug encapsulation.[26,92–95] The gaseous properties of $scCO_2$ enable the molecules to diffuse into the accessible free volume between polymer chains. Here the $CO_2$ acts like a Lewis acid and interacts with any basic sites along the polymer backbone, reducing the number of intermolecular interactions between polymer chains.[96] In the case of PLA, PLGA and PCL, $CO_2$ can interact with the carbonyl groups, increasing chain separation and mobility resulting in a reduction in $T_g$ and viscosity.[91] The observed effect is greater for amorphous polymers compared to crystalline polymers. As a consequence of their regular structure, crystalline polymers have a higher density of intermolecular interactions and less accessible free volume making $CO_2$ penetration more difficult.[97] Accessible free volume surrounding the polymer backbone will also affect the degree of $CO_2$ penetration, hence polymers with bulky side chains will absorb more $CO_2$ because they have more accessible free volume.[93]

This plasticising effect is particularly useful for processing polymers for pharmaceutical applications because it enables the mixing of the polymers and drugs without the need for high temperatures. Some small molecule drugs are soluble in $CO_2$ and can be more readily impregnated into polymer matrices under these conditions.[95] On the other hand large protein or peptide drugs are insoluble in $CO_2$ and so its ability to reduce the viscosity and $T_g$ of the polymers is key for processing. A further advantage of replacing organic solvents with $CO_2$, especially in pharmaceutical applications, is that when $CO_2$ is removed from the system there are no solvent residues and all the $CO_2$ can be completely removed.[82] This process occurs naturally via venting without the need for extraction or drying steps because the $CO_2$ diffuses out of the product and into the atmosphere. On top of this, the $CO_2$ does not interact with the APIs so they maintain their full activity and efficacy.[93] There are three major $scCO_2$ processing techniques for the production of polymer

microparticles for drug delivery: rapid expansion of supercritical solutions (RESS), anti-solvent techniques and particles from gas saturated solutions (PGSS).[98,99]

#### 1.5.1.1 Rapid Expansion of Supercritical Solutions (RESS)

This technique requires both the polymer and the drug to be soluble in $scCO_2$.[26] The components are exposed to $CO_2$ at a specific temperature and pressure above the critical point to give a high pressure solution. The mixture is then expanded through a capillary nozzle into a low pressure collection vessel. The rapid decompression results in the expansion and subsequent evaporation of $CO_2$ leading to microparticle precipitation.[93] Particle size can be altered by adjusting processing conditions and nozzle geometry. Examples of RESS used in drug delivery system preparation include deferasirox (Exjade) which is used to reduce iron overload in patients receiving long term blood transfusions[100] and Naproxen, a poorly water soluble drug.[101] Exploiting the high diffusivity and low surface tension of $scCO_2$, RESS has been used to impregnate polymers with pharmaceutical agents.[102] As the polymer is swollen by $CO_2$ the soluble drug can be dispersed through the polymer matrix.

However very few polymers are soluble in $CO_2$ making RESS unsuitable for most products. Co-solvents, like acetone,[103] can be used to improve solubility but this is unfavourable since it leads back to issues with residual solvent, product purification and solvent disposal. Often high temperatures are required and there is the potential for the drug and polymer to precipitate separately if they have different solubilities in $CO_2$, therefore affecting particle morphology.[93]

#### 1.5.1.2 Anti-Solvent Techniques

As a consequence of being a poor solvent for many polymers, $scCO_2$ makes a very good anti-solvent. Several $scCO_2$ anti-solvent techniques have been developed for the preparation of drug delivery systems including gas anti-solvent (GAS),[104,105] supercritical anti-solvent (SAS),[106,107] precipitation with compressed anti-solvent (PCA),[108] aerosol solvent extraction system (ASES)[105] and solution enhanced dispersion by $scCO_2$ (SEDS)[109,110] processing. The basis of these techniques is to dissolve the drug and polymer in an organic solvent and precipitate them using $scCO_2$

as the anti-solvent. As $CO_2$ concentration in the solution increases, the solvating power of the liquid phase is reduced, resulting in co-precipitation.[111] For these techniques it is not always necessary for the $CO_2$ to be supercritical e.g. GAS. Processing parameters, namely temperature and pressure are used to manipulate particle morphology leading to particle size control.[105] However, once again this technique requires organic solvents and is limited by the need for solutes that are soluble in such solvents.

#### 1.5.1.3 Particles from Gas Saturated Solutions (PGSS)

This technique exploits the plasticising effect of $CO_2$ on polymers, where a decrease in $T_g$ and viscosity facilitates the encapsulation of drug molecules without the need for high temperatures.[93] The drug and polymer are exposed to $CO_2$ at conditions above the critical point in a sealed vessel. Under these conditions, the polymer is in a liquefied state, while the drug remains solid. The components are mixed together to form a homogeneous blend, and the product is collected once the pressure is released.[74] There are two methods of collection; either the sample remains in the mixing chamber as pressure is released resulting in a foam or scaffold, or the mixture is sprayed through a nozzle into a collection vessel yielding small, uniform particles. For certain applications e.g. injectable or nasal drug administration these scaffolds can be ground to give the required particle size. The second method is preferable for the preparation of injectable doses because smaller particle sizes can be obtained (Figure 1.7). In order to produce a spray the collection vessel is at low pressure, causing the $CO_2$ to expand and evaporate; this increases the $T_g$ of the polymer so the particles solidify and are collected as a dry powder.[71,74] Control of particle size, shape and morphology is achieved through the speed of depressurisation and processing parameters.[112]

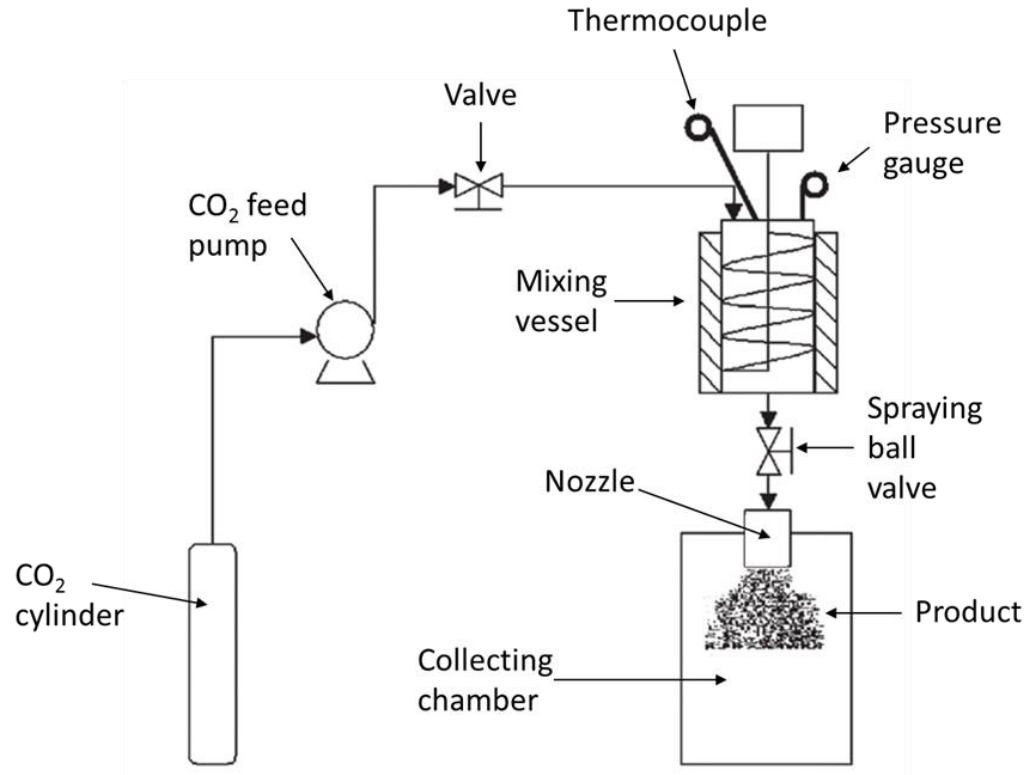



Figure 1.7. Schematic of the PGSS apparatus. The starting materials are placed in the mixing chamber, which is then brought to the desired temperature and pressure. The mixture is stirred and then released into the low pressure collecting chamber where the particulate product forms upon evaporation of the $CO_2$. Adapted with permission of Royal Society of Chemistry from supercritical fluid assisted melting of poly(ethylene glycol): a new solvent-free route to microparticles, J. Hao, M. Whitaker, G. Serhatkulu, K. M. Shakesheff, S. M. Howdle, Copyright (2005), Journal of Materials Chemistry.[252]

This process has many advantages over the other techniques, including being a solvent free, fast, one pot technique that can be operated at mild conditions and which does not rely on the solubility of polymers or APIs in $CO_2$.[93] Furthermore, in general the drug is not modified or affected by $CO_2$. However, it does come with its own challenges, control of depressurisation and solidification rates are important because they need to be fast enough to prevent particle aggregation caused by residual $CO_2$, but slow enough to allow time for droplet formation.[93] The high viscosity of the polymer melt makes mixing difficult, resulting in an uneven distribution of the drug throughout the polymer matrix. This is unfavourable and leads to issues with batch-to-batch reproducibility, which ultimately filters through to give inconsistent release profiles. The polymers also appear to behave differently in the presence of the drug molecules.[111] These problems need to be addressed for this method to become a viable preparation for drug delivery systems. Therefore,

the polymer melt viscosity in the presence of $CO_2$ is a major consideration for these systems and can be investigated using high pressure rheology. The systems investigated in this thesis are based on this method of polymer processing using the foam/scaffold collection method.

## 1.6 Rheology

Rheology is the study of deformation and flow of matter under an applied stress.[113] It is utilised in many industries to characterise materials based on their resistance to flow.[114] How a material behaves under stress can be classified on a scale, from ideally viscous liquids to ideally elastic solids. Ideally viscous liquids, such as oils and water are Newtonian fluids with shear-independent viscosities that follow Newton's law of viscosity. Newton's law of viscosity states that the stress applied to fluid layers is directly proportional to the velocity gradient.[115] Ideally elastic solids are rigid materials such as stone and steel that follow Hooke's Law of elasticity, which states that "the power of any spring is in the same proportion with the tension therefore".[114] Materials that have properties somewhere in between these two extremes, such as glues, shampoos, gels, pastes and rubbers, are described as viscoelastic because they exhibit both viscous and elastic behaviours (Figure 1.8).[114,116] Polymers are also classified as viscoelastic materials; their behaviour is determined by experimental conditions including temperature, the frequency and amplitude of stress and the shear rate. For example, at high temperature and low frequency, polymers reside in a rubbery state, while at low temperature and high frequency they are in a glassy state; and, at very high temperatures, they become viscous liquids.[117]




Figure 1.8. Rheology road shows the classification of material behaviours from ideally viscous liquids through to ideally elastic solids with common examples.[116]

Viscosity ($\eta$) is the internal friction between molecules of a flowing material and is a measure of a material's resistance to flow.[114] The earliest use of viscosity dates back to ancient Egypt and the invention of a water clock for the measurement of time. This device comprised of a vessel filled with water and equipped with an outlet. The water would be allowed to flow from the vessel and by controlling the initial volume of water and the outlet size could be used as a rudimentary timer.[118] For example, 5 litres of water has a flow time of about 6 minutes, depending on the outlet size. This device forms the basis for gravimetric and capillary viscometers where the flow time of a known amount of an ideally viscous liquid is used to determine the kinematic (weight dependent) viscosity.[119,120] It is expected that flow time will increase with increased viscosity. The capillary or flow cup must have precisely defined dimensions and a precise distance that the sample travels. In order to calculate $\eta$ the instruments are calibrated with a known sample, such as water. These systems are simple to use because they rely on gravity as the driving force and so do not require technical equipment or maintenance. However, it is not possible to alter gravity and therefore these instruments are unsuitable for high viscosity and non-Newtonian samples.[119] In addition, each capillary is only capable of determining a narrow range of viscosities because a different size capillary is needed for different viscosities. It is possible to measure high viscosity materials by applying pressure to force the sample through the capillary. This is particularly useful for polymer melts to predict their behaviour

during processing. It also allows for a range of shear stresses and shear rates to be accessed, depending on the instrument used.[119]

Falling ball viscometers expand on these principles and measure the falling time of a ball bearing to travel a defined distance through a sample fluid. Again, precise dimensions are needed, not just of the capillary but also of the ball bearing including its density.[121] By adjusting the angle of the instrument, is it possible to control the driving force, too steep an angle will result in turbulent flow while too shallow an angle will result in too long travel times. The product of the rolling time, the difference in density of the ball and the sample, and a constant, *K*, gives the dynamic viscosity of the sample. However, they are limited to transparent, low viscosity liquids and shear dependent viscosity is difficult to elucidate because the fluid viscosity and the density of the falling object determine the shear rate.[119]

Rotational rheometers are motor driven and so can measure a wide range of viscosities.[119] These instruments consist of a cup which holds the sample and a bob which is submerged in the sample. The measurement can be performed via two different principles: the Couette principle where the driving force is applied to the cup[122] or the Searle principle where the driving force is applied to the bob. In both cases, the $\eta$ is related to the torque of the motor and so the dynamic $\eta$ is determined i.e. the viscosity of the material as a function of stress. The drive is set to a defined speed and the motor torque required to overcome the viscous forces is a measure of the sample $\eta$. The Couette principle reduces the probability of turbulent flow but the drive shaft must be leak-tight against any liquids used for temperature control. Therefore, there are only a few instruments on the market.[123] In 1912, George Frederick Charles Searle designed a rotational viscometer with a concentric cylinder geometry and to this day, most commercial rheometers employ this principle.[119] There are many different designs of bob that can be used depending on the application, allowing the measurement of $\eta$ from 1-4,000,000 mPa.s. These designs include commonly used cylindrical bobs, disc spindles and some speciality geometries such as a t-bar or a vane (Figure 1.9). Some of the geometries do not have specific approved dimensions and therefore can only be used to determine the relative $\eta$. Concentric cylinders, double gap cylinders, cone plate and parallel plate

geometries are all precisely defined, approved geometries for measuring the absolute $\eta$.[119]




Figure 1.9. Examples of typical geometries used in rotational rheology.[119]

### 1.6.1 Rheology of Polymers

As hinted previously, rheology is a vital tool in many industries for predicting material behaviours during and post processing. For example, in the food industry, the viscosity of oils can be used to determine the long-term storage stability of dressings. The viscosity of paint is important because if the viscosity is too low the paint will drip but if it is too high, it will not level correctly and brush strokes will be left behind. Information about the melt viscosity of polymers is vital to determine appropriate processing conditions and to predict the properties of the final product. Generally, a high viscosity material yields stronger mechanical properties but will require higher processing pressures and temperatures and more robust equipment to withstand such conditions, making it more difficult to process. On the other hand, a polymer with a lower melt viscosity will be more easily processed with weaker mechanical properties in the final product.[124] Polymer melts have extremely high viscosities that can be measured using rotational rheometers or inferred using a capillary extruder

similar to that described in Chapter 3. By selecting the appropriate equipment it is possible to measure the viscoelastic properties of polymers under conditions similar to those used during processing. For example, a rotational rheometer can measure in a shear range from $10^{-3}$-$10^{3}$ $s^{-1}$, which is equivalent to processes from sagging and levelling that occur at very low shear, up to extrusion, which employs very high shear. To access even higher shear rates, such as those experienced during spraying, researchers use capillary rheometers, which typically measure from $10^{-1}$-$10^{6}$ $s^{-1}$. Polymers are non-Newtonian, shear thinning materials that have a non-linear relationship where $\eta$ decreases with increasing shear rate.[113,125] At low shear rates the polymer chains have enough time between deformations to relax and return to their original structure. At these low shear rates the polymer behaves like a Newtonian material where its viscoelastic properties are independent of shear, this region of Newtonian behaviour is described as the linear viscoelastic (LVE) region. As shear rate is increased this time decreases until the chains become permanently aligned in the direction of deformation, and shear thinning behaviour is observed. The viscoelastic response of a polymer is defined by the complex shear modulus (*G**), which is a measurement of material stiffness. *G** is a combination of elastic contributions from the storage modulus (G') and viscous contributions from the loss modulus (*G''*). By performing small deformations within the LVE region while increasing the temperature it is possible to determine the thermal transitions of the materials by monitoring the viscoelastic response of *G'* and *G''* (more detail provided in Chapter 2). Increasing temperature will also result in a decrease in $\eta$, making rheology a useful tool for determining appropriate polymer processing temperatures.[70] Polymers also exhibit a yield point where applied external forces exceed the network forces of the internal structure, causing the material to flow or break. Determination of the yield stress is important for application testing of polymers, as the manufacturer needs to know that the materials are fit for purpose. It is therefore unsurprising that the field of polymer rheology has been established for as long as polymers have been made. Thus, as new developments in polymer processing technologies emerge, such as those that use $CO_2$, the area of polymer rheology must adapt.

### 1.6.2 High Pressure Rheology

The use of $CO_2$ as an aid for polymer processing has long been established and extensively reported on, especially for use in the pharmaceutical industry, as described in Section 1.5.1.[126] Hence it follows that the viscosity of polymers in the presence of $CO_2$ has been reported for years, in fact there is a plethora of literature available on the use of high pressure rheology.[127–132] The earliest reports date back to the mid-1990s where researchers investigated the effect of $CO_2$ on the viscosity of poly(dimethyl siloxane) (PDMS).[133,134] There are four main types of high pressure rheometer; pressure driven capillary, falling body, vibrating wire and rotational (described in more detail in Chapter 3).[135] All the literature confirms that the use of $CO_2$ can effectively reduce the $\eta$ of a number of polymers.[128,130,131,136–139] Literature published by the Howdle group has attempted to correlate changes in $\eta$ with the properties of the particles produced after processing via a modified PGSS technique.[112,140] The aim of this thesis is to correlate the viscosity of a drug loaded polymer formulation with its release profile. Hence, it is necessary to understand the effect of APIs on the viscosity of the polymer melt.

### 1.6.3 Effect of APIs on Polymer Melt Viscosity

Several reports have been published on the effect of drug molecules on the polymer melt viscosity.[59,141–146] It is desirable to keep the number of excipients in a pharmaceutical formulation to a minimum, in order to reduce the chances of unwanted side effects upon administration. Therefore, the ratio of API to polymer matrix is generally high and the flow behaviours of the formulation will be influenced by API particle size, shape and interactions.[147] How the API will effect $\eta$ is also dependent on its miscibility and solubility in the polymer matrix.[59] Investigators can predict whether the API and polymer will be miscible based on the difference between their solubility parameters. Hildebrand solubility parameters can be calculated from the cohesive energy density, where the cohesive energy is the energy required to separate the atoms or molecules in a substance such that they no longer possess any potential energy. If two substances have similar cohesive energy then they are likely to be miscible and soluble in one another because they require

the same amount of energy to break any intermolecular interactions.[148] Greenhalgh et al. categorised a variety of drug/carrier systems based on their visible miscibility and their solubility parameters.[148] They found that in most cases there was a strong correlation between the difference in solubility parameter and miscibility. Systems with similar solubility parameters, i.e. a solubility parameter difference below 7 $MPa^{0.5}$ were more likely to be miscible than those with a solubility parameter difference above 10 $MPa^{0.5}$.[148] However, there were also many cases where systems with a small solubility parameter difference were immiscible. This could be attributed to inaccuracies in the solubility parameters, especially in the case of polymer carriers, and by considering that solubility is also dependent on factors such as polydispersity, molecular weight, solute-solvent interactions and temperature.[145,148]

The miscibility and solubility of an API in a carrier material can be confirmed by DSC and rheology. For example, small molecule APIs are likely to be miscible and act as plasticisers for the polymer matrix, reducing the $T_g$ and $\eta$. On the other hand, $\eta$ will increase in the presence of an immiscible or insoluble API because it will behave like a filler.[142,143,145,146,149] Chomcharn and Xanthos showed that aspirin exhibited some miscibility with Eudragit® and acted as a plasticiser by reducing the $T_g$ and $\eta$. A plot of the relative viscosity ($\eta/\eta_0$) where $\eta$ is the viscosity of mixture and $\eta_0$ is the viscosity of the polymer matrix versus aspirin content revealed that above 20 wt.% aspirin the miscibility begins to decrease.[145] Chokshi et al. investigated the effect of indomethacin (INM) on the thermal and rheological properties of a selection of polymers based on comparable solubility parameters.[143] They found that, despite having comparable solubility parameters, one of the polymers was only partially miscible while the others exhibited total miscibility. The miscible mixtures exhibited a single $T_g$ while two melting transitions were observed for the partially miscible mixture. In accordance with other reports, the miscible mixtures showed reduced viscosity in comparison with the pure polymer.[62,144,146] For the partially miscible mixture the opposite was true, and increased drug loading resulted in increased viscosity.[143] Given the temperature of the experiment this is unsurprising as the drug would be a solid particle in a molten matrix and would therefore behave as a filler.[149]

Suwardie et al. performed an extensive rheological study on the solubility of acetaminophen (APAP) in poly(ethylene oxide) (PEO). They showed that several different rheology measurements can produce comparable solubility data. Generally, the plots of viscosity versus drug loading were parabolic, with the solubility of APAP in PEO being determined as the minima of the curve. Although the viscosity data at high shear rates are more representative of those expected during processing, the effect of drug loading becomes less pronounced due to the shear thinning behaviour of the material. Therefore, solubility seems to have some dependence on shear rate and it is suggested that solubility data should be collected at low shear rates.[146]

A handful of studies have attempted to relate rheological properties to therapeutic release, see Chapter 5 for more detail.[150–153] However, in most cases the release was dependent on product properties such as the degradation rate, internal structure, and presence of additives or other stabilising components. There was also a strong dependence on the processing method that was not directly linked to the rheological properties. In the current work, the formulations were produced via a modified PGSS method. The components were exposed to high pressure $CO_2$ and moderate temperature (140 bar $CO_2$, 40 °C), mixed at constant shear to ensure incorporation of API within the polymer matrix and collected as a solid powder upon removal of the $CO_2$. It was therefore expected that the formulation would be akin to an amorphous solid dispersion and the presence of the API would increase the viscosity of the polymer melt.

However, the majority of the cited investigations are performed at ambient pressure because the authors seek to use the data as a tool for process optimization. Although there have been a several reports acknowledging the ability of $CO_2$ to reduce the viscosity of polymer-drug mixtures, the processing temperatures are still incredibly high (110-190 °C) and there is no mention of high pressure rheological characterisation.[154–156]

Hence, the aim of this thesis is to develop a method to measure the effect of a model protein API on the viscosity of a polymer melt, in the presence of high pressure $CO_2$ and relate this to the release of the API.

## 1.7 Aims and Objectives

This chapter has provided an overview of the growing use of biodegradable polymers in pharmaceutical applications and the development of greener polymer processing techniques using $CO_2$. The most significant factor governing the success of these new techniques is the viscosity of the mixtures to be processed. Therefore, rheology is a vital tool for the development of new drug delivery technologies. In order for $CO_2$ to become a truly viable aid for polymer processing, its effect on the viscosity must be quantified.

Therefore, this thesis aims to establish a robust and reliable method for the analysis of the viscosity of complex pharmaceutical formulations. Specifically, this method will be used to assess the viscosity during processing in the presence of dense phase $CO_2$. This work then looks to explore whether there is a correlation between the rheological data and the release profiles of a formulation. Present legislation states that all potential drug delivery systems have to be subjected to *in vitro* release studies.[157] In the case of sustained release formulations this means long term, large scale, costly investigations, sometimes only to find that the formulations are not suitable. Therefore, if rheological properties could be related to release profiles; then rheology could be used as a probe for formulation development, thereby reducing the number of *in vitro* release studies that need to be performed. The hypothesis being that if a formulation can be readily processed to produce a homogeneous, well dispersed system then its release should be reproducible and comparable on a batch to batch basis.[146] The homogeneity and processability of a formulation could be assessed by rheology.

In order to achieve this the work has been split into three distinct areas:

Chapter 3 describes the development of a high pressure rheology method suitable for the analysis of polymer formulations containing thermosensitive APIs. Initially a method will be developed for the analysis of polymers above their $T_g$ in the presence and absence of $CO_2$. Following this, a method for the measurement of the polymer viscosity below the ambient pressure $T_g$ will be developed.

As polymer melt viscosities are notoriously high, it has been reported that the use of $CO_2$ alone is not enough to sufficiently reduce the viscosity to enable homogeneous mixing.[111] Also, the stability of the drug during processing and storage and controlled released is paramount for the success of a formulation. Therefore, many formulations contain excipients that can act as plasticisers, stabilising agents or release enhancing moieties. Hence, Chapter 4 investigates the effect of a polymer plasticiser on the melt viscosity of the original polymer. This work aims to determine whether the plasticiser has any added benefits to the use of $CO_2$ and confirm that the methods developed in Chapter 3 are suitable for the measurement of more complex systems.

The work presented in Chapter 5 describes the rheological properties of a series of formulations produced via a $CO_2$ mixing procedure similar to the PGSS technique. This data was then compared to the results of a content assay to assess the success of mixing and homogeneity of the formulations. Finally, a month long *in vitro* release study was performed using tablets of the formulations, and the release profiles compared to the viscosity data measured using rheology.

# Chapter 2

## General Experimental Details

## 2.1 Overview

This Chapter provides a general overview of the methods used in this thesis. Details of the naming system used to distinguish the polymers, blends and formulations used throughout this thesis are also provided. In addition, the high pressure equipment used is described in detail along with the general operating procedures. Specific experimental details are provided in the individual results chapters.

# 2.2 Contents

Chapter 2 ..... 2-31

2.1 Overview ..... 2-32

2.2 Contents ..... 2-33

2.3 Sample Naming System ..... 2-34

2.3.1 Purchased Polymers Naming System ..... 2-34

2.3.2 Synthesised Polymers Naming System ..... 2-34

2.3.3 Polymer Blends Naming System ..... 2-35

2.3.4 Formulation Naming System ..... 2-37

2.4 Rheology ..... 2-38

2.4.1 Oscillatory Measurement Mode ..... 2-38

2.4.2 Rotational Measurement Mode ..... 2-41

2.5 High Pressure Equipment ..... 2-45

2.5.1 High Pressure Rheometer ..... 2-47

2.5.2 View Cell ..... 2-51

2.5.3 MKIII Clamp Sealed Autoclave ..... 2-53

2.6 Characterisation Methods ..... 2-55

2.6.1 Differential Scanning Calorimetry ..... 2-55

2.6.2 Gel Permeation Chromatography ..... 2-55

2.6.3 $^{1}$H Nuclear Magnetic Resonance Spectroscopy ..... 2-56

2.6.4 SEM ..... 2-56

2.6.5 Micro Raman Spectroscopy ..... 2-56

## 2.3 Sample Naming System

Throughout this thesis a series of polymers have been purchased and synthesised for use in polymer blend and formulation samples. For ease of reference a naming system for the polymers, blends and formulations was developed and is detailed here.

### 2.3.1 Purchased Polymers Naming System

For the purchased polymers, sample names consisted of the polymer acronym followed by its weight average molecular weight ($M_w$, x$10^3$ g/mol) determined by gel permeation chromatography (GPC) or quoted from the supplier (Table 2.1).

Table 2.1. Details of the naming system for the purchased polymers used throughout this thesis.

| ID | Polymer | $M_w$ (g/mol) | Chapter |
|---|---|---|---|
| $PCL_{112}$ | Polycaprolactone | 112,000 | 3 |
| $PLA_{11}$ | Poly($_{D,L}$-lactide) | 11,000 | 3,4 |
| $PLA_{12}$ | Poly($_{D,L}$-lactide) | 12,000 | 3,5 |
| $PLGA_{36}$ | Poly($_{D,L}$-lactide-*co*-glycolide) | 36,000 | 3,5 |
| $PEG_5$ | Poly(ethylene glycol) | 5000 | 4 |
| $PEG_{10}$ | Poly(ethylene glycol) | 10,000* | 4 |
| $PEG_{0.4}$ | Poly(ethylene glycol) | 400* ($M_n$) | 5 |
| $PEG_6$ | Poly(ethylene glycol) | 6000* ($M_n$) | 5 |
| $PCL_{14}$ | Polycaprolactone | 14,000* | 5 |

*Nominal molecular weight provided by the supplier.

### 2.3.2 Synthesised Polymers Naming System

The homopolymers and block copolymers synthesised for use in Chapter 4 were produced by ring opening polymerisation (ROP) of $_{D,L}$-lactide. The initiator to monomer ratio was chosen to yield polymers with targeted number average

molecular weights ($M_n$). Therefore, the ID's of the polymers consist of the acronym followed by the targeted $M_n$ (x$10^3$ g/mol) (Table 2.2).

Table 2.2. Details of the naming system for the synthesised polymers used in Chapter 4.

| ID | Polymer | PEG $M_w$ (g/mol) | Targeted $P_{D,L}LA$ $M_n$ (g/mol) |
|---|---|---|---|
| $PLA_5$ | Poly($_{D,L}$-lactide) | - | 5040 |
| $PEG_5$-*b*-$PLA_5$ | Poly(ethylene glycol)-*block*-Poly($_{D,L}$-lactide) | 5000 | 5040 |
| $PEG_5$-*b*-$PLA_{10}$ | Poly(ethylene glycol)-*block*-Poly($_{D,L}$-lactide) | 5000 | 10,080 |

### 2.3.3 Polymer Blends Naming System

A series of polymer blends were produced for use in Chapters 4 and 5 of this thesis. In order to describe the blends succinctly, the naming system includes the acronym of the polymers, followed by their $M_w$ (x$10^3$ g/mol) in subscript, followed by the polymer content in the blend (wt.%). For example a blend containing 50 wt.% $PLA_{11}$ and 50 wt.% $PEG_5$ would be denoted as $PLA_{11}$50:$PEG_5$50 (Table 2.3).

Table 2.3. Details of the naming system for the polymer blends produced for use in Chapters 4 and 5.

| Chapter 4 | | | | |
|---|---|---|---|---|
| **ID** | **Polymer 1** | **wt.%** | **Polymer 2** | **wt.%** |
| $PLA_{11}100$ | Poly($_{D,L}$-lactide) | 100 | - | - |
| $PEG_5$5:$PLA_{11}$95 | Poly(ethylene glycol) | 5 | Poly($_{D,L}$-lactide) | 95 |
| $PEG_5$10:$PLA_{11}$90 | Poly(ethylene glycol) | 10 | Poly($_{D,L}$-lactide) | 90 |
| $PEG_5$33:$PLA_{11}$67 | Poly(ethylene glycol) | 33 | Poly($_{D,L}$-lactide) | 67 |
| $PEG_5$50:$PLA_{11}$50 | Poly(ethylene glycol) | 50 | Poly($_{D,L}$-lactide) | 50 |
| $PEG_5100$ | Poly(ethylene glycol) | 100 | - | - |
| $PEG_{10}100$ | Poly(ethylene glycol) | 100 | - | - |
| $PEG_{10}$50:$PLA_{11}$50 | Poly(ethylene glycol) | 50 | Poly($_{D,L}$-lactide) | 50 |
| $PLA_5100$ | Poly($_{D,L}$-lactide) | 100 | - | - |
| $PLA_5$10:$PLA_{11}$90 | Poly($_{D,L}$-lactide) | 10 | Poly($_{D,L}$-lactide) | 90 |
| **Chapter 5** | | | | |
| **ID** | **Polymer 1** | **wt.%** | **Polymer 2** | **wt.%** |
| $PLGA_{36}$18.75:$PEG_{0.4}$81.25 | Poly($_{D,L}$-lactide-*co*-glycolide) | 18.75 | Poly(ethylene glycol) | 81.25 |
| $PLGA_{36}$18.75:$PEG_6$81.25 | Poly($_{D,L}$-lactide-*co*-glycolide) | 18.75 | Poly(ethylene glycol) | 81.25 |
| $PLGA_{36}$18.75:$PCL_{14}$81.25 | Poly($_{D,L}$-lactide-*co*-glycolide) | 18.75 | Polycaprolactone | 81.25 |
| $PLGA_{36}$18.75:$PLA_{12}$81.25 | Poly($_{D,L}$-lactide-*co*-glycolide) | 18.75 | Poly($_{D,L}$-lactide) | 81.25 |

### 2.3.4 Formulation Naming System

For Chapter 5 a series of formulations were produced containing a model active pharmaceutical ingredient (API), bovine serum albumin (BSA), encapsulated in a polymer matrix. These formulations contained two different particle sizes of BSA produced by two different grinding methods. The first method consisted of manually grinding the BSA using a pestle and mortar and subsequently sieving the particles to yield an approximate particle diameter of 200 µm. The second utilised a jet milling process to produce much smaller BSA particles with an approximate diameter of 5 µm. BSA particles produced using the first method are hereon in referred to as BSAg, while those produced using the jet milling method are referred to as BSAm. The polymer matrix used for the formulations consisted of a blend of $PLGA_{36}$ and $PLA_{12}$, and two different ratios of polymer were used. Two different BSA loadings were also used in the formulations. Therefore, the naming system developed for the formulations included the $PLGA_{36}$ content, the size of the BSA particles used and the BSA content. For example a formulation containing 30 wt.% $PLGA_{36}$, 50 wt.% $PLA_{12}$ and 20 wt.% of BSA with the smaller particle size was denoted as $PLGA_{36}$30:BSAm20 (Table 2.4).

Table 2.4. Details of the naming system developed for the formulations containing BSA encased in a polymer matrix.

| ID* | Approx. BSA particle size (µm) | BSA content (wt.%) | $PLGA_{36}$ content (wt.%) | $PLA_{12}$ content (wt.%) |
|---|---|---|---|---|
| $PLGA_{36}$11.25:BSAg40 | 200 | 40 | 11.25 | 48.75 |
| $PLGA_{36}$11.25:BSAm40 | 5 | | | |
| $PLGA_{36}$15:BSAg20 | 200 | 20 | 15 | 65 |
| $PLGA_{36}$15:BSAm20 | 5 | | | |
| $PLGA_{36}$30:BSAm20 | 5 | 20 | 30 | 50 |

## 2.4 Rheology

Rheology is the study of deformation and flow of materials under an applied stress.[113] There are two modes of measurement used to describe different rheological behaviours exhibited by materials. Dynamic oscillatory measurements are used to define viscoelastic behaviour while transient rotational measurements provide information about the sample shear viscosity. In this work, a parallel plate geometry was employed for all measurements.

### 2.4.1 Oscillatory Measurement Mode

By oscillating the upper plate back and forth, a shear strain ($\gamma$) is applied to the sample. The resultant stress ($\tau$) of the sample is quantified by measuring the torque and is related to the viscoelastic behaviour of the sample.[158] The amplitude of the displacement of the upper plate is defined by the deflection angle ($\phi$); tan($\phi$) is equal to the strain ($\gamma$, %) a dimensionless quantity (Figure 2.1).

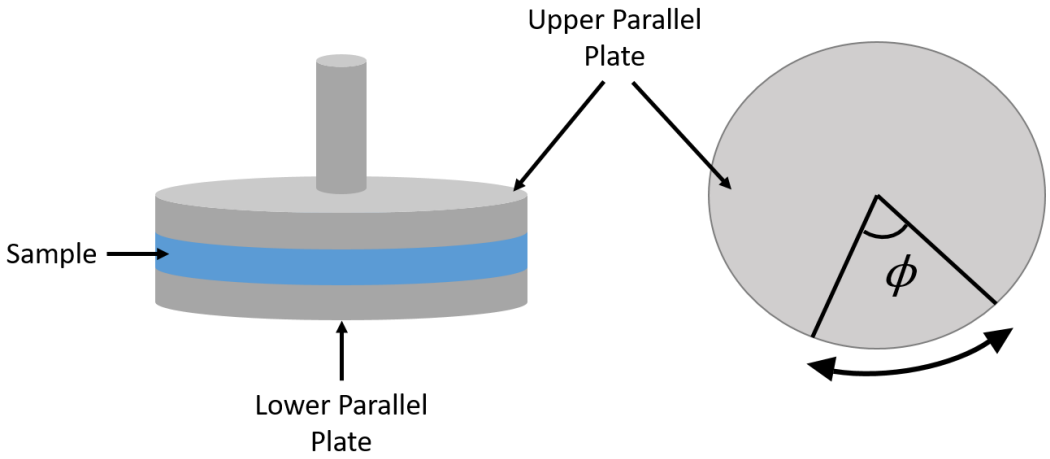



Figure 2.1. Diagram demonstrating the oscillatory motion of the upper plate, where $\phi$ is the deflection angle.

Wave forms of the shear stress ($\sigma$) and shear strain ($\gamma$) can be described by Equations 2.1a and b, respectively.

$$\text{a) } \sigma = \sigma_0 \cos(\omega t) \qquad \text{b) } \gamma = \gamma_0 \cos(\omega t - \delta) \qquad 2.1$$

Where $\sigma_0$ and $\gamma_0$ are the shear stress and shear strain amplitudes, respectively, $\omega$ is the angular frequency (i.e. the speed of the oscillation) and $t$ is the time. The phase shift ($\delta$) defines a lag between the $\sigma$ and $\gamma$ caused by viscosity (Figure 2.2).[159]

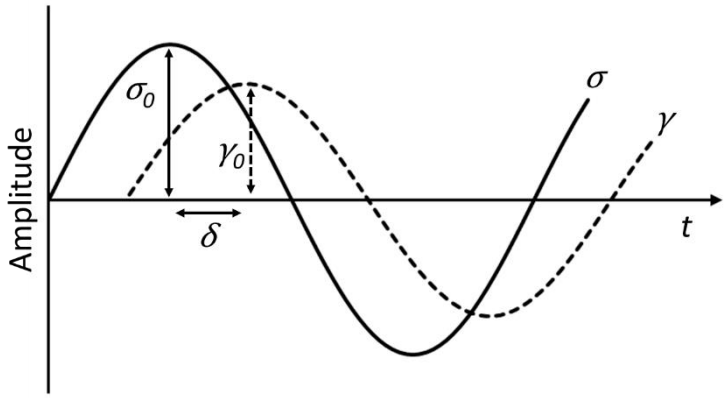



Figure 2.2. The wave forms of shear stress ($\sigma$) and shear strain ($\gamma$) have a phase shift ($\delta$) caused by the viscosity. The stress and strain amplitudes ($\sigma_0$ and $\gamma_0$, respectively) are also shown.[159]

Ideal solids are purely elastic with no viscosity and as such the stress and strain responses are in phase, i.e. $\delta$ = 0°. Conversely, Newtonian fluids give a purely viscous response, where the stress and strain are out of phase, i.e. $\delta$ = 90°.[158] Viscoelastic materials such as polymers are somewhere in between, with in-phase and out-of-phase contributions i.e. 0° < $\delta$ < 90°. The in-phase contributions are characterised by the storage modulus (*G'*), which accounts for stored energy associated with the elastic behaviour, defined by Equation 2.2a. A parameter called the loss modulus (*G''*) accounts for lost energy and deformation associated with the viscous behaviour and defines the out-of-phase behaviour (Equation 2.2b).[159]

$$\text{a) } G' = \frac{\sigma_0}{\gamma_0}\cos(\delta) \qquad \text{b) } G'' = \frac{\sigma_0}{\gamma_0}\sin(\delta) \tag{2.2}$$

The viscoelastic behaviour is defined by a single complex modulus (*G**) which is a combination of the elastic (*G'*) and viscous (*G''*) contributions as shown in Equation 2.3a. The balance between the stored and lost energy is quantified by tan($\delta$), which is the ratio of the storage and loss moduli, Equation 2.3b.[159]

$$\text{a) } G^* = G' + jG'' \text{ where } j = \sqrt{-1} \qquad \text{b) } \tan(\delta) = \frac{G''}{G'} \tag{2.3}$$

These parameters provide important information about the physical properties of the material. For example, when $G' > G''$ the material is in a solid-like state and when $G'' > G'$ the material is more fluid-like. Viscoelastic materials often exhibit a Linear Viscoelastic (LVE) region, where the $G'$ and tan($\delta$) responses are independent of deformation. In this region, the amplitude and frequency of deformation is so small that the materials' behaviour is stable. At higher amplitudes and frequencies the internal structure begins to break down and the material begins to flow, as demonstrated by a decrease in $G'$ accompanied by an increase in tan($\delta$) (Figure 2.3). The LVE region can be determined by performing strain sweeps at constant frequency and frequency sweeps at constant strain.

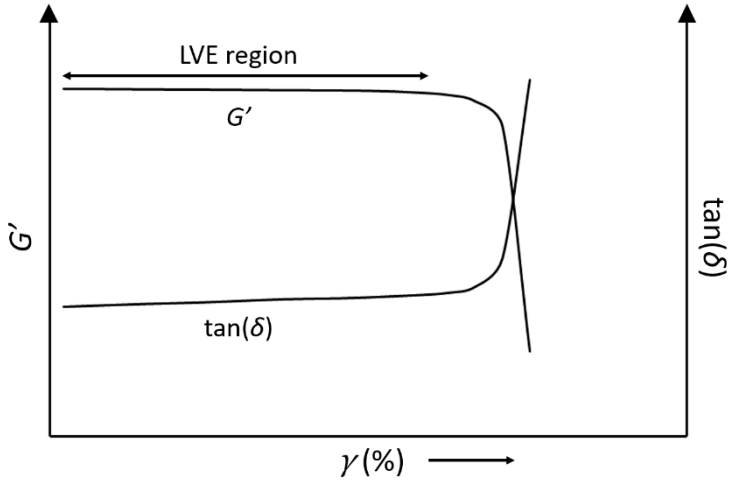



Figure 2.3. A plot of $G'$ and tan($\delta$) against shear strain ($\gamma$) shows a plateau at low strain, which defines the linear viscoelastic (LVE) region. As strain is increased the sample begins to flow resulting in a sharp decline in G' accompanied by an incline in tan($\delta$).

Information about the effect of temperature on the material properties can be obtained by performing temperature sweeps at constant strain and frequency within this LVE region. As the temperature is increased, more energy is delivered to the molecules resulting in increased chain mobility and a transition from a solid state to a fluid like state. Again, this is demonstrated by a decrease in G' and an increase in tan($\delta$) (Figure 2.4).[125]

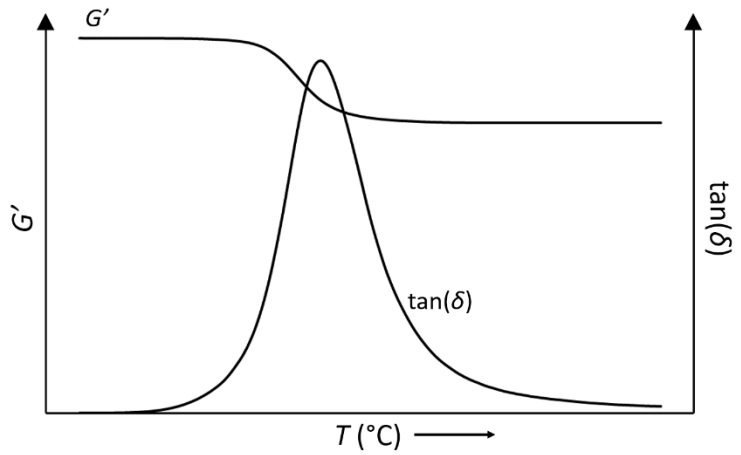



Figure 2.4. Typical plot of *G′* and tan(*δ*) vs temperature.

These measurements were used in Chapter 3 of this thesis to determine the minimum temperature at which the ambient pressure rotational measurements could be performed.

### 2.4.2 Rotational Measurement Mode

Viscosity is caused by frictional forces between molecules which results in resistance to flow. By applying a controlled force to a sample and measuring the torque required to maintain that force, the viscosity can be determined. In this thesis, all measurements were performed using a parallel plate geometry with a fixed gap of 1 mm, which was filled with sample. In this measurement system, the lower plate remained stationary while a certain amount of force was applied to rotate the upper plate. A simple two plate model can be used to describe the rheological parameters and demonstrate how viscosity is determined (Figure 2.5).[160]

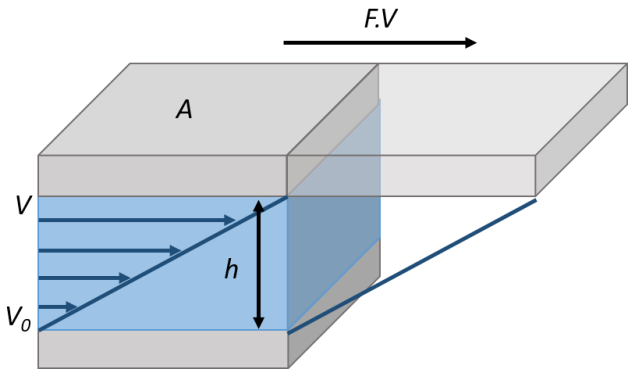



Figure 2.5. Simple two plate model to describe the rheological parameters: shear stress and shear rate. The upper plate has an area (*A*) which is moved by a force (*F*) at a velocity (*V*), while the lower plate remains stationary (*V*=0). The two plates are separated by a defined gap (*h*), which is filled with sample.[160]

The force applied per unit area to move the top plate is called the shear stress, $\tau$, while the speed of the rotation is the shear rate, $\dot{\gamma}$, as defined by equations 2.4a and b, respectively. Viscosity, $\eta$, is given by the ratio of the shear stress and the shear rate at a specific shear rate, as shown in equation 2.4c.[160,161]

$$\text{a) } \tau = \frac{F}{A} \qquad \text{b) } \dot{\gamma} = \frac{V}{h} \qquad \text{c) } \eta = \frac{\tau}{\dot{\gamma}} \tag{2.4}$$

During a typical rotational measurement, the shear rate is increased and the shear stress is measured at each shear rate. Plotting shear stress against shear rate allows the viscosity to be calculated from the gradient of the slope. Three different material behaviours can be identified depending on the shape of the curve (Figure 2.6).[161–163] Newtonian fluids exhibit a linear relationship between the shear stress and shear rate, resulting in constant viscosity over the shear rate range.[164] A material that exhibits a non-linear relationship between the shear stress and shear rate is classed as a non-Newtonian material. There are two different types of non-Newtonian systems: shear thickening, where viscosity increases with increasing shear rate and shear thinning, where viscosity decreases with increasing shear rate.[113] Examples of shear thickening materials are rare but include corn starch solutions in water.

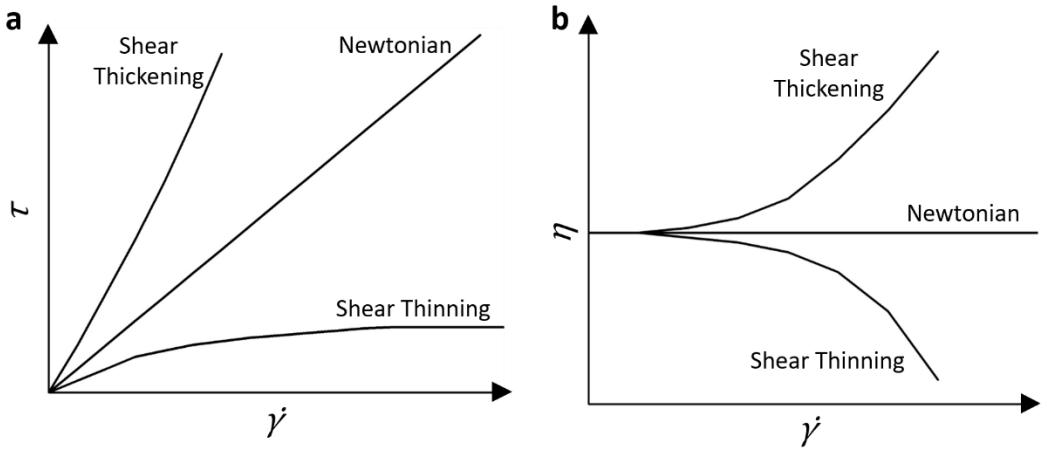



Figure 2.6. Plots showing the different relationships between (a) shear rate ($\dot{\gamma}$) and shear stress ($\tau$) and (b) shear rate ($\dot{\gamma}$) and viscosity ($\eta$) for different fluid behaviours. Newtonian fluids show a linear relationship between shear stress and shear rate resulting in constant viscosity as shear rate is varied. Non-Newtonian fluids show non-linear behaviours.[5]

Polymers are complex materials that exhibit Newtonian behaviour at low shear rates followed by a region of shear thinning as the shear rate is increased (Figure 2.7). The Newtonian region is observed at sufficiently low shear rates where the sample viscosity is independent of shear rate, defined as the zero shear viscosity ($\eta_0$). As shear rate is increased, the polymer chains disentangle and align in the direction of shear, resulting in a decrease in viscosity. The shear rate at which the viscosity begins to decrease is called the critical shear rate ($\dot{\gamma}_{cr}$). As shear rate continues to be increased the polymer chains can completely align such that the viscosity no longer drops and a second viscosity plateau, called the infinite shear viscosity ($\eta_\infty$) is achieved. In this work, it was not possible to observe the $\eta_\infty$ because the high shear rates required were beyond the limits of the instrument ($\dot{\gamma} > 3000\ s^{-1}$).[125]

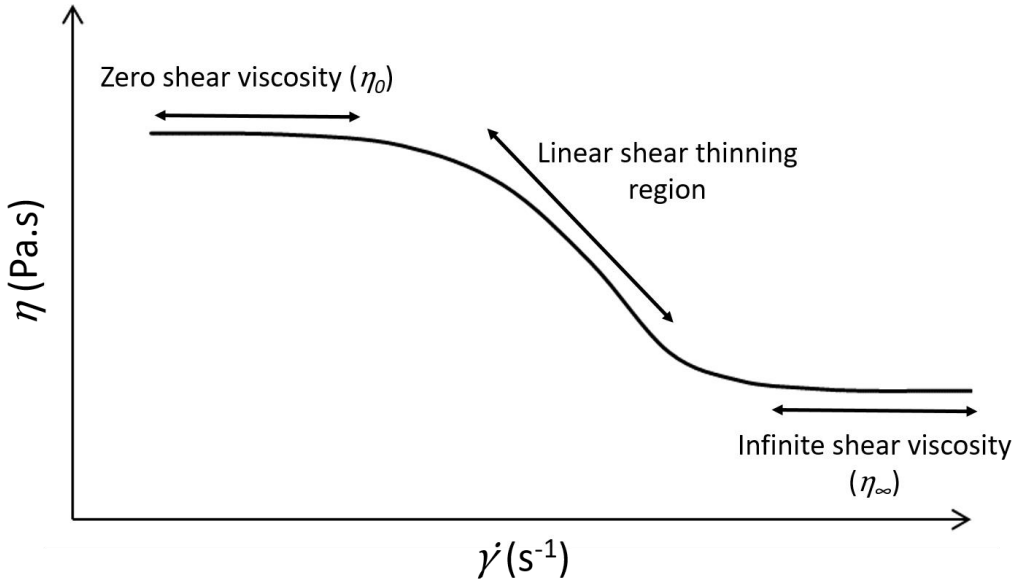



Figure 2.7. A typical plot of viscosity ($\eta$, Pa.s) vs shear rate ($\dot{\gamma}$, s$^{-1}$) of a polymer melt demonstrating the zero shear viscosity plateau ($\eta_0$), the linear shear thinning region and the infinite shear viscosity plateau ($\eta_\infty$).[125]

Two models are commonly used to describe this relationship, the Cross model[165] and the Carreau model;[166] despite being developed almost half a century ago they are still used today. The Cross model is shown in equation 2.5, where *C* is the Cross constant and *p* is the Cross exponent.

$$\eta(\dot{\gamma}) = \eta_\infty + \frac{\eta_0 - \eta_\infty}{1 + (C\dot{\gamma})^p} \qquad 2.5$$

For the purpose of this work, all the experimental data were fitted to the Carreau model given in equation 2.6, to give calculated values for the zero shear viscosity ($\eta_0$, Pa.s).

$$\eta(\dot{\gamma}) = \eta_0[1 + (\dot{\gamma}\lambda)^2]^{-c} \qquad 2.6$$

Where $\eta(\dot{\gamma})$ is the viscosity (Pa.s) at the specific shear rate ($\dot{\gamma}$, s$^{-1}$). $\lambda$ (s) is the relaxation time and describes the mobility of the polymer chains. *c* is the Carreau constant related to the power law and is derived from the gradient of the shear thinning region (Figure 2.8).[130, 131]

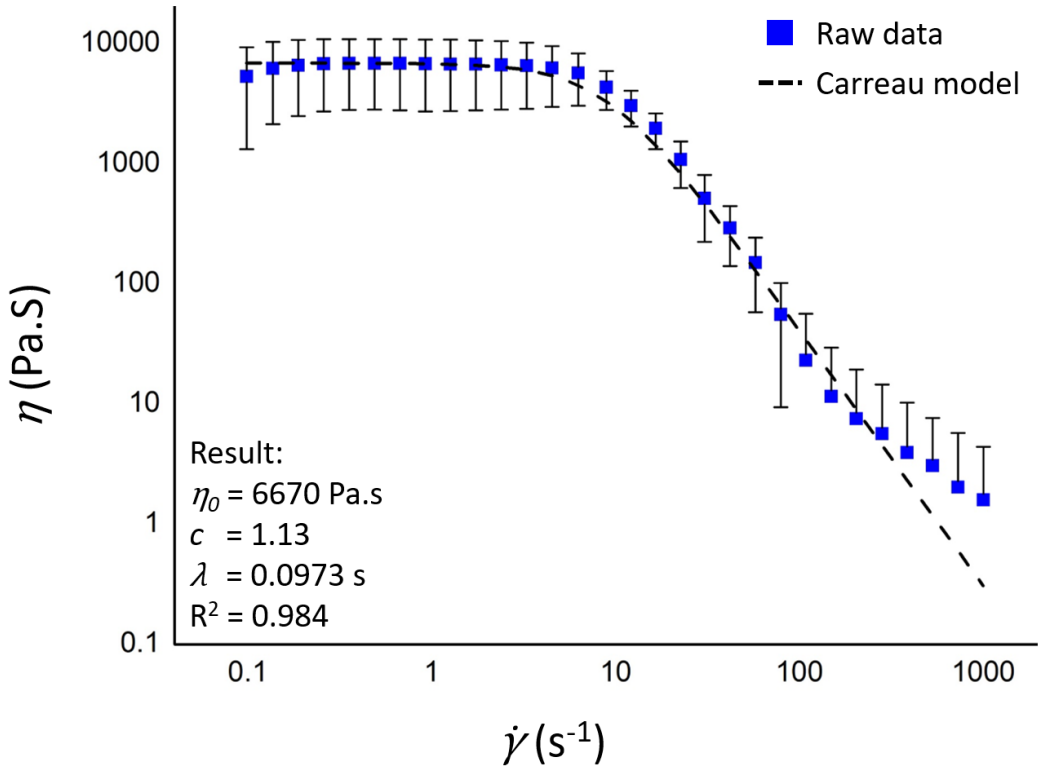



Figure 2.8. The raw data given by the viscosity measurement (blue squares) was fitted to the Carreau model (black dashed line) to give quantitative values for the zero shear viscosity, $\eta_0$ (Pa.s) and relaxation time, $\lambda$ (s). Data is from a representative sample of $PLA_{11}$ measured at ambient pressure. Error bars represent ±1 standard deviation from the mean. $T$ = 80 °C.

## 2.5 High Pressure Equipment

The high pressure equipment used consisted of a Pickel pump to deliver the $CO_2$ connected to the high pressure stainless steel vessel via high pressure Swagelok® tubing and fittings (Figure 2.9). The temperature and pressure of the system was monitored continuously via K-type thermocouples and piezoelectric pressure transducers that fed back to a digital output.

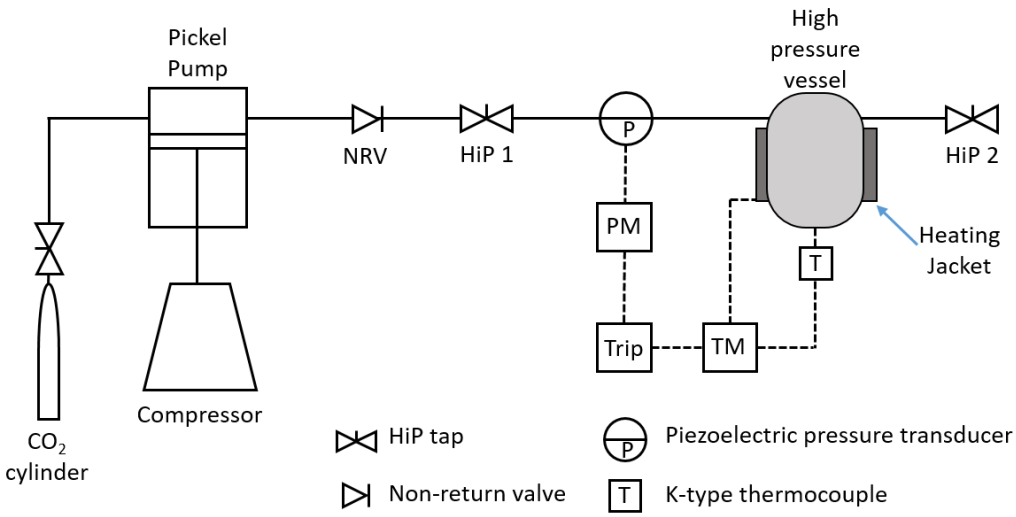



Figure 2.9. Rig diagram for a typical high pressure set up. Including the pressure monitor (PM), the trip and the temperature monitor (TM).

The PM-101 SFE Pickel pump (New Ways of Analytics, Germany) was used to condense the $CO_2$ gas (55 bar) from the cylinder into a liquid that could be compressed and delivered to the system at elevated pressure (250-300 bar). The pump consisted of a gas inlet to draw the $CO_2$ from the cylinder, a refrigerator unit to condense the gas and an outlet to deliver the compressed liquid $CO_2$. Compressed air, at a pressure of 3-5 bar, was used to compress the $CO_2$ liquid to achieve the desired output pressure. A non-return valve (NRV) was placed on the high pressure line, after the pickle pump, to prevent any back flow and subsequent contamination of the $CO_2$ line and the pump. Manual HiP taps (High Pressure Equipment Company, USA) were used to control the inlet and outlet flow of $CO_2$ through the rig. The system also contained a trip switch connected to the pressure and temperature monitors. In the event of the pressure exceeding the prescribed safety limits (~275 bar) the power to the heating jacket would be cut off causing the system to cool and subsequently, the pressure to drop.

The high pressure equipment was brought to experimental conditions following the same general procedure (unless otherwise stated). The system was first pressurised to 55 bar at ambient temperature. The temperature was then increased to the desired conditions unless the required temperature was above 80 °C. In this instance the temperature was first increased to 60 °C and then increased in 20 °C increments

until the desired temperature was achieved. The system was then left to equilibrate for 5 minutes at the operating temperature before the pressure was increased to the final working conditions.

### 2.5.1 High Pressure Rheometer

A high pressure rheology method was developed for the analysis of the viscosity of the polymers, blends and formulations in the presence of $CO_2$. All rheology measurements were performed using an MCR 102 rheometer (Anton Paar) controlled using the Rheoplus/32 software. The system consisted of a high pressure measuring cup equipped with a $CO_2$ inlet/outlet and a pressure release valve. The measuring cup was sealed with a pressure head. A parallel plate geometry was employed for the analysis of all samples, where the base of the measuring cup acted as the stationary, lower plate with an approximate diameter of 32 mm. The rotating upper plate was contained within the pressure head and had an approximate diameter of 20 mm. A magnetic coupling was used to control the rotation of the upper parallel plate (Figure 2.10).

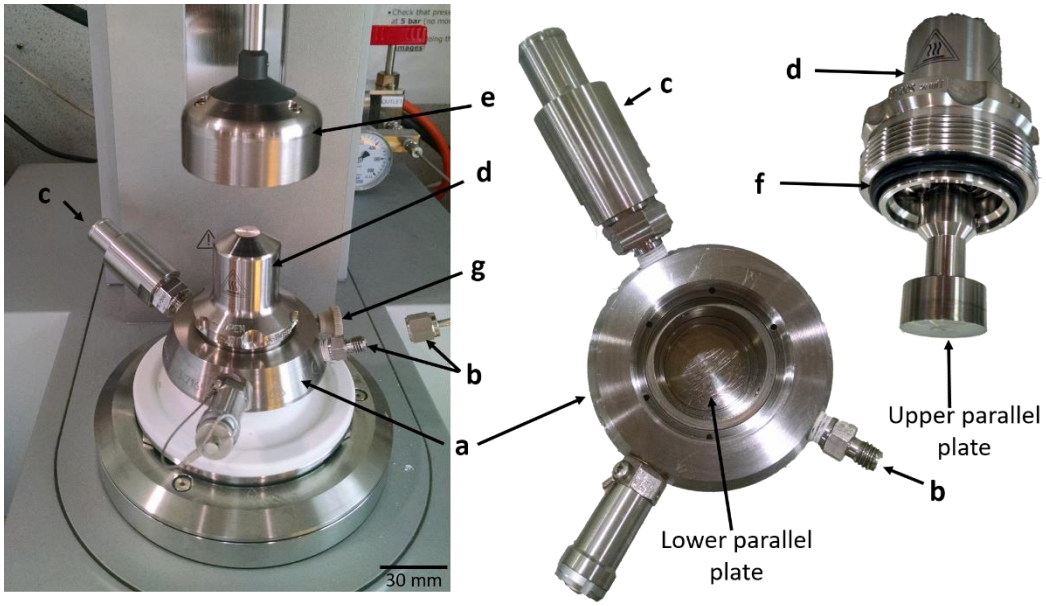



Figure 2.10. Images of the MCR 102 rheometer used throughout this thesis. **a**) High pressure measurement cup, the base of which acts as the stationary lower parallel plate. **b**) $CO_2$ inlet/outlet. **c**) Pressure release valve. **d**) Pressure head containing the rotating upper parallel plate. **e**) Magnetic coupling used to control the rotation of the upper parallel plate. **f**) Ethylene propylene diene monomer (EPDM) rubber O-ring used to produce an airtight seal. **g**) Built-in clamp to secure the measuring cup in place.

The rheometer used air bearings and mechanical bearings to reduce the frictional forces exerted on the measurement system that would affect the viscosity result. The mechanical bearings, which were located in the pressure head, were replaced after every measurement. A series of service tests were performed before each measurement to take into account the internal friction of the system and to check the suitability of the new bearings.

For high pressure measurements the $CO_2$ was delivered to the system via a 260D syringe pump (Teledyne ISCO, USA). This was connected to a Pickel pump using a high pressure line consisting of HiP Taps and Swagelok® tubing and fittings (Figure 2.11). The use of the syringe pump provided reproducible control over the amount of $CO_2$ supplied to the measuring cup. By leaving HiP taps 4, 6, 7 and the rheometer inlet tap open (Figure 2.11), the pressure in the measuring cup was maintained during the measurements, counteracting the effect of any temperature changes or leaks. The pressure was delivered and maintained by the displacement of a piston within the syringe pump chamber. In addition to the pressure transducer in the syringe pump there was also a piezoelectric pressure transducer on the high pressure line which was connected to a digital output (P1 in Figure 2.11) and a Bourdon-tube gauge integrated on the rheometer inlet line (P2 in Figure 2.11).

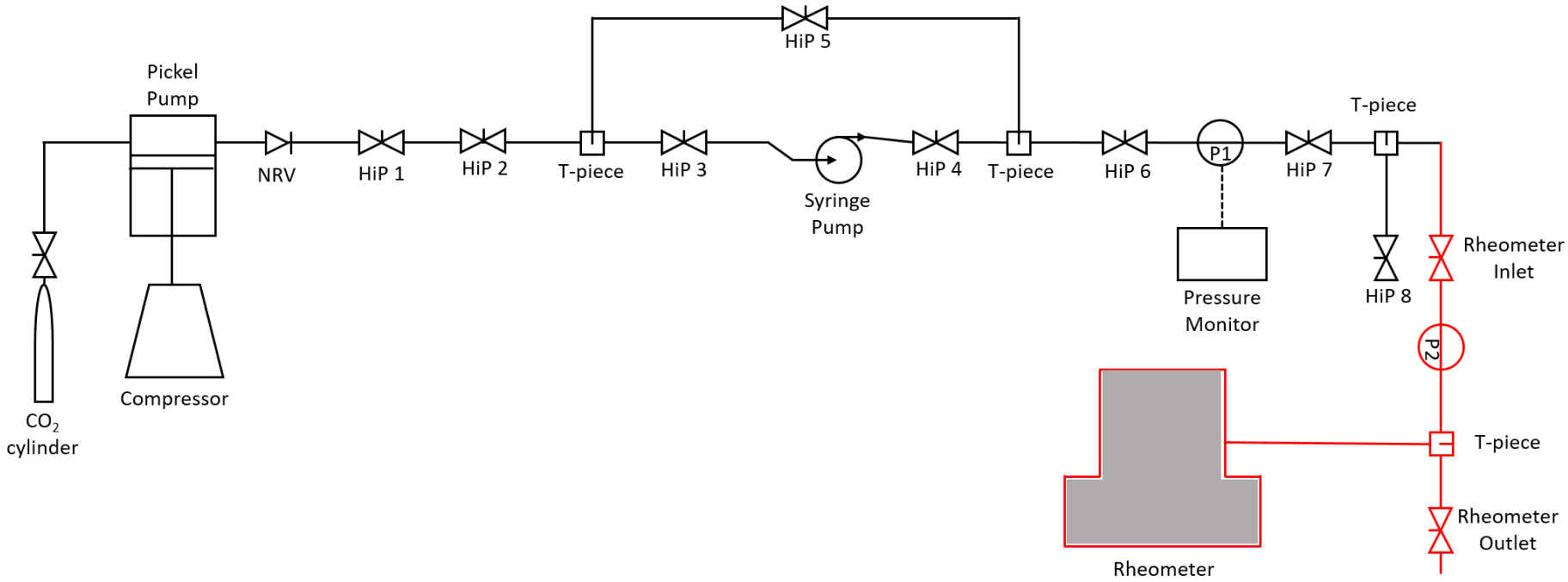



Figure 2.11. Rig diagram of the high pressure rheometer. Here, the red indicates the commercially bought components.

#### 2.5.1.1 Experimental Procedure

Typically, the high pressure experiments were performed directly after the ambient pressure experiments. Therefore, it was necessary to perform a leak test of the system before the sample could be loaded. An ethylene propylene diene monomer rubber (EPDM) O-ring (Figure 2.10f) was fitted to the pressure head (Figure 2.10d) before it was screwed onto the measuring cup (Figure 2.10a), forming an airtight seal. The inlet pipe was then connected (Figure 2.10b) and the cup secured in place using the built-in clamp (Figure 2.10g). A polycarbonate shield was placed in front of the rheometer whenever high pressure was used. A leak test was then performed by pressurising the system to 55 bar using the syringe pump and heating to 40 °C. The pressure was monitored and all the fittings checked for leaks using Snoop® (Sigma) a leak detecting fluid. If any leaks were detected, the system was cooled and vented and the fittings were adjusted. The leak test was repeated until no leaks were present.

After the leak test the system was vented to ambient pressure and cooled to room temperature. The sample to be tested was weighed into a vial and decanted into the measurement cup. The pressure head was then screwed into place, sealing the sample inside the measuring cup. The cup was then heated to the measurement temperature and the sample left to equilibrate for 1 hour. The cup was secured in place using the built-in clamp and the magnetic coupling (Figure 2.10e) was lowered until the Normal Force on the RheoPlus software read between -0.05 and 0.05 N. The ambient pressure measurements were then performed as described in Chapter 3. For the high pressure measurements the $CO_2$ was delivered via the syringe pump. The measurement cup could hold a volume of approximately 40 mL of $CO_2$. Therefore, to ensure there was enough $CO_2$ present, in case of temperature fluctuations or leaks, the syringe pump had to contain at least 60 mL of $CO_2$. The syringe pump was filled by opening the HiP taps between the Pickel pump and the syringe (Figure 2.11 HiP 1, 2 and 3). Once the desired volume was achieved these taps were closed and HiP taps 4, 6, 7 and the rheometer inlet tap (Figure 2.11) were opened to deliver the $CO_2$ to the measurement cup. The desired pressure was set on

the syringe pump, and once this value was achieved, the flow of $CO_2$ was stopped automatically. These taps were then left open to account for any temperature fluctuations or leaks. Once the high pressure measurements were complete the taps were closed and the system was allowed to cool. Once the temperature was below 30 °C the $CO_2$ was vented via HiP 8 (Figure 2.11) and the sample could be removed.

### 2.5.2 View Cell

A fixed volume (100 mL) view was used to observe the behaviour of the materials used in Chapter 5 as they were exposed to high pressure $CO_2$ conditions. The view cell is a stainless steel high pressure vessel equipped with two sapphire windows which was designed and built in-house at the University of Nottingham. Briefly, it is comprised of a cylindrical chamber capped with two sapphire windows in stainless steel housings (Figure 2.12). The windows are secured using a clamp and key system, where the key is specific to the clamp and also acts as the safety needle for the high pressure vessel. Hence, in order to remove the clamps, the vessel must be at ambient pressure before the safety needle can be removed and used as the key.

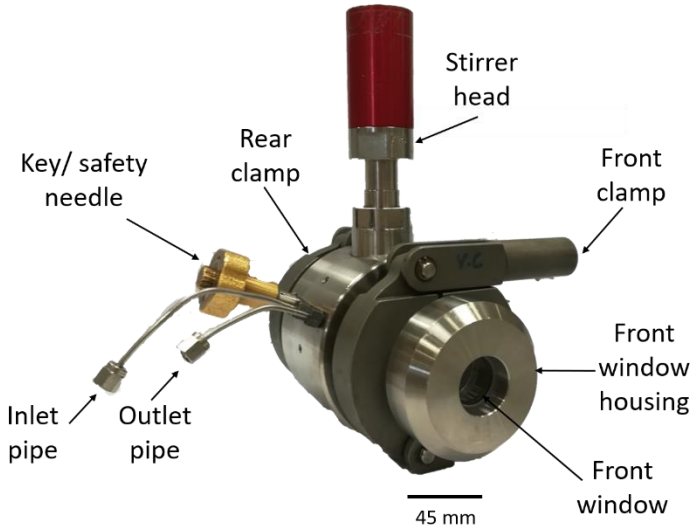



Figure 2.12. Image of the fixed volume view cell.

$CO_2$ is delivered to the view cell through the inlet pipe, which is connected to the Pickel pump via the high pressure tubing and fittings as described in section 2.5. Due to the volume and horizontal orientation of the view cell the heating elements sit within in the cell wall. As a result of the wall material being thicker, two

thermocouples are required. One is located in the cell wall and used to monitor the external temperature of the cell and to control the power delivered to the heating cartridges. The second is used to monitor the internal temperature. The view cell also contains a mechanical stirrer but this was not used during any of the experiments in this work. An external lamp was placed behind the rear window to provide light and improve visibility inside the cell. The maximum working pressure of the view cell was 300 bar at 100 °C, with the sapphire windows being the weakest point.

#### 2.5.2.1 Experimental Procedure

Prior to any experiments, the view cell was fully assembled and leak tested at experimental conditions. First the windows were fitted with an EPDM O-ring and secured in each of the housings, a Kel-F spacer was placed between the windows and the housing to provide a soft surface for the sapphire windows. Another EPDM O-ring was placed at the rear of the cell and the rear window housing secured in place using the clamp and key mechanism. The view cell was placed on a purpose built stand in the fumehood, in front of the lamp. The heating cartridges were then inserted into the cell wall before the front window was secured in place, not forgetting the EPDM O-ring. The inlet and outlet pipes were then connected to the high pressure tubing and the fittings tightened. Finally, the key was inserted into the body of the view cell and screwed into place to seal the vessel. The external thermocouple and the heating cartridges were connected to a control box, which was connected to the trip switch. The internal thermocouple was connected to separate temperature monitor.

The leak test was performed by first pressurising the cell to 55 bar and checking the fittings for leaks using Snoop® leak detecting fluid. Following this, the cell was heated and left to equilibrate until the internal thermocouple reached the desired temperature, again the system was checked for leaks. Next, the cell was pressurised to experimental conditions and a final leak test performed using the Snoop® leak detecting fluid to check all fittings. If a leak was detected at any point, the system was cooled and vented and the necessary fittings tightened. The leak test was repeated until the system was free of leaks.

After the leak test, the cell was returned to ambient temperature and pressure, and the experiment was performed. In a typical experiment ~500 mg of the sample was weighed into a glass vial (10 x 10 mm, height x diameter) and placed on a platform in the view cell. The view cell was then sealed and pressurised to initial conditions of ~55 bar and ambient temperature. The cell was then heated to 40 °C and the temperature allowed to equilibrate for approximately 5 minutes before increasing the pressure to the final conditions of 140 bar $CO_2$. The sample was then left for 1 hour before the heating supply was disconnected and system vented over approximately 20 minutes and left to cool. Photos were taken at various intervals throughout the experiment to document any phase changes.

### 2.5.3 MKIII Clamp Sealed Autoclave

A standard MKIII clamp sealed autoclave was used in Chapter 5 of this thesis to produce a series of polymer blends and API containing formulations. The autoclave consisted of a 60 mL 316 stainless steel vessel made up of a head and a base, which was designed in-house at the University of Nottingham (Figure 2.13). The head was connected to the base using the same clamp and key system used for the view cell. The head of the autoclave was equipped with an inlet and outlet pipe connected to the high pressure $CO_2$ line, a K-type thermocouple and a mechanical stirrer. A heating jacket surrounded the base of the autoclave, and was connected to the temperature control box. As well as the standard trip switch, a second safety measure was installed in the head of the autoclave. A spring loaded relief valve would release the pressure in the system, should the maximum pressure limit (345 bar) be exceeded. This was set above the value of the trip switch because in the event of a pressure release, the reaction mixture may also be released which was undesired.

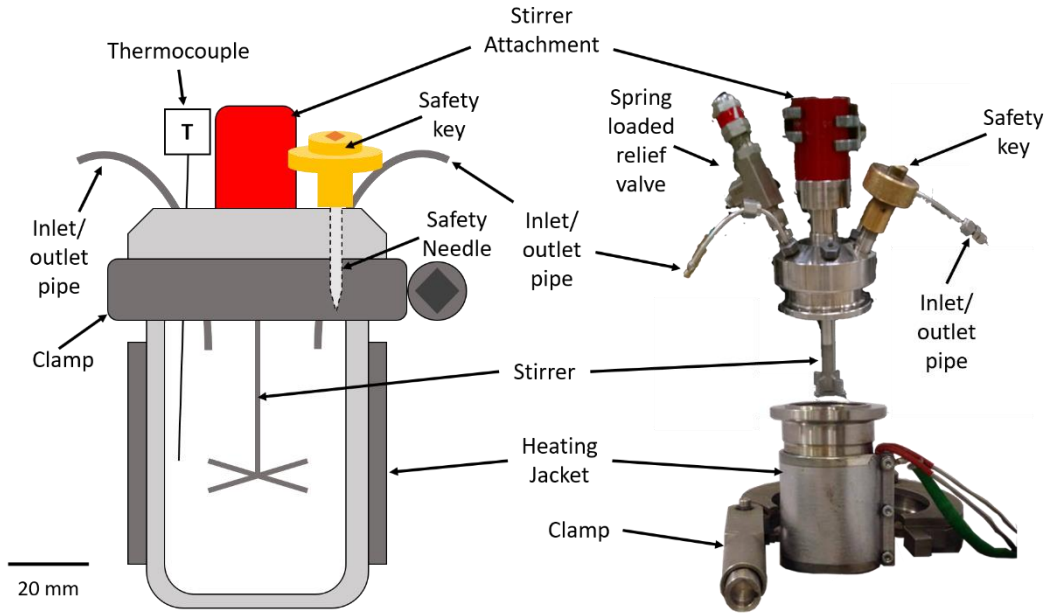



Figure 2.13. Image and a schematic of the 60 mL MKIII autoclave.

The maximum working pressure of the autoclave once it was fully assembled with the EPDM O-ring was 300 bar at 150 °C.

### 2.5.3.1 Experimental Procedure

Before use the autoclave was assembled and leak tested. An EPDM O-ring was placed in the head of the autoclave and it was attached to the base using the clamp and key mechanism. Once the clamp had been tightened, the key was inserted into the autoclave head and screwed tight creating a seal. The leak test was then performed following the same procedure described in section 2.5.2.1. Once the system was found to be leak free and had returned to ambient temperature and pressure the $CO_2$ mixing procedure could be carried out.

Prior to loading into the autoclave, the components were weighed into vials and physically mixed. The autoclave was sealed and the same pressurising procedure as described for the view cell experiments was followed to achieve the final conditions of 140 bar $CO_2$ and 40 °C. The blends were left stirring at 300 rpm for 1 hour after which time the sample was allowed to cool without stirring. Once the system was at a temperature below 25 °C, the $CO_2$ was removed and the sample was collected and ground using a pestle and mortar.

## 2.6 Characterisation Methods

The polymers were characterised by the following standard analytical techniques.

### 2.6.1 Differential Scanning Calorimetry

Differential Scanning Calorimetry (DSC) analysis was performed to determine the thermal transitions of the polymers. Analysis was carried out on a TA-Q2000 (TA instruments) DSC calibrated with an indium standard under a flow of nitrogen. 1-3 mg of sample was weighed into a T-zero sample pan (TA instruments) while a second reference T-zero pan remained empty. Both pans were heated at 10 °C/min, from -20 °C to 120 °C. Three samples of each polymer were analysed with two heating cycles per sample in order to erase any thermal history of the individual samples. The results from the second cycle were averaged.

### 2.6.2 Gel Permeation Chromatography

Gel Permeation Chromatography (GPC) was used to determine the molecular weight of the polymers before use, and in some cases after exposure to $CO_2$. GPC was also used in Chapter 5 to determine the API content and release of the pharmaceutical formulations.

#### 2.6.2.1 Molecular Weight Analysis

Molecular weight analysis was performed using an Agilent 1260 infinity multidetector GPC/SEC (size exclusion chromatography) system with a Wyatt Optilab light scattering detector. Columns consisted of 2 x Agilent PLGEL 5 µm Mixed D (7.5 mm X 300 mm) and a PLGEL 5 µm guard column (7.5 mm X 50 mm). THF was used as the eluent at a flow rate of 1 mL/min and the following differential index of refraction values (dn/dc) were used for evaluation: 0.042 mL/g for $P_{D,L}LA$ and PLGA[167], 0.072 mL/g for PCL[168] and 0.067 mL/g for PEG.[169] For the block copolymers dn/dc values of 0.055 and 0.051 mL/g for the $PEG_5$-*b*-$PLA_5$ and $PEG_5$-*b*-$PLA_{10}$, respectively, were calculated using the weight percent as determined from $^1$H NMR (see Chapter 4 for details).

#### 2.6.2.2 BSA Content Assay and Release

The BSA content of each formulation was determined using the RI signal of a multidetector SEC system. SEC was carried out using a 1200 Infinity series system equipped with a Polymer Labs aquagel-OH guard column (50 x 7.5 mm, 8 µm) followed by a PL aquagel-OH MIXED-H analytical column. Standard Dulbecco's Phosphate Buffered Saline (DPBS) was used as the mobile phase, with a flow rate of 1 mL/min.

In order to determine the BSA concentration, a series of known concentrations of BSA in DPBS solution were analysed for calibration (see Chapter 5 for more detail).

### 2.6.3 $^{1}$H Nuclear Magnetic Resonance Spectroscopy

$^{1}$H Nuclear Magnetic Resonance spectroscopy (NMR) was performed to analyse the number average molecular weights ($M_n$) and conversions of the synthesised polymers in Chapter 4. It was also used to assess any changes in $M_n$ of the polymers after they had been exposed to high pressure $CO_2$. All samples were analysed in deuterated chloroform ($CDCl_3$) using a Bruker Avance III 400 MHz spectrometer. The spectra were referenced to the solvent peak at $\delta$ = 7.26 ppm corresponding to $CDCl_3$. Details of the calculations used can be found in the individual chapters.

### 2.6.4 SEM

Carbon tape (Agar) was placed on an SEM stub (Agar), the sample was then loaded onto this in a thin layer and sputter coated for 90 seconds with platinum. The images were obtained under vacuum with a typical accelerating voltage of 10 kV, using a Phillips XL30 scanning electron microscope.

### 2.6.5 Micro Raman Spectroscopy

Micro Raman spectroscopy was performed using a Horiba Jobin Yvon LabRAM HR Raman spectrometer equipped with an automated xyz stage (Märzhäuser). Spectra were acquired using a 785 nm laser at 24 mW power, a 50× objective and a 300 µm confocal pinhole. To scan a range of Raman shifts simultaneously, a 600 lines/mm rotatable diffraction grating along a path length of 800 mm was employed. Spectra

were detected using a Synapse CCD detector (1024 pixels) which was thermoelectrically cooled to −60 °C. Before spectra collection, the instrument was calibrated using the Rayleigh line at 0 $cm^{-1}$ and a standard Si(100) reference band at 520.7 $cm^{-1}$.

For single point measurements, the deposited component solids were laser irradiated for 10 minutes to reduce the background fluorescence by photo-bleaching. Spectra were then acquired in the range of 100-4000 $cm^{-1}$ with an acquisition time of 10 seconds and 8 accumulations to improve the signal to noise ratio. Spectra were baseline corrected for residual fluorescence using a third-order polynomial fitting model.

The surface maps of the pressed formulations were obtained by acquiring spectra over the range of 720-1820 $cm^{-1}$ at 100 µm steps within a square of 3000 x 3000 microns (961 spectra per map). The DuoScan functionality was employed to increase the effective laser spot size, conferring a spatial resolution of ~100 and ~30 µm in the lateral (xy) and axial (z) dimensions respectively. As each individual spectrum was collected for 13 seconds, and repeated once (to remove the spikes due to cosmic rays) the whole map required approximately 17 hours of acquisition time. The intensity (as height) of bands in the range of 1540-1720 (blue, BSA) and 1720-1820 cm-1 (green, polymers) and the intensity ratio of the bands (i.e. BSA relative to the polymers) were evaluated within the respective maps using univariate analysis. Classic least square regression analysis was employed to quantify the concentration of the non-polymer component utilising the multivariate analysis module within Labspec 6 software.

Optical micrographs of the compacts were obtained using a 10x objective lens and the Montage function within the instrument software.

# Chapter 3

## Development of a High Pressure Rheology Method

## 3.1 Abstract

Advances in the pharmaceutical industry have led to new developments in drug delivery systems. In particular, encapsulating drugs in polymers to produce controlled and sustained release has received considerable attention.[17,18] Traditional encapsulation methods require heat or volatile organic solvents (VOCs) to reduce the polymer viscosity.[170] These conditions have been shown to be detrimental to the active pharmaceutical ingredients (APIs) and in some cases, extensive purification steps are required. Therefore new techniques of processing polymers at mild conditions are being developed using $scCO_2$.[98,99]

In order to optimise these techniques, the effect of $CO_2$ and APIs on the polymer melt viscosity has to be quantified. Hence, the aim of this chapter is to develop a high pressure rheology method that can measure the polymer melt viscosity reliably and reproducibly.

Initial measurements were performed on a semi-crystalline polymer: polycaprolactone ($PCL_{112}$). As this polymer has been previously well studied within the group, it provides the perfect starting point for the method development. Once a method has been established for PCL the chapter moves on to study the rheology of an amorphous polymer: poly($_{D,L}$-lactic acid) ($P_{D,L}LA$). Further development of the method investigates the feasibility of performing measurements at a temperature below the normal $T_g$ of the polymers, suitable for use with thermosensitive APIs.

Once a reliable and reproducible high pressure rheology method has been developed, it is necessary to confirm that this method has no detrimental effects on the polymers. For example, if the polymers are kept at high temperatures for a long time they could undergo thermal degradation. Therefore, the polymers will be characterised before and after the rheology measurements using GPC, $^1$H NMR and DSC.

Following successful development, this high pressure rheology method will be employed throughout the remainder of this thesis.

## 3.2 Contents

Chapter 3 ..... 3-59

3.1 Abstract ..... 3-60

3.2 Contents ..... 3-61

3.3 Introduction ..... 3-62

3.4 Materials ..... 3-68

3.5 Methods ..... 3-69

3.5.1 Rheology Measurements ..... 3-69

3.5.2 Characterisation of the Polymers ..... 3-74

3.6 Results ..... 3-76

3.6.1 Rheology of $PCL_{112}$ ..... 3-76

3.6.2 Rheology of $PLA_{11}$ ..... 3-81

3.6.3 Rheology at 140 bar and 40 °C ..... 3-87

3.6.4 Characterisation of the Polymers Before and After Rheology ..... 3-93

3.7 Summary ..... 3-97

3.8 Conclusions ..... 3-99

## 3.3 Introduction

Characterisation of the polymer melt viscosity is necessary given that many processing operations involve working with polymer melts, mixtures or solutions. One such application where the viscosity of the polymer melt is important is the encapsulation of drugs in polymers for the pharmaceutical industry. Traditional methods of encapsulating drugs in polymers include emulsion, precipitation, spray drying and extrusion techniques.[170] In order for the polymer and the drug to mix, the polymer must be in a liquefied state, typically, this would be done by heating or dissolving in a solvent. However, high temperatures can be detrimental to the integrity of the protein or peptide drugs for which these systems are designed.[14,71] The use of solvents, although often less damaging to the drug is also unfavourable as intensive purification steps are required to remove excess solvent. Even then, residual solvent can remain in the final product, which can be toxic for patients. Furthermore, disposal of the waste solvent can be expensive and environmentally harmful; therefore, green solvents, in particular $scCO_2$, are being investigated as alternatives. Another benefit of using $scCO_2$ is that the drugs are not modified during processing, leaving them with full activity and efficacy.[93] A "Particles from Gas Saturated Solutions" (PGSS) technique (described in Chapter 1) has been explored as a route to produce protein loaded polymer microparticles.[111] However, this process is only successful for some formulations and it is thought that the complexity of the API/polymer/$CO_2$ system results in unpredictable melt properties.[111] Therefore determining polymer viscosity at high pressure during these processes is necessary to address and solve these problems.

The viscosity of polymer melts is an essential parameter to be considered during process development and so has been measured for almost as long as the polymer industry has been around.[161] The earliest reports on the effect of pressure on polymer melt viscosity date back to the 1960s where hydrostatic pressure was seen to increase viscosity.[171] It is now known that if a gas, such as $CO_2$, is soluble in the polymer melt, the free volume is increased resulting in a reduction in viscosity and $T_g$ in a process known as gas plasticisation.[127,135,139,172] In order to assess the

efficiency of $CO_2$ as a processing aid, several high pressure rheology techniques have been developed.[127,128,176,130,131,135,136,138,173–175] There are four categories of high pressure rheometer: pressure driven, falling body, vibrating wire and rotational.[135]

Pressure driven rheometers replicate polymer flow during conventional processing where flow is driven by pressure. Examples include capillary rheometers that generate flow from an upstream piston (Figure 3.1) or slit die extrusion rheometers that employ an extruder. Viscosity is calculated from the drop in pressure and the flow rate. The simplicity of the flow field and small sample quantities along with precise and reproducible results make this a popular method for high pressure viscosity measurements. However, the pressure drop not only affects the viscosity but also leads to phase separation meaning this method is only suitable for low pressures. It is also necessary to apply mathematical corrections to account for additional pressure drops at the exit of the device.[135] Gerhardt et al. employed a high pressure capillary rheometer to measure the viscosity of polydimethylsiloxane (PDMS) in the presence of low concentrations of $CO_2$ (up to 2 wt.%).[127] The results suggest that an increase in free volume in the polymer is the main mechanism for viscosity reduction with the addition of $CO_2$. A slit-die extrusion rheometer was employed by Royer et al. to investigate the effect of $CO_2$ on the viscosity of a range of polymers.[128,177] In all cases the observed viscosity decreased with the addition of $CO_2$.

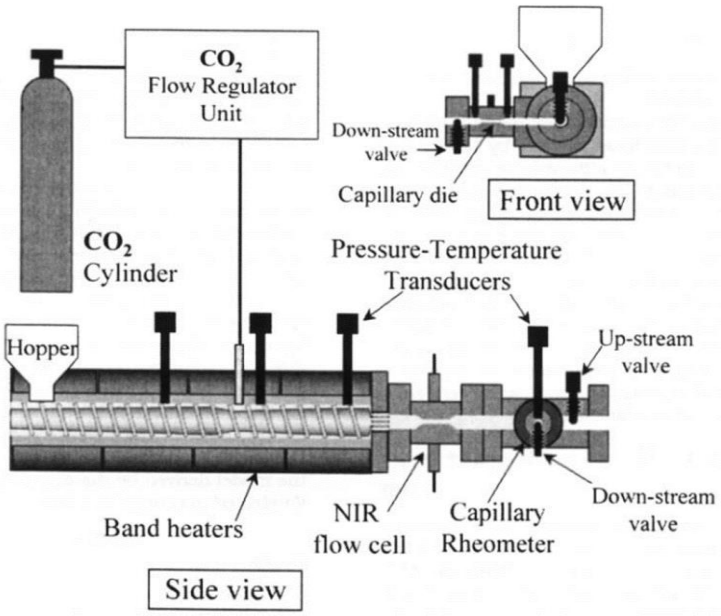



Figure 3.1. Schematic of a capillary tube rheometer with a $CO_2$ injection system. Reprinted with permission of John Wiley & Sons, Inc. from measurement and prediction of LDPE/$CO_2$ solution viscosity, S. Areerat, T. Nagata and M. Oshima, Copyright (2002) Polymer Engineering and Science.[253]

Falling body rheometers relate viscosity to the amount of time it takes an object to fall through a known distance of the sample fluid. These measurements are performed at constant pressures but are limited to low viscosities (mPa.s). Since the experiment is governed by gravity, high viscosities result in impractical measurement times. Quantification of viscosity as a function of shear rate is also difficult to calculate because the shear rate is determined by the fluid viscosity and object density. However, there is the capability for high pressures and the simplicity of the experiment makes it ideal for Newtonian fluids. Bae and Gulari used this technique to show that small quantities of $CO_2$ are capable of significantly decreasing the viscosity of PDMS.[178] Royer et al. have expanded on this technique to develop a magnetically levitated sphere rheometer.[174] In this instrument, a sphere is held in place using an electromagnet, and a cylindrical sample chamber is moved vertically to generate shear flow. The change in magnetic force required to keep the sphere stationary is related to the shear stress. From this, the viscosity can be calculated directly, with no need for theoretical modelling. Unlike traditional falling body rheometers, these measurements are not limited to low viscosity because the

response is based on electronic control and not the viscosity of the sample fluid. It is also possible to decouple concentration versus pressure effects of the dissolved gas.

The high precision vibrating wire instrument allows for the simultaneous measurement of the viscosity and density of materials. This technique exploits the buoyancy force acting on a solid sinker supported by a metallic wire (Figure 3.2). A current is passed through the wire at a specific frequency to generate a uniform and constant magnetic field. By performing frequency sweeps the wire is forced through a series of oscillations and the resonant curve can be determined. The presence of a sample fluid results in changes to the resonant frequency compared to that observed in a vacuum. The viscosity is obtained from the width of the resonance curve at one-half of its height. Gourgouillion et al. investigated the effect of $CO_2$ of the viscosity of a low molecular weight poly(ethylene glycol) (PEG, 400 g/mol), and demonstrated that viscosity decreased with increasing $CO_2$ pressures.[136] However, once again these measurements were performed on extremely low viscosity polymers (mPa.s).[136]

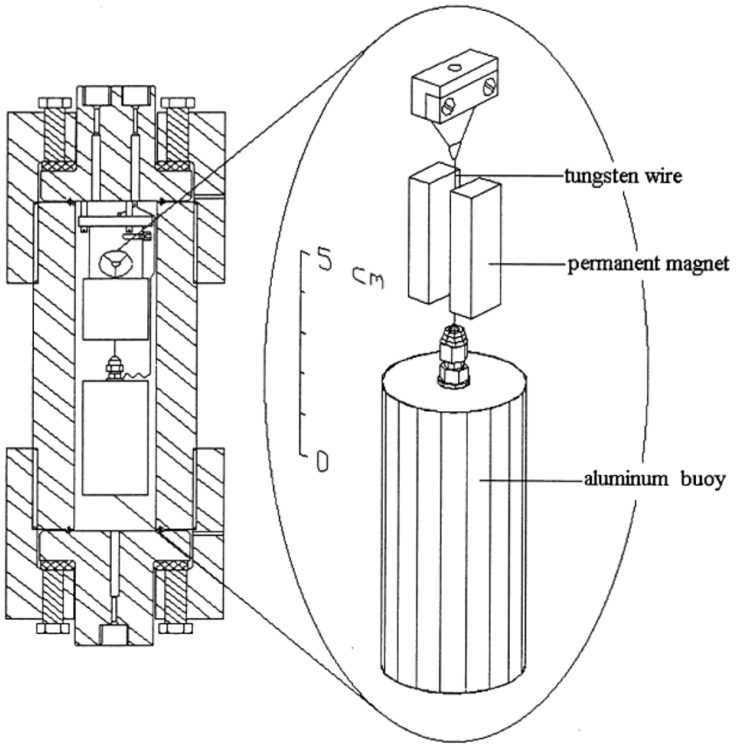



Figure 3.2. Schematic of the vibrating wire device used to determine densities and viscosities within a high pressure vessel. Reprinted with permission of Elsevier from simultaneous viscosity and density measurement of supercritical $CO_2$-saturated PEG 400, D. Gourgouillon, H. M. N. T. Avelino, J. M. N. A. Fareleira, M. Nunes da Ponte, Copyright (1998) The Journal of Supercritical Fluids.[136]

Of the four different types of rheometer, rotational rheometers are the most versatile and therefore the most widely used (Figure 3.3). In addition to viscosity, they can provide viscoelastic information through oscillatory measurements and can be used to perform continuous and sequential measurements. Not only this, they exhibit a uniform distribution of shear rate through the whole sample resulting in a good control of deformation that is not possible with capillary rheometers. They can be easily modified for use with high pressure using magnetic couplings. However, some sensitivity is lost at low viscosities (mPa.s), as the torque used for the viscosity calculations is no longer measured through direct contact with the sample.[135] Handge and Alstädt analysed the viscoelastic, thermal and diffusion properties of polystyrene (PS) melts treated with $CO_2$ using a rotational rheometer with a parallel plate geometry.[179] At 50 bar of $CO_2$ and 170 °C the viscosity of the PS melt decreased and a saturation time of 12 hours was observed.[179] Raps et al. also used a parallel plate geometry to demonstrate the viscosity reduction of polypropylene (PP) melts under $CO_2$ loading.[139]

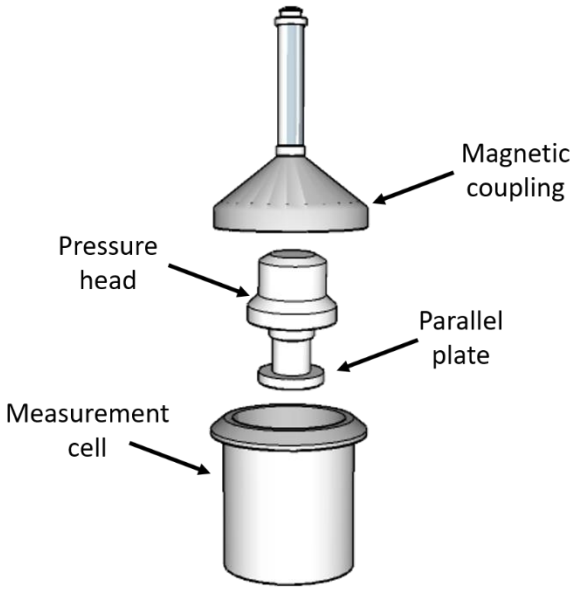



Figure 3.3. Schematic diagram of the high pressure rheometer attachment.

In all cases it has been shown that $CO_2$ can effectively reduce the viscosity of many different polymers, ranging from PE,[137] PP[139] and PS[128] through to PEG,[136] PCL[131,138] and PLA.[130]

In recent years, several papers have been published by the Howdle group investigating the effect of $CO_2$ on polymer melt systems with notoriously high viscosities.[112,129–132,138] These reports all use a rotational rheometer as it is possible to access a wide range of shear rates, pressures and temperatures, as well as being sufficiently accurate for high viscosity systems.[179] In order to measure the viscosity of $P_{D,L}LA$ during the PGSS process Hao et al. developed their own rotational instrument.[112] This instrument related viscosity to the load placed on a stirrer motor by calibrating the changes in electronic current with four commercial grade PDMS polymers of known viscosity. More recently, a commercial high pressure rheometer (MCR, Anton Paar) has been purchased and used to quantify the effects of $CO_2$ on the viscosity of $P_{D,L}LA$[129,130] and PCL.[131,138] In these studies the authors have tried to relate the trends in viscosity to particle formation. For example Hao et al. demonstrated that to generate uniform particle sizes, a low viscosity must be maintained in the early stages of depressurisation.[112] Kelly et al. demonstrated that blending $P_{D,L}LA$ with PEG at certain ratios also had an impact on yield and particle size.[140]

The aim of this thesis is to relate the viscosity of a drug loaded polymer formulation to its release profile. With the idea being that if the viscosity is sufficiently low to enable thorough mixing; then a formulation with an even distribution of drug can be produced, therefore resulting in a reproducible release profile. High pressure rheology of polymers and polymer blends has long been established and will be discussed in more detail in Chapter 4. However, the presence of a drug particle will also have an effect on the polymer melt properties (see Chapter 5 for more detail).[59] To date, several reports have been published investigating the effect of APIs on polymer melt viscosity.[59,141–146] However, in these reports the authors are interested in utilising rheology to optimise the hot melt extrusion (HME) process for pharmaceutical applications. Hence, all the rheology is carried out at ambient pressure and at relatively high temperatures. There have been several reports on the $CO_2$ assisted melt processing of polymers for pharmaceutical applications.[154] Although the authors acknowledge that $CO_2$ is capable of lowering the viscosity of

the polymer-drug mixture the processing temperatures are still incredibly high (130-190 °C) and there is no mention of any high pressure rheology.[155,156]

Hence, this chapter will describe the development of a high pressure rheology method suitable for the analysis of polymer formulations containing thermosensitive APIs. Initially a method will be established for the analysis of neat polymers above their $T_g$. This will be extended to the analysis of the viscosity of polymers in the presence of high pressure $CO_2$ while maintaining a temperature above the polymer $T_g$. Following this, a method will be developed where the viscosity of the polymers in the presence of high pressure $CO_2$ can be measured at temperatures below their ambient pressure $T_g$.

## 3.4 Materials

Polycaprolactone with molecular weight of 112,000 g/mol, by GPC ($PCL_{112}$) was purchased from Sigma Aldrich and stored at room temperature. All other polymers were purchased from Evonik and stored at -20 °C; see Table 3.1 for details (Figure 3.4). The polymers, Food grade $CO_2$ (99.8%; BOC, UK) for the high pressure rheology experiments, THF (HPLC grade, Fisher Scientific) and $CDCl_3$ (<99%, Sigma Aldrich) were used as received.

Table 3.1. Details of the polymers purchased for use in this chapter.

| Polymer[a] | $M_n$[b] (g/mol) | $M_w$[b] (g/mol) | Đ[b] | $T_g$[c] (°C) | $T_m$[c] (°C) |
|---|---|---|---|---|---|
| $PCL_{112}$ | 76,000 | 112,000 | 1.475 | - | 53 |
| $PLA_{11}$ | 7,000 | 11,000 | 1.649 | 49 | - |
| $PLA_{12}$ | 7,000 | 12,000 | 1.620 | 44 | - |
| $PLGA_{36}$ | 24,000 | 36,000 | 1.510 | 47 | - |

a) Subscript numbers refer to the $M_w$ (x$10^3$ g/mol) of the polymer. b) Measured by triple detection GPC in THF using dn/dc values of 0.072 and 0.042 mL/g for PCL and PLA/PLGA respectively. c) Measured by DSC.

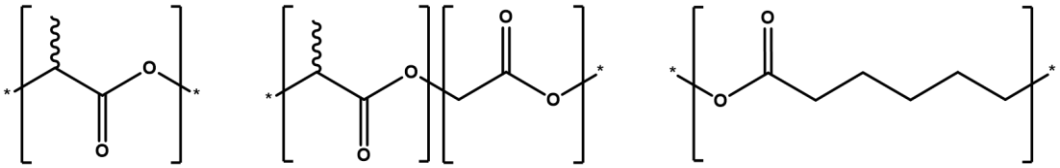



Figure 3.4. Structures of the polymers used in this chapter.

# 3.5 Methods

## 3.5.1 Rheology Measurements

All rheology measurements were performed using an Anton Paar MCR 102 rheometer with high pressure capabilities, as described in Chapter 2. The polymers were weighed directly into the measurement cell and left to equilibrate at measurement temperature for 1 hour, unless otherwise stated. All data was fitted to the Carreau model,[166] given by equation 2.6, to give calculated values for the zero shear viscosity ($\eta_0$, Pa.s). Multiple samples and measurements were carried out per polymer and the results averaged.

The amount of sample required was determined by loading an estimated amount of polymer into the measurement cell and heating to form a molten disk. The pressure head, containing the upper parallel plate, was then sealed in place. After a few minutes, the cell was opened and the upper plate checked for sample contact. In order to produce reproducible and reliable results the sample must make contact with both the upper plate and the lower plate during the entire measurement. If the sample had not made sufficient contact with the plates, more polymer was added.

Ambient pressure viscosity measurements were made by performing consecutive rotational shear ramps on each specimen. The shear rate was increased logarithmically from 0.1-1000 $s^{-1}$ across 30 measurement points with a measurement point duration of 120 to 10 seconds. The longer measurement point duration at lower shear rates was required to give the sample time to equilibrate between each point, reducing the noise of the measurement. A 1 minute pause at constant shear (0.1 $s^{-1}$) was implemented between each run to allow the sample time to relax. The

samples were then pressurised to 140 bar $CO_2$ using a syringe pump. High pressure measurements were carried out using the same shear ramp profile as for the ambient pressure measurements. After an initial 1 hour soaking period, measurements were performed every hour for 6 hours and again at 9, 12, 15 and 18 hours to ensure complete $CO_2$ saturation. The saturation time of the individual samples ($t_{sat}$) was determined by fitting the $\eta_0$ values at each time interval determined from the Carreau model to an empirical formula described in Equation 3.1. This represents the transition from a linear drop in log($\eta_0$) with time ($t$), at short time scales, to a constant saturation viscosity ($\eta_{sat}$) at longer times (Figure 3.5). Equation 3.2 was then used to calculate $t_{sat}$, defined by the time at the intercept of the two linear segments.

$$\eta = 10^{-m(t^*-t)} + \eta_{sat} \quad 3.1$$

$$t_{sat} = t^* + \frac{1}{m}(\log_{10}\eta_{sat}) \quad 3.2$$

In the above equations $m$ is the gradient as log($\eta$) decreases with time and $t^*$ is an interim parameter which relates to the time at which $\log_{10}(\eta - \eta_{sat}) = 0$.

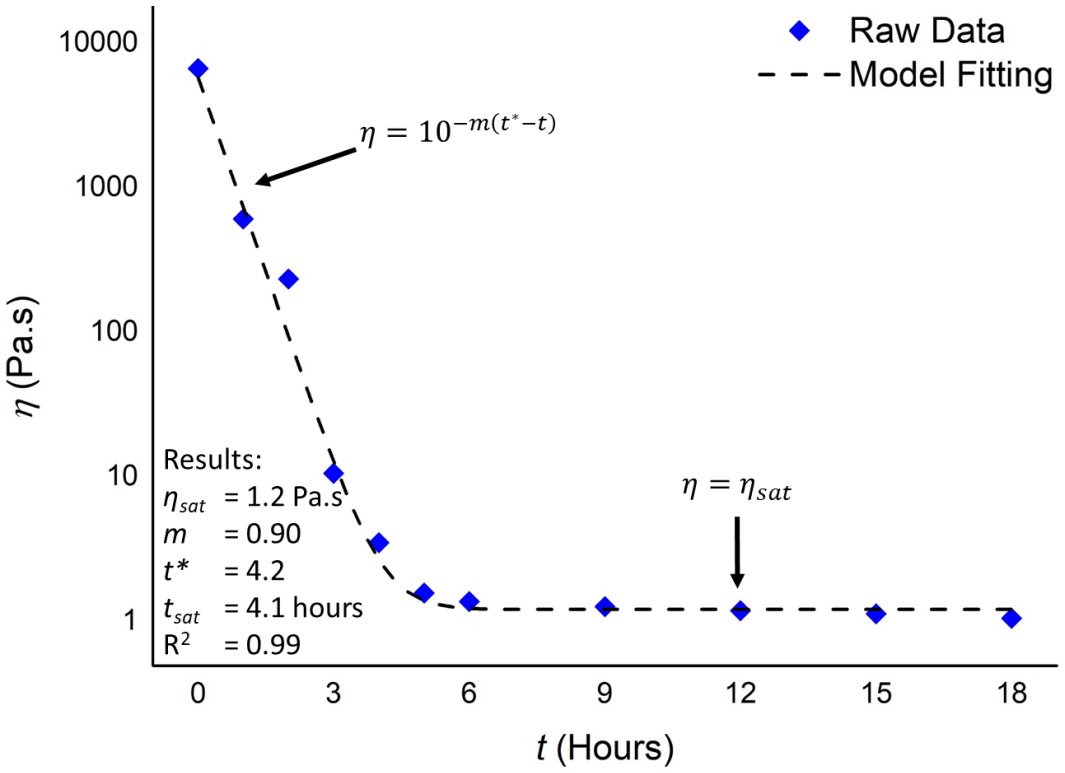



Figure 3.5. Raw data of the $\eta_0$ vs time from an individual sample (blue diamonds) is fitted to equation 3.1 (black dashed line). From this it is possible to determine the saturation viscosity ($\eta_{sat}$ (Pa.s)), the gradient of the slope ($m$) and the saturation time, ($t_{sat}$ (hours)), along with the $R^2$ value. Error bars represent ±1 standard deviation from the mean. $T$ = 80 °C, $P$ = 140 bar. Data from $PLA_{11}$ as a representative sample.

Following this, the datasets with soak times greater than the transition time, $t_{sat}$ (where the viscosity is no longer decreasing with soak time) were averaged (Figure 3.6). In this example, $t_{sat}$ was calculated as 4.1 hours; therefore, the average $\eta_{sat}$ is taken from the average of the results from 5 hours onwards. The overall $\eta_{sat}$ and $t_{sat}$ values for each polymer were calculated from the averages of the values obtained via the fitting model of each individual sample.

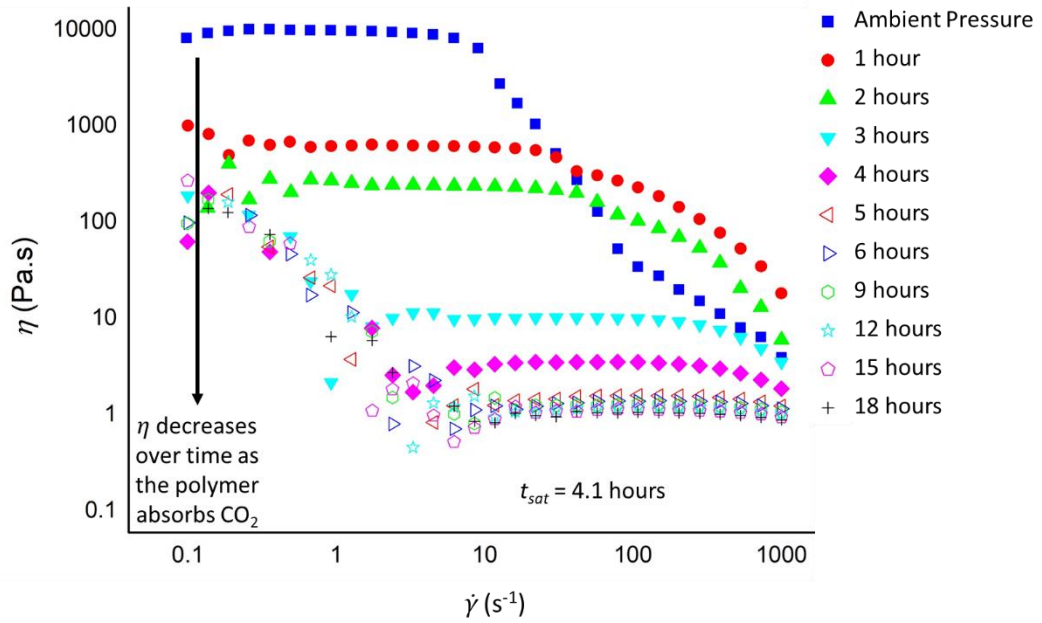



Figure 3.6. Viscosity of $PLA_{11}$ at regular time intervals during soaking with $CO_2$ at 140 bar and 80 °C. Data is from one representative sample.

The viscosity of $PLA_{11}$ was measured after the $CO_2$ had been vented from the sample to assess whether the use of $CO_2$ had any lasting effects on viscosity. The cell was vented over 20 minutes, during which time the sample was sheared constantly while temperature was maintained, the ambient pressure measurement profile was then applied. Multiple repetitions and detailed analysis confirmed that $CO_2$ could be completely removed from the $PLA_{11}$ sample with no lasting effects. Therefore, it was not necessary to carry out this test on all the polymers, as it has previously been reported in the literature.[131,155]

#### 3.5.1.1 Oscillatory Measurements

Oscillatory measurements were performed in order to determine the measuring temperature for the rotational measurements. Oscillations performed at constant strain and frequency over a temperature ramp allowed the storage and loss moduli (*G'* and *G''* respectively) to be plotted against temperature. The point at which the transition begins is clearly seen as *G'* begins to decrease and *G''* increases. A plot of tan($\delta$) (= G"/G') vs temperature results in a peak. In order for these measurements to be reliable, they must be performed in the linear viscoelastic (LVE) region (see Chapter 2 for more information).

A strain sweep, increased logarithmically from 0.1-1000% strain over 2 minutes at a constant frequency and temperature (1 Hz and 20 °C) was used to identify the LVE region. Prior to this measurement, the samples were loaded into the rheometer measuring cell and heated to 120 °C to form a molten disk. The samples were then left to cool overnight to 20 °C.

The temperature ramp was carried out at 1% strain and 1 Hz at a heating rate of 2 °C/min from 25 °C up to 130 °C.

#### 3.5.1.2 Rotational Measurements

##### 3.5.1.2.1 Recovery Test

Recovery measurements were made to establish how well the samples recovered after being exposed to high shear rates and to determine how long should be left between sequential measurements. The samples were sheared at low shear rates (0.1 $s^{-1}$ for 65 seconds) before being exposed to high shear (50 $s^{-1}$ for 20 seconds) followed by a second period of low shear (0.1 $s^{-1}$ for 150 seconds).

##### 3.5.1.2.2 Rheology of $PLA_{11}$ at 40 °C and 140 bar $CO_2$

The samples were loaded into the measurement cell and left to equilibrate at 80 °C for 1 hour in order to form a molten disk. They were then left to cool to 40 °C and then pressurised with 140 bar $CO_2$ using the syringe pump. An oscillatory measurement was then carried out over 40 hours at 1% strain and 1 Hz. Immediately following this the standard rotational shear ramp profile (described in section 3.5.1) was applied to generate the viscosity measurement.

##### 3.5.1.2.3 Rheology of the Other Polymers at 40 °C and 140 bar $CO_2$

For the measurements performed directly at 40 °C and 140 bar $CO_2$ the samples were loaded into the measurement cell and immediately pressurised to 55 bar $CO_2$ using the syringe pump. The temperature was then increased to 40 °C and the samples allowed to equilibrate at this temperature for 10 minutes. The pressure was then increased to 140 bar and the measurement started in accordance with the standard high pressure shear ramp profile (described in section 3.5.1).

For the measurements performed after cooling from 80 °C the samples were first analysed according to the standard measurement profile i.e. first at ambient pressure and 80 °C, then at 140 bar $CO_2$ and 80 °C. After the measurements at 140 bar $CO_2$ and 80 °C were completed, the samples were left to cool to 40 °C over 2 hours while the pressure was maintained at 140 bar. The viscosity was then measured according to the standard shear ramp profile for seven consecutive measurements.

### 3.5.2 Characterisation of the Polymers

The polymers were analysed by DSC, GPC and $^1$H NMR before use as described in Chapter 2. The $P_{D,L}LA$ and PLGA polymers were also analysed after the rheology experiments to confirm whether the methods had caused any thermal degradation.

#### 3.5.2.1 $^1$H NMR

$^1$H NMR spectroscopy was performed as described in section 2.6.3. Comparisons were made by normalising against the signal at 6.5 ppm corresponding to the methine group in the polymer backbone (**a'**, $\delta$ = 5.18 ppm Figure 3.7) and calculating the mol.% of lactide (equation 3.3). The $P_{D,L}LA$ $M_n$ was calculated by comparing the signals of the methine end group (**a''**, $\delta$ = 4.37 ppm Figure 3.7) and the polymer methine signal (equation 3.4).

$$\text{Mol.\% lactide} = \frac{\int(\boldsymbol{a})}{\int(\boldsymbol{a'}) + \int(\boldsymbol{a})} \times 100 \qquad 3.3$$

$$M_n = \frac{\int(\boldsymbol{a'})}{\int(\boldsymbol{a''})} \times 144 \qquad 3.4$$

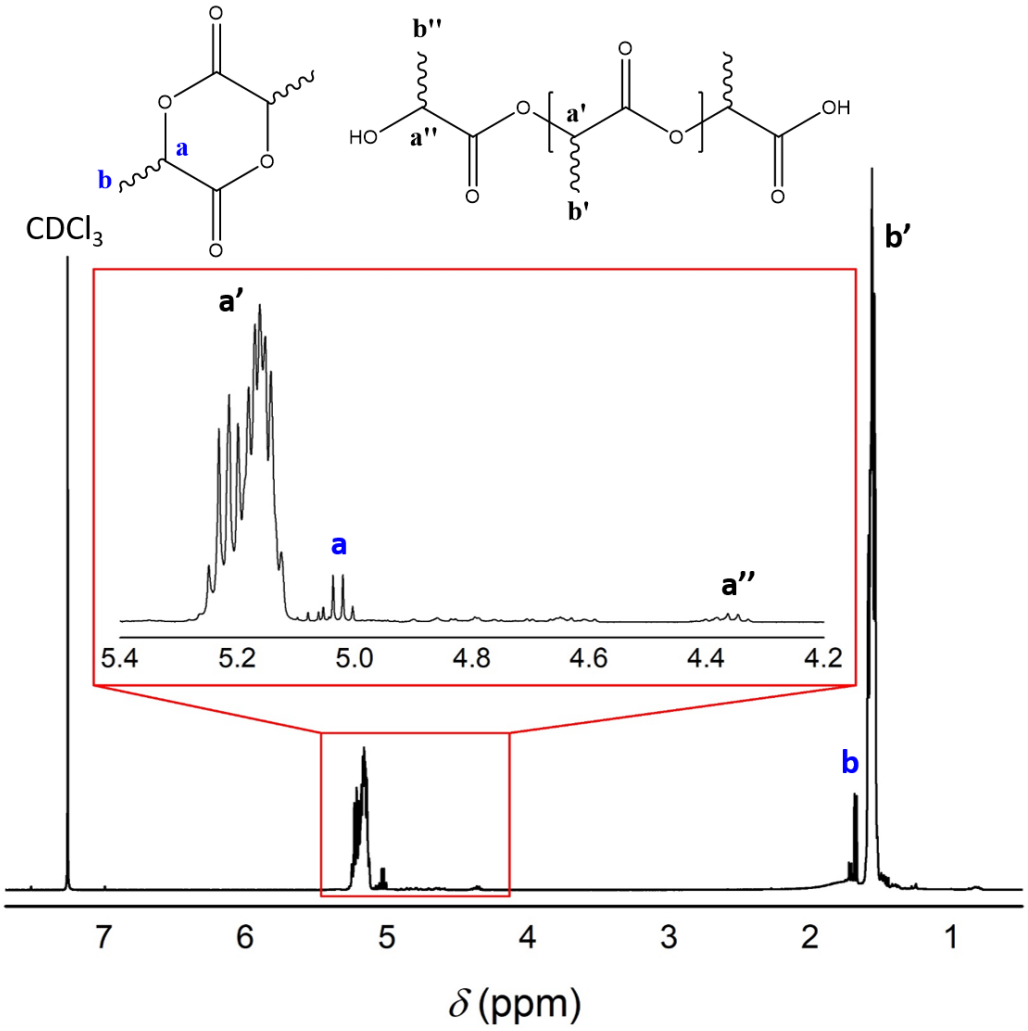



Figure 3.7. Typical $^{1}$H NMR spectrum of $P_{D,L}LA$ analysed in $CDCl_3$.

The $M_n$ of the $PLGA_{36}$ was calculated by adding together the $M_n$ of the lactide and the glycolide polymeric components (equation 3.5, Figure 3.8).

$$M_n(PLGA) = \left(\frac{\int(\boldsymbol{a}')}{\int(\boldsymbol{a}'')} \times 144\right) + \left(\frac{\int(\boldsymbol{c}')}{2\int(\boldsymbol{a}'')} \times 116\right) \qquad 3.5$$

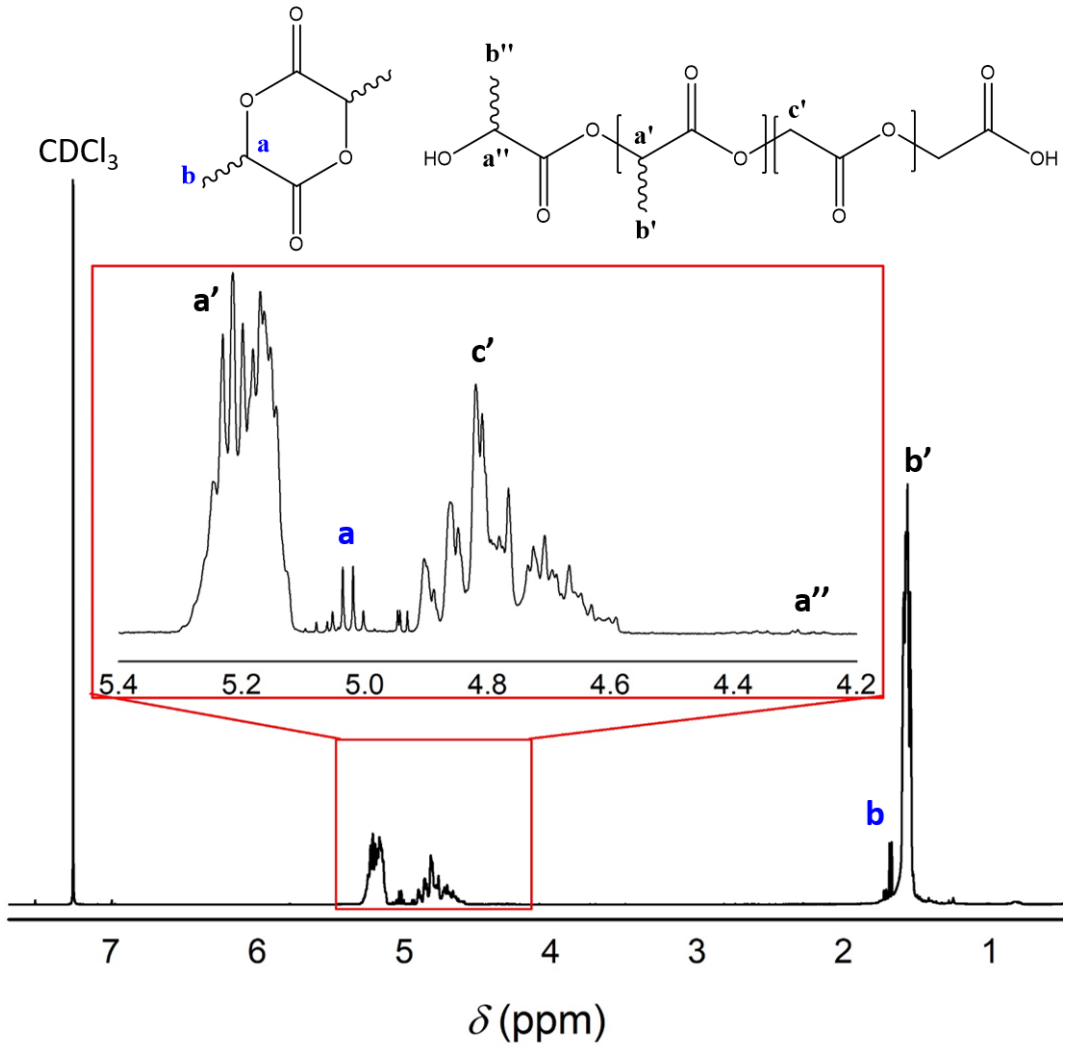



Figure 3.8. Typical $^{1}$H NMR spectrum of PLGA analysed in $CDCL_3$.

## 3.6 Results

### 3.6.1 Rheology of $PCL_{112}$

PCL is a semi-crystalline polymer that previous members of the group have extensively analysed using high pressure rheology.[131,138] Specifically, work by Curia et al. compared the effect of high pressure $CO_2$ on the viscosity and melting temperature of a high molecular weight ($M_n$ = 76,000 g/mol, $M_w$ = 112,000 g/mol, $PCL_{112}$) and low molecular weight ($M_n$ = 10,000 g/mol, $M_w$ = 14,000 g/mol, $PCL_{14}$) PCL.[131] The methods developed in that work provide the basis for the methods developed in this chapter, which once optimised will be applied throughout this thesis.

Since a method had already been established for PCL, a similar procedure was followed to measure the viscosity of the same $PCL_{112}$ at ambient pressure and 140 bar $CO_2$, at 90 °C (Figure 3.9, blue squares). In these measurements, the sample was loaded into the measurement cup, heated to 90 °C and left to equilibrate for 1 hour to allow a homogeneous melt to form. After this time, the cell was sealed, and sequential measurements performed at ambient pressure ($p_{amb}$), as described in section 3.5.1. Under these conditions $PCL_{112}$ had a zero shear viscosity ($\eta_0$) of 35,000 Pa.s (derived from the Carreau model, section 3.5.1) which was comparable to 50,000 Pa.s reported by Curia et al,[131] given the temperature difference (90 °C in this work and 80 °C used by Curia et al.). In order to confirm that this method was robust and gave reproducible results, two individual samples were measured a multiple of times. The average was then obtained, and the error calculated as ±1 standard deviation from the mean.

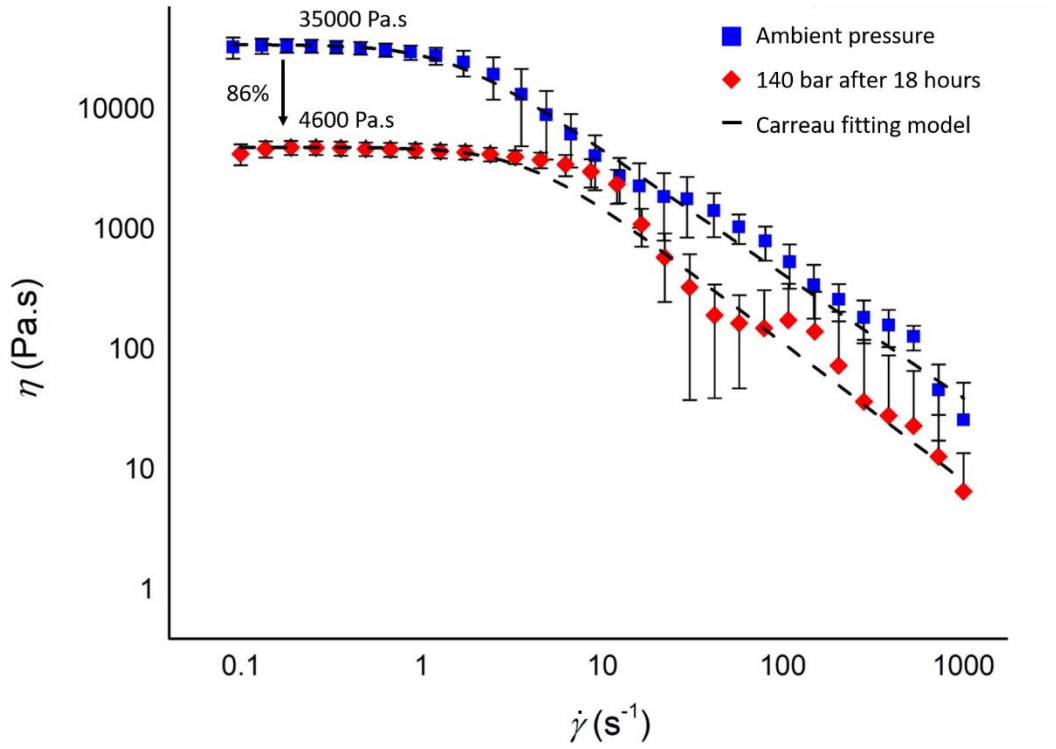



Figure 3.9. The ambient pressure viscosity (blue squares) of $PCL_{112}$ was much higher than the viscosity after saturation with 140 bar $CO_2$ (red diamonds). The Carreau model (black dashed lines) was a good fit for both measurements ($R^2$ > 0.95). Error calculated as ±1 standard deviation from the mean. ($T$ = 90°C)

Directly following the ambient pressure measurements, the system was pressurised to 140 bar with $CO_2$ via a syringe pump while the temperature was maintained at 90 °C. The samples were then analysed following the same measurement profile as the ambient pressure tests. The viscosity reported in Figure 3.9 (red diamonds) is that of the sample once it had been saturated with $CO_2$ and had reached its saturation viscosity, $\eta_{sat}$. Here an 86% decrease from the ambient pressure viscosity ($\eta_0(p_{amb})$) of 35,000 Pa.s down to 4600 Pa.s was observed. These results were compared to those obtained previously and any differences were attributed to variations in the measurement and instrument (Table 3.2).[131] This work was carried out at 90 °C compared to 80 °C previously used and so the $\eta_0(p_{amb})$ was lower, but also the decrease caused by $CO_2$ was smaller. This was because the current study used a much lower pressure of $CO_2$ (140 bar compared to the 300 bar used by Curia et al.) and so the relative concentration of $CO_2$ was lower.

Table 3.2. The reported viscosities for $PCL_{112}$ were comparable to those previously presented by Curia et al.[131]

| Source | Temperature (°C) | $\eta_0(p_{amb})$ (Pa.s) | Pressure (bar) | $\eta_{sat}$ (Pa.s) | % decrease from $\eta_0(p_{amb})$ |
|---|---|---|---|---|---|
| This work | 90 | 35,000 | 140 | 4600 | 86 |
| Curia | 80 | 50,000 | 300 | 2600 | 95 |

In the work performed by Curia,[131] viscosity in the presence of $CO_2$ was recorded after a 50 minute soaking period. However, in this work, a further drop in viscosity was observed during sequential measurements after the initial 50 minutes (Figure 3.10). This was because a longer shear ramp profile was used in this work than in previous work to allow longer measurement times at low shear rates in order to eliminate noisy measurements. This led to the polymer being exposed to $CO_2$ for a longer time in the first measurement than the sample was exposed to in the whole of Curia's measurements.

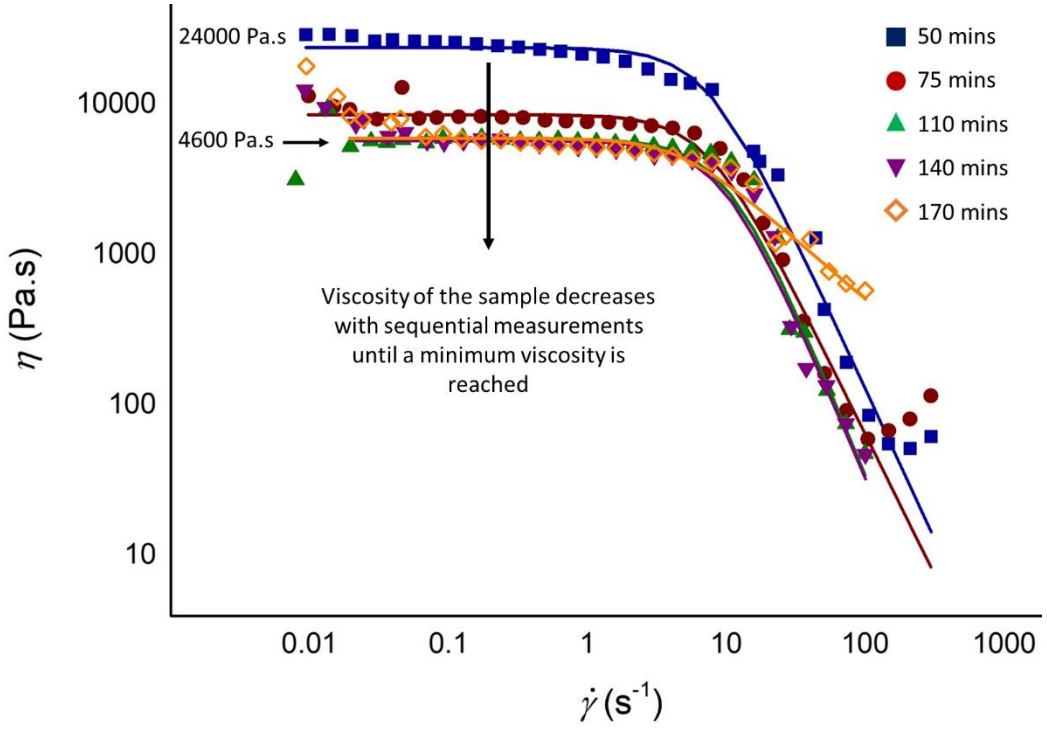



Figure 3.10. The viscosity of $PCL_{112}$ in the presence of 140 bar $CO_2$ was measured sequentially over 3 hours after an initial 50 minute soaking period. As the $PCL_{112}$ was exposed to $CO_2$ for longer periods of time the viscosity decreased until a minimum was reached and the sample was deemed to be saturated with $CO_2$. ($T$ = 90 °C).

In this work, the first sample reached its $\eta_{sat}$ after being exposed to $CO_2$ for 110 minutes (Figure 3.11 Sample 1- blue). It was therefore decided that a second sample (sample 2) should be left to soak for 110 minutes before the first measurement was made. However, sample 2 did not reach its $\eta_{sat}$ until it had been exposed to the $CO_2$ for 180 minutes (Figure 3.11 red). Sample 3 was analysed following a 175 minutes soak period, and this time the $\eta_{sat}$ was achieved after 195 minutes (Figure 3.11 green). Overall, it was clear that shear had an effect on $CO_2$ absorption into the samples. In each case, the first one or two measurements for each sample had a high viscosity, but once the sample had been sheared, allowing for better absorption of the $CO_2$, the $\eta_{sat}$ was achieved (Figure 3.11).

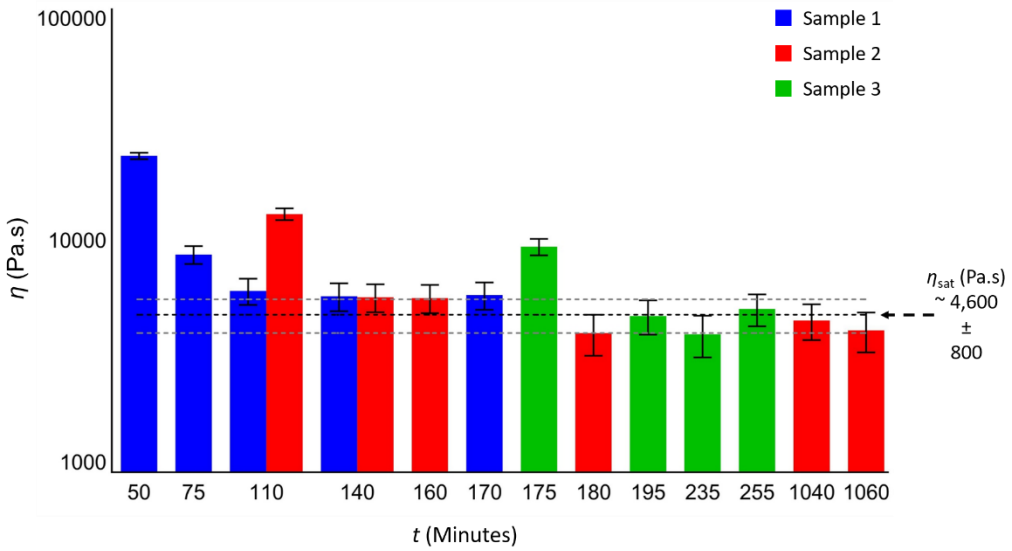



Figure 3.11. The viscosity of three individual samples of $PCL_{112}$ was measured after soaking in $CO_2$ at 140 bar for different initial soaking times. Each sample reached a comparable $\eta_{sat}$, but at different exposure times, with the first measurements of each sample having an exaggerated viscosity. The black dashed line denotes the average $\eta_{sat}$ with the standard deviation represented by the two grey dashed lines. ($T$ = 90 °C). Error calculated as ±1 standard deviation from the mean.

Following this experiment, a new method was developed where the samples were sheared at 10 $s^{-1}$ during the initial soak and in between sequential measurements. The samples were first analysed at ambient pressure as previously described and then pressurised with $CO_2$. After an initial 1 hour soaking period, measurements were performed every hour for 6 hours and again at 9, 12, 15 and 18 hours to ensure complete $CO_2$ saturation. From this method, the Carreau model was used to determine the $\eta_0$ of the sample at each time point, and these were plotted against

time. This data was then fitted to an empirical formula (section 3.5.1) which described the transition from a linear drop in log($\eta$) with time at short time scales, through to a constant saturation viscosity ($\eta_{sat}$) at longer times. From this, the time at which saturation was reached ($t_{sat}$) was calculated. $PCL_{112}$ at 140 bar and 90 °C had a $\eta_{sat}$ of 4600 Pa.s and a $t_{sat}$ of 0.35 hours (Figure 3.12). This was less time than the 50 minutes used by Curia and showed how important the effect of shear is for the absorption of $CO_2$ into the polymer samples.

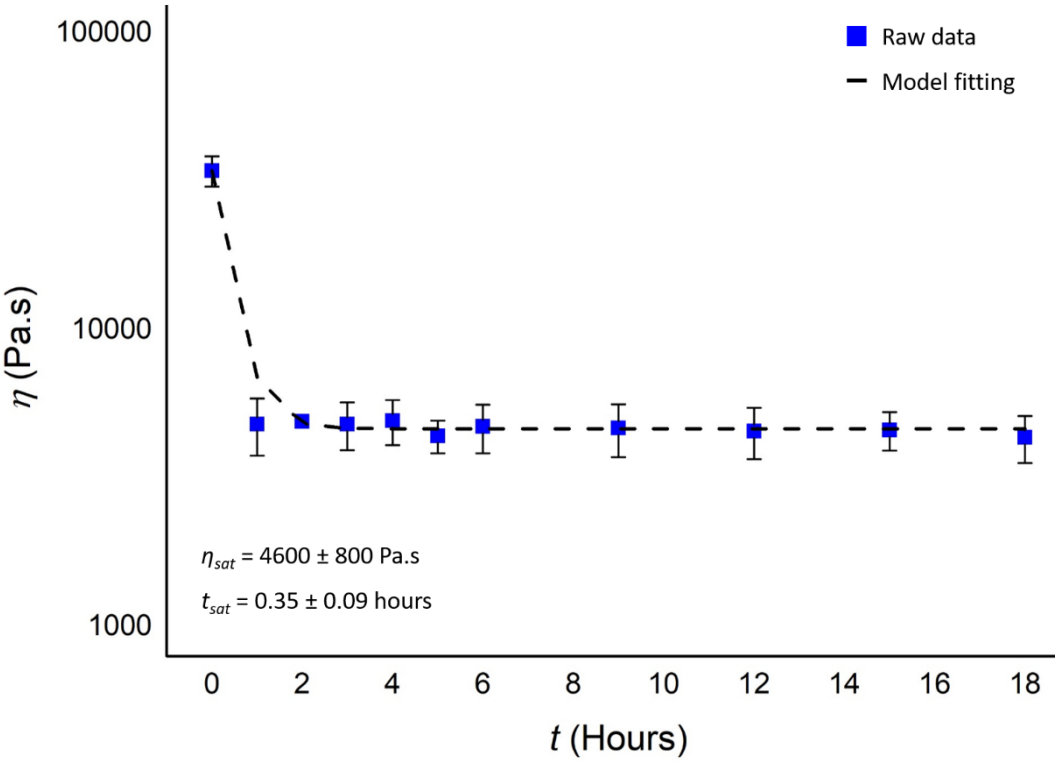



Figure 3.12. Viscosity vs time for $PCL_{112}$ in the presence of 140 bar $CO_2$ was determined from the Carreau model (blue squares) and was fitted with equation 3.1 (black dashed line). From this, the saturation viscosity ($\eta_{sat}$) and the saturation time ($t_{sat}$) of the sample were determined. $R^2 > 0.99$, error calculated as ±1 standard deviation from the mean. ($T$ = 90 °C).

Given that these methods proved to be reproducible with a known system they could now be applied to another polymer: amorphous poly($_{D,L}$-lactide) ($PLA_{11}$).

## 3.6.2 Rheology of $PLA_{11}$

### 3.6.2.1 Oscillatory Measurements

Oscillatory measurements were performed at constant strain and frequency over a temperature ramp in order to determine the temperature for the rotational

measurements. For these measurements to be reliable, they must be carried out in the linear viscoelastic (LVE) region. Therefore, samples were first heated and then cooled to 20 °C to form a homogeneous disc, and a strain sweep applied at constant frequency (1 Hz) for 2 minutes. The LVE region extended over a region greater than 0.1-10% strain (Figure 3.13) thus, it was decided that the temperature sweep should be carried out at 1 Hz and 1% strain as this was in the centre of the LVE region.

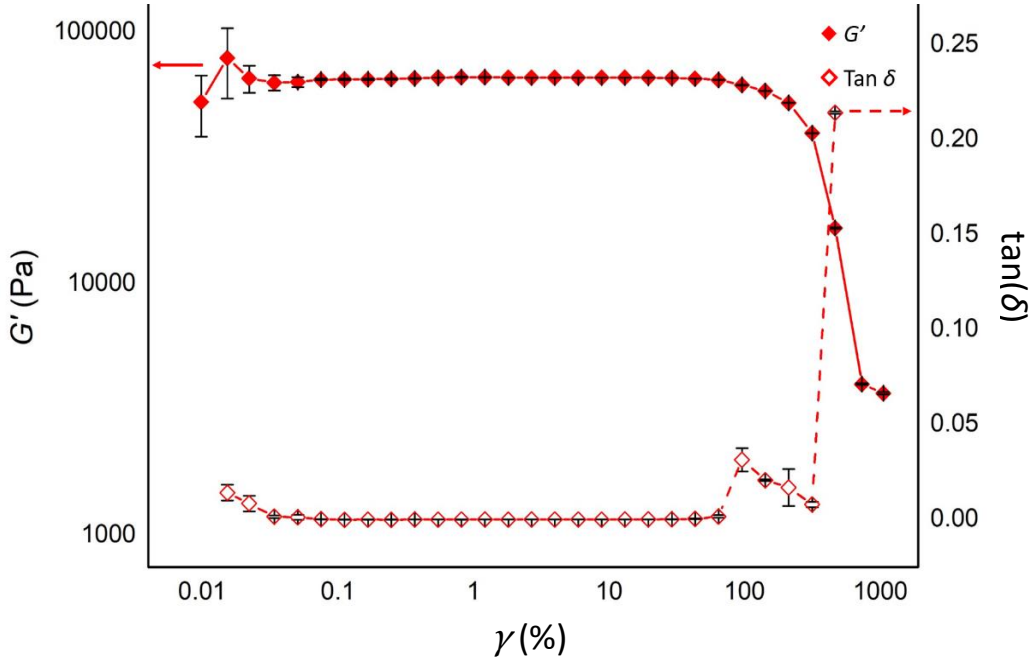



Figure 3.13. A strain sweep of $PLA_{11}$ showed that the LVE region extended from 0.01 to 100% strain. Error calculated as ±1 standard deviation from the mean. ($T$ = 20 °C).

Following the temperature sweep, it was decided that the rotational viscosity should be measured at 80 °C (Figure 3.14) as it was shown to be the onset temperature of the glass transition.

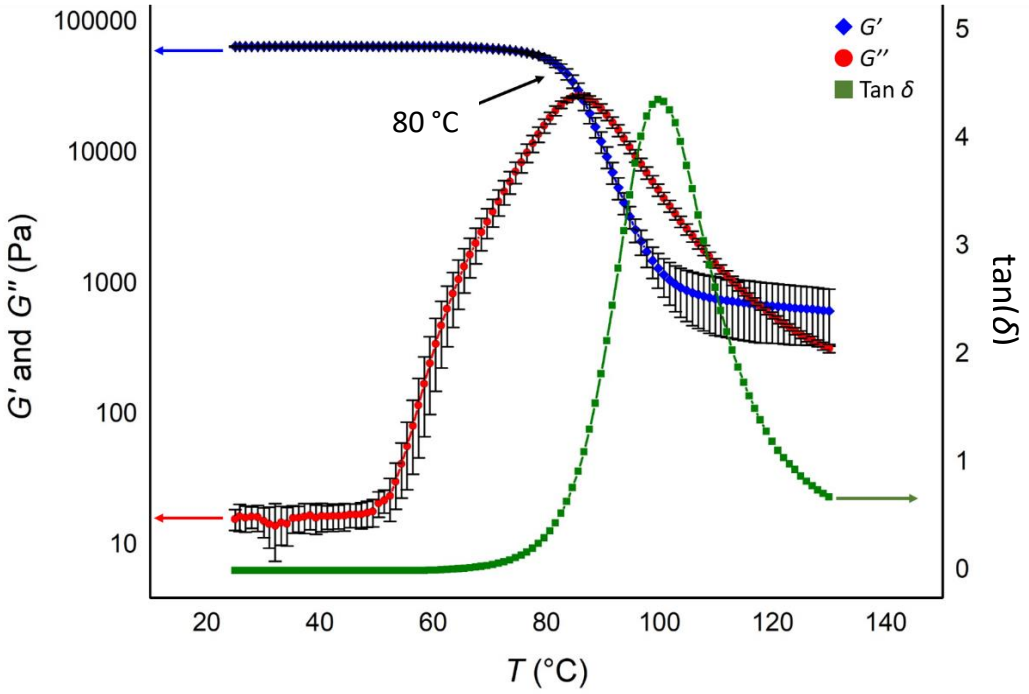



Figure 3.14. Storage modulus (*G'*, blue), loss modulus (*G''*, red) and tan(*δ*) (green) of $PLA_{11}$ were measured as temperature was increased from 25 to 140 °C at a constant strain and frequency of 1% and 1Hz respectively. Error calculated as ±1 standard deviation from the mean.

### 3.6.2.2 Rotational Measurements

Rotational measurements were used to determine viscosity and for each sample three consecutive measurements were made.

#### 3.6.2.2.1 Recovery Tests

In order to perform sequential measurements of one sample, knowledge about sample recovery was required. Therefore, recovery tests were implemented by plotting viscosity against time to determine how long the polymer took to recover its initial viscosity, and therefore how much time was needed between each measurement. These tests showed that the samples recovered sufficiently within 20 seconds of returning to low shear. To ensure full sample recovery all sequential measurements were performed with a 1 minute delay at 1 $s^{-1}$ shear in between (Figure 3.15).

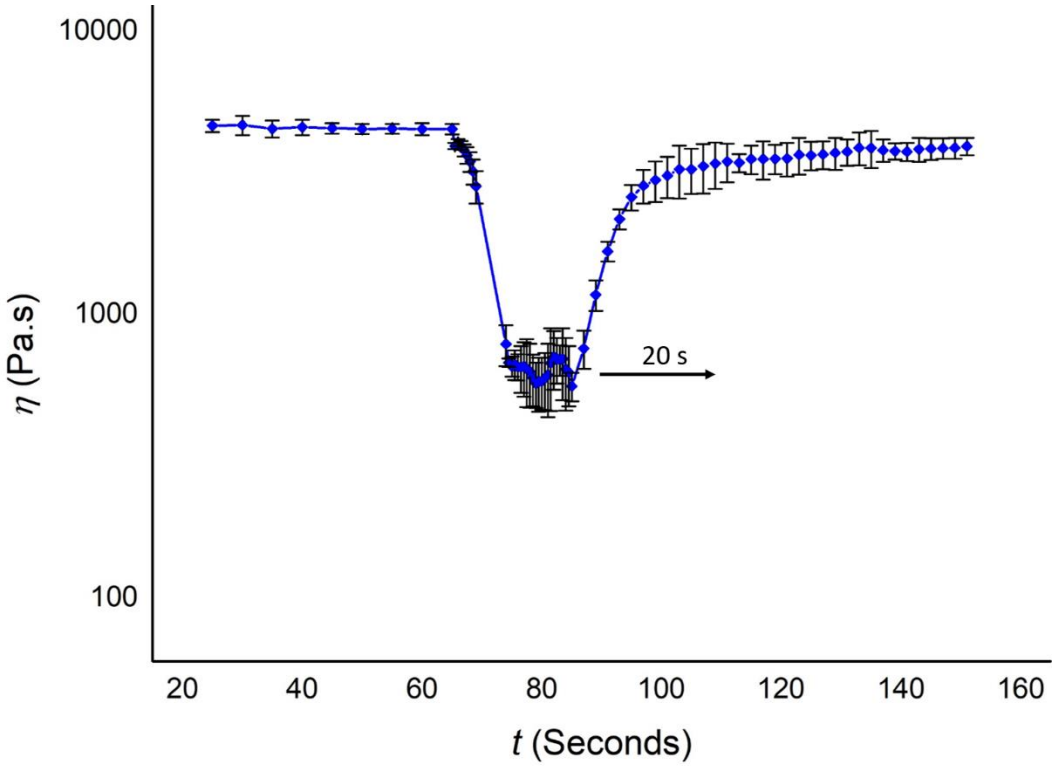



Figure 3.15. Recovery test showed that the viscosity of $PLA_{11}$ recovered sufficiently after 20 seconds of returning to low shear rates. Error calculated as ±1 standard deviation from the mean. ($T$ = 80 °C).

#### 3.6.2.2.2 Viscosity at 140 bar and 80 °C

The viscosity was first measured at ambient pressure after 1 hour soaking at 80 °C and fitted to the Carreau model (Figure 3.16 blue squares) giving a $\eta_0$ of 6800 Pa.s. The sample was then exposed to 140 bar $CO_2$ and the viscosity measured periodically over 18 hours as described in section 3.5.1. At 80 °C and in the presence of 140 bar $CO_2$ $PLA_{11}$ had a $\eta_{sat}$ of 1.2 Pa.s (Figure 3.16). The observed decrease in viscosity for the amorphous $PLA_{11}$ (>99%) was significantly larger than that of the semi-crystalline $PCL_{112}$ (86%). This was because the $CO_2$ could interact more favourably with the carbonyl rich backbone of the $P_{D,L}LA$ resulting in greater penetration, and therefore a greater increase in free volume. Along with the larger molecular weight, the long hydrocarbon backbone of the $PCL_{112}$ hindered the interaction of the $CO_2$ reducing its plasticising effect (Figure 3.4). In addition, the viscosity of $PCL_{112}$ was measured at a higher temperature, which reduced the solubility of $CO_2$ in the polymer and so reduced its plasticising effect. It should be noted that for low viscosity samples, such

as those measured in the presence of $CO_2$, the torque at low shear rates was less than the lower limit of the instrument and hence the viscosity could not be measured.

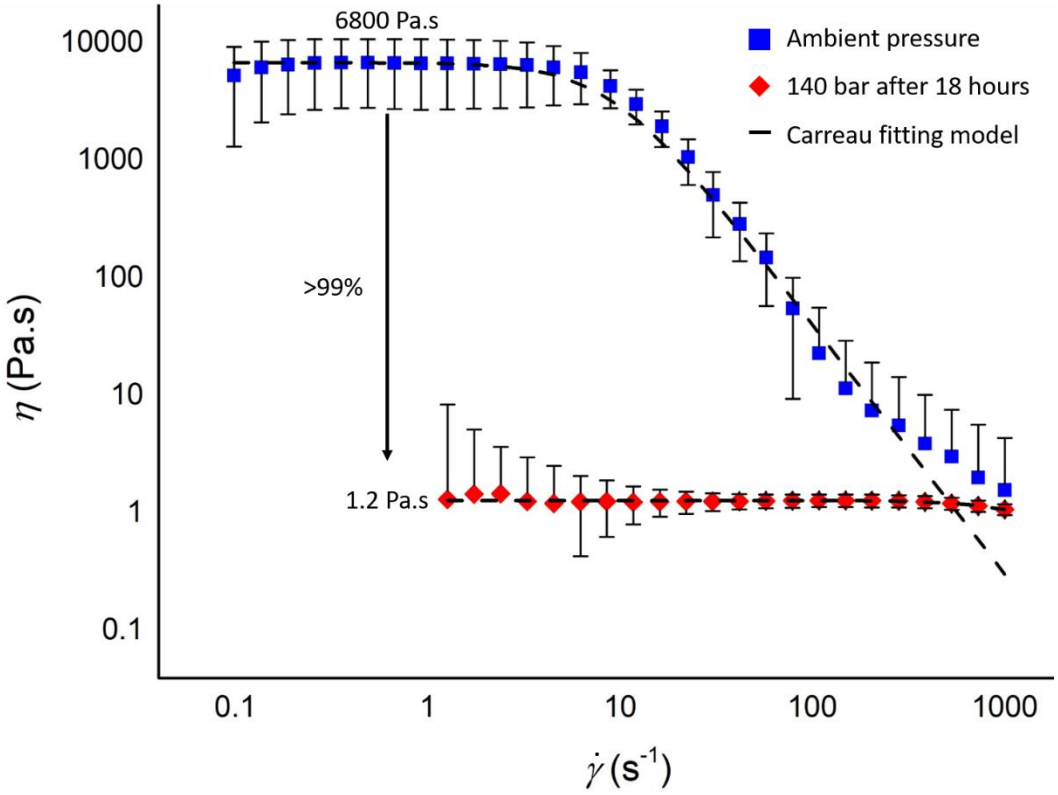



Figure 3.16. Comparison of the viscosity of $PLA_{11}$ at ambient pressure (blue squares) and 140 bar $CO_2$ (red diamonds) showed a substantial decrease with the addition of $CO_2$. Error calculated as ±1 standard deviation from the mean. ($T$ = 80 °C).

The viscosity in the presence of high pressure $CO_2$ was measured and the time to saturation fitting model applied to the data (Figure 3.17). It took approximately 5 hours for the $PLA_{11}$ to achieve $\eta_{sat}$; this was much longer than the 20 minutes required for the $PCL_{112}$ to become saturated. This could be because PCL was semi-crystalline and at measurement temperature (90 °C) was in a liquefied state. Therefore, despite the longer chain lengths there were no entanglements to prevent $CO_2$ penetration. On the other hand, $PLA_{11}$ was an amorphous polymer, which even at elevated temperatures consisted of entangled polymer chains that can delay the absorption of $CO_2$.

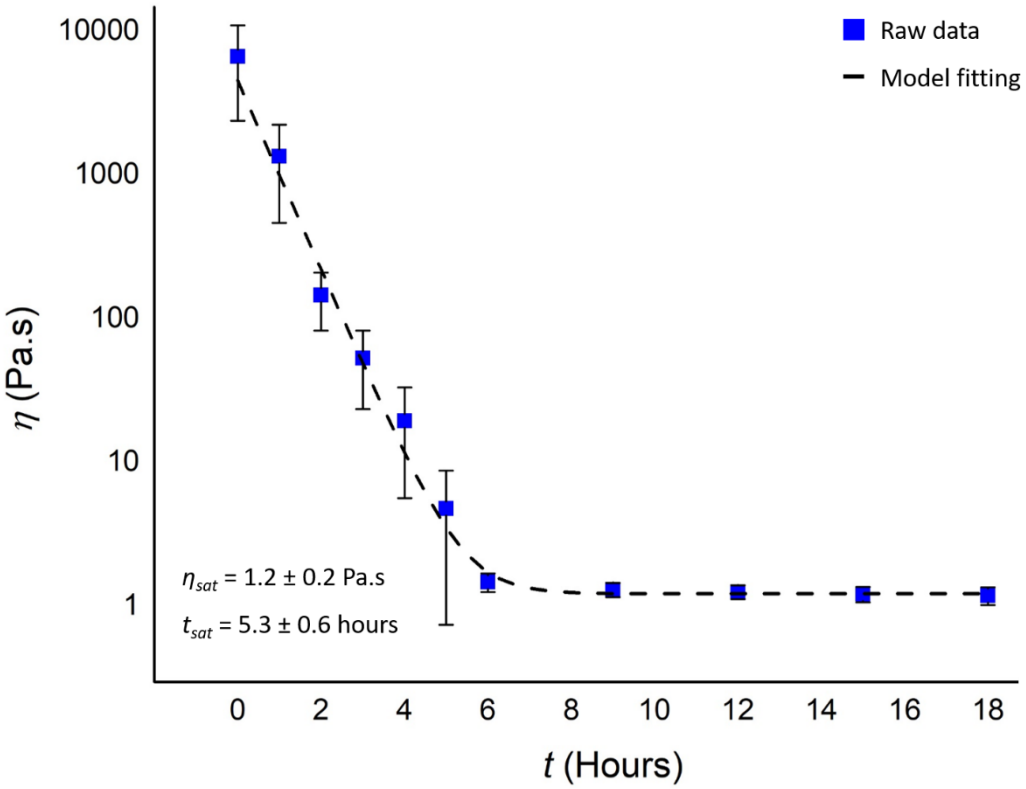



Figure 3.17. Viscosity vs time profile for $PLA_{11}$ showed that saturation viscosity ($\eta_{sat}$) was achieved after a saturation time ($t_{sat}$) of approximately 5 hours. Error calculated as ±1 standard deviation from the mean. ($T$ = 80 °C).

#### 3.6.2.2.3 Viscosity After Venting

Previous literature reports have indicated that the use of $CO_2$ for processing of polymers has no residual or long lasting effects on the polymers.[131,155] This was investigated via rheology by venting the samples over 20 minutes with constant shear and repeating the ambient pressure measurements. After venting, it was clear that the viscosity of the polymer had recovered in agreement with the literature (Figure 3.18).[131,155]

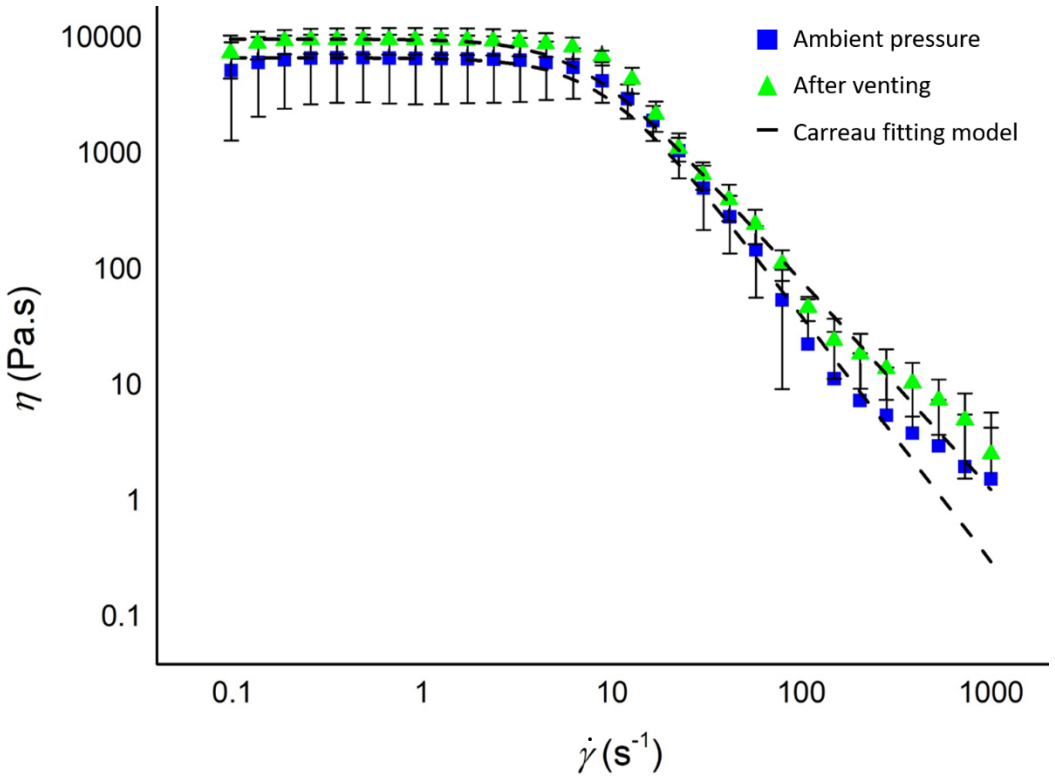



Figure 3.18. Comparison of the viscosity of $PLA_{11}$ before and after exposure to $CO_2$ showed that the viscosity had fully recovered and the use of $CO_2$ was completely reversible. Error calculated as ±1 standard deviation from the mean. ($T$ = 80 °C).

These experiments showed that this method of measuring the viscosity of polymers at ambient pressure and in the presence of $CO_2$ was robust, reliable and reproducible. However, the aim of this thesis is to measure the rheology of a formulation containing a thermally sensitive API and 80 °C could potentially damage protein or peptide based APIs. Typically, a protein will denature at temperatures above physiological conditions, therefore, the next step of this work was to develop a method to measure the viscosity at 40 °C, which will be less detrimental to the integrity of the APIs.

## 3.6.3 Rheology at 140 bar and 40 °C

### 3.6.3.1 $PLA_{11}$

$PLA_{11}$ was supplied as a voluminous powder and required melting in the measurement cell in order to load the correct amount of material. Hence, the sample had to be heated to 80 °C and allowed to equilibrate before being cooled to 40 °C for the lower temperature measurements. It was not possible to perform the ambient

pressure measurements at 40 °C because the sample was effectively still solid (Figure 3.14). Thus, the sample was pressurised with $CO_2$ and allowed to soak under oscillatory mode (1% strain and 1 Hz) to monitor the absorbance of the $CO_2$ (Figure 3.19). After 30 hours the storage modulus (*G'*) began to decrease while the loss modulus (*G''*) increased, indicating that the polymer was transforming from a rigid solid structure into a more liquid like state as the $CO_2$ caused it to plasticise. Eventually, the moduli plateaued out showing the end of the transition where the sample was saturated with $CO_2$. Although *G'* had been significantly reduced it remained greater than *G''* which meant that the polymer was not in the fully liquid state and retained some rigidity (see Chapter 2).

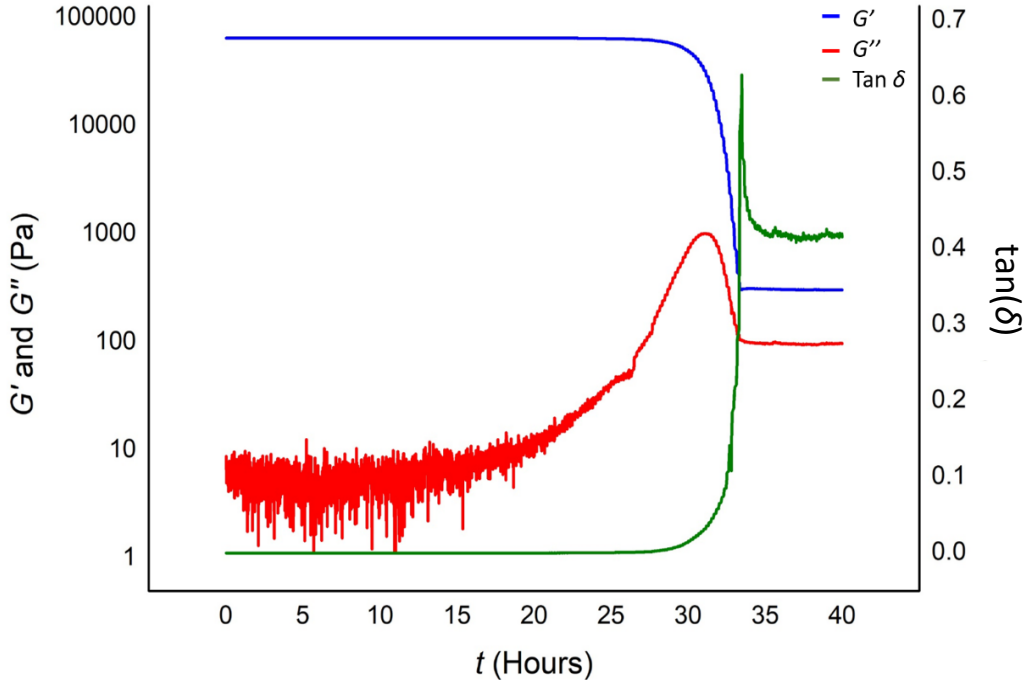



Figure 3.19. Oscillatory measurement of $PLA_{11}$ during the 40 hour soak in 140 bar $CO_2$ showed the plasticisation onset after 30 hours soaking. ($T$ = 40 °C).

Directly following the 40 hour soak, the rotational mode was employed to measure the viscosity and this was compared to the viscosity at 80 °C. The decrease in temperature resulted in a minimal increase in viscosity from 1.2 Pa.s at 80 °C to 1.5 Pa.s at 40 °C (Figure 3.20).

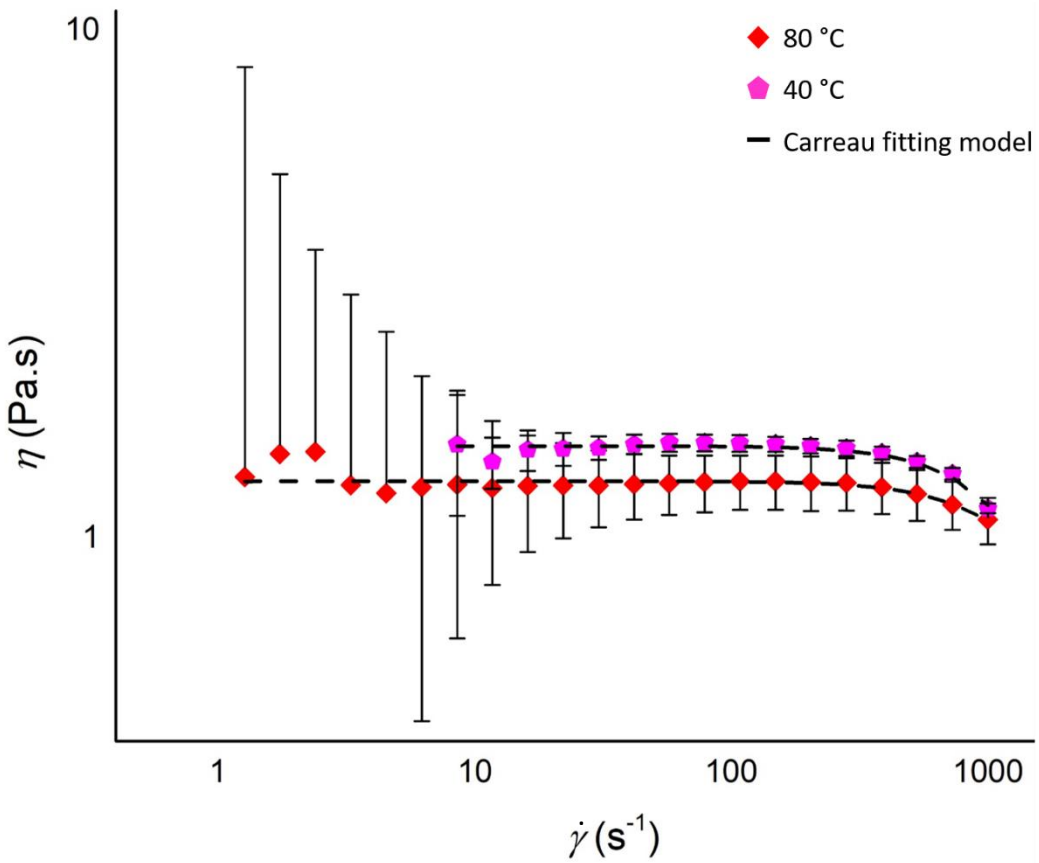



Figure 3.20. Comparison of the viscosity of $PLA_{11}$ at 80 °C (red diamonds) and 40 °C (pink pentagons) in the presence of 140 bar $CO_2$. Error calculated as ±1 standard deviation from the mean.

However, because of the initial 80 °C melting step, this method of sample preparation was still not suitable for thermally sensitive APIs and so it was necessary to use a different grade of polymer, which would enable loading of the measurement cell without preheating. A $P_{D,L}LA$ with a similar molecular weight to $PLA_{11}$ but a different D:L lactide ratio and a PLGA were found to be suitable for rheology measurements without preheating. These polymers had been manufactured differently and were more dense and granular in comparison with the $PLA_{11}$. Hence, they could be loaded into the measurement cell without heating to form a disc. A comparison of the polymers is presented in Table 3.3.

Table 3.3. Characteristics of the polymers used in this section compared to the $PLA_{11}$ used initially.

| Polymer | $M_n$[a] (g/mol) | $M_w$[a] (g/mol) | $Đ$[a] | $T_g$[b] (°C) |
|---|---|---|---|---|
| $PLA_{11}$ | 7000 | 11,000 | 1.649 | 49 |
| $PLA_{12}$ | 7000 | 12,000 | 1.620 | 44 |
| $PLGA_{36}$ | 24,000 | 36,000 | 1.510 | 47 |

a) Measured by triple detection GPC in THF using dn/dc value of 0.042 mL/g.[167] b) Measured by DSC.

### 3.6.3.2 Direct measurements

The new polymers were loaded into the rheometer, and their viscosities measured at 40 °C and 140 bar $CO_2$ over 18 hours, following the procedure as described in section 3.5.1.2.3.

It was expected that as the temperature decreased, the viscosity would increase. Hence, the viscosity was also measured at 40 °C and 140 bar after cooling from 80 °C to determine whether the increase in viscosity was consistent over the two methods. However, the viscosity of the $P_{D,L}LA$ measured at 40 °C after cooling from 80 °C did not exhibit a significant increase compared to the viscosity measured at 80 °C (Figure 3.21). In addition to this, the viscosity measured directly at 40 °C and 140 bar $CO_2$ was higher than that of the viscosity measured after cooling, with this observation being more pronounced for the $PLGA_{36}$ (Table 3.4). This could be down to a combination of the increased molecular weight of the $PLGA_{36}$ and its reduced ability to absorb $CO_2$ due to the reduced number of methyl groups along the polymer chain reducing the available free volume (Figure 3.4).

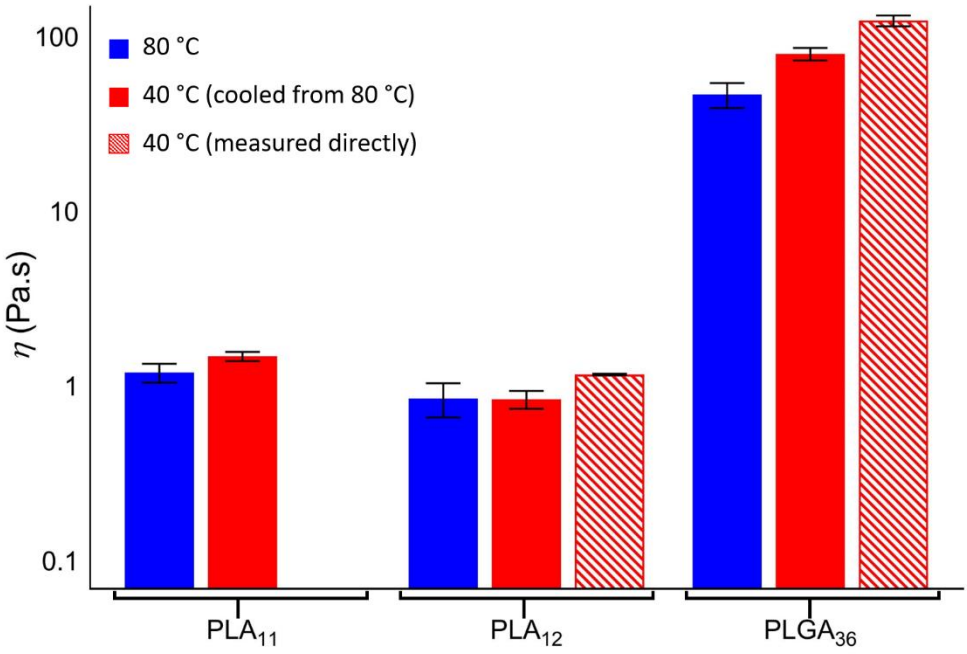



Figure 3.21. Comparison of the viscosities measured at 140 bar $CO_2$ at 80 °C (blue) and 40 °C (red). The viscosity measured at 40 °C after cooling from 80 °C (block red) was lower than that measured directly at 40 °C (red stripes) suggesting that this was not a viable method. Error calculated as ±1 standard deviation from the mean.

Table 3.4. Comparison of the viscosities measured at 140 bar $CO_2$ and different temperatures and methods.

| Polymer | $\eta_{sat}$ at 80 °C (Pa.s) | $\eta_{sat}$ at 40 °C cooled from 80 °C (Pa.s) | $\eta_{sat}$ measured directly at 40 °C (Pa.s) | % increase from cooled to direct measurement |
|---|---|---|---|---|
| $PLA_{11}$ | 1.2 | 1.5 | - | - |
| $PLA_{12}$ | 0.86 | 0.85 | 1.2 | 39 |
| $PLGA_{36}$ | 47 | 81 | 125 | 55 |

This was investigated further using the case of the PLGA. Initially, it was thought that cooling had not expelled the $CO_2$ from the polymer melt sufficiently, supressing the viscosity. Hence, the sample was left to equilibrate for 52 hours after cooling from 80 °C to 40 °C. However, although the viscosity had increased in comparison with the viscosity at 80 °C, even after this time it had not recovered to match the viscosity achieved directly at 40 °C (Figure 3.22).

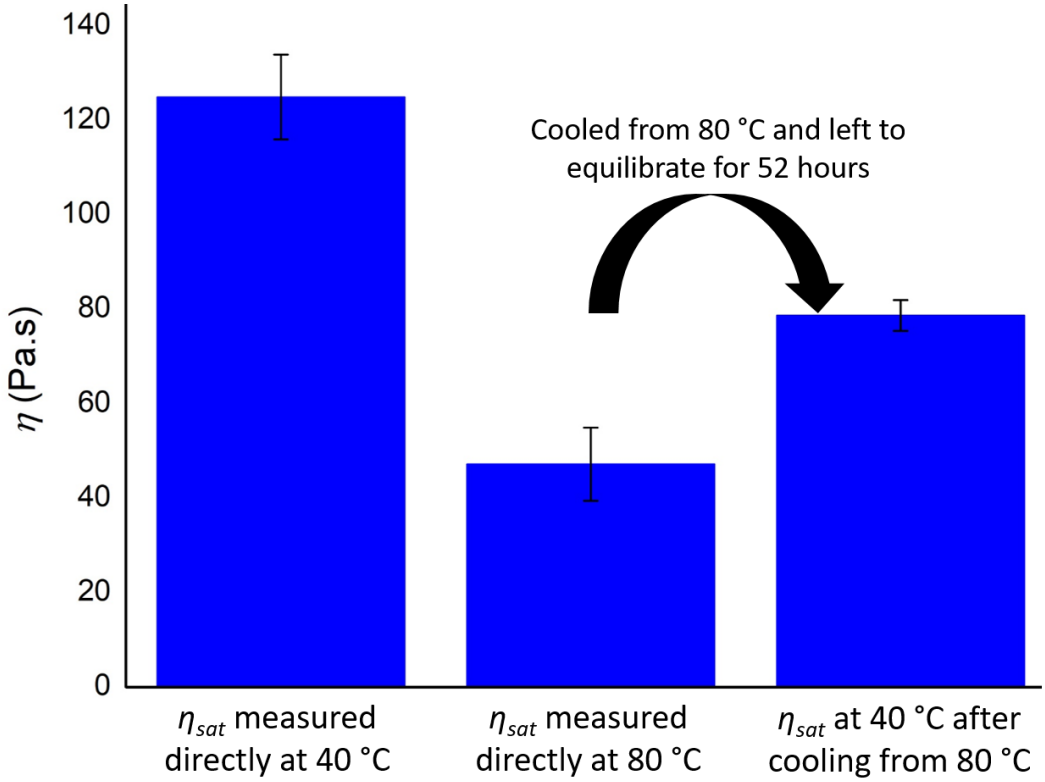



Figure 3.22. Comparison of the viscosity of $PLGA_{36}$ measured directly at 40 °C and 80 °C, and at 40 °C after cooling from 80 °C and equilibrating for 52 hours. ($P$ = 140 bar) Error calculated as ±1 standard deviation from the mean.

It was then considered that the PLGA was degrading as a consequence of the long measurement times at elevated temperature possibly exacerbated by the potential presence of water from the $CO_2$. GPC analysis revealed that after the measurements at 80 °C the PLGA had indeed suffered a reduction in molecular weight ($M_w$); from 36,000 g/mol to 30,000 g/mol. Given that viscosity scales with molecular weight it is possible that this could account for the reduced viscosity at 40 °C after cooling from 80°C. The scale factor for a pair of polymers can be determined from equation 3.6. For $PLGA_{36}$, $n$ = 2.9 which is comparable to the expected scale factor for an entangled polymer; $\eta \propto M^{3.4}$.[180]

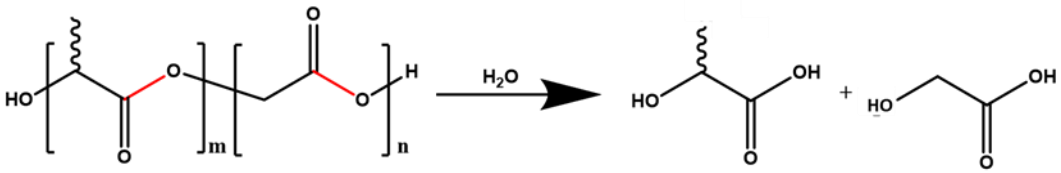
$$n = \frac{\log \eta_1 - \log \eta_2}{\log M_1 - \log M_2} \qquad 3.6$$

This data confirmed that cooling from 80 °C to 40 °C was not a viable method of measuring the viscosity at these conditions. Therefore, it is necessary to select polymers that are suitable for the measurement parameters that are being

employed. Henceforth, for all measurements performed at 40 °C and 140 bar $CO_2$ these polymers ($PLA_{12}$ and $PLGA_{36}$) were used instead of the $PLA_{11}$ because these polymers did not require heating prior to the measurement.

### 3.6.4 Characterisation of the Polymers Before and After Rheology

Now that a reliable and reproducible high pressure rheology method had been developed for the measurement of polymer melt viscosity, it was necessary to confirm that this method had no detrimental effects on the polymers. For example, as the polymers were kept at high temperatures for a long time they could undergo thermal degradation. In addition, the Food grade $CO_2$ used for these experiments contained water which can result in hydrolysis of the polymers (Scheme 3.1). The polymers were characterised before and after the rheology measurements using GPC, $^1$H NMR and DSC (Table 3.5).




Scheme 3.1. Hydrolysis of PLGA, the red bonds indicate the ester bonds that will be broken.

Table 3.5. Characterisation of the polymers before and after rheology.

| Polymer | Conditions | GPC[a] | | | NMR[b] | | DSC[c] |
|---|---|---|---|---|---|---|---|
| | | $M_n$ (g/mol) | $M_w$ (g/mol) | $Đ$ | Mol.% Lactide | $M_n$ (g/mol) | $T_g$ (°C) |
| $PLA_{11}$ | Before | 7,000 | 11,000 | 1.6 | - | 5,000 | 48 |
| | After 80 °C | 9,000 | 12,000 | 1.3 | - | 3,000 | 46 |
| $PLA_{12}$ | Before | 7,000 | 12,000 | 1.6 | 3 | 7,000 | 44 |
| | After 40 °C | 8,000 | 12,000 | 1.6 | 2 | 8,000 | 46 |
| | After 80 °C | 7,000 | 10,000 | 1.4 | 2 | 6,000 | 44 |
| $PLGA_{36}$ | Before | 24,000 | 36,000 | 1.5 | 3 | 14,000 | 46 |
| | After 40 °C | 20,000 | 35,000 | 1.7 | 2 | - | 45 |
| | After 80 °C | 19,000 | 30,000 | 1.6 | 2 | 11,000 | 47 |

a) Measured using triple detection GPC with a dn/dc value of 0.042 mL/g.[167] b) Calculated from $^1$H NMR in $CDCl_3$. c) Determined by DSC, values taken from the second heating scan.

#### 3.6.4.1 GPC

Characterisation of the $PLA_{12}$ and the $PLGA_{36}$ after the rheology measurements at 80 °C showed a small reduction in $M_w$, while the molecular weight was maintained after the measurements at 40 °C (Figure 3.23a and b, respectively). Conversely, $PLA_{11}$ appeared to maintain its molecular weight even after the measurement at 80 °C (Figure 3.23c). These temperatures are very low for thermal degradation but it is thought that the water present in the $CO_2$ could accelerate any degradation via hydrolysis of the ester bonds given that the experiments were performed over a long time. PLA is known to degrade more slowly than PLGA because of the steric hindrance afforded by the increased number of methyl groups on the polymer backbone and its increased hydrophobicity (Figure 3.4). Therefore, the reduction in molecular weight for $PLA_{12}$ was negligible. However, the reduction observed for $PLGA_{36}$ was more significant and could result in reduced viscosity as described in Section 3.6.3.2. Hence, viscosity measurements at 80 °C can be performed on PLA without detrimental effects, but should be avoided for $PLGA_{36}$.

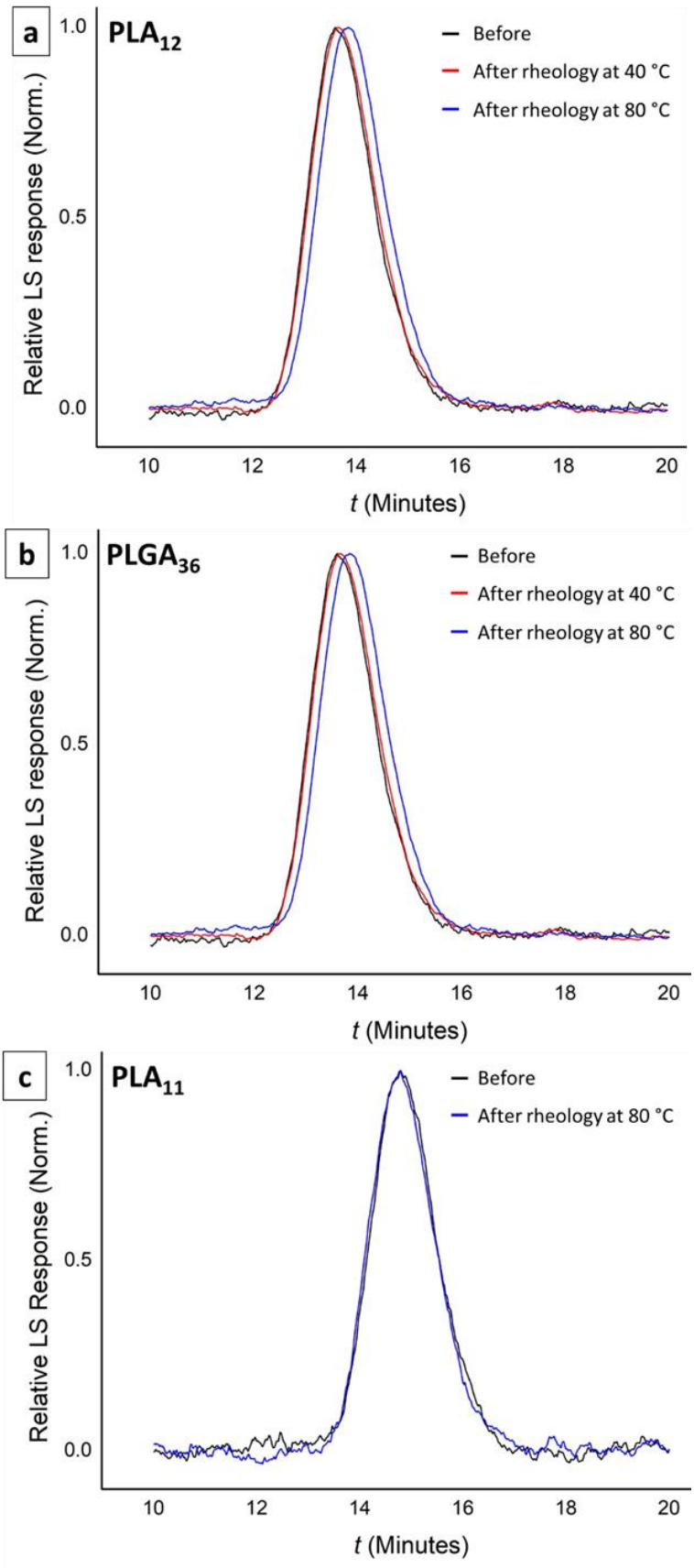



Figure 3.23. GPC traces of the polymers before and after the rheology measurements. A shift to higher retention time (a and b after rheology at 80°C) indicated a reduction in $M_w$.

### 3.6.4.2 $^{1}$H NMR

By comparing the lactide signal at ~5.0 ppm with the methine signal at ~5.2 ppm the mol.% of residual lactide monomer was approximated (equation 3.3). Following the rheology measurements the amount of lactide monomer present was reduced slightly (Table 3.5). As the monomer is soluble in $CO_2$ under certain conditions, it is possible that a small quantity was removed upon venting of the system. It was not possible to detect any residual monomer in $PLA_{11}$.

The $M_n$s of the $P_{D,L}LA$s were calculated from the $^{1}$H NMR following equation 3.4. Where the integral of the resonance corresponding to the methine on the polymer backbone ($\delta$ ~5.2 ppm) was compared to the integral of the resonance of the PLA end group ($\delta$ ~4.4 ppm). The $M_n$ of the $PLGA_{36}$ was calculated according to equation 3.5, where the $M_n$ of the lactide portion was added to the glycolide. Hence, the integral of the resonance corresponding to the PGA backbone ($\delta$ ~4.8 ppm) was compared to that of the PLA end group. In accordance with the GPC, small reductions in $M_n$ were observed after the measurements at 80 °C, showing some degradation (Table 3.5).

### 3.6.4.3 DSC

Thermal transitions of the polymers were determined from the second heating scan of the DSC traces. The $T_g$ was determined using the TA Universal Analysis software and taken as the mid-point of the transition (Figure 3.24). All samples had $T_g$'s in the range of 44-48 °C and showed very little variation after the rheology measurements, in accordance with the GPC and $^{1}$H NMR data and as expected with such small changes in $M_w$ (Table 3.5).

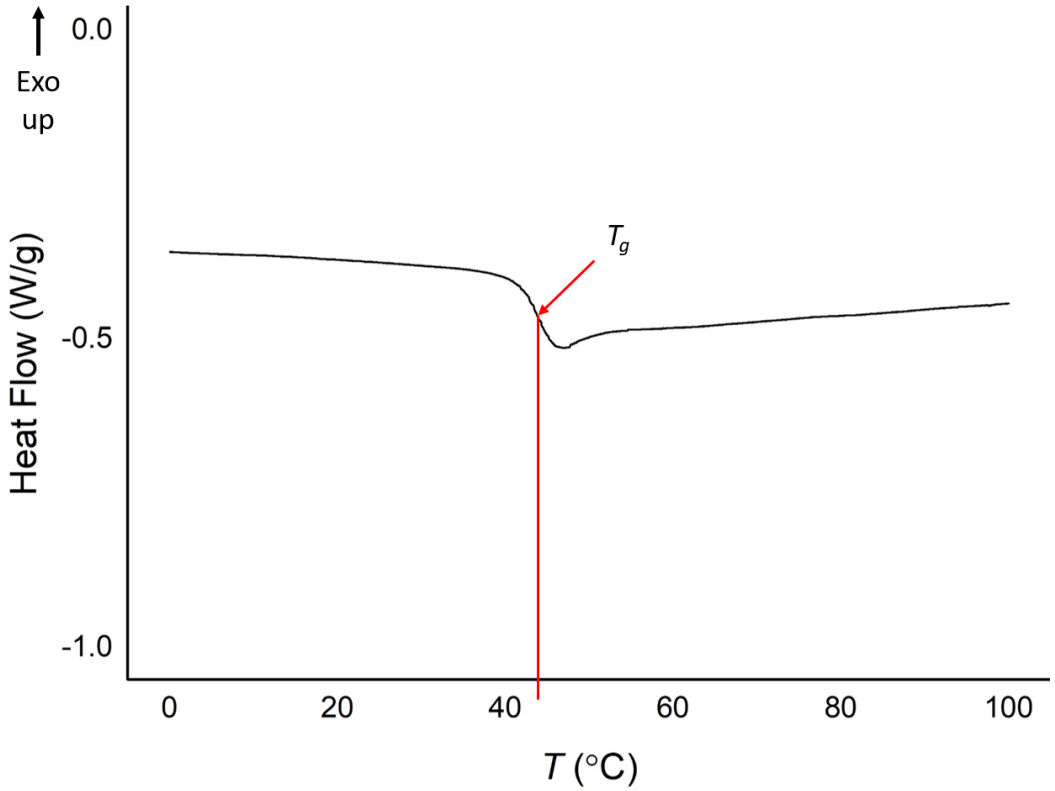


Figure 3.24. Typical DSC trace of an amorphous polymer (specifically $PLA_{12}$).

## 3.7 Summary

The aim of this chapter was to develop a robust and reliable high pressure rheology method that could be implemented throughout the remainder of this thesis, enabling the quantification of polymer melt viscosity at various conditions.

The viscosity of semi-crystalline PCL was assessed following a previously established protocol.[131] This was found to be insufficient to fully describe the viscosity profile of a high molecular weight polymer in the presence of $CO_2$ (Figure 3.10). In the previous work reported by Curia et al.[131] the PCL reached $\eta_{sat}$ after 50 minutes of soaking. However, in the current work a further drop in viscosity was observed during sequential measurements performed after the initial 50 minutes. Hence, a new measurement profile was developed which measured the viscosity at regular intervals during exposure to $CO_2$. Once these data had been fitted to the Carreau Model, the $\eta_0$ values were plotted against time. Furthermore, fitting these data to an empirical formula provided approximate values for $\eta_{sat}$ and $t_{sat}$ (Figure 3.12). In the current study, $PCL_{112}$ was found to have an $\eta_0(p_{amb})$ of 35,000 Pa.s, a $\eta_{sat}$ of

4600 Pa.s and a $t_{sat}$ of 0.35 hours. By analysing the data using these models, it was possible to eliminate some uncertainty associated with arbitrary data selection. The new method of measuring viscosity in the presence of $CO_2$ also highlighted the effect of shear on the absorption time of $CO_2$ into the samples. Initial studies suggested that 50 minutes was not long enough to allow complete saturation of the sample with $CO_2$. However, the new method, in which the sample was sheared during the soaking periods, revealed that only 20 minutes was required for the sample to reach saturation.

Next, this method was applied to the viscosity analysis of an amorphous $P_{D,L}LA$ widely investigated for use in drug delivery systems. Prior to measuring the rotational viscosity of the new polymer, it was necessary to determine the optimal measuring temperature. Following a series of oscillatory measurements, a temperature of 80 °C was found to be suitable for measurements at both ambient pressure and in the presence of $CO_2$ (Figure 3.14). Thus, the aforementioned method was employed at 80 °C for the viscosity analysis of $PLA_{11}$ giving a $\eta_0(p_{amb})$ of 6800 Pa.s, a $\eta_{sat}$ of 1.2 Pa.s and a $t_{sat}$ of 5.3 hours (Figure 3.16 and Figure 3.17). The polymer viscosity was also quantified after the removal of the $CO_2$ to certify that the effect of $CO_2$ on the polymer viscosity was reversible (Figure 3.18). In accordance with literature reports, the viscosity recovered after $CO_2$ exposure, confirming that this was a viable technique for the quantification of the effect of $CO_2$ on polymer melt viscosity.

Ultimately, the aim of this thesis is to assess the effect of APIs on polymer melt viscosity by measuring the viscosity of formulations containing APIs. For this to be a viable tool for use in industry this method must be suitable for use with thermally sensitive APIs. Therefore, a secondary method was developed to measure the viscosity at lower temperatures, specifically 40 °C, which would be less detrimental to the integrity of the APIs. Initial studies were performed using $PLA_{11}$ but it soon became apparent that the polymer itself was not suitable for such measurements. As the polymer was supplied as a voluminous powder, it required melting in order to load the correct amount of material. The initial melting could only be achieved at temperatures above 80 °C and so measurements could not be made directly at 40 °C or with thermally sensitive APIs present. Consequently, a $P_{D,L}LA$ with a similar

molecular weight ($PLA_{12}$) was sourced along with a PLGA ($PLGA_{36}$). These polymers had been manufactured differently so were more granular and could be loaded into the measurement cell without heating. Ambient pressure measurements at 40 °C were still not possible with these polymers but the desired conditions of 40 °C and 140 bar $CO_2$ could be accessed directly. Once the system was at measurement conditions the now standard soaking procedure was followed giving $\eta_{sat}$ values of 1.2 Pa.s for $PLA_{12}$ and 125 Pa.s for $PLGA_{36}$. For completion, the viscosity of all three polymers at 40 °C and 140 bar was also measured after cooling from 80 °C and the values compared. It was clear from Table 3.4 that cooling from 80 °C was not a viable method for achieving measurements at lower temperatures, as there were significant differences between the results from the two methods. This could be because the polymers were degrading slightly, as demonstrated with $PLGA_{36}$ where the molecular weight had decreased after the measurement at 80 °C accounting for the reduced viscosity at 40 °C.

It was also necessary to confirm that these methods had no detrimental effects on the polymers. For example, as the polymers were kept at high temperatures for a long time they could undergo thermal degradation. Therefore, the polymers were characterised before and after the rheology measurements using GPC, $^1$H NMR and DSC. Although small variations were detected in the characteristics of the polymers, these were not found to be significant for the $P_{D,L}LAs$ (Table 3.5). The $PLGA_{36}$ was more sensitive to degradation especially after measurements performed at 80 °C and so shall only be used for low temperature measurements.

## 3.8 Conclusions

In conclusion, two robust and reliable high pressure rheology methods have been developed to measure the viscosity at two different temperatures (80 °C and 40 °C). Both methods were found to be non-detrimental to the polymers and were used throughout this thesis to produce comparable viscosity data. Chapter 4, utilises the method at 80 °C to assess the effect of a combination of $CO_2$ and poly(ethylene glycol) (PEG) on the viscosity of $PLA_{11}$. Following this, the method at 40 °C will be employed in Chapter 5 to analyse the viscosity of formulations containing APIs.

# Chapter 4

## Effect of PEG and Dense Phase $CO_2$ on the Viscosity of Poly($_{D,L}$-lactic acid) Melts

## 4.1 Abstract

The processing of thermoplastic polymers generally involves very high temperatures, pressures or the presence of volatile organic solvents (VOCs) in order to overcome the high viscosity of the polymer melt. However, these processing conditions are not suitable for the incorporation of thermally labile active pharmaceutical ingredients (APIs) in biodegradable polymers, such as the encapsulation of drugs in poly($_{D,L}$-lactide) ($P_{D,L}LA$). Therefore, new methods of reducing viscosity without the use of high temperatures or VOCs are being investigated. Both poly(ethylene glycol) (PEG) and $CO_2$ are approved excipients in drug delivery and it is well established that both can individually reduce the viscosity and the glass transition temperature ($T_g$) of $P_{D,L}LA$. This chapter investigates if further benefits arise from a combination of PEG and $CO_2$.

The robust and reliable high pressure rheology method, which was developed for the analysis of polymer melt viscosities (Chapter 3), is used to assess the effect of PEG on the viscosity of $P_{D,L}LA$ in combination with dense phase $CO_2$. This chapter also explores other benefits arising from the use of both PEG and $CO_2$ as potential processing aids, such as reduced processing times.

By investigating PEG as a blended excipient, the effect of increasing PEG content on the viscosity of $P_{D,L}LA$ is determined. Subsequently, the effect of covalently linking PEG to $P_{D,L}LA$ in a PEG-*b*-$P_{D,L}LA$ block copolymer is studied, exploring both the influence of the overall molecular weight of the block copolymer and the molecular weight ratios of the blocks. Ultimately, the impact of the mode of introducing the PEG on the viscosity of the $P_{D,L}LA$ is compared.

A summary of this work can be found in the article:

K.J. Pepper, T. Masson, D. De Focatiis, S.M. Howdle, *Can a combination of poly(ethylene glycol) and dense phase carbon dioxide improve processing of polylactide? A high pressure rheology investigation,* The Journal of Supercritical Fluids, (2018) 133, 343–348. doi:10.1016/j.supflu.2017.10.014.

# 4.2 Contents

Chapter 4 ..... 4-101

4.1 Abstract ..... 4-102

4.2 Contents ..... 4-103

4.3 Introduction ..... 4-104

4.4 Materials ..... 4-106

4.5 Methods ..... 4-107

4.5.1 Polymer Synthesis ..... 4-107

4.5.2 Polymer Characterisation ..... 4-109

4.5.3 Rheological Measurements ..... 4-110

4.6 Results and Discussion ..... 4-112

4.6.1 Polymer Synthesis ..... 4-112

4.6.2 Viscosity Analysis ..... 4-118

4.7 Summary ..... 4-129

4.8 Conclusions ..... 4-130

## 4.3 Introduction

In order to process thermoplastic polymers it is often necessary to reduce the high viscosity of the polymer melt. Typically, this is done using extremely high temperatures and pressures (up to 350 °C and 500 bar)[124] for methods such as extrusion or injection moulding. Alternatively, VOCs can be used to produce low viscosity solutions allowing the use of lower temperatures for methods such as spray drying. However, both options have significant drawbacks such as high-energy costs or the need for extensive purification steps. Moreover, high temperatures and the use of VOCs are detrimental to the activity of APIs rendering these methods inapplicable for processing polymers for drug delivery.[71]

Plasticisers are usually small molecules which are used to facilitate the processing of high viscosity polymers,[73,181] by penetrating and disrupting the secondary intermolecular forces between polymer chains. This results in an increased free volume, and less energy is therefore required for molecular motion. The overall outcome is a decrease in $T_g$ and viscosity, which in turn allows for easier processing at lower temperatures. However, plasticizers remain in the final product, making them unsuitable when processing polymers for pharmaceutical applications, as they will be released into the body.

The use of PEG as a polymeric plasticiser for $P_{D,L}LA$ has long been established and documented in the literature.[30] As it is FDA approved for use in the body it is a particularly good candidate for use in drug delivery applications. In particular, PEG has been utilised in drug delivery devices to improve release profiles by introducing hydrophilic channels and enhancing the rate of diffusion of water in and out of microparticles.[24] Previously, studies have focused on investigating the effect of PEG on the viscosity of PEG/PLA blends. Work by Li *et. al*. showed that as the content of PEG in the blends increased, the viscosity decreased,[182] with similar observations reported throughout the literature.[183–187] However, in all these studies, the properties and characteristics are determined after blending and high temperatures are still required. This is problematic particularly when processing proteins or peptides. Another avenue of investigation is the mode of incorporation of PEG. Block

copolymers as drug delivery vehicles have been extensively investigated in the literature,[18,188–190] and in the past twenty years PEG derived block copolymers in combination with biodegradable PLA and PLGA have garnered particular interest.[18,31,191–196] Varying the block ratio and molecular weights of the polymers may have different effects on the viscosity and thus allow tailoring of the processing aids to specific purposes.[197]

Exceptional benefits of using block copolymers of PEG and PLA for pharmaceutical applications, such as improved hydrophilicity, degradation rates, crystallization, increased drug loading, reduced burst release and increased residence time of APIs have been reported.[191,198] Despite these advantages, the effect of copolymerisation on polymer processing parameters such as temperature and viscosity reduction leading to improved API dispersion, has not yet been investigated in detail.

As described in Chapter 1, $CO_2$ has been extensively investigated as a viable route to low temperature processing of polymers. It is well documented that $CO_2$ can effectively and significantly reduce the viscosity of a range of polymers from PE,[137] PP[139] and PS[128] to PEG,[136] PCL[131,138] and PLA.[130] It is especially promising as a processing aid since it is capable of reducing the thermal transitions and viscosity without the use of solvents.[71,93] However, the viscosity of the polymer remains relatively high which impedes the efficient incorporation of active components, such as APIs, and thorough mixing of the components, ultimately impairing the final product properties.[111] Therefore, this chapter investigates whether the combination of PEG and dense phase $CO_2$ can overcome these challenges and further reduce the viscosity and required processing temperatures of $P_{D,L}LA$. To investigate this a high pressure rheometer was employed.

Polymer blends have been investigated using rheology at ambient pressure for many years with an early review dating back to 1982.[199] A more recent review explores the importance of using rheology to investigate polymer properties for processing.[200] Various characteristics of polymer blends have been studied such as phase transitions and morphologies of immiscible polymers,[201] as well as the viscoelastic properties and interactions of blended polymers.[202] In the past decade a plethora of research has focused on the melt rheology of polymer blends to provide vital

information for polymer processing optimisation.[182,203–209] Over the years several high pressure rheology techniques have been developed in order to assess the efficiency of $CO_2$ as a processing aid.[127,174–176,210] Some of the earliest experiments were performed using a high precision vibrating wire method reported by Gourgouillon.[136] Most recently Curia et al. investigated the effect of $CO_2$ on the viscosity of semi-crystalline PCL using a high pressure rotational rheometer.[131] In Chapter 3 of this thesis, the viscosity study of PCL is used as a basis for the development of the high pressure rheology method.

Despite PEG and $CO_2$ significantly reducing viscosity and processing temperature, the viscosity of the polymer melt remains sufficiently high that it inhibits complete mixing of the components of the formulation.[111] It is well established that both PEG and $CO_2$ can individually facilitate the processing of $P_{D,L}LA$, but are there further benefits to combining them? Using high pressure rheology, the viscosity of different molecular weight $P_{D,L}LA$ and PEG polymers at ambient pressure and in $CO_2$ is compared. Then the effect of PEG as a blended excipient at varying weight content is investigated. Subsequently, the effect of covalently linking the processing aid in a PEG-*b*-$P_{D,L}LA$ block copolymer is studied, exploring the impact of molecular weight and block ratios. Ultimately, the aim is to determine how the mode of introducing PEG affects the viscosity of the $P_{D,L}LA$.

## 4.4 Materials

$_{D,L}$-lactide (99%, Acros Organics) was stored at 2-8 °C. Benzyl alcohol (99.8%, Sigma Aldrich) and tin (II) 2-ethylhexanoate ($Sn(Oct)_2$) (> 92.5%, Sigma Aldrich) were stored at room temperature. Poly(ethylene glycol) methyl ether with molecular weight 5000 g/mol by GPC ($PEG_5$ Table 4.1) and poly(ethylene glycol) with molecular weight of 10,000 g/mol as given by the supplier ($PEG_{10}$ Table 4.1) were purchased from Sigma Aldrich and stored at room temperature. Amorphous poly($_{D,L}$-lactide) with molecular weight 11,000 g/mol by GPC was purchased from Evonik and stored at -20 °C ($PLA_{11}$ Table 4.1). The monomer, initiators and catalyst were dried at reduced pressure (room temperature vacuum oven, 100 mbar) over night before being used for the synthesis. The polymers, chloroform (Laboratory Reagent Grade,

Fisher Scientific), ethanol (Analytical Reagent Grade, Fisher Scientific), Food grade $CO_2$ (99.8%; BOC, UK) for the high pressure rheology experiments; and SFC grade $CO_2$ (99.99%; BOC, UK) for the synthesis, were all used as received.

THF (HPLC grade, Fisher Scientific) and deuterated chloroform, $CDCl_3$ (<99%, Sigma Aldrich) were also used as received. Synthesised products were stored at -20 °C.

Table 4.1. Details of purchased polymers used in this chapter.

| Polymer[a] | Description | $M_w$ (g/mol) | $T_g$[c] (°C) | $T_m$[c] (°C) |
|---|---|---|---|---|
| $PLA_{11}$ | Poly($_{D,L}$-lactide) | 11,000[b] | 50 | - |
| $PEG_5$ | Poly(ethylene glycol) methyl ether | 5000[b] | - | 59 |
| $PEG_{10}$ | Poly(ethylene glycol) | 10,000* | - | 61 |

a) Subscript numbers refer to the molecular weight (x$10^3$ g/mol) of the polymer. b) Measured by triple detection GPC in THF using dn/dc values of 0.042 and 0.067 mL/g for $P_{D,L}LA$ and PEG respectively. c) Measured by DSC. *Nominal molecular weight provided by supplier.

## 4.5 Methods

### 4.5.1 Polymer Synthesis

Polymers were synthesised via ring opening polymerisation (ROP) of $_{D,L}$-lactide with tin (II) 2-ethyl ethanoate ($Sn(oct)_2$) catalyst via conventional bulk methods and in $CO_2$ (Table 4.2). Benzyl alcohol was used as the initiator for the homopolymers while block copolymers were produced using a 5000 g/mol PEG methyl ether macroinitiator ($PEG_5$). All polymers were characterised according to the procedures detailed below.

Table 4.2. Molar ratios used for the synthesis of the $P_{D,L}LA$ homopolymer and the PEG-*b*-$P_{D,L}LA$ block copolymers.

| | Molar ratio | | | | Target $P_{D,L}LA$ $M_n$ (g/mol) |
|---|---|---|---|---|---|
| | $_{D,L}$-Lactide | $Sn(oct)_2$ | $PEG_5$ | Benzyl Alcohol | |
| $PLA_5100$ | 35 | 0.1 | - | 1 | 5040 |
| $PEG_5$-*b*-$PLA_5$ | 35 | 0.1 | 1 | - | 5040 |
| $PEG_5$-*b*-$PLA_{10}$ | 70 | 0.1 | 1 | - | 10080 |

Subscript number in polymer name refers to molecular weight (x$10^3$ g/mol) of the preceding block.

#### 4.5.1.1 Synthesis of $PLA_5$ via ROP in the Bulk

$_{D,L}$-lactide (3.00 g, 20.8 mmol), benzyl alcohol (66.6 mg, 0.614 mmol) and $Sn(Oct)_2$ (21.6 mg, 0.1 mol.% with respect to initiator) were weighed into a 50 mL round bottom flask and the reaction mixture was degassed with argon. The flask was submerged in a preheated oil bath at 120 °C and the reaction was left to proceed for 1 hour whilst stirring. The reaction was stopped by removing the flask from the oil bath and the reaction mixture dissolved in a minimal volume of chloroform. The solvent was subsequently removed under reduced pressure. A monomer conversion of typically 89% was determined by $^1$H NMR.

To remove the residual $_{D,L}$-lactide, the polymer was washed with an excess of ethanol (~50 mL). The resulting polymer was dried under vacuum overnight to remove any excess solvent, yielding a voluminous white powder. The purification process was repeated until <1% monomer remained (as quantified by $^1$H NMR). $^1$H NMR (400 MHz, Chloroform-*d*): δ (ppm) = 7.40 – 7.29 (m, 5H, C***H***), 5.30 – 5.10 (m, 1H, C***H***), 4.35 (q, 1H, HOC***H***($CH_3$)), 1.66 – 1.52 (m, 3H, C***H***$_3$) (Table 4.4, Entry B1).

#### 4.5.1.2 Synthesis of the Block Copolymers via ROP in the Bulk

The block copolymers $PEG_5$-*b*-$PLA_5$ and $PEG_5$-*b*-$PLA_{10}$ were synthesized following the general procedure described above in section 4.5.1.1. For the $PEG_5$-*b*-$PLA_5$ a $_{D,L}$-lactide:$PEG_5$ initiator ratio of 35:1 was used, whereas a 70:1 $_{D,L}$-lactide:$PEG_5$ initiator ratio was used for the $PEG_5$-*b*-$PLA_{10}$ (Table 4.2).

$^{1}$H NMR (400 MHz, Chloroform-*d*) δ 5.30 – 5.10 (m, 1H, C***H***), 4.41 – 4.32 (q, 1H, HOC***H***($CH_3$)), 4.32 – 4.19 (m, 4H, C***H***$_2$), 3.64 (s, 4H, C***H***$_2$), 3.38 (s, 3H, C***H***$_3$), 1.62 – 1.50 (m, 3H, C***H***$_3$) (Table 4.4, Entry B2 and B3).

#### 4.5.1.3 ROP in Dense Phase $CO_2$

The polymer syntheses in the presence of $CO_2$ were carried out in the standard 60 mL autoclave described in Chapter 2. As previously described, before the reaction could commence the system had to be leak tested at reaction conditions (120 °C and 240 bar of $CO_2$). Synthesis in dense phase $CO_2$ was carried out using the same reagent quantities as described in sections 4.5.1.1 and 4.5.1.2 and detailed in Table 4.2. The $_{D,L}$-lactide, initiator and catalyst were weighed directly into the autoclave base and the system was assembled as described in Chapter 2. The system was then purged with $CO_2$ at 2-3 bar for 5-10 minutes to remove any residual water and oxygen. Following this, the autoclave was then sealed and pressurised to the reaction conditions of 240 bar and 120 °C in accordance with the general procedure described in Chapter 2. The reaction was left to proceed for 1 hour with stirring after which time the vessel was cooled on ice to a temperature below 25 °C. The system was then vented and a sample removed for $^{1}$H NMR analysis. A $CO_2$ extraction method for the removal of any residual $_{D,L}$-lactide has previously been reported and was adapted for use in this work.[211] A small amount of ethanol (2 mL) was injected into the reaction vessel and the system pressurised to 240 bar with $CO_2$ at 45 °C. The vessel was then flushed with $CO_2$ while maintaining these conditions until there was no trace of the residual monomer visible in the $^{1}$H NMR spectra. The $P_{D,L}$LA homopolymer was flushed with $CO_2$ for 30 minutes, while the block copolymers were exposed to the $CO_2$ flow for up to 2 hours. Upon cooling and venting the samples were collected (entries S1-S3, Table 4.4).

### 4.5.2 Polymer Characterisation

Both the purchased and the synthesised polymers were characterised by DSC, GPC and $^{1}$H NMR as described in Chapter 2.

#### 4.5.2.1 $^1$H NMR

$^1$H NMR were obtained as described in section 2.6.3. The NMR spectra were used to calculate conversion and molecular mass of the polymers and the dn/dc values of the block copolymers for GPC. The dn/dc values of the block copolymers were calculated from equation 4.1 using the weight percent of the individual blocks as determined from $^1$H NMR and the known dn/dc values of the individual blocks (0.042 and 0.067 mL/g for $P_{D,L}LA$ and PEG in THF, respectively).[167,169,212] The weight fractions of the $P_{D,L}LA$ and PEG blocks, *x* and *y* respectively can be determined from the ratio of the integrals corresponding to the polymer backbones (signals **a'** and **c**, Figure 4.2). This gave a dn/dc value of 0.055 and 0.051 mL/g for the $PEG_5$-*b*-$PLA_5$ and $PEG_5$-*b*-$PLA_{10}$ block copolymers, respectively.

$$\frac{dn}{dc} = x\left(\frac{dn}{dc}\right)_{\mathrm{PEG}} + y\left(\frac{dn}{dc}\right)_{\mathrm{PLA}} \qquad 4.1$$

### 4.5.3 Rheological Measurements

All rheology measurements were performed following the high temperature method described in Chapter 3 (Section 3.5.1.2).

Homopolymer samples and the block copolymers were weighed directly into the measurement cell. The blends were weighed into a vial and physically mixed prior to being loaded into the measurement cell. Table 4.3 gives the composition details of the blends of PEG and $P_{D,L}LA$ homopolymers, and the PEG-*b*-$P_{D,L}LA$ block copolymers.

Table 4.3. Composition details of PEG/$P_{D,L}LA$ blend and PEG-*b*-$P_{D,L}LA$ block copolymer samples investigated in this chapter. Subscript numbers give the number average molecular weight (x $10^3$ g/mol) of the preceding polymer.

| Sample Name | $PEG_5$ [wt.%] | $PLA_{11}$ [wt.%] |
|---|---|---|
| $PLA_{11}100$ | 0 | 100 |
| $PEG_5$5:$PLA_{11}$95 | 5 | 95 |
| $PEG_5$10:$PLA_{11}$90 | 10 | 90 |
| $PEG_5$33:$PLA_{11}$67 | 33 | 67 |
| $PEG_5$50:$PLA_{11}$50 | 50 | 50 |
| $PEG_5100$ | 100 | 0 |
| **Sample Name** | **$PEG_{10}$ [wt.%]** | **$PLA_{11}$ [wt.%]** |
| $PEG_{10}100$ | 100 | 0 |
| $PEG_{10}$50:$PLA_{11}$50 | 50 | 50 |
| **Sample Name** | **$PLA_5$ [wt.%]** | **$PLA_{11}$ [wt.%]** |
| $PLA_5100$ | 100 | 0 |
| $PLA_5$10:$PLA_{11}$90 | 10 | 90 |
| **Sample Name** | **$M_w$ PEG block [g/mol] / PEG block [wt.%]** | **$M_w$ $P_{D,L}LA$ block [g/mol] / $P_{D,L}LA$ block [wt.%]** |
| $PEG_5$-*b*-$PLA_5$ | 5000 / 50 | 5000 / 50 |
| $PEG_5$-*b*-$PLA_{10}$ | 5000 / 33 | 10,000 / 67 |

Before the measurement commenced, the samples were heated to 80 °C and left to equilibrate for 1 hour to allow the formation of a molten disk. Initial viscosity was measured at ambient pressure by performing consecutive rotational shear ramps from 0.1 to 1000 $s^{-1}$ (described in detail in Chapter 3). Following these measurements, the sample was pressurised to 140 bar $CO_2$ using the syringe pump and the high pressure viscosity analysis performed as described in Chapter 3. After the high pressure measurement was complete all samples had reached their minimum viscosity (saturation viscosity ($\eta_{sat}$)). After the high pressure measurements, the cell was vented over 20 minutes with constant shearing to remove all the $CO_2$, while temperature was maintained at 80 °C. The ambient

pressure measurements were then repeated to assess whether or not the use of $CO_2$ had any long lasting effects on viscosity.

The saturation time of the samples was determined by fitting the $\eta_0$ values to an empirical formula as described in Chapter 3.

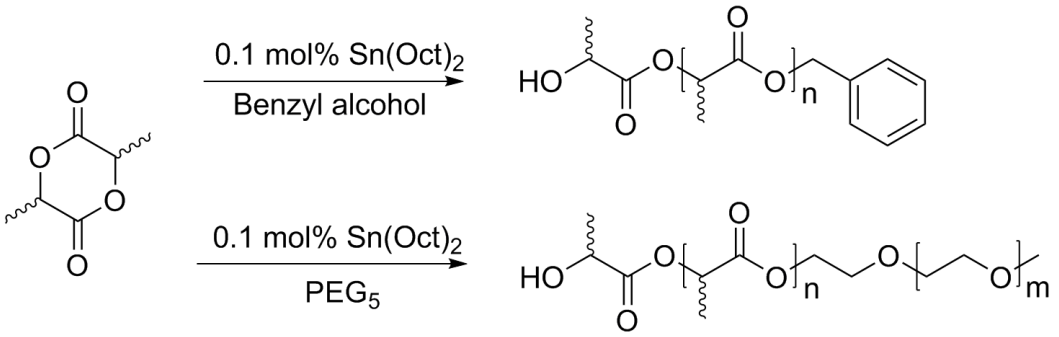
## 4.6 Results and Discussion

In order to investigate the effect of PEG and $CO_2$ on the viscosity of $P_{D,L}LA$ it was necessary to produce the blend and block copolymer samples. Following this, the benefits of PEG and $CO_2$ as processing aids for $P_{D,L}LA$ were quantified using a high pressure rheometer. Finally, the influence of PEG on the system as either a blended excipient or as a component of a diblock copolymer were compared.

### 4.6.1 Polymer Synthesis

Typically, the homopolymers and the block copolymers were synthesised by ROP of $_{D,L}$-lactide initiated by the hydroxy end groups using tin (II) 2-ethyl ethanoate catalyst. Due to the toxicity of heavy metals other catalysts have been investigated.[194,213,214] Here a supercritical ROP method previously established in the group was followed to produce the polymers,[211] and the resultant polymers were compared to those produced via conventional methods.

An amorphous $P_{D,L}LA$ and two PEG-*b*-$P_{D,L}LA$ copolymers of target $P_{D,L}LA$ molecular weights of 5000, 5000, and 10,000 g/mol ($PLA_5100$, $PEG_5$-*b*-$PLA_5$ and $PEG_5$-*b*-$PLA_{10}$ respectively, Table 4.2) were synthesised by ROP of $_{D,L}$-lactide (Scheme 4.1). Polymers synthesised via bulk ROP were purified by repeated washing with ethanol while those synthesised in $CO_2$ were purified by a $CO_2$ extraction method (see section 4.5.1.3 for further details).[211] All polymers were characterised by $^1$H NMR, GPC and DSC and the results are reported in Table 4.4 and Table 4.5.




Scheme 4.1 Reaction scheme for the ring opening polymerisation of D,L-lactide to give the homopolymers and the block copolymers.

Table 4.4. Characterisation of polymers synthesised by ROP in the bulk (entries B1-B3) and in $CO_2$ (entries S1-S3).

| Entry | Polymer | Conv. (%)[a] | PEG $M_n$ (g/mol)[a] | $P_{D,L}LA$ $M_n$ (g/mol)[a] | Total $M_n$ (g/mol)[a] | $M_n$ (g/mol)[b] | $M_w$ (g/mol)[b] | Đ[b] |
|---|---|---|---|---|---|---|---|---|
| B1 | $PLA_5100$ | 92 | - | 5200 | 5200 | 4100 | 4800 | 1.2 |
| B2 | $PEG_5$-*b*-$PLA_5$ | 94 | 5500 | 4900 | 10,000 | 8900 | 9400 | 1.1 |
| B3 | $PEG_5$-*b*-$PLA_{10}$ | 90 | 5600 | 9700 | 15,000 | 12,000 | 1300 | 1.1 |
| S1 | $PLA_5100$ | 99 | - | 5200 | 5200 | 5500 | 6300 | 1.1 |
| S2 | $PEG_5$-*b*-$PLA_5$ | 91 | 5300 | 4600 | 10,000 | 8600 | 9600 | 1.1 |
| S3 | $PEG_5$-*b*-$PLA_{10}$ | 94 | 5200 | 9400 | 15,000 | 11,000 | 13,000 | 1.1 |

Subscript number in polymer name refers to molecular weight (x$10^3$ g/mol) of the preceding block, while the letter B denotes that the polymer was synthesised via conventional bulk methods and S refers to polymers synthesised in $CO_2$. (a) Calculated from $^1$H NMR. (b) Determined from triple detection GPC. dn/dc values for block copolymers were calculated from NMR to give 0.055 and 0.051 mL/g for the $PEG_5$-*b*-$PLA_5$ and $PEG_5$-*b*-$PLA_{10}$ block copolymer respectively (equation 4.1), a dn/dc value of 0.042 mL/g was used for the $P_{D,L}LA$ homopolymer.[167,169]

The conversion was calculated from the $^1$H NMR spectrum of the crude samples by taking the ratios of the integrals of the methine signal in the polymer backbone (**a'**, δ = 5.18 ppm, Figure 4.2 top) and the corresponding monomer signal (**a,** δ = 5.03 ppm) following equation 4.2. The $M_n$ of the $P_{D,L}LA$ was calculated from the $^1$H NMR spectrum of the pure samples by comparing the integrals of the benzyl signals from the initiator (**c**, δ = 7.34 ppm) and the polymer methine signal (**a'**, δ = 5.16 ppm) (Figure 4.1) using equation 4.3, where 72 g/mol corresponds to the molecular weight of the lactide repeating unit, and 5 is the number of protons associated with the initiator signal.

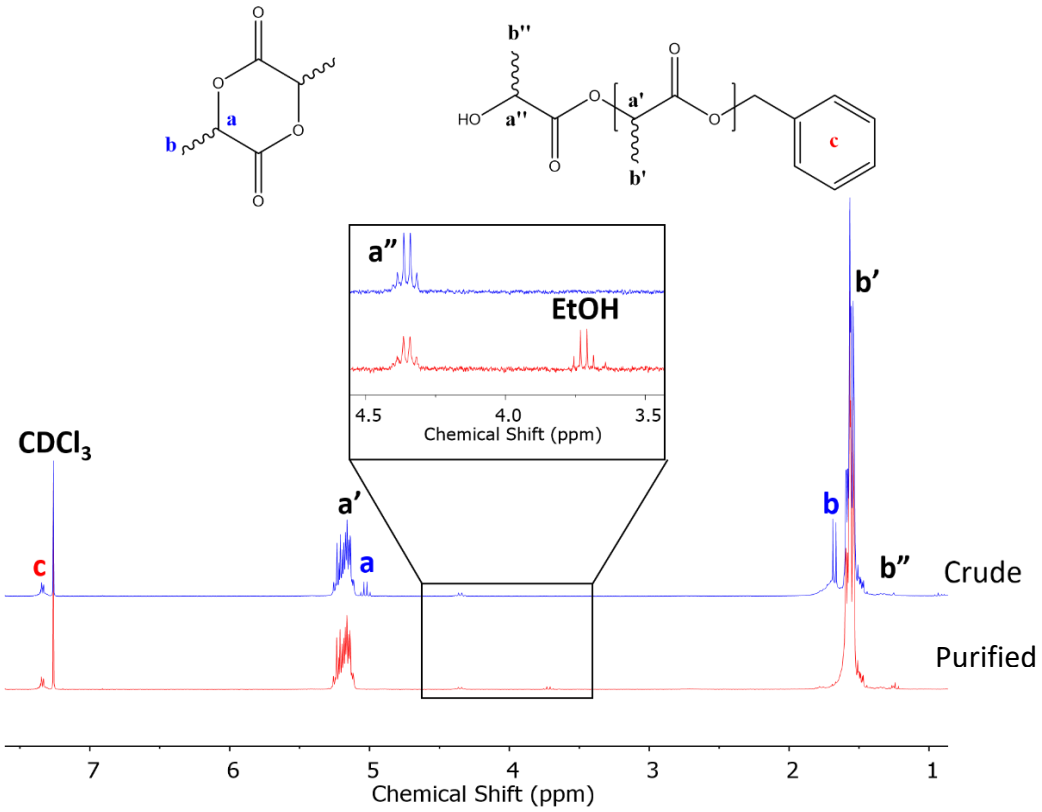



Figure 4.1. $^{1}$H NMR spectrum of crude and purified PLA$_5$100 synthesised by ring opening of $_{D,L}$-lactide with benzyl alcohol initiator in $CO_2$, analysed in $CDCl_3$.

$$\text{Conversion } (\%) = \frac{\int(\boldsymbol{a}')}{\int(\boldsymbol{a}') + \int(\boldsymbol{a})} \times 100 \qquad 4.2$$

$$M_n = \frac{\int(\boldsymbol{a}')}{\int(\boldsymbol{c}) \div 5} \times 72 \qquad 4.3$$

In order to calculate the $M_n$ of the block copolymers the integral of the $P_{D,L}LA$ polymer signal (**a'**, δ = 5.18 ppm) was compared to that of the methyl signal associated with the PEG macroinitiator (**c''**, δ = 3.38 ppm) as described by equation 4.4 (Figure 4.2). The molecular weight of the PEG macroinitiator was also confirmed by $^{1}$H NMR analysis by taking the integral of the signal associated with the PEG polymer backbone (**c**, δ = 3.64 ppm) and multiplying by the molecular weight of the ethylene glycol repeating unit, 44 g/mol, following equation 4.5 (Figure 4.2).

$$M_n = \frac{3\int(\boldsymbol{a}')}{\int(\boldsymbol{c}'')} \times 72 \qquad 4.4$$

$$M_n = \frac{3\int(\boldsymbol{c})}{4\int(\boldsymbol{c}'')} \times 44 \qquad 4.5$$

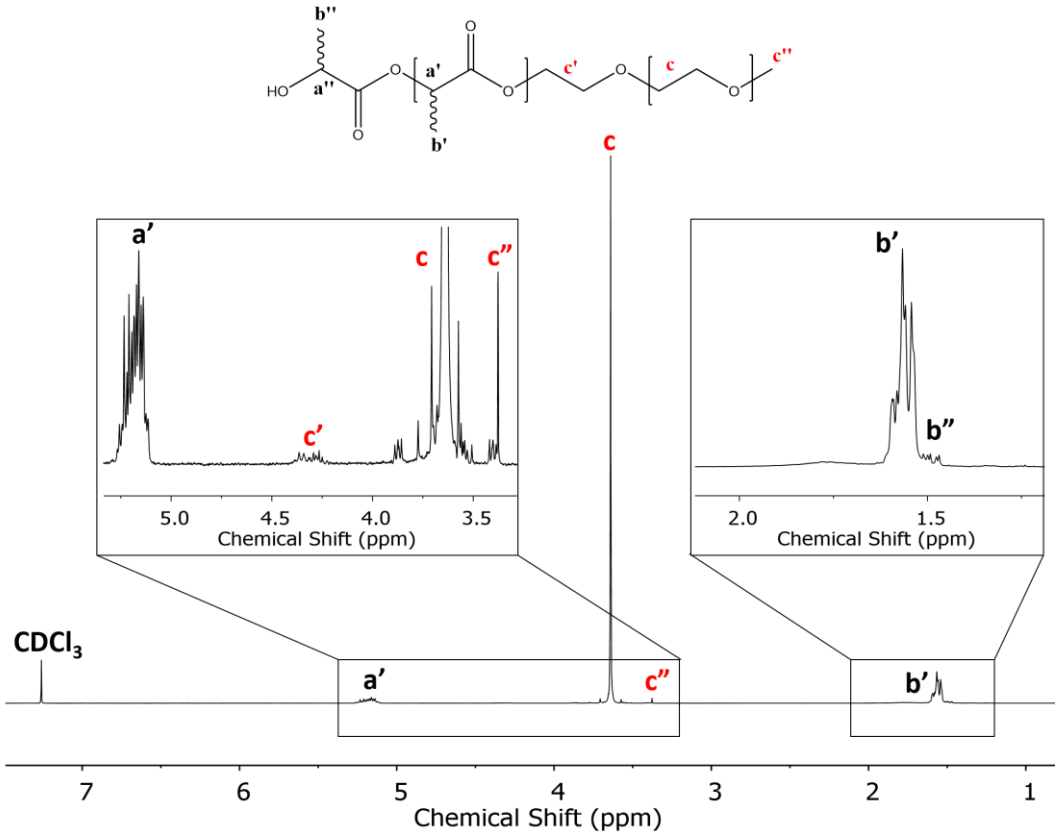



Figure 4.2. $^{1}$H NMR spectrum of pure $PEG_5$-*b*-PLAx block copolymer synthesised by ring opening of $_{D,L}$-lactide with $PEG_5$ macroinitiator in $CO_2$, analysed in $CDCl_3$.

The polymers were also analysed by GPC to obtain the weight average molecular weight ($M_w$) and dispersity ($Đ$) along with the $M_n$ which compared favourably with that calculated from $^{1}$H NMR (Table 4.4). Comparison of the block copolymers with the PEG macroinitiator ($PEG_5$) showed a transition to higher molecular weight in accordance with the growing PLA chain (Figure 4.3). This confirmed the successful synthesis of PEG-*b*-$P_{D,L}$LA block copolymers, both via conventional polymerisation in bulk and via synthesis in $CO_2$.

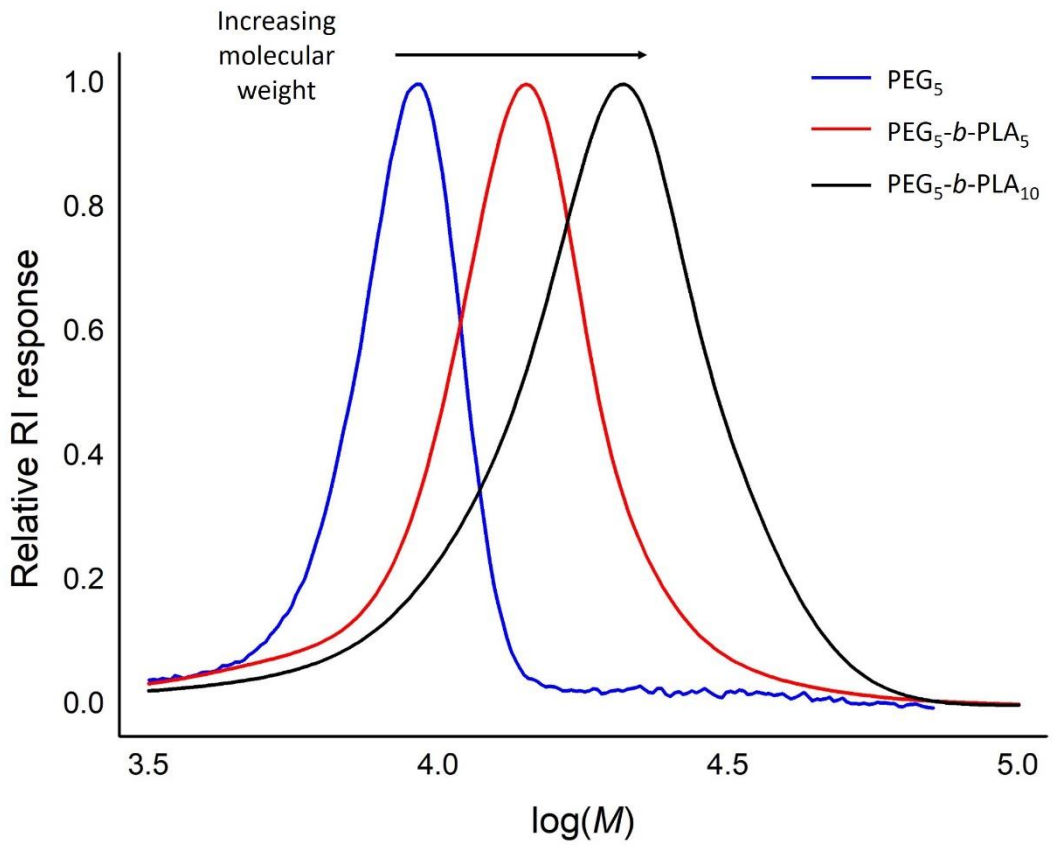



Figure 4.3. Typical GPC traces of synthetic polymers showed an increase in overall molecular weight as the target molecular weights increase from 5000 g/mol for $PEG_5$ homopolymer, to 10000 g/mol and 15000 g/mol for $PEG_5$-*b*-$PLA_5$ and $PEG_5$-*b*-$PLA_{10}$ block copolymers, respectively.

The thermal transitions of the polymers were detected by DSC (Table 4.5). The $PLA_5$ homopolymers had a $T_g$ around 35-38 °C which was close to the expected value of 40 °C.[215] The block copolymers showed a reduction in $T_m$ compared to that of $PEG_5$, which had a $T_m$ of 60 °C. This was possibly due to some miscibility between the PEG and the $P_{D,L}LA$ components. In fact, this phenomenon became more pronounced in the $PEG_5$-*b*-$PLA_{10}$ copolymers where a $T_g$ and a $T_m$ were detected.

Table 4.5. Thermal transition of synthesised polymers determined by DSC.

| Entry | Polymer | $T_g$ (°C) | $T_m$ (°C) |
|---|---|---|---|
| B1 | $PLA_5100$ | 35 ± 0.79 | - |
| B2 | $PEG_5$-*b*-$PLA_5$ | - | 51 ± 0.24 |
| B3 | $PEG_5$-*b*-$PLA_{10}$ | -15 ± 3.1 | 51 ± 1.1 |
| S1 | $PLA_5100$ | 38 ± 0.69 | - |
| S2 | $PEG_5$-*b*-$PLA_5$ | - | 52 ± 0.69 |
| S3 | $PEG_5$-*b*-$PLA_{10}$ | -13 ± 0.70 | 50 ± 1.1 |
| 4 | $PEG_5$ | -41* | 59 ± 0.19 |

*Value taken from literature[216]

#### 4.6.1.1 Comparison of Polymerisations Performed in the Bulk and in $CO_2$

Both methods of synthesis were performed in duplicate and produced polymers at high conversion with reproducible molecular weights and narrow dispersity. Polymers synthesised in the bulk were purified by washing with an excess of ethanol. It was necessary to repeat the purification process multiple times over several days before an acceptable level of purity was achieved (<1% monomer by $^1$H NMR). Even after several hours of drying, a significant amount of ethanol (~2 % with respect to polymer by $^1$H NMR) remained in the final product (Figure 4.4 red trace). By comparison, purification via $CO_2$ extraction required only a very small amount of ethanol (2 mL) and was completed in one step in less than 2 hours. The resultant polymers contained trace amounts of ethanol (~0.3 wt.% with respect to the polymer by $^1$H NMR) but showed complete removal of the residual monomer (Figure 4.4 blue trace). Based on the higher purity of the polymers synthesised in $CO_2$ these were chosen for the following rheological studies.

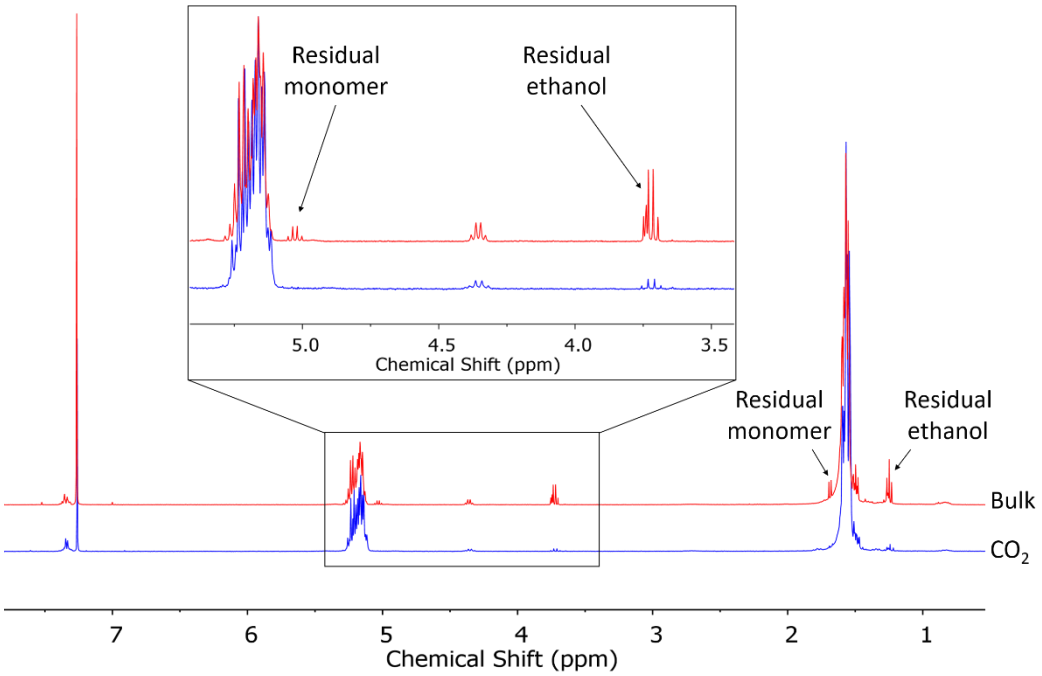



Figure 4.4. Comparison of $^{1}$H NMR spectra of $PLA_5$ synthesised and purified in the bulk (red) vs $CO_2$ (blue). All of the residual monomer had been removed from the sample synthesised in $CO_2$ and only trace amounts of ethanol were present.

## 4.6.2 Viscosity Analysis

### 4.6.2.1 Effect of Molecular Weight on Viscosity

It is well established that lower molecular weight polymers have lower viscosity than higher molecular weight polymers. This is because lower molecular weight polymers have shorter polymer chains and therefore fewer chain entanglements compared to higher molecular weight polymers with longer chain lengths.[114] This results in materials that will flow more easily and have lower viscosity. The viscosity of $PLA_5$ was determined at ambient pressure and at 140 bar in dense phase $CO_2$ ($T$ = 80 °C) and compared to commercially obtained $PLA_{11}$ (Figure 4.5). At ambient pressure it was apparent that the $PLA_5$ had a much lower $\eta_0$ of 1200 Pa.s than the commercial $PLA_{11}$ (6800 Pa.s). Upon treatment with 140 bar $CO_2$ both polymers underwent a significant viscosity reduction, with the lower molecular weight polymer maintaining a lower viscosity than the $PLA_{11}$. The same trend was seen for PEG, with $PEG_{10}$ having a larger viscosity at both ambient pressure and at 140 bar in dense phase $CO_2$ compared to that of $PEG_5$.

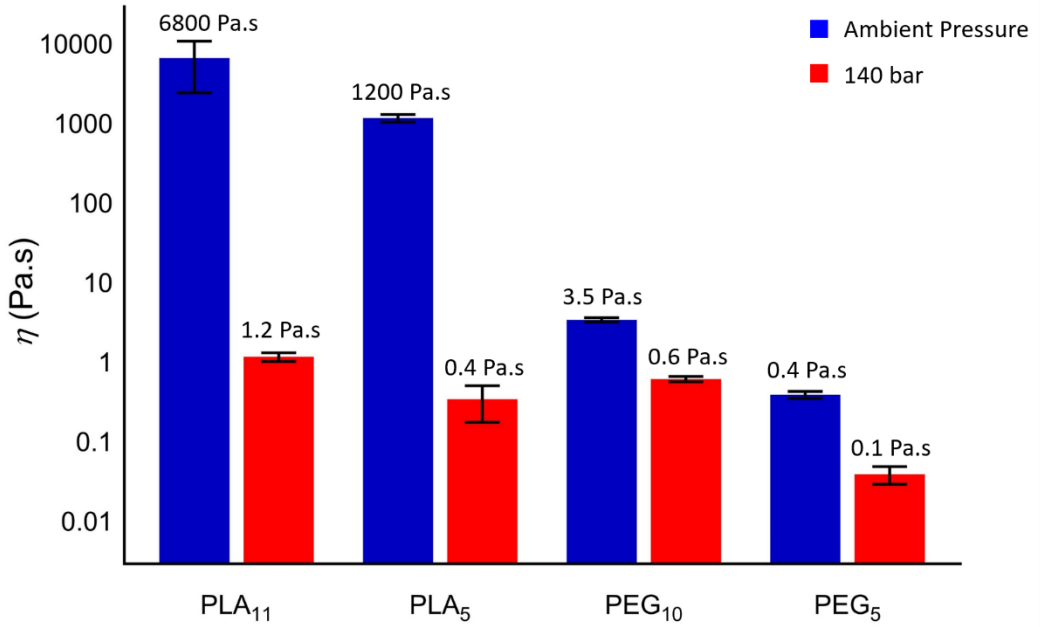



Figure 4.5. Comparison of the viscosities of 10000 g/mol and 5000 g/mol $P_{D,L}LA$ and PEG at ambient pressure and after saturation with 140 bar $CO_2$. Error bars represent ±1 standard deviations from the mean. ($T$ = 80 °C).

Depending on whether the polymer chains are entangled or not, zero shear viscosity scales either linearly with molecular weight ($M$) or with a much higher power of $M$ (typically 3.4)(equation 4.6).[180] For a pair of polymers the scale factor is calculated from equation 4.7. From this, $P_{D,L}LA$ viscosity scaled as $M^{2.3\pm1}$ at ambient pressure and as $M^{1.6\pm0.8}$ once the polymer was saturated with $CO_2$. The entanglement molecular weight ($M_e$) for PLA has been reported as ~9000 g/mol[217]. Therefore, the value of 2.3 ± 1 was in line with a transition across $M_e$. The viscosity scaled as $M^{3.5\pm0.6}$ at ambient pressure and as $M^{4.1\pm0.8}$ for PEG. This was in agreement with the expected correlation of $M^{3.4}$ as PEG is reported to have an $M_e$ of 1900 g/mol. It should be noted that there was increased uncertainty associated with the low viscosity measurements and possible solvent effects of $CO_2$.[218]

$$\eta \propto M^n \tag{4.6}$$

$$n = \frac{\log \eta_1 - \log \eta_2}{\log M_1 - \log M_2} \tag{4.7}$$

In the above equations $\eta$ is the viscosity, $M$ is the molecular weight and $n$ is the power. The uncertainty was propagated from the uncertainty in the viscosity and molecular weight measurements.[219]

#### 4.6.2.2 Effect of PEG as a Blended Excipient

In order to assess the effect of PEG as an excipient, blends of different ratios of $PLA_{11}$ and $PEG_5$ were prepared (Table 4.3). The aim of these experiments was to give an indication of how increasing amounts of PEG could influence processing parameters by reducing the viscosity of the polymer melt.

Rheological measurements were performed at 80 °C and ambient pressure, and immediately following this, the samples were pressurised to 140 bar with $CO_2$ and sequential measurements performed over 18 hours. After the viscosity had been measured at 140 bar, the samples were depressurised over 20 minutes and the viscosity at ambient pressure was measured again. This protocol was designed to give information not only regarding the viscosities of the system at ambient and high pressure but also during the $CO_2$ soaking procedure and to investigate how well the system recovered after $CO_2$ removal. Increasing the PEG content (wt.%) resulted in a decrease in viscosity across all stages of the experiment (Figure 4.6). These data were in agreement with other results reported in the literature[140] and confirmed that PEG can be employed as a processing aid for $P_{D,L}LA$ systems. At ambient pressure a significant decrease in zero shear viscosity of 64% was evident even at relatively low PEG content (5 wt.%), with $PEG_5$5:$PLA_{11}$95 having a viscosity of 2400 Pa.s compared to 6800 Pa.s for $PLA_{11}$100. This suggested that PEG does indeed efficiently plasticise $P_{D,L}LA$, given the effect of such a small quantity of additive.

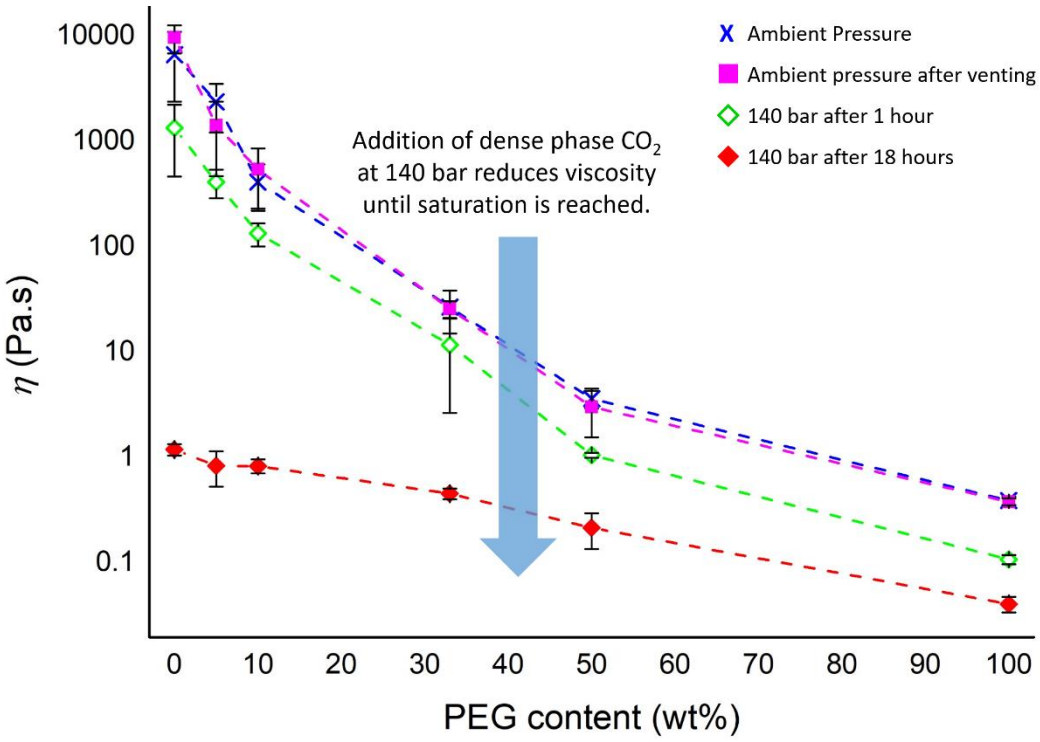



Figure 4.6. Increasing PEG content (wt.%) resulted in decreasing viscosity of PEG:$P_{D,L}LA$ blends at ambient pressure, with 140 bar $CO_2$ after 1 and 18 hours soaking and after venting. Error bars represent ±1 standard deviations from the mean ($T$ = 80 °C).

The addition of 10 wt.% PEG ($PEG_5$10:$PLA_{11}$90) yielded a drastic reduction in viscosity of 94% to 400 Pa.s compared to the ambient pressure viscosity ($\eta_0(p_{amb})$) of $PLA_{11}$. Comparison with a blend of $P_{D,L}LA$ homopolymers of different molecular weights, where 10 wt.% $PLA_5$ was mixed with 90 wt.% $PLA_{11}$ ($PLA_5$10:$PLA_{11}$90) was carried out to assess whether it was merely the presence of shorter polymer chains which reduced viscosity or the PEG molecules themselves. This experiment was performed as recent literature studies have reported that short chain PLA oligomers can be used as plasticisers.[220] The data shown in Table 4.6 demonstrate that the presence of 10 wt.% short chain $PLA_5$ had a negligible effect on the viscosity of the $PLA_{11}$ at ambient pressure. The addition of 10 wt.% $PEG_5$ significantly decreased viscosity; confirming that it is not the presence of short polymer chains causing the reduction in viscosity but the plasticising effect of the PEG molecules themselves.

Table 4.6. Zero shear viscosities of $PLA_{11}$ blended with 10 wt.% $PLA_5$ and $PEG_5$ at ambient pressure. Error reported as ±1 standard deviation from the mean ($T$ = 80 °C).

| Sample | $\eta_0(p_{amb})$ Average ± SD (Pa.s) | % Decrease relative to $PLA_{11}100$ |
|---|---|---|
| $PLA_{11}100$ | 6800 ± 4300 | - |
| $PLA_5 10$:$PLA_{11}90$ | 7500 ± 1100 | -11 |
| $PEG_5 10$:$PLA_{11}90$ | 400 ± 200 | 94 |

Pressurising the samples to 140 bar with $CO_2$ resulted in a decrease in viscosity of over 50% for all compositions even after 1 hour of soaking at 10 $s^{-1}$ (Figure 4.6-green symbols, Table 4.7). The viscosity was measured at regular intervals over an 18 hour period to ensure all samples had experienced the same soaking procedure and were saturated with $CO_2$. The saturation time ($t_{sat}$) and the saturation viscosity ($\eta_{sat}$) were calculated as described in Chapter 3. Saturated samples had such a low viscosity that the effect of additional PEG was minimal (Figure 4.6- red symbols), although a decrease in the time required for complete saturation was observed (as discussed later in the chapter).

Once the viscosity had been measured at 140 bar, the pressure was released and the viscosity at ambient pressure was measured again. This provided an insight into the reversibility of the effects of $CO_2$ treatment on the polymer samples. It has previously been reported that the effects of $CO_2$ as a plasticiser are completely reversible upon depressurisation.[131] In this study, all samples recovered their viscosities (Figure 4.6-pink symbols) and therefore this data agreed with the literature reports.

Allowing the samples to soak for 18 hours resulted in complete $CO_2$ saturation and a more reliable comparison, but it should be noted that this timescale was purely a function of the measurement geometry. Inside the measurement cell there was limited accessible surface area available for the $CO_2$ to contact the sample, giving rise to longer diffusion times (Figure 4.7). Previous studies from the group have demonstrated that in our view cells the polymers liquefy within minutes at pressures as low as 20 bar.[221] When using the high pressure rheometer geometry the $P_{D,L}LA$ homopolymer took approximately 5 hours to become fully saturated with $CO_2$.

Introducing PEG as a blended excipient resulted in a decrease in the time taken for samples to reach equilibrium viscosity, to 1 hour for the 50 wt.% PEG blend ($PEG_5$50:$PLA_{11}$50) (Figure 4.8). It was not possible to calculate the exact $t_{sat}$ for the $PEG_5$100 homopolymer as the sample reached its minimum viscosity before the first measurement was performed after 1 hour of soaking. Table 4.8 details the time taken for each sample to reach saturation.

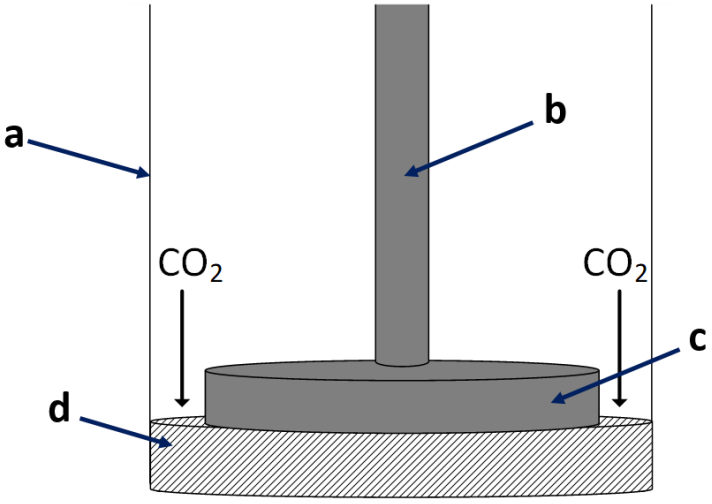



Figure 4.7. Schematic of the inside of the rheometer measuring cell showing how the $CO_2$ contact area is relatively small compared to the sample size, where **a** is the measuring cell wall, **b** is the spindle of the measuring geometry, **c** is the upper parallel plate and **d** is the polymer sample.

Owing to the PEG molecules having greater mobility than the $P_{D,L}LA$ molecules the relaxation time and viscosity of the blends at ambient pressure was substantially reduced in comparison to $PLA_{11}$. Accordingly, the $CO_2$ penetration through the polymer occured more quickly with increased PEG content, reducing the saturation time.

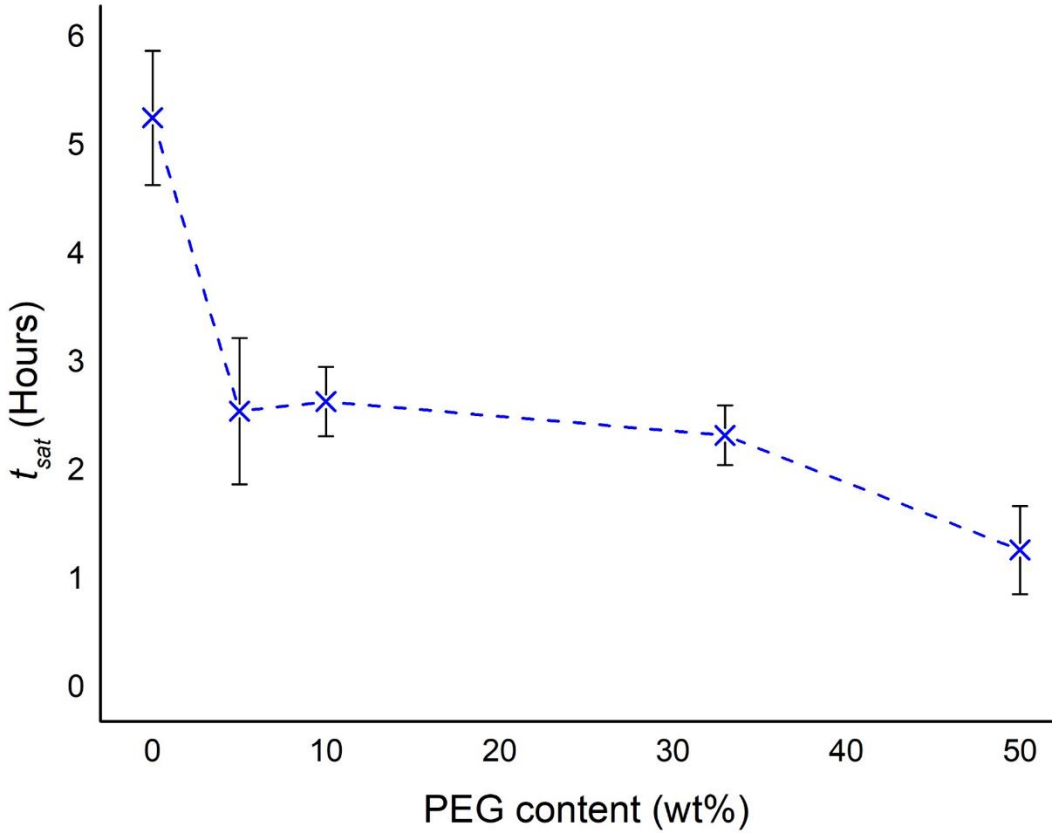
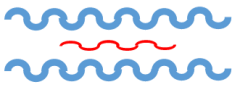



Figure 4.8. Saturation time ($t_{sat}$) of $PEG_5$:$PLA_{11}$ blends. Increasing PEG content resulted in a decrease in $t_{sat}$. Error bars represent ±1 standard deviations from the mean ($T$ = 80 °C).

#### 4.6.2.3 Effect of PEG as a Covalently Linked Block on the Viscosity of $P_{D,L}LA$

With a view to making a comparison between the effect of PEG as a blended excipient and as part of block copolymer, two PEG-*b*-$P_{D,L}LA$ copolymers were synthesised by ROP in dense phase $CO_2$ using a 5000 g/mol PEG macroinitiator, as detailed above (section 4.5.1, Table 4.2). Two different PEG:$P_{D,L}LA$ ratios were targeted and these block copolymers were compared to polymer blends of similar polymer weight fractions. To this end the viscosity of a block copolymer with a 1:1 PEG:$P_{D,L}LA$ ratio ($PEG_5$-*b*-$PLA_5$) was compared to that of a 50 wt.% 10,000 g/mol PEG blend ($PEG_{10}$50:$PLA_{11}$50, Table 4.3); and the viscosities of a second block copolymer with a 1:2 PEG:$P_{D,L}LA$ ratio ($PEG_5$-*b*-$PLA_{10}$) and a 33 wt.% PEG blend ($PEG_5$33:$PLA_{11}$67) were compared. A summary of the polymers being discussed is given in Scheme 4.2.

| Sample | Schematic | $M_w$ (g/mol) | $\eta_0(p_{amb})$ (Pa.s) |
|---|---|---|---|
| $PLA_{11}100$ |  | 11000 | 6800 |
| $PLA_5100$ |  | 5000 | 1200 |
| $PEG_{10}100$ |  | 10000 | 3.5 |
| $PEG_5100$ |  | 5000 | 0.4 |
| $PEG_5$-*b*-$PLA_5$ |  | 10000 | 5.6 |
| $PEG_{10}50$:$PLA_{11}50$ |  | 11000 PLA + 10000 PEG | 17 |
| $PEG_5$-*b*-$PLA_{10}$ |  | 15000 | 44 |
| $PEG_5$33:$PLA_{11}$67 |  | 11000 PLA + 5000 PEG | 27 |

Scheme 4.2. A series of schematics depicting the various block copolymers and their comparable blends, along with the homopolymers for reference. $P_{D,L}LA$ is shown in blue and PEG is shown in red. Viscosities at ambient pressure ($\eta_0(p_{amb})$) and molecular weights ($M_w$) are also given.

Taking first the data obtained at ambient pressure it was found that the block copolymers had notably lower viscosities than the $P_{D,L}LA$ homopolymer; 5.6 Pa.s and 44 Pa.s for $PEG_5$-*b*-$PLA_5$ and $PEG_5$-*b*-$PLA_{10}$ respectively in comparison with 6800 Pa.s for $PLA_{11}100$ and 1200 Pa.s for $PLA_5100$ (Figure 4.9- blue bars). Surprisingly, the viscosity observed for the weight equivalent $PEG_5$33:$PLA_{11}$67 blend ($\eta_0(p_{amb})$ 27 Pa.s) was significantly lower than the viscosity of the $PEG_5$-*b*-$PLA_{10}$ ($\eta_0(p_{amb})$ 44 Pa.s). This can be explained by thinking of the composition of the samples in terms of their composition and chain mobility. The blend was composed of highly mobile, shorter PEG chains and less mobile, longer $P_{D,L}LA$ chains. On the other hand, the block

copolymer represents the covalently linked counterpart and as such had a reduced degree of freedom in the PEG chains (Scheme 4.2). This resulted in less mobility and therefore increased viscosity by comparison. The overall molecular weight of the block copolymer (15,000 g/mol) is also larger than either component of the blend (5000 g/mol PEG plus 10,000 g/mol $P_{D,L}LA$) and contributes to the elevated viscosity.

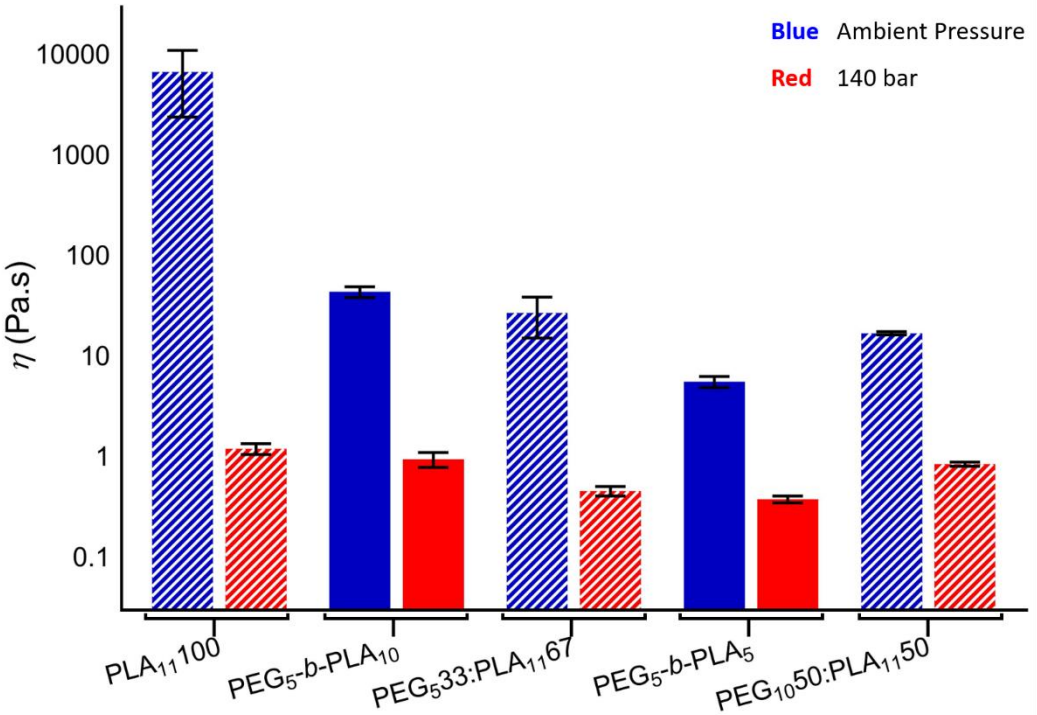



Figure 4.9. The viscosities of PEG:PLA blends and PEG-*b*-$P_{D,L}LA$ copolymers at ambient pressure and after 18 hours in $CO_2$ at 140 bar pressure are compared. The hatched bars represent the blends while the block colours represent the block copolymers. Error bars represent ±1 standard deviation from the mean ($T$ = 80 °C).

By contrast, a reversal of this trend is seen for the comparison of the $PEG_5$-*b*-$PLA_5$ block copolymer ($\eta_0(p_{amb})$ 5.6 Pa.s) which had a lower viscosity than its equivalent blend $PEG_{10}50$:$PLA_{11}50$ ($\eta_0(p_{amb})$ 17 Pa.s). Once again, this can be explained by considering the molecular weights of the individual components. Here the molecular weight of the block copolymer is equivalent to the two homopolymers of the blend. Therefore it consists of a less mobile but much shorter (5000 g/mol) $P_{D,L}LA$ chain covalently bound to a highly mobile PEG moiety (5000 g/mol) resulting in a much lower viscosity than $PLA_{11}$ (Scheme 4.2). The blend is a mixture of two individual polymers both with $M_n$ = 10,000 g/mol and so the viscosity correlates with the molecular weights of the individual polymers being much larger than the separate

blocks. This is coupled with a dominance of the $P_{D,L}LA$ and becomes apparent when the viscosity of the corresponding $P_{D,L}LA$ chains is considered. The $PLA_5$ has a viscosity of 1200 Pa.s while the $PLA_{11}$ has a much greater viscosity of 6800 Pa.s. Even for the highly mobile PEG, increased chain length results in increased viscosity from 0.4 Pa.s for $PEG_5$ to 3.5 Pa.s for $PEG_{10}$.

The same trends follow for both block copolymers when they are exposed to $CO_2$.

Based on previous work it was expected that the samples with a 33 wt.% PEG content would be more miscible than those containing 50 wt.% PEG.[140] This correlates with the data presented in Table 4.5, where an intermediate $T_g$ was observed for the $PEG_{5}$-*b*-$PLA_{10}$ indicating partial miscibility of the two component polymers. A $T_g$ was not detected at all for the $PEG_{10}$-*b*-$PLA_{10}$ copolymer due to it being masked by the PEG $T_m$. Where polymers exhibit greater miscibility, it has been reported that a greater decrease in viscosity is observed.[140] However, the viscosities observed in Scheme 4.2 do not follow this trend, indicating that although miscibility can influence viscosity, in this case it is not a dominating factor.

As both block copolymer formation and blending with PEG significantly reduce the viscosity of $P_{D,L}LA$, either strategy could be employed to improve processability and the decision of which to use will be based on other properties of the block copolymer or blends, which may be desirable for the final application. For example, the enhancement of hydrolytic degradation is important for drug delivery applications and can be achieved by the introduction of hydrophilic channels via blending. Conversely, the use of block copolymers could result in improved drug solubility.[222]

Table 4.7. Calculated zero shear viscosity values (Pa.s) obtained using the Carreau model fitting ($T$ = 80 °C)

| Sample | Viscosity at ambient pressure ($\eta_0(p_{amb})$) | | Viscosity at 140 bar after 1h soak | | | Saturation viscosity ($\eta_{sat}$)[a] | | | Viscosity after venting | | | % decrease from $PLA_{11}100$ |
|---|---|---|---|---|---|---|---|---|---|---|---|---|
| | Average | Standard deviation | Average | Standard deviation | % drop from $p_{amb}$* | Average | Standard deviation | % drop from $p_{amb}$* | Average | Standard deviation | % difference from $p_{amb}$* | |
| $PLA_{11}100$ | 6800 | 4300 | 1400 | 900 | 79.75 | 1.2 | 0.15 | 99.98 | 9800 | 2900 | +45.96 | - |
| $PEG_5$5:$PLA_{11}$95 | 2400 | 1200 | 420 | 130 | 82.61 | 0.85 | 0.31 | 99.96 | 1400 | 970 | -39.94 | 64.35 |
| $PEG_5$10:$PLA_{11}$90 | 420 | 200 | 140 | 34 | 67.36 | 0.84 | 0.13 | 99.80 | 550 | 320 | +31.95 | 93.82 |
| $PEG_5$33:$PLA_{11}$67 | 27 | 12 | 12 | 9.2 | 56.09 | 0.46 | 0.05 | 98.30 | 26 | 4.8 | -3.97 | 99.60 |
| $PEG_5$50:$PLA_{11}$50 | 3.7 | 0.69 | 1.1 | 0.06 | 70.77 | 0.22 | 0.08 | 94.02 | 3.1 | 1.5 | -16.18 | 99.95 |
| $PEG_5100$ | 0.40 | 0.04 | 0.11 | 0.01 | 72.26 | 0.04 | 0.01 | 89.57 | 0.39 | 0.03 | -2.73 | |
| $PEG_{10}100$ | 3.5 | 0.21 | 1.6 | 0.11 | 53.37 | 0.63 | 0.05 | 81.82 | 2.9 | 0.24 | -15.35 | - |
| $PEG_{10}$50:$PLA_{11}$50 | 17 | 0.59 | 7.6 | 0.55 | 55.64 | 0.85 | 0.04 | 95.00 | 14 | 0.46 | -14.99 | 99.75 |
| $PEG_5$-*b*-$PLA_5$ | 5.6 | 0.71 | 1.8 | 0.26 | 66.48 | 0.38 | 0.03 | 93.26 | 6.00 | 0.67 | +6.82 | 99.92 |
| $PEG_5$-*b*-$PLA_{10}$ | 44 | 5.3 | 14 | 1.8 | 67.40 | 0.95 | 0.16 | 97.84 | 41 | 2.6 | -6.08 | 99.35 |
| $PLA_5100$ | 1200 | 130 | 520 | 30 | 54.90 | 0.35 | 0.17 | 99.97 | 1100 | 95 | -7.13 | - |
| $PLA_5$10:$PLA_{11}$90 | 7500 | 1100 | 1500 | 580 | 80.29 | 0.95 | 0.04 | 99.99 | 5300 | 1200 | -28.64 | -10.70 |

*% drop from $p_{amb}$ = The percentage drop in viscosity from the ambient pressure ($p_{amb}$) viscosity. a) Calculated from equation 3.2.

Table 4.8. Time to saturation as determined from equation 3.2.

| Sample | Time to saturation, $t_{sat}$ (hours) | |
|---|---|---|
| | Average | Standard Deviation |
| $PLA_{11}100$ | 5.26 | 0.62 |
| $PEG_5$5:$PLA_{11}$95 | 2.56 | 0.67 |
| $PEG_5$10:$PLA_{11}$90 | 2.65 | 0.32 |
| $PEG_5$33:$PLA_{11}$67 | 2.34 | 0.28 |
| $PEG_5$50:$PLA_{11}$50 | 1.28 | 0.41 |
| $PEG_5100$ | - | - |
| $PEG_{10}100$ | 1.25 | 0.01 |
| $PEG_{10}$50:$PLA_{11}$50 | 2.34 | 0.04 |
| $PEG_5$-*b*-$PLA_5$ | 1.61 | 0.07 |
| $PEG_5$-*b*-$PLA_{10}$ | 2.49 | 0.18 |
| $PLA_5100$ | 4.43 | 0.36 |
| $PLA_5$10:$PLA_{11}$50 | 5.13 | 0.47 |

## 4.7 Summary

Homopolymers of $P_{D,L}LA$ and PEG-*b*-$P_{D,L}LA$ block copolymers were synthesised and purified by conventional bulk methods and were comparable to those produced in $CO_2$. Both techniques gave good conversions, molecular weights and narrow dispersities. However, following purification, the bulk polymers contained a significant amount of residual ethanol and it was not possible to remove all of the residual $_{D,L}$-lactide monomer via conventional methods. Whereas the polymers made via ROP in $CO_2$ had only trace amounts of ethanol and no residual monomer. Although the synthesis of PLA in $CO_2$ has previously been reported, this is first time that the established method of ROP of $_{D,L}$-lactide in $CO_2$ has been extended to the synthesis of a PEG-*b*-$P_{D,L}LA$ copolymer. The $CO_2$ synthetic method yielded polymers with good agreements between theoretical and experimental molecular weights and narrow dispersities.

Rheological analysis of $P_{D,L}LA$ and PEG samples of different molecular weights (5000 and 10,000 g/mol) showed that viscosity scaled with molecular weight as expected.[223]

The addition of PEG as a processing agent along with the use of $CO_2$ can dramatically reduce the viscosity of $P_{D,L}LA$, improving the processability of the polymer. The effect of PEG is apparent whether its role is as a blended excipient or as a component of a block copolymer. Viscosity reductions from 6800 Pa.s (for $PLA_{11}$ homopolymer) to less than 1 Pa.s were observed when the $P_{D,L}LA$ was treated with PEG and $CO_2$.

Furthermore, this work also showed that PEG reduces the saturation time of $CO_2$ through the polymer melt resulting in shorter processing times. A soaking time of 5 hours was required to saturate the $P_{D,L}LA$ homopolymer with $CO_2$. This was immediately reduced to approximately 2 hours with the addition of just 5 wt.% PEG (Table 4.8). Rheology measurements also confirmed that the use of $CO_2$ has no lasting effects, as upon its removal all samples recovered their viscosity.

## 4.8 Conclusions

The rheological data in this chapter documents the quantification of the process improvements that $CO_2$ and PEG could provide. The reduction in saturation time required for $CO_2$ to reduce the viscosity of the polymer melt is a key benefit of the combination of PEG and $CO_2$. This is also the first time that the effect of PEG on the melt viscosity of $P_{D,L}LA$ has been quantified both as a component of a PEG/$P_{D,L}LA$ blend and a PEG-*b*-$P_{DL}LA$ block copolymer in $CO_2$. In these studies reduced viscosity was achieved at 80 °C; over 100 °C lower than contemporary processing temperatures. However, this temperature is still too high for use with thermally labile APIs such as the proteins used in the formulations in the following chapter. In order to measure the viscosity at lower temperatures an alternative system of polymer blends was employed. The following chapter aims to exploit these data to aid formulation design.

# Chapter 5

## Can the Rheological Properties of a Formulation Provide an Insight into the Drug Release Profile?

## 5.1 Abstract

The previous chapters describe the development of a high pressure rheology method to investigate the effect of $CO_2$ and additives on the viscosity of polymer melts. This chapter aims to use the knowledge and skills previously acquired to investigate the viscosity of polymer-based formulations containing a model drug for sustained release. The data presented herein are used to investigate whether the rheological properties of a formulation correlate with its performance during an *in vitro* dissolution study.

At present, it is necessary to perform *in vitro* dissolution studies for all potential drug delivery systems in order to establish whether they have promising release properties for sustained or controlled drug delivery. These studies are time consuming and sometimes carried out only to find that the formulations are not suitable for successful drug delivery based on their poor and inconsistent release profiles. In addition, these studies are costly, especially when performed on large batch sizes. They are also prone to large experimental uncertainties resulting in the need for multiple repeats and large sample pools.

It is expected that a formulation with a homogeneous distribution of API throughout the polymer matrix will produce reproducible release profiles during *in vitro* dissolution studies. It is hypothesised that rheology could be used to assess the homogeneity of a formulation, and therefore be used to predict how well a formulation will perform in a dissolution study. Rheology could be used as a preliminary test to aid the development of sustained release formulations. This would not only reduce the number of long-term *in vitro* dissolution studies that need to be carried out but also save costs and time within the formulation development process.

This chapter addresses this question by first using the high pressure rheology method along with other high pressure techniques to determine a suitable polymer matrix. Following this a series of formulations were produced using a $CO_2$ mixing procedure. The viscosity of these formulations was then measured using the high pressure rheology method described in Chapter 3. A content assay and micro Raman

spectroscopy provided information on the success of blending and on the homogeneity of the formulations. Finally, a one-month *in vitro* release study was performed and the release profiles were compared to the rheology data.

## 5.2 Contents

Chapter 5 ..... 5-131

5.1 Abstract ..... 5-132

5.2 Contents ..... 5-134

5.3 Introduction ..... 5-135

5.4 Materials ..... 5-141

5.5 Methods ..... 5-142

5.5.1 Jet Milling of the BSA ..... 5-142

5.5.2 Rheology ..... 5-143

5.5.3 BSA Content Assay ..... 5-143

5.5.4 *In Vitro* Dissolution Study ..... 5-145

5.6 Results ..... 5-145

5.6.1 Polymer Matrix Selection ..... 5-146

5.6.2 Formulations Containing BSA ..... 5-153

5.7 Summary ..... 5-180

5.8 Conclusions ..... 5-182

## 5.3 Introduction

The process of developing a new route for sustained drug delivery for the pharmaceutical market is cost and time consuming. Whilst, the active pharmaceutical ingredient (API) is often well studied and understood, the impact of the polymer and additives on the stability and release behaviour is often unknown. Therefore, all formulations must undergo rigorous testing before being submitted for pre-clinical *in vivo* studies. These tests include monitoring the stability of the API in the presence of the formulation components, during processing and during storage via the appearance of degradation products. Assessing the toxicology of the proposed formulation using cell culture studies is also a key test. Not least, *in vitro* dissolution testing is required for all dosage forms in which absorption of the API is necessary to achieve the desired therapeutic effect.[157]

For most APIs to be effective they must be absorbed into the systemic circulation before they become bioavailable. This is a two-phase process that involves dissolution of the API from the formulation into the surrounding environment followed by absorption of the API into systemic circulation. Dissolution of the API into the surrounding environment has been shown to be critical for bioavailability and in many cases is the rate-limiting step for successful absorption of the drug.[224,225] This can be assessed by *in vitro* dissolution studies, where the dissolution of the API into the solution media is directly related to the rate of release of the API from a formulation.

Therefore, *in vitro* dissolution studies are invaluable for the optimisation of drug release, and are also used to detect physical changes in the API and the formulated product, such as the formation of degradation products. They are one of the most important quality control tools for ensuring batch-to-batch consistency, as well as serving as a comparative study for *in vitro- in vivo* correlation (IVIVC) or relations (IVIVR).[226] An *in vitro- in vivo* correlation is a rational relationship between biological properties or parameters derived from the physiochemical properties associated with a dosage form. The first dissolution study was performed in 1897 investigating the chemical and physical dissolution of sparingly soluble benzoic acid and lead

chloride in water.[227] However, the pharmaceutical importance of dissolution was not recognised until the early 1950s[225,228] and the impact of dissolution on the therapeutic effect of drugs was not investigated until the 1960s.[224] In 1971, a study by Lindenbaum et al. investigated the intestinal absorption of digoxin from tablets prepared by a variety of manufacturers.[229] This was prompted by increased reports of variations in bioavailability and reports of low serum concentrations despite the administration of large doses. Their study showed significant differences in serum concentration levels despite supposedly equal digoxin tablet concentration. These differences were not only observed between different manufacturers, but also between different batches produced by the same manufacturer. This led to an investigation by the U.S Food and Drug Administration (FDA) into the dissolution of 44 formulations of digoxin from 32 different manufacturers.[224] This study complemented the results reported by Lindenbaum, exposing a wide variation in the *in vitro* release profiles of the different formulations and thus rationalising the differences in bioavailability. Herein, the FDA and United Sates Pharmacopeia (USP) introduced official dissolution requirements for the evaluation of the *in vitro* release characteristics of pharmaceutical formulations. The test soon became a standard quality control tool for the pharmaceutical industry and to date there are seven specified apparatus for *in vitro* dissolution testing that adhere to those requirements.[157,224] In 1997, the FDA published four guidances that revolutionised the use of the dissolution test in drug delivery research. These guidances cover the general expectation of the test for immediate release (IR) dosage forms,[230] general expectations on the development, evaluation and application of IVIVC for modified release (MR) forms[231] and regulations on the scale up and post approval for IR[232] and MR dosage forms.[233] These guidances cemented the reliance on *in vitro* dissolution studies to rule out bioequivalence and to predict *in vivo* bioavailability.

The conditions of the *in vitro* dissolution tests are determined by the characteristics of the dosage form and the route of administration i.e. the dissolution media, apparatus and agitation rate should all be suitable for the product. A good dissolution study should be robust, free of artefacts, have low variability and discriminate between different formulations while having sufficient day-to-day reproducibility.[157]

By selecting experimental conditions that replicate *in vivo* conditions, it is possible to predict a trend in *in vivo* performance, generating successful IVIVC, and hence perform biorelevant dissolution studies.[234] Such correlations are of the utmost importance for the development of sustained release dosage forms because carrying out *in vivo* release studies of this nature would be impractical due to the long time scales and the need for multiple sampling occasions over the course of the study. The *in vitro* method also allows developers to ensure each batch of the same formulation performs identically before being tested *in vivo*.[157]

The Biopharmaceutics Classification Scheme suggested that, where possible, *in vivo* clinical studies should be substituted by biorelevant *in vitro* dissolution studies.[235] These *in vitro* dissolution studies act as a guide for formulation development and help to determine or reduce the need for bioavailability/bioequivalence tests in animals and humans.[234] Therefore, they are undoubtedly necessary for the development of drug delivery systems. However, the extended timescales required for the *in vitro* dissolution study of sustained release formulations means that it can take years of development until a formulation can enter the *in vivo* preclinical trial phase. In the case of sustained release formulations each dissolution study could last for 1, 3 or 6 months depending on the desired residence time of the API. The large experimental uncertainty associated with these tests means that large batch sizes and many reiterations have to be performed to ensure statistically accurate results. Therefore, although these tests are necessary, they are inefficient, time consuming and costly to the industry. Hence, this chapter explores the possibility of using a high pressure rheology technique as a pre-screening process to determine whether a formulation should be subjected to *in vitro* dissolution studies. It is expected that a homogeneous formulation would generate reproducible release profiles from *in vitro* dissolution studies. It is hypothesised that the homogeneity of a formulation during processing could be assessed by rheology. Hence, the rheology could be related to how well the formulation performs during the dissolution studies, and the number of unnecessary dissolution studies could be reduced.

Rheology is already a vital technique for the optimisation of polymer processing and as described in Chapter 1 biodegradable polymers such as poly($_{D,L}$-lactide) and its

derivatives have been investigated for use in the pharmaceutical industry for decades.[18,22–25] These polymers are chosen as they are generally biocompatible and break down into non-toxic water-soluble molecules.[22] By encapsulating APIs in a polymer based matrix it is possible to produce delivery systems with controlled release. These systems also offer some protection of the drug molecules against degradation.[17–19] There are many methods for producing these polymer-based systems including emulsion, spray drying and extrusion techniques, described in more detail in Chapter 1. In particular hot melt extrusion (HME) processing of polymers is gaining ground in the pharmaceutical industry,[59] and the key to its success as a processing technique lies in the characterisation of the polymer viscoelastic properties to aid processing and formulation design. Rheology has been used extensively in pharmaceutical HME to determine processing parameters such as melt temperature and screw rotation speed. For instance, reliable and accurate rheology data can be used in flow simulation and reduce the need for trial and error approaches to process design. In turn, this can save time, labour, materials and ultimately reduce waste and costs.[59]

It is well documented that the addition of APIs can alter the viscosity and viscoelastic properties of the polymer matrix, as covered in detail in Chapter 1.[59] The solubility and miscibility of the API in the polymer matrix will influence the flow properties of the formulation and these can be detected using rheology.[145,146] For example, miscible small molecule APIs act as plasticisers for the polymer matrix and lead to reduced $T_g$ and viscosity.[142,143] Conversely if the API is immiscible or insoluble it will act as a filler, increasing the viscosity of the formulation.[143,149] It is clear that these rheological investigations are invaluable for process development and for the determination of processing parameters. The question is, can the data obtained from rheology also be used to predict how well a formulation could perform in *in vitro* dissolution studies?

Various studies have been carried out to try to relate rheological properties to release. Lyons et al. reported on the use of agar as a filler for monolithic matrices.[150] Their study showed that an increased filler content resulted in an increase in viscosity and a decrease in the rate of release of the API. However, they attributed the

decrease in rate of release to a lack of disintegration and not the increased viscosity. Avgerinos et al. investigated the correlation between the mechanical properties of solid matrices, specifically cylindrical pellets and mini tablets, and the release of a model drug.[151] They found that in some cases, the release kinetics were inversely proportional to the tensile strength of the tablet but this was dependent on the processing method. Andrews et al. demonstrated that release from highly structured gel platforms is related to the elasticity and viscosity of the gel.[152] They showed that an increase in viscosity is related to increased internal structure, which in turn slows the rate of release; but this is also governed by the presence of different additives. Similarly, Aminabhavi et al. concluded that although the viscosity of a formulation has some influence over its release profile, it is the composition of a formulation that ultimately determines the release kinetics.[153] In all cases, the authors have tried to relate the rate of release to the rheological properties of the final product rather than the rheological properties of the formulation during processing. This work analysed the rheological properties of the formulations during processing with a view to assess the homogeneity of the formulation. It is assumed that a homogenous formulation will exhibit batch-to-batch reproducibility during *in vitro* dissolution studies. Therefore, if rheology can be used to describe the homogeneity of a formulation it could predict the *in vitro* release performance of the formulation, thereby improving the efficiency of the development process by reducing the number of *in vitro* studies that are required.

The cited investigations were performed at ambient pressure, because the authors sought to use the rheology data as a tool for process optimization for conventional polymer processing techniques. In all cases, the polymer must be in a liquefied state to enable thorough mixing of the formulation components. Typically, this would involve heating the polymer above its $T_g$ or $T_m$ or dissolving the components in an organic solvent. However, both of these methods can be detrimental to the API, especially those derived from proteins or peptides.[14,71] Temperatures above 40 °C can lead to the thermal degradation of protein and peptide based APIs. As described in Chapter 1, $CO_2$ has been extensively investigated as a potential green solvent alternative, to enable processing to occur at lower temperatures.[93] Although there

have been several reports acknowledging the ability of $CO_2$ to reduce the viscosity of the polymer-drug mixture, the processing temperatures are still high (110-190 °C) and there is no mention of high pressure rheology.[154–156] Lyons et al. report on the use of supercritical $CO_2$ ($scCO_2$) as a polymer plasticiser during hot melt extrusion processing of oral drug delivery devices.[155] The torque and die head pressure of the extruder are directly related to the viscosity of the mixture. Their results show a decrease in die pressure and torque with the use of $CO_2$ which they extrapolate to a reduction in viscosity. The use of $CO_2$ also increased the dissolution rate of the API, but this was attributed to the increased surface area on the monolith due to foaming upon $CO_2$ release.[155] Verreck et al. also investigated the use of $CO_2$ as a temporary plasticiser for hot melt extrusion processes.[156] Again there is no report of any high pressure rheology, and the ability of the $CO_2$ to successfully act as a plasticiser is inferred from the torque of the extruder. In this report, the authors show that $CO_2$ can sufficiently reduce the processing temperature, allowing for the incorporation of a thermally labile drug.[156]

This chapter focuses on investigating whether a high pressure rheology technique can be used to assess the homogeneity of pharmaceutical formulations. The hypothesis is that a homogeneous formulation will exhibit batch-to-batch reproducibility and comparable release profiles during *in vitro* dissolution testing. Therefore, rheology could be used to predict the performance of formulations reducing the need for multiple, lengthy release studies on every single formulation produced. This would also lower costs, save time and improve the efficiency of the whole formulation development process. Therefore, a series of formulations containing a model protein drug, BSA, encapsulated in a biodegradable polymer matrix were produced using a $CO_2$ mixing technique, similar to the particles from gas saturated solutions method described in Chapter 1. It was expected that the BSA would remain solid throughout the process and therefore the formulation would be akin to an amorphous solid dispersion and the presence of the API would increase the viscosity of the polymer melt.[149] The rheological properties under high pressure processing conditions were assessed using the high pressure rheology method developed previously. Micro Raman spectroscopy and a content assay provided

information on the homogeneity and BSA content of the formulations. Finally, an *in vitro* release study was performed and the results were compared to the rheology data.

## 5.4 Materials

Poly(ethylene glycol) with molecular weights of 400 g/mol and 6000 g/mol ($PEG_{0.4}$ and $PEG_6$, respectively) (Sigma Aldrich) and polycaprolactone with a molecular weight of 14,000 g/mol ($PCL_{14}$) (Sigma Aldrich) were stored at room temperature. The poly($_{D,L}$-lactic acid) with a molecular weight of 12,000 g/mol ($PLA_{12}$) (100 DL 2A, Evonik Industries) and poly($_{D,L}$-lactide-*co*-glycolide) with a molecular weight of 36,000 g/mol ($PLGA_{36}$) (7525 DLG 4A, Evonik Industries) were stored at -20 °C, see Table 5.1 for details. $PEG_6$ was ground using a pestle and mortar before use, while the other polymers were used as received.

Table 5.1. Details of the polymers used in this chapter.

| Polymer[a] | $M_n$[b] (g/mol) | $M_w$[b] (g/mol) | $Đ$[b] | $T_m$[c] (°C) | $T_g$[c] (°C) |
|---|---|---|---|---|---|
| $PEG_{0.4}$ | 400* | - | - | 6 | -41[#] |
| $PEG_6$ | 6000* | - | - | 61 | -41[#] |
| $PCL_{14}$ | 10,000* | 14,000* | 1.4 | 53 | -60[#] |
| $PLA_{12}$ | 7000 | 12,000 | 1.620 | - | 44 |
| $PLGA_{36}$ | 24,000 | 36,000 | 1.510 | - | 47 |

a) Subscript numbers refer to the molecular weight ($x10^3$ g/mol) of the polymer. b) Measured by triple detection GPC in THF using dn/dc value of 0.042 mL/g. c) Measured by DSC.*Nominal molecular weights from supplier. [#]Values taken from literature.[29,216,236–239]

Bovine serum albumin (BSA, Sigma Aldrich) was stored at 2-8 °C. Before use, the BSA was ground and milled to produce two different particle sizes. Large, irregular particles with an approximate diameter of 200 µm were produced using a pestle and mortar, herein referred to as BSAg. Jet milling was used to produce smaller, uniform

particles with an approximate diameter of 5 µm, herein referred to as BSAm. The particle sizes were estimated from SEM images (Figure 5.8).

Dialysis tubes with a molecular weight cut off of 100,000 g/mol (Spectrum Laboratories, Float-A-Lyzer G2, 1 mL) were purchased for use in the *in vitro* release study. Before use, the dialysis tubes required pre-wetting in an 10% alcohol/water solution in order to remove the glycerin coating as stated in the operator manual.[240] Dulbecco's phosphate buffered saline (DPBS, modified without calcium chloride and magnesium chloride, liquid, sterile-filtered, suitable for cell culture, Sigma Aldrich) was used as received.

Food grade $CO_2$ (99.8%; BOC, UK) for the high pressure rheology experiments, SFC grade $CO_2$ (99.99%; BOC, UK) for the $CO_2$ mixing, THF (HPLC grade, Fisher Scientific), propan-2-ol (Reagent grade, VWR) and deionised water were all used as received.

## 5.5 Methods

The materials were characterised by DSC, GPC, SEM, and Micro Raman Spectroscopy as described in Chapter 2. View cell experiments of the polymer blends were carried out according to the procedure described in Section 2.5.2.1. The $CO_2$ mixing procedure described in Section 2.5.3.1 was used to produce the final formulations.

### 5.5.1 Jet Milling of the BSA

In order to reduce the particle size of the BSA an Atritor M3 microniser was used (Upperton Pharma Solutions, August 2017). 15 g of BSA was manually fed into the venture of the microniser over a period of approximately 3 minutes. The venturi pressure was set to 6 bar; the maximum achievable in the lab. Initially, the grinding air pressure was set to 2 bar and increased to 4 bar during the first 10 seconds of the procedure. In order to achieve the desired particle size the micronised BSA was collected and passed through the microniser a second time. The processing time of the two runs was 9 minutes in total.

### 5.5.2 Rheology

All rheology measurements were performed following the low temperature method as described in Chapter 3 (Section 3.5.1 and 3.5.1.2.3). The measurements were performed directly at 40 °C and 140 bar $CO_2$. All data was fitted to the Carreau model[166] to give calculated values for the zero shear viscosity ($\eta_0$, Pa.s) as described in Chapter 2. The results of a minimum of four measurements per sample with a minimum of two samples per formulation were averaged.

The saturation viscosity ($\eta_{sat}$) and saturation time ($t_{sat}$) of the samples was determined by fitting the $\eta_0$ values to an empirical formula as described in Chapter 3.

### 5.5.3 BSA Content Assay

The BSA loading of each formulation was determined using the RI signal of a multidetector SEC system as described in Section 2.6.2. In order to determine the BSA concentration, a series of known concentrations of BSA in DPBS solution were analysed for calibration, and the integral of the sample peak ($I$) was plotted against the BSA concentration ($C$, mg/mL) (Figure 5.1).

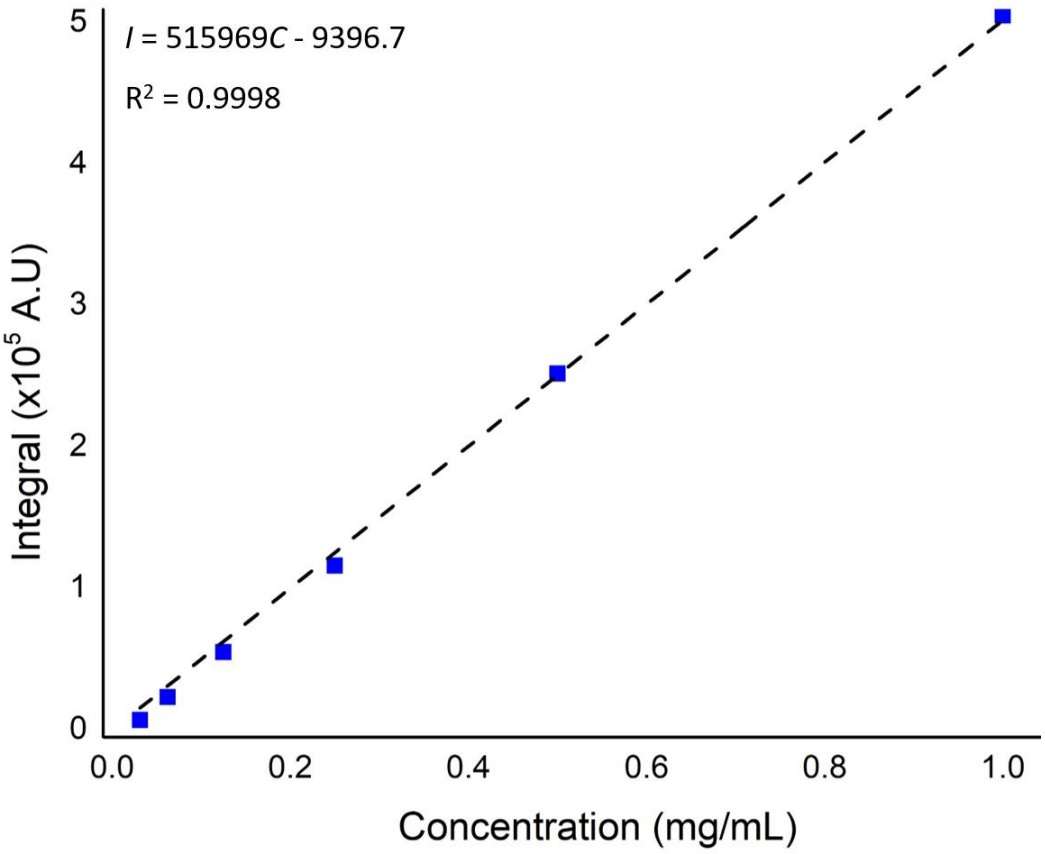



Figure 5.1. The integral of the resolving peak is plotted against the known BSA concentrations (blue squares) and fitted to a linear equation (black dashed line).

To ensure this method of analysis would be suitable for the formulations, polymer solutions in DPBS were spiked with known amounts of BSA and analysed. The results of the content assay demonstrated the suitability of this method for determining the BSA content of the formulations (Table 5.2, $R^2$ = 0.979).

Table 5.2. Comparison of the actual and calculated BSA content of the spiked polymer solutions.

| Sample | Actual BSA concentration (mg/mL) | Integral of the resolving peak | Calculated BSA concentration (mg/mL) |
|---|---|---|---|
| 1 | 2.2 | 1133967.6 | 2.22 |
| 2 | 1.9 | 863556.1 | 1.69 |
| 3 | 0.9 | 302794.3 | 0.61 |

This GPC method was also used to assess the amount of BSA that was released during the dissolution study.

### 5.5.4 *In Vitro* Dissolution Study

The *in vitro* dissolution study was carried out using 1 mL dialysis tubes (Float-A-Lyser G2 100,000 g/mol) submerged in 25 mL of DPBS. Prior to use the dialysis tubes were pre-wetted in a 10 v/v% solution of propan-2-ol in deionised water for 10 minutes. Subsequently, the membranes were rinsed repeatedly with deionised water then soaked in DPBS buffer overnight.[240]

The release study was performed on two tablets from each batch of the formulations. Tablets were pressed from 50 mg of sample using a 5 mm diameter mould at 2 tonnes of pressure for 30 seconds. Prior to loading into the dialysis tubes, the weight of each tablet was recorded and the approximate mass of BSA calculated from the content assay.

The tablets were loaded into individual dialysis tubes along with 1 mL DPBS buffer. These were then submerged in 25 mL DPBS buffer. A zero hour sample of each tablet was taken before being placed in the incubator shaker (Thermoscientific MaxQ 6000) at 180 rpm and 37 °C. Samples were then taken every 30 minutes for the first 4 hours and then every hour for the next 4 hours. Following this, samples were taken at 11, 24 and 48 hours to cover the initial burst period. As the study progressed, further samples were taken at 4, 7, 10, 15, 22 and 29 days. Samples were taken by removing 1 mL of the surrounding buffer and replacing with 1 mL of fresh DPBS; they were then analysed using the SEC-MALS method described previously in section 5.5.3.

## 5.6 Results

The aim of this chapter was to determine whether the rheology of a formulation could be used to predict how well it will perform during an *in vitro* dissolution study. The first aspect was to determine which blend of polymers would be most suitable for the polymer matrix. This blend must have a low enough viscosity to enable thorough mixing and yield a solid, homogeneous product upon removal of the $CO_2$. Once the polymer matrix was selected, a series of formulations containing the model drug, BSA, were produced using the $CO_2$ mixing procedure, as described in section 2.5.3.1. These formulations were then analysed by rheology and an *in vitro*

dissolution study was carried out to assess whether there was any correlation between the rheological properties of the formulation and its performance in the *in vitro* dissolution study.

### 5.6.1 Polymer Matrix Selection

Following discussions with Critical Pharmaceuticals Ltd (UK) a series of polymer blends were suggested based on a formulation for the extended release of ketamine. This formulation exhibited extended release over 3 months with minimal burst release and consisted of 60 wt.% API, 7.5 wt.% $PLGA_{36}$ and 32.5 wt.% PLA. However, due to the high molecular weight of the $PLGA_{36}$, it was difficult to process, resulting in low yield and poor API encapsulation. Oral communications with Critical Pharmaceuticals revealed that the high molecular weight $PLGA_{36}$ was required to promote extended release and to reduce burst release. Therefore, other polymers were investigated for use as a second polymer, which should have a lower viscosity than the $PLGA_{36}$ in order to improve processability and API incorporation without negatively affecting the burst release. PEG was chosen as an option for Polymer 2 as it is more hydrophilic than the PLGA and could improve the miscibility of hydrophilic drugs with the polymer matrix. Conversely, PCL and PLA are more hydrophobic than PLGA and will therefore reduce the dissolution rate of the formulation, further extending the release. All the polymers investigated for use as Polymer 2 had a lower viscosity than the $PLGA_{36}$; as demonstrated in Chapters 3 and 4 for the viscosities of $PLA_{12}$ and $PEG_5$, respectively. The viscosity of $PCL_{14}$, (47 Pa.s at ambient pressure and 80 °C) was reported by Curia et al.[131] Thus, all the chosen polymers matched the requirements of having a lower viscosity than $PLGA_{36}$. In order to determine which polymer was the most suitable for the polymer matrix, blends of $PLGA_{36}$ with the various second polymers were produced and their behaviour under processing conditions investigated. The ratio of the two polymers was based on the ketamine formulation as specified by Critical Pharmaceuticals and maintained at 18.75 wt.% $PLGA_{36}$ to 81.25 wt.% Polymer 2, see Table 5.3 for details.

Table 5.3. Properties of the polymers used for polymer 2 in the blends.

| Blend ID[#] | Polymer 2 | $M_n$[a] (g/mol) | $M_w$[a] (g/mol) | $Đ$[a] | $T_m$[b] (°C) | $T_g$[b] (°C) |
|---|---|---|---|---|---|---|
| $PLGA_{36}$18.75:$PEG_{0.4}$81.25 | $PEG_{0.4}$ | - | 400[$] | - | 6 | -41* |
| $PLGA_{36}$18.75:$PEG_{6}$81.25 | $PEG_{6}$ | 6000[$] | - | - | 61 | -41* |
| $PLGA_{36}$18.75:$PCL_{14}$81.25 | $PCL_{14}$ | 10,000[$] | 14,000[$] | 1.4 | 53 | -60* |
| $PLGA_{36}$18.75:$PLA_{12}$81.25 | $PLA_{12}$ | 7000 | 12,000 | 1.620 | - | 44 |

[#]Subscript number details the $M_w$ (x$10^3$ g/mol) of the preceding polymer, large number depicts the content (wt.%) of the preceding polymer. a) Measured by triple detection GPC. b) Determined by DSC. [$]Nominal molecular weights provided by the supplier. *Values obtained from literature.[29,216,236–239]

View cell experiments were performed on the blends containing $PEG_6$ and $PCL_{14}$ ($PLGA_{36}$18.75:$PEG_6$81.25 and $PLGA_{36}$18.75:$PCL_{14}$81.25, respectively) in order to determine whether these blends would be suitable for rheology studies. The components of the blend containing $PLA_{12}$ ($PLGA_{36}$18.75:$PLA_{12}$81.25) had already been characterised in detail in Chapter 3 and so it was not necessary to perform the view cell experiment. The blend containing $PEG_{0.4}$ ($PLGA_{36}$18.75:$PEG_{0.4}$81.25) was not investigated in the view cell since $PEG_{0.4}$ is a liquid at room temperature and thus, all the components would certainly be liquefied under processing conditions.

#### 5.6.1.1 View Cell Experiments

View cell experiments were performed on the neat $PLGA_{36}$ and the blends containing $PEG_6$ and $PCL_{14}$ ($PLGA_{36}$18.75:$PEG_6$81.25 and $PLGA_{36}$18.75:$PCL_{14}$81.25, respectively). The samples were placed in small vials inside the view cell and exposed to experimental conditions of 140 bar $CO_2$ at 40 °C. Photos were taken during pressurisation to observe any changes in the samples with $CO_2$ addition (Figure 5.2). The neat $PLGA_{36}$ began to plasticise at 55 bar $CO_2$ without heating (Figure 5.2b). By the time the cell was at 40 °C (~ 62 bar), the polymer was mostly liquefied (Figure 5.2c). Upon addition of $CO_2$ to reach a final pressure of 140 bar the sample is

completely liquefied confirming that a melt is obtained, which allows for rheological characterisation of the sample (previously reported in Chapter 3) (Figure 5.2d).

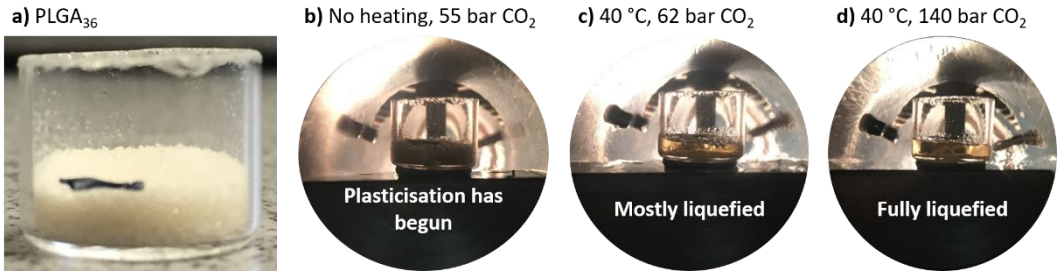



Figure 5.2. Images of $PLGA_{36}$ during the view cell experiment. **a**) $PLGA_{36}$ is a pale yellow granular solid and ambient pressure and temperature. **b**) Exposure to $CO_2$ causes plasticisation to begin. Increasing temperature (**c**) and then pressure (**d**) leads to completely liquefaction of the polymer. This experiment confirmed that it is possible to perform rheology studies at these conditions on the neat $PLGA_{36}$.

The blend consisting of 18.75 wt.% $PLGA_{36}$ and 81.25 wt.% $PEG_6$ ($PLGA_{36}$18.75:$PEG_6$81.25) remained solid under these experimental conditions (Figure 5.3). Hence, it was not possible to perform the rheology experiments and this blend was discarded as a potential formulation matrix. It has been well documented that PEG liquefies at 55 °C in the presence of $CO_2$[140] and so our observation at 40 °C was not unexpected. For the formulations used in this work, a temperature of 55 °C is too high, as it would result in the thermal degradation of the protein drug. However, this blend could be explored in future experiments for use with formulations that can withstand higher processing temperatures.

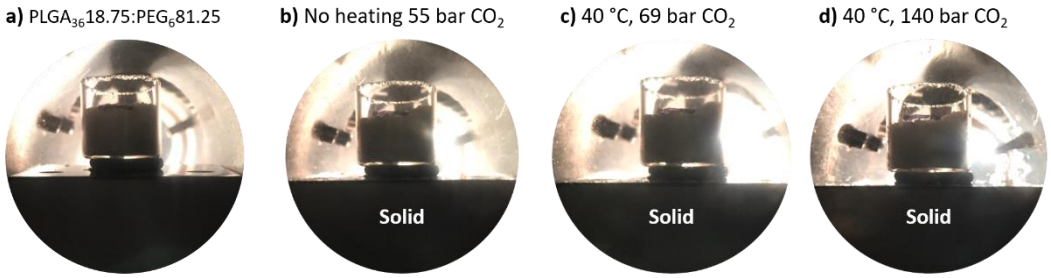



Figure 5.3. View cell images of $PLGA_{36}$18.75:$PEG_6$81.25 show that the sample remains solid throughout the experiment indicating that this blend is not suitable for further studies.

For the next blend ($PLGA_{36}18.75:PCL_{14}81.25$), the $PEG_6$ was replaced with $PCL_{14}$, another semi-crystalline polymer with a similar $T_m$. Curia at al. demonstrated that $CO_2$ can reduce the $T_m$ of PCL by 25 °C; using high pressure rheology and showed that these results were consistent with DSC and FTIR analysis.[131] In this study, the sample partially liquefied after 45 minutes of exposure to $CO_2$ at 140 bar and 40 °C (Figure 5.4b). The sample was left for a further 18 hours to see if over time it would liquefy completely (Figure 5.4d).

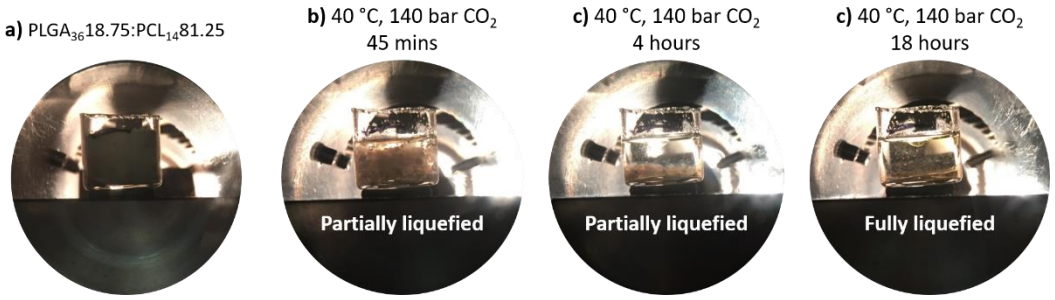



Figure 5.4. View cell images of $PLGA_{36}18.75:PCL_{14}81.25$ show that the sample is partially liquefied after being exposed to 140 bar $CO_2$ at 40 °C for 45 minutes (**b**). Leaving the sample for longer allows the $CO_2$ to plasticise the sample until it is fully liquefied (**d**).

As none of the samples were stirred during this experiment and the absence of stirring increases the soaking time (Chapter 3) it was decided that rheology measurements might be possible for this blend. Especially since Curia et al. showed that the $PCL_{14}$ homopolymer liquefied completely after 50 minutes of exposure to $CO_2$ at 120 bar and 45 °C.[131]

These view cell experiments suggest that it is not possible to analyse the blend containing $PEG_6$ ($PLGA_{36}18.75:PEG_6 81.25$), as it remained solid throughout the experiment. However, it should be possible to measure the viscosity of the blend containing $PCL_{14}$ ($PLGA_{36}18.75:PCL_{14}81.25$), as the shearing mechanism could promote plasticisation. Therefore, the blends containing $PEG_{0.4}$, $PCL_{14}$ and $PLA_{12}$ ($PLGA_{36}18.75:PEG_{0.4}81.25$, $PLGA_{36}18.75:PCL_{14}81.25$ and $PLGA_{36}18.75:PLA_{12}81.25$, respectively) were analysed using the low temperature, high pressure rheology method developed in Chapter 3 and their viscosities were compared to that of the neat $PLGA_{36}$.

### 5.6.1.2 Rheology of the Blends

The viscosities of the blends were significantly lower than that of the neat $PLGA_{36}$: $PLGA_{36}18.75:PEG_{0.4}18.25$ had a $\eta_{sat}$ of 0.2 Pa.s, while $PLGA_{36}18.75:PCL_{14}18.25$ and $PLGA_{36}18.75:PLA_{12}18.25$ both had a $\eta_{sat}$ of 3 Pa.s (Figure 5.5). This equates to a reduction in viscosity of > 99%, 97% and 98%, for the blends, respectively, compared to the $\eta_{sat}$ of 125 Pa.s of $PLGA_{36}$.

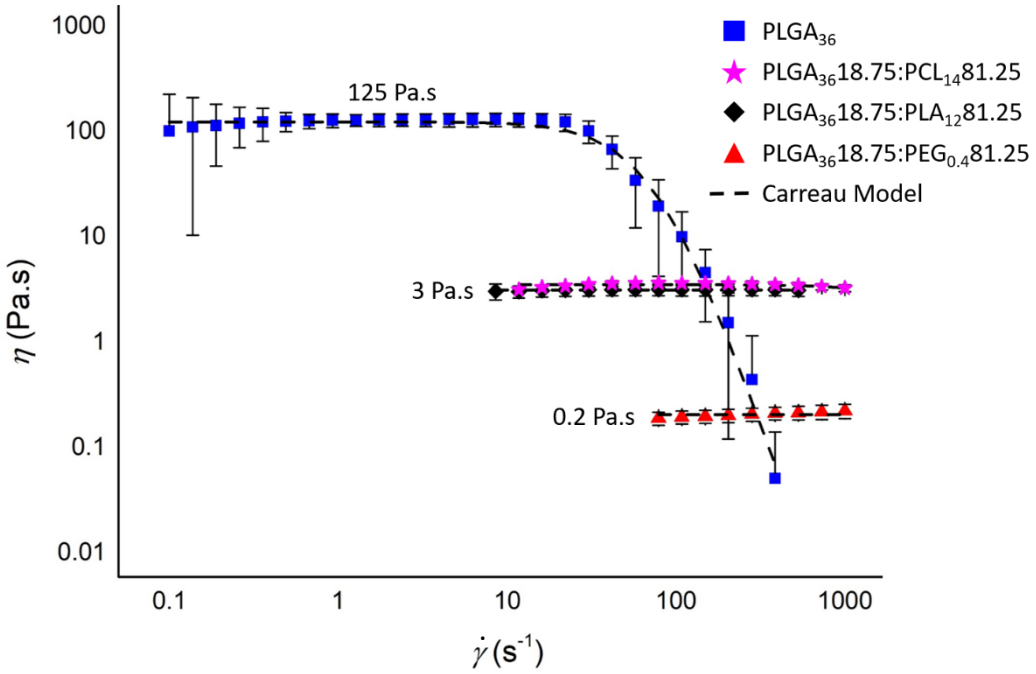



Figure 5.5. The viscosities of the blends were lower compared to that of the neat $PLGA_{36}$. Error calculated as ±1 standard deviation from the mean. $T$ = 40 °C, $P$ = 140 bar.

Given that $PEG_{0.4}$ was a viscous liquid, there were significant inconsistencies with the sample loading for that blend, resulting in the samples having a range of compositions and final loading weights. Also due to the low viscosity of the blend it was not possible calculate $t_{sat}$, so it was assumed that the sample reached $\eta_{sat}$ after less than 1 hour soaking in $CO_2$. After venting of the rheometer (i.e. after processing) the sample remained liquid which is not suitable for drug delivery formulations. Liquid formulations can be less stable than solid formulations so are generally considered unsuitable.

The viscosities of the blends containing $PCL_{14}$ and $PLA_{12}$ were very similar (3.56 and 3.06 Pa.s, respectively) (Figure 5.5). However, upon removal of $CO_2$, the blend containing $PCL_{14}$ phase separated. This was observed during the view cell experiments (Figure 5.6) and by DSC.

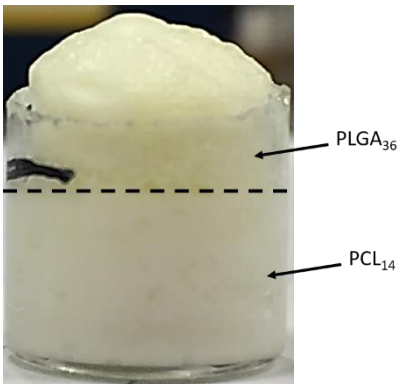



Figure 5.6. Image of $PLGA_{36}$18.75:$PCL_{14}$81.25 after the view cell experiment. Removal of the $CO_2$ results in phase separation of the two polymers.

In the view cell experiments 81.25 wt.% $PCL_{14}$ was physically mixed with 18.75 wt.% $PLGA_{36}$. In order to investigate whether the polymers exhibited a region of miscibility at lower $PCL_{14}$ concentrations DSC was performed on blends of three different ratios of $PCL_{14}$:$PLGA_{36}$: 10:90, 25:75 and 50:50 (Figure 5.7). The blends were produced *via* $CO_2$ blending as described in section 2.5.3.1 and ground to form a homogeneous powder. The Fox equation, shown in equation 5.1, predicts that if the polymers are miscible then a single $T_g$ should be detected at an intermediate value:[241]

$$\frac{1}{T_{g,blend}} = \sum_i \frac{w_i}{T_{g,i}} \qquad 5.1$$

Where $T_{g,blend}$ is the predicted glass transition temperature of the blend, $T_{g,i}$ is the glass transition temperature of the individual components and $w_i$ is the weight fraction of the components. Neat $PLGA_{36}$ has a $T_g$ of 47 °C while $PCL_{14}$ has a $T_m$ of 53 °C and a $T_g$ of -60 °C.[29] Due to the crystallinity of the PCL it was not possible to detect its $T_g$. Given that there was no significant difference in $T_g$ for the blends compared to the $PLGA_{36}$ homopolymer and that the values were not comparable with the predicted $T_g$s, it was concluded that the two polymers were not miscible at

any composition (Figure 5.7). Therefore, this blend is not suitable for future formulations as the immiscibility would lead to partitioning of the drug through the matrix and an uneven distribution of the drug. However, this could be useful for future work, where partitioning of the drug into different polymer phases might be exploited to result in controlled delivery.[242] In addition, the blend could not be readily ground to produce a fine powder.

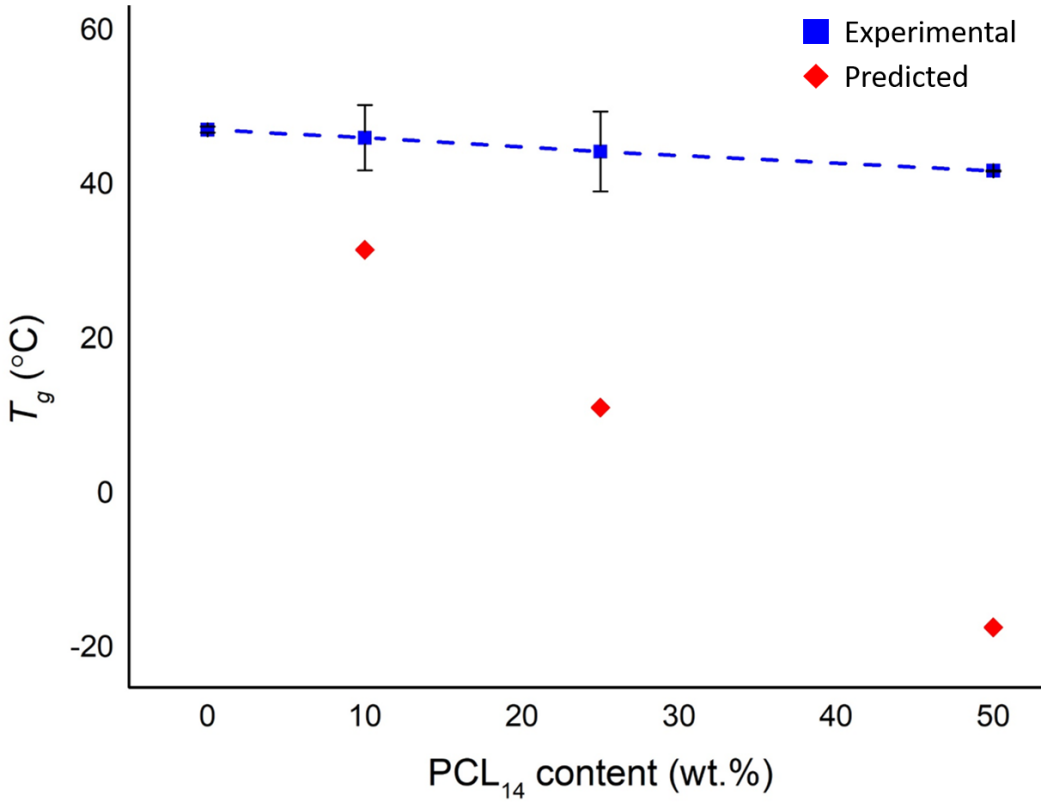



Figure 5.7. The $T_g$ of the blends does not change significantly with increasing $PCL_{14}$ content and does not agree with the predicted values from the Fox equation. Therefore, these two polymers are not miscible at any composition. Error calculated as ±1 standard deviation from the mean.

The viscosity of the blend containing $PLA_{12}$ was deemed to be sufficiently low to enable good mixing of the drug molecules during processing. In comparison to the blend containing $PCL_{14}$, the samples of $PLGA_{36}$18.75:$PLA_{12}$18.25 could be recovered from the rheometer after venting as a homogeneous solid and easily ground using a pestle and mortar to produce a fine powder. The neat $PLGA_{36}$ was difficult to grind, while the $PLA_{12}$ homopolymer and the blend of the two ($PLGA_{36}$18.75:$PLA_{12}$18.25) were brittle and easily manipulated. Although, other polymers were investigated for

use as Polymer 2, $PLA_{12}$ was the most suitable and its blend with $PLGA_{36}$ ($PLGA_{36}$18.75:$PLA_{12}$18.25) was used for the polymer matrix of the formulations.

### 5.6.2 Formulations Containing BSA

In this work, BSA was chosen as the model drug as it is readily available and is a common substitution for protein formulation work. As proteins have also been shown to be stable in the presence of high pressure $CO_2$ at mild temperatures BSA is a good candidate for this investigation.[243] As explained in Chapter 1, the ratio of API to polymer is usually high; in order to eliminate the possibility of unwanted side effects from the use of excipients. However, it was decided that the amount of API in the formulation should be reduced so that the polymers were the main component by weight. This would improve API encapsulation efficiency but by investigating two different compositions (40 and 20 wt.% BSA), it would still be possible to document the effect of API on the rheological properties of the formulation. Two different particle sizes of BSA (200 µm and 5 µm approximate particle diameter) were also investigated in order to assess if particle size affected the viscosity of the formulation and therefor the release profile. The large, irregular particles were produced by grinding using a pestle and mortar and subesequent sieving, BSAg (Figure 5.8a), while the smaller, uniform particles were produced by jet milling, BSAm (Figure 5.8b).

Thus, five formulations were produced *via* the $CO_2$ mixing procedure (section 2.5.3.1), and are detailed in Table 5.4; two batches were produced per formulation. For the first four formulations, the polymer ratio was maintained at $PLGA_{36}$18.75:$PLA_{12}$18.25 while taking into account the addition of the BSA. For the final formulation, the BSA content was maintained at 20 wt.% and the polymer ratio adjusted. It was possible to grind all formulations to produce homogeneous powders for rheology and BSA content analysis, and to press tablets for the *in vitro* release study.

Table 5.4. Composition details of the five formulations containing BSA.

| ID* | Approx. BSA particle size (μm)[a] | BSA content (wt.%) | $PLGA_{36}$ content (wt.%) | $PLA_{12}$ content (wt.%) |
|---|---|---|---|---|
| $PLGA_{36}$11.25:BSAg40 | 200 | 40 | 11.25 | 48.75 |
| $PLGA_{36}$11.25:BSAm40 | 5 | | | |
| $PLGA_{36}$15:BSAg20 | 200 | 20 | 15 | 65 |
| $PLGA_{36}$15:BSAm20 | 5 | | | |
| $PLGA_{36}$30:BSAm20 | 5 | 20 | 30 | 50 |

*subscript number refers to the $M_w$ (x$10^3$ g/mol) of the preceding polymer, large number refers to the content (wt.%) of the preceding component. a) Approximated from SEM.

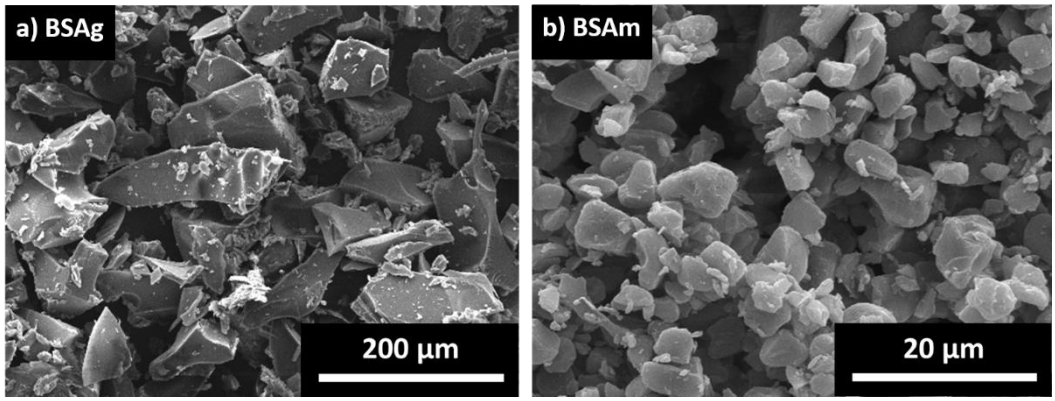



Figure 5.8 SEM images of BSA particles of different sizes. **a**) BSAg- large, irregular particles with an approximate diameter of 200 μm, produced by grinding and sieving. **b**) BSAm- small, uniform particle with an approximate diameter of 5 μm, produced by jet milling.

### 5.6.2.1 Rheology of the BSA Formulations

The addition of BSA increased the viscosity of the formulations in comparison to the polymer blend, which had a $\eta_{sat}$ of 3 Pa.s (Table 5.5). This is expected as the BSA particles remained solid in the polymer matrix and therefore acted as a filler for the formulation. In addition, the data can be fitted to the Krieger-Dougherty relationship, described by equation 5.2 (Figure 5.9).[244–246] Where $\eta_r$ is the relative viscosity, $\eta$ is the viscosity of the formulation, $\eta_0$ is the viscosity of polymer matrix, $\phi$ is the volume fraction of particles, $\phi_m$ is the maximum packing and $[\eta]$ is the intrinsic viscosity which is equivalent to 2.5 for spherical particles.

$$\eta_r = \frac{\eta}{\eta_0} = \left(1 - \frac{\phi}{\phi_m}\right)^{-[\eta]\phi_m} \quad 5.2$$

An increased loading of BSA resulted in an increase in viscosity; as evident from the viscosity of the blends containing 40 wt.% BSA and 11.25 wt.% $PLGA_{36}$ (24 Pa.s) compared to the viscosity of the blends containing 20 wt.% BSA and 15 wt.% $PLGA_{36}$ (5 Pa.s).

Table 5.5. $\eta_{sat}$ and $t_{sat}$ values determined from the Carreau model fitting and the time to saturation calculation.

| Blend ID[a] | $\eta_{sat}$ (Pa.s) | | | $t_{sat}$ (hours) | |
|---|---|---|---|---|---|
| | Average | SD | RSD (%) | Average | SD |
| $PLGA_{36}$18.75:$PLA_{12}$81.25 | 3.1 | 0.1 | 3.2 | 1.7 | 0.6 |
| $PLGA_{36}$11.25:BSAg40 | 24* | 5 | 21 | < 1** | - |
| $PLGA_{36}$11.25:BSAm40 | - | - | - | < 2h** | - |
| $PLGA_{36}$15:BSAg20 | 5.8 | 0.1 | 1.7 | 1.8 | 0.01 |
| $PLGA_{36}$15:BSAm20 | 5.0 | 0.3 | 6.0 | 2.5 | 0.4 |
| $PLGA_{36}$30:BSAm20 | 14 | 0.9 | 6.4 | 1.8 | 0.04 |

a) BSAg particles were produced by grinding and subsequent sieving and BSAm particles were produced by jet milling. *Calculated from the average of the $\eta_0$ values determined from the Carreau Model. **Could not be calculated using the $t_{sat}$ calculation. Error calculated as ±1 standard deviation from the mean. $T$ = 40 °C, $P$ = 140 bar.

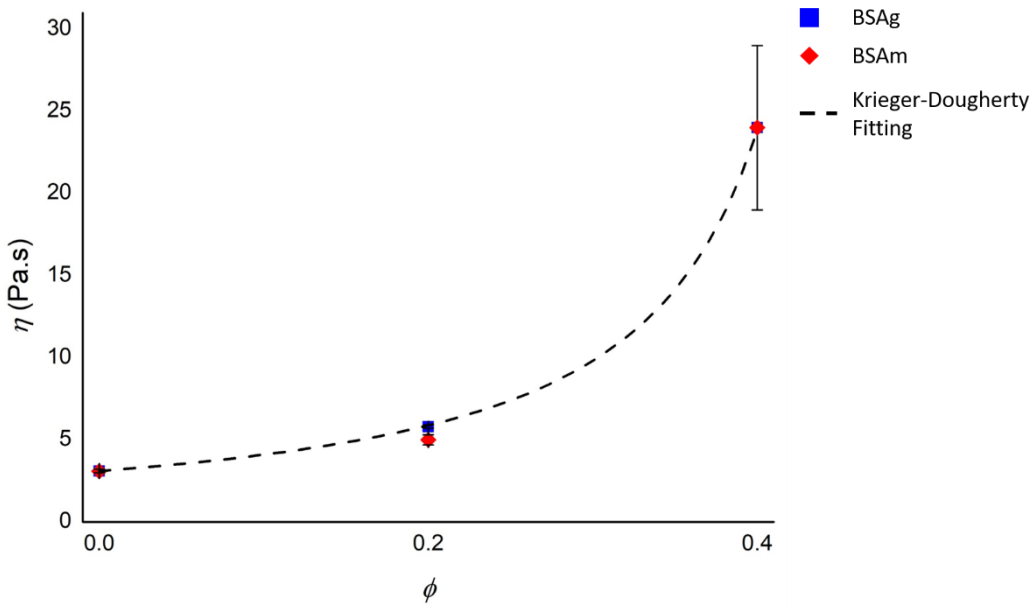



Figure 5.9. As the concentration of solid BSA in the formulations was increased, the viscosity increased for both particle sizes of BSA. The trend could be fitted with the Krieger-Dougherty relationship.

Overall, the addition of 40 wt.% BSA resulted in reduced reproducibility, demonstrated by the large relative standard deviation (RSD) in the viscosity measurements compared to that associated with the formulations containing 20 wt.% BSA (Table 5.5). This prevented the calculation of $t_{sat}$ and the standard calculation of $\eta_{sat}$ for both the blends containing 40 wt.% BSA. It was possible to fit the viscosity of the blend containing 40 wt.% BSAg ($PLGA_{36}$11.25:BSAg40, Figure 5.10a blue squares) to the Carreau model and so the $\eta_{sat}$ was estimated from the average of all the $\eta_0$ values generated from the Carreau model. In general, the particle size of the BSA did not have any significant impact on the viscosity profile. However, for the blend containing 40 wt.% BSAm ($PLGA_{36}$11.25:BSAm40) a second plateau was observed at high shear rates which meant it could not be fitted to the Carreau model, preventing the evaluation of $t_{sat}$ and $\eta_{sat}$ (Figure 5.10a red diamonds). On the other hand, analysis of the blends containing 20 wt.% BSA were much more reproducible with lower RSDs (Table 5.5). Additionally, the data could be fitted to the Carreau model and subsequently $t_{sat}$ and $\eta_{sat}$ could be calculated (Figure 5.10b). Increasing the ratio of $PLGA_{36}$ with respect to $PLA_{12}$ resulted in an increase in viscosity (14 Pa.s for $PLGA_{36}$30:BSAm20), this was due to the increased amount of $PLGA_{36}$ which has a much higher viscosity than the $PLA_{12}$ homopolymer (Figure 5.10b).

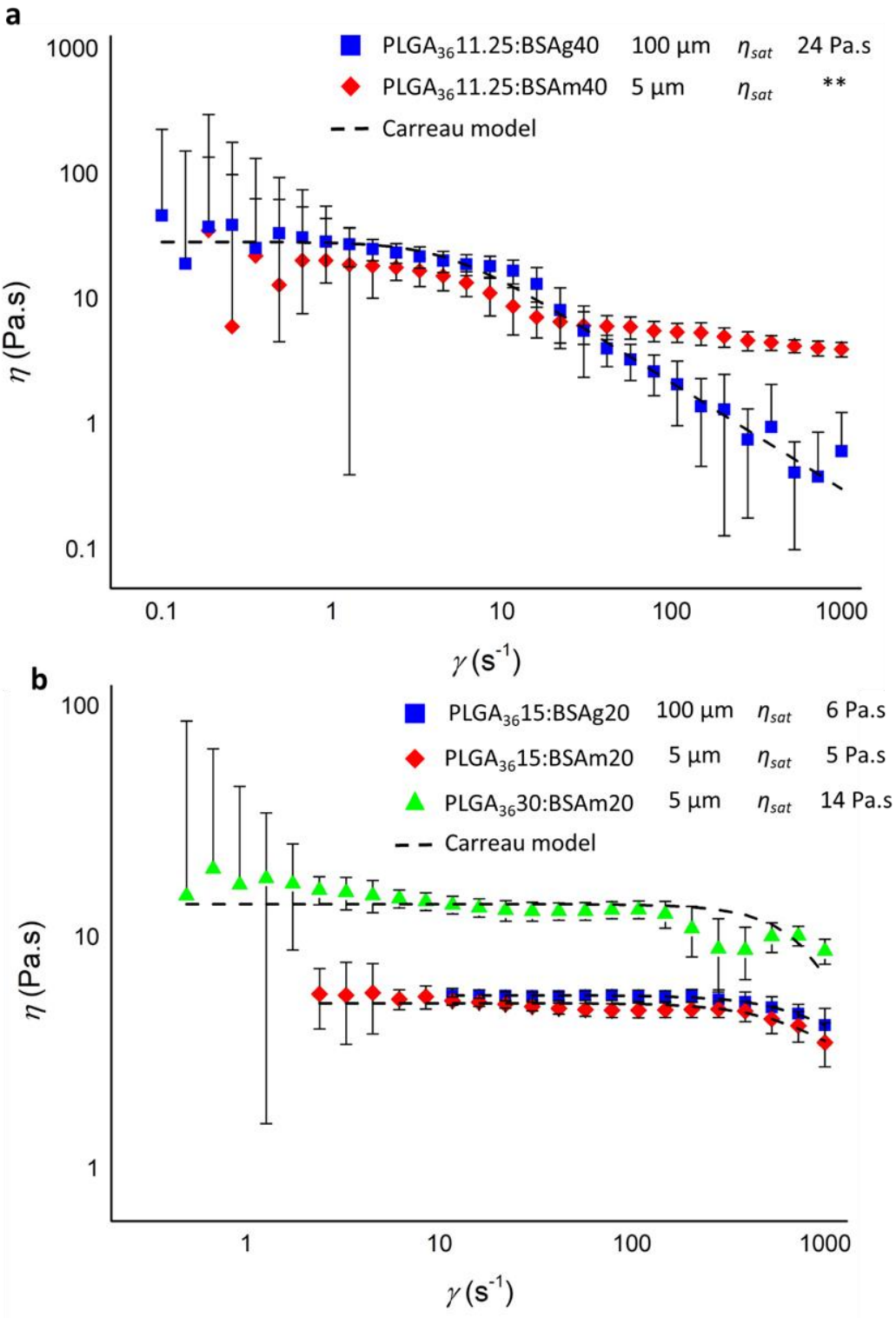



Figure 5.10. The viscosities of the formulations with different BSA loadings and different particle sizes are compared. **a**) Formulations containing 40 wt.% BSA. **The blend containing BSAm (red diamonds) could not be fitted to the Carreau model and thus the $\eta_{sat}$ could not be quantified. **b**) Formulations containing 20 wt.% BSA. Error calculated as ±1 standard deviation from the mean. $T$ = 40 °C, $P$ = 140 bar. *Large error bars are observed at low shear rates because the measurement is approaching the lower toque limit of the instrument, as explained in Chapter 2.

Overall the rheology data could imply that the formulations containing 40 wt.% BSA were not very homogeneous, or the BSA content was too high and the presence of the solid particles disrupted the rheology measurements. Conversely, the reproducibility of the formulations containing 20 wt.% BSA could suggest that the drug was evenly distributed throughout the matrix. The formulation containing 40 wt.% BSAg had a comparatively large RSD, compared to that of the formulations containing 20 wt.% BSA (Table 5.5). However, all the RSD values (that could be evaluated) are considered to be acceptable for this type of measurement.

#### 5.6.2.2 Content Assay of BSA Formulations

An *in vitro* release study was designed in order to assess the release profile of the formulations and determine whether there was any correlation to the viscosity measurements. Before the release study could commence it was necessary to quantify the BSA loading of each batch of each formulation. The samples were analysed by GPC and the area of the peak corresponding to the BSA was evaluated using a previously established calibration to generate the BSA concentration (Section 5.5.3). The loading of each batch of each formulation was determined in triplicate and then averaged. The loadings were then used to calculate the mass of BSA in each tablet, which was then used to determine the percentage of BSA being released during the *in vitro* dissolution study (Table 5.6).

Table 5.6. Loading of BSA formulations determined by GPC compared to the targeted loading.

| Blend ID | Target BSA loading (wt.%) | Actual BSA loading (wt.%) | | | Percentage difference from target loading (%) |
|---|---|---|---|---|---|
| | | Average | SD | RSD (%) | |
| $PLGA_{36}$11.25:BSAg40 | 40 | 48 | 0.6 | 1 | 20 |
| | | 48 | 0.7 | 2 | 20 |
| $PLGA_{36}$11.25:BSAm40 | 40 | 42 | 0.7 | 2 | 5 |
| | | 40 | 0.8 | 2 | 0 |
| $PLGA_{36}$15:BSAg20 | 20 | 25 | 1.3 | 5 | 25 |
| | | 25 | 0.7 | 3 | 25 |
| $PLGA_{36}$15:BSAm20 | 20 | 19 | 0.4 | 2 | 5 |
| | | 18 | 1.8 | 10 | 10 |
| $PLGA_{36}$30:BSAm20 | 20 | 10 | 1.8 | 18 | 50 |
| | | 12 | 2.6 | 22 | 40 |

In general, the formulations containing BSAm and the standard polymer ratio ($PLGA_{36}$11.25:BSAm40 and $PLGA_{36}$15:BSAm20) are closer to the desired BSA content than the ones containing BSAg ($PLGA_{36}$11.25:BSAg40 and $PLGA_{36}$15:BSAg20). Across both particle sizes the formulations containin 40 wt.% BSA are also closer to the target loading than those containing 20 wt.% BSA. When the actual BSA loading values were compared with the $\eta_{sat}$ values the following trend was observed: $PLGA_{36}$15:BSAm20<$PLGA_{36}$15:BSAg20<$PLGA_{36}$11.25:BSAm40<$PLGA_{36}$11.25:BSAg40, as expected. The BSA content of the blend containing increased $PLGA_{36}$ content ($PLGA_{36}$30:BSAm20) is significantly lower than the targeted loading, and is not as uniform across the two batches as for the previous blends. This could be a direct consequence of the increased viscosity of this formulation resulting in reduced mixing and therefore an uneven distribution of BSA through the formulation. This did not influence the uniformity of the $\eta_{sat}$ value which has a similar RSD to that of the other blend containing 20 wt.% BSAm ($PLGA_{36}$15:BSAm20). However, there is an increased variance in the overall rheology profile of $PLGA_{36}$30:BSAm20 compared to $PLGA_{36}$15:BSAm20 in accordance with an uneven distribution of BSA.

The RSD values for the formulations containing BSAm were larger than those containing BSAg suggesting these formulations had a less homogenous distribution of BSA. The same observation was made for the RSD values of the rheological profiles and the $\eta_{sat}$ values indicating that rheology could be used to predict the homogeneity of a formulation. Conversely, when the RSD values of the formulations containing 40 wt.% BSA are compared with those containing 20 wt.% the same trend is not seen for the loading as the rheology. For the loading data the formulations containing 20 wt.% BSA have the larger RSD, while the 40 wt.% formulations have the larger RSD values in the rheology data. Overall, the RSD values for the blends (excluding $PLGA_{36}$30:BSAm20) are relatively low suggesting that in general the BSA is evenly distributed through the formulations.

#### 5.6.2.2.1 Distribution of BSA in the Polymer Matrix

Micro Raman spectroscopy was employed to assess the distribution of BSA through the polymer matrix. Each batch of each formulation was pressed into 50 mg tablets and analysed by collecting individual point spectra within a defined area to produce false colour surface maps where the individual components can be identified and spatially located. Discrimination of the $PLGA_{36}$ and $PLA_{12}$ proved to be particularly challenging due to their similarities in chemical structure. However, it was possible to distinguish between the polymer matrix and the BSA, using the intensity of the bands at 1769 $cm^{-1}$ (C=O stretching) and 1656 $cm^{-1}$ (Amide I band), respectively (Figure 5.11). The spectra are all in agreement with previous literature studies.[247–249]

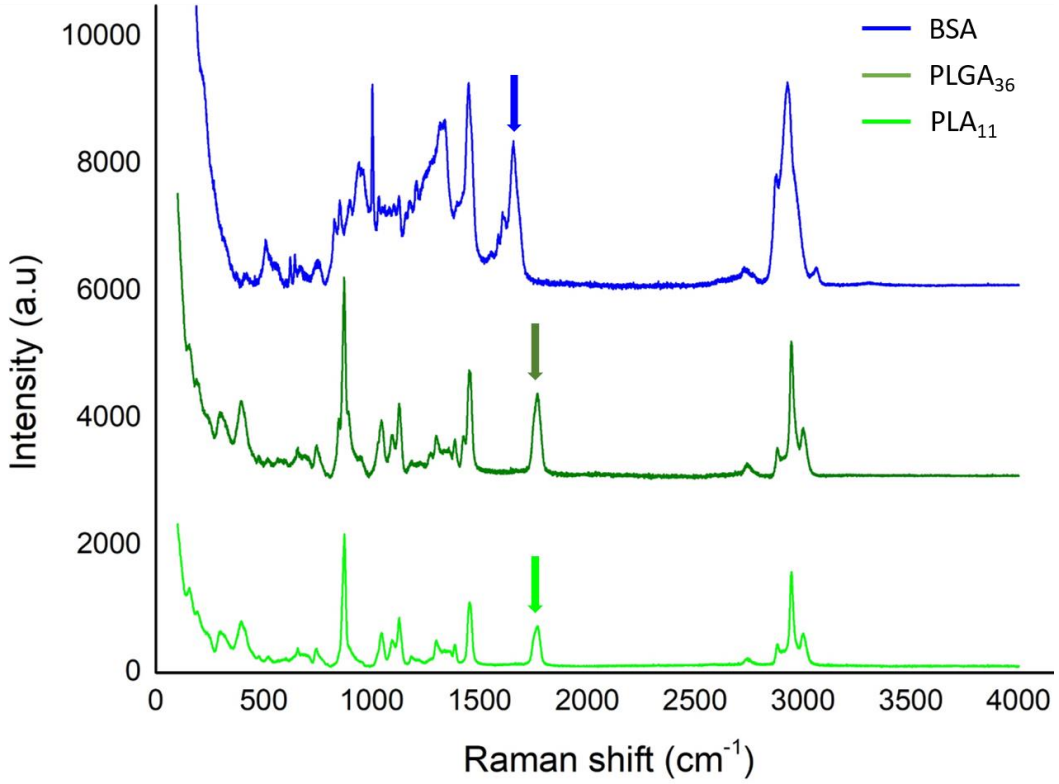



Figure 5.11. Component Raman spectra of BSA, $PLGA_{36}$ and $PLA_{12}$ where the arrows indicate the diagnostic bands of the components at 1656 $cm^{-1}$ for BSA (blue) and 1769 $cm^{-1}$ for the polymers (green).

The spectra of the formulations contain signals from the individual components. A visual comparison of the peak ratios for the Amide I band at 1656 $cm^{-1}$ confirms the increased loading of BSA in the 40 wt.% blends compared with those containing 20 wt.% BSA (Figure 5.12).

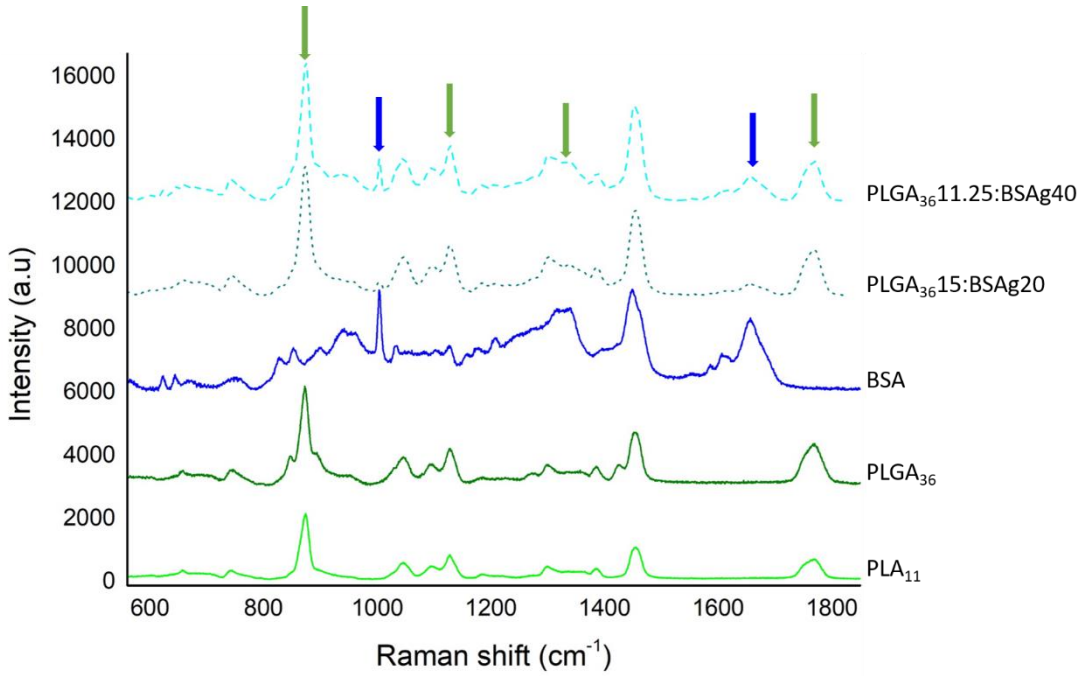



Figure 5.12. Raman spectra of the formulations contain peaks attributed to the presence of BSA (blue arrows) and the polymer matrix (green arrows). The increase in BSA content is confirmed by the increase in peak intensity of the band at 1656 $cm^{-1}$. The spectra of blends containing 40 and 20 wt.% BSAg ($PLGA_{36}$11.25:BSAg40 and $PLGA_{36}$15:BSAg20, respectively) are displayed as representative examples of all the blends.

The surface maps were obtained by acquiring spectra over the range 540-1820 $cm^{-1}$ at 100 µm steps within a 3 $mm^2$ area. The intensities (as height) of the bands were evaluated using univariate analysis (UVA) in the range 1540-1720 $cm^{-1}$ and 1720-1825 $cm^{-1}$ for BSA (blue) and the polymers (green), respectively (Figure 5.13). Classic least squares (CLS) regression analysis was used to quantify the BSA content of the formulations, along with the intensity ratio of the BSA and the polymer ($I_{BSA}/I_{polymer}$) from UVA.

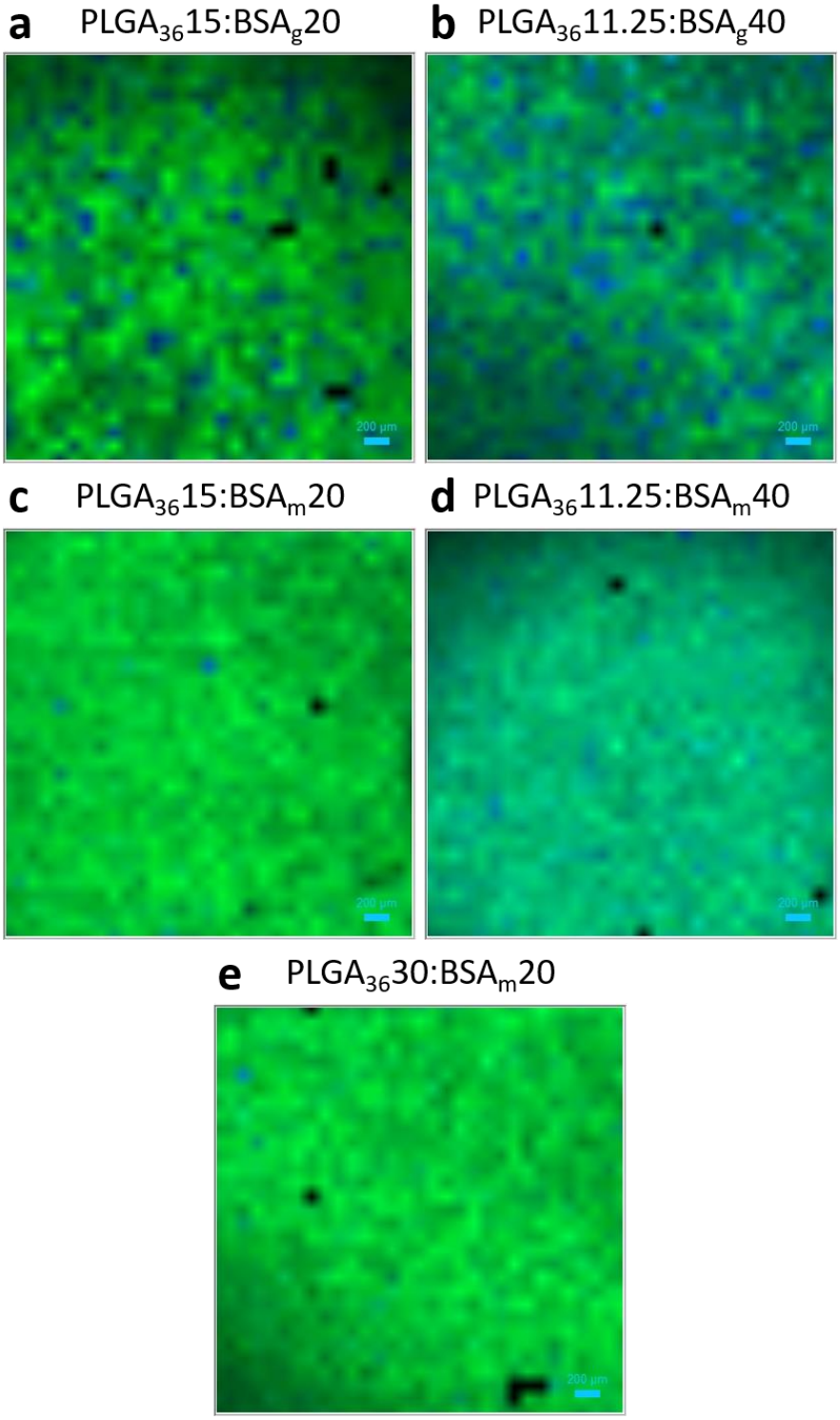



Figure 5.13. Surface maps of the tablets generated by Raman spectroscopy. The maps obtained by UVA describe the distribution of BSA (blue) and the polymers (green) with the intensity and concentration of the blue being lower for the blends containing 20 wt.% BSA (**a**, **c** and **e**) than for the blends containing 40 wt.% BSA (**b** and **d**). Note that the black pixels are due to fluorescence and therefore the contents at those pixels could not be accurately determined.

As expected there is increased spacing between the blue domains for the blend containing 20 wt.% BSA ($PLGA_{36}$15:BSAg20, Figure 5.13a) compared to the blend containing 40 wt.% BSA ($PLGA_{36}$11.25:BSAg40, Figure 5.13b) in agreement with the reduced BSA content. The BSA appears to be evenly distributed throughout out the mapped area of both blends suggesting good mixing has occurred. In comparison, there was very little BSA visible in the maps associated with the formulations containing 20 wt.% BSAm. This could be attributed to the size of the BSA particles being much smaller than the size of the pixels, 5 µm compared to 100 µm, respectively. Another explanation could be that the BSA was small enough to be encapsulated within polymer microparticles and is therefore not visible on the tablet surface (Figure 5.14).

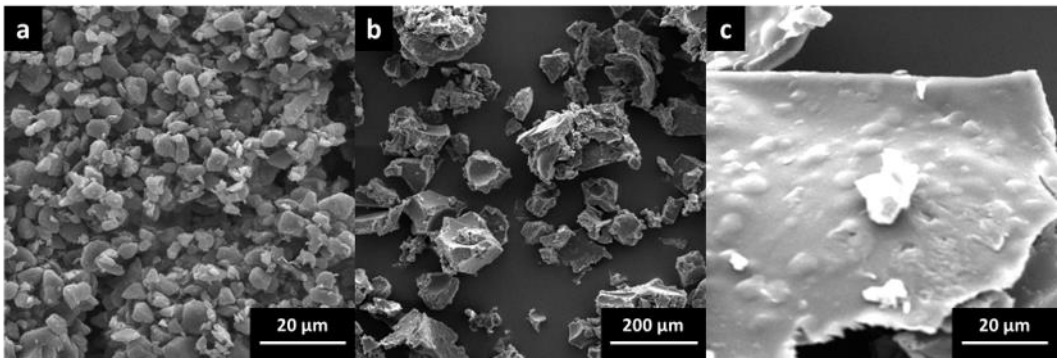



Figure 5.14. SEM images of BSAm (**a**), the formulation containing 20 wt.% BSAm (**b**) and an expanded area of b showing BSAm particles in a polymer matrix (**c**).

The average particle diameter of the BSAm was 5 µm (Figure 5.14a), while the formulation had an average particle diameter of 100-200 µm (Figure 5.14b). Therefore, the BSAm was small enough to be encapsulated within the polymer matrix (Figure 5.14c). Conversely, the BSAg had an average particle diameter of 100-200 µm (Figure 5.15a) which was similar to average particle diameter observed for the formulation (Figure 5.15b). This meant it was not possible to encapsulate the BSAg within the polymer for the formulations containing BSAg (Figure 5.15c). Hence, the BSA was clearly visible in surface maps of the formulations containing BSAg.

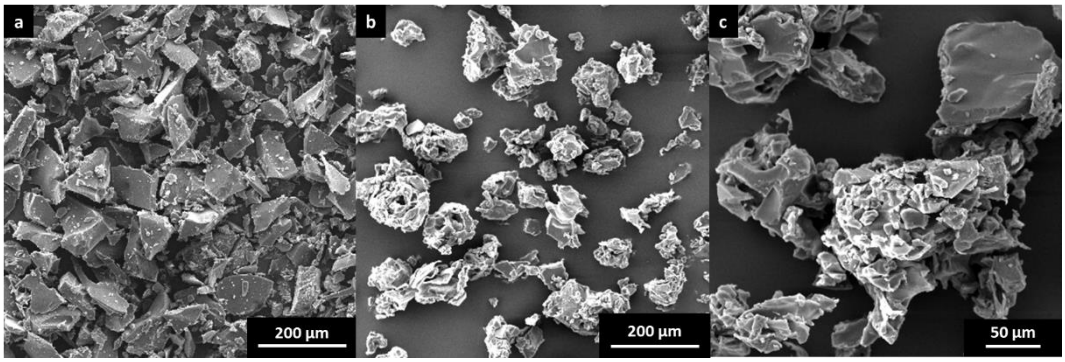



Figure 5.15 SEM images of BSAg (**a**), the formulation containing 40 wt.% BSAg (**b**) and an expended area of b with no evidence of encapsulation (**c**).

Intensity bars allowed for a quantitative description of the BSA concentration as determined by CLS fitting (0-100%, scores normalised at each location). By extracting the normalised BSA score from the CLS fitting from each pixel within the map it is possible to quantify the BSA content (Table 5.7).

Table 5.7. Loading of BSA formulations determined by CLS fitting compared to the targeted loading.

| Blend ID | Target BSA Loading (wt.%) | Measured BSA Loading (wt.%) | | | Percentage difference from target loading (%) |
|---|---|---|---|---|---|
| | | Average | SD | RSD | |
| $PLGA_{36}$11.25:BSAg40 | 40 | 38 | 9 | 23 | 5 |
| | | 39 | 9 | 22 | 3 |
| $PLGA_{36}$11.25:BSAm40 | 40 | 42 | 2 | 5 | 5 |
| | | 43 | 4 | 8 | 8 |
| $PLGA_{36}$15:BSAg20 | 20 | 22 | 12 | 55 | 10 |
| | | 18 | 12 | 65 | 10 |
| $PLGA_{36}$15:BSAm20 | 20 | 24 | 4 | 16 | 20 |
| | | 25 | 4 | 15 | 25 |
| $PLGA_{36}$30:BSAm20 | 20 | 32 | 3 | 9 | 60 |
| | | 32 | 3 | 8 | 60 |

In agreement with the content assay, the loading values were within a similar range and the loading of the 40 wt.% formulations were closer to the target value than the

20 wt.% formulations. However, the loading values of the formulations containing elevated levels of $PLGA_{36}$ were substantially higher than expected at 30 wt.% compared to a target of 20 wt.%. These were also higher than the values determined by the content assay, although the RSD values were smaller. It was concluded that this was a result of photoluminescence associated with the $PLGA_{36}$ content, which manifested as a non-zero-baseline. This was due to the slight yellow colouration of the PLGA in the samples. As the $PLGA_{36}$30:BSAm20 formulations contained double the amount of $PLGA_{36}$ compared to the other formulations, it follows that the influence of photoluminescence is greatest in these samples. Therefore, the quality of the fit was significantly reduced for the samples where one or more of the components contribute to a non-zero baseline.

As an alternative to the CLS fitting, the BSA loading was quantified by determining the intensity of the peak heights using UVA and taking the ratio the BSA to polymer ($I_{BSA}/I_{Polymer}$). This avoided any issues with photoluminescence, and although the absolute loading values could not be calculated, the loading was defined and followed a general trend (Table 5.8). For example, the results for the formulations containing 40 wt.% BSA were approximately double that of the formulations containing 20 wt.% BSA (0.7 compared to 0.35 for BSAg and 0.65 compared to 0.27 for BSAm). In addition, the values for the formulations containing increased $PLGA_{36}$ (0.3) were also consistent with the other formulations containing 20 wt.% BSA. Furthermore, the trend observed for the $I_{BSA}/I_{Polymer}$ values was the same as that seen in the content assay and the $\eta_{sat}$ values.

Table 5.8. Loading of BSA formulations determined by UVA compared to the targeted loading.

| Blend ID | Target BSA Loading (wt.%) | $I_{BSA}/I_{Polymer}$ | | |
|---|---|---|---|---|
| | | Average | SD | RSD |
| $PLGA_{36}$11.25:BSAg40 | 40 | 0.69 | 0.40 | 58 |
| | | 0.70 | 0..40 | 57 |
| $PLGA_{36}$11.25:BSAm40 | 40 | 0.64 | 0.09 | 14 |
| | | 0.65 | 0.12 | 18 |
| $PLGA_{36}$15:BSAg20 | 20 | 0.35 | 0.38 | 109 |
| | | 0.32 | 0.33 | 103 |
| $PLGA_{36}$15:BSAm20 | 20 | 0.27 | 0.07 | 26 |
| | | 0.26 | 0.08 | 31 |
| $PLGA_{36}$30:BSAm20 | 20 | 0.28 | 0.07 | 25 |
| | | 0.27 | 0.07 | 26 |

Overall, the formulations containing BSAg were more variable, with larger RSDs than those containing BSAm, which was in contrast with the content assay and the rheology data. This was attributed to the size of the BSA in each case, relative to the size of the map pixel. For the formulations containing BSAm, the BSA size was significantly smaller (5 µm) than the pixel (100 µm) and as such there is an effect of averaging that homogenises the BSA distribution. Conversely, the size of the BSAg (100-200 µm) was comparable to the mapping pixel. Hence, the chance of finding BSA within any given pixel is much more variable making the distribution appear less homogeneous. Referring back to the surface maps, where the colour of each pixel is very similar throughout the entire map (Figure 5.13c and d), then the BSA loading per pixel is more uniform, with the effect being more pronounced at lower loadings.

In agreement with the content assay, the formulations containing 20 wt.% BSA demonstrated larger RSD values than those containing 40 wt.% BSA. However this does not correspond with the rheology data, where the 40 wt.% formulations were found to have the larger RSD values.

### 5.6.2.3 Dissolution Study of the BSA Formulations

The formulations were pressed into 50 mg tablets (Figure 5.16) for the release study. At least two tablets were produced from each batch, as there were two batches per formulation, the release profiles of each formulation are representative of an average of four results.

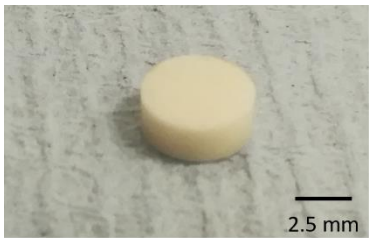



Figure 5.16. Tablets with 5 mm diameter were pressed from 50 mg of formulation.

For the larger BSA particles (BSAg, 200 μm), the results from the initial dissolution study of the blend containing 40 wt.% BSA ($PLGA_{36}11.25$:BSAg40) were inconclusive, as there were two distinct trends over the four tablets. One tablet from each batch released the majority of the BSA (up to 80%) in the first 5 days (Figure 5.17a tablets a2 and b2), while the other two tablets showed slower release over the course of the study (Figure 5.17a tablets a1 and b1). Since *in vitro* dissolution studies are prone to large experimental uncertainty, the study was repeated with another two tablets (one from each batch). However, two different trends were observed (Figure 5.17 a3 and b3). These are preliminary results but they could support the hypothesis that rheology could be used to predict the performance of a formulation during *in vitro* dissolution studies. It was not possible to calculate the $t_{sat}$ and $\eta_{sat}$ values for this formulation due to the poor rheology (Table 5.5), and the release profiles are very inconsistent across the different tablets from two batches of the same formulation (Figure 5.17b).

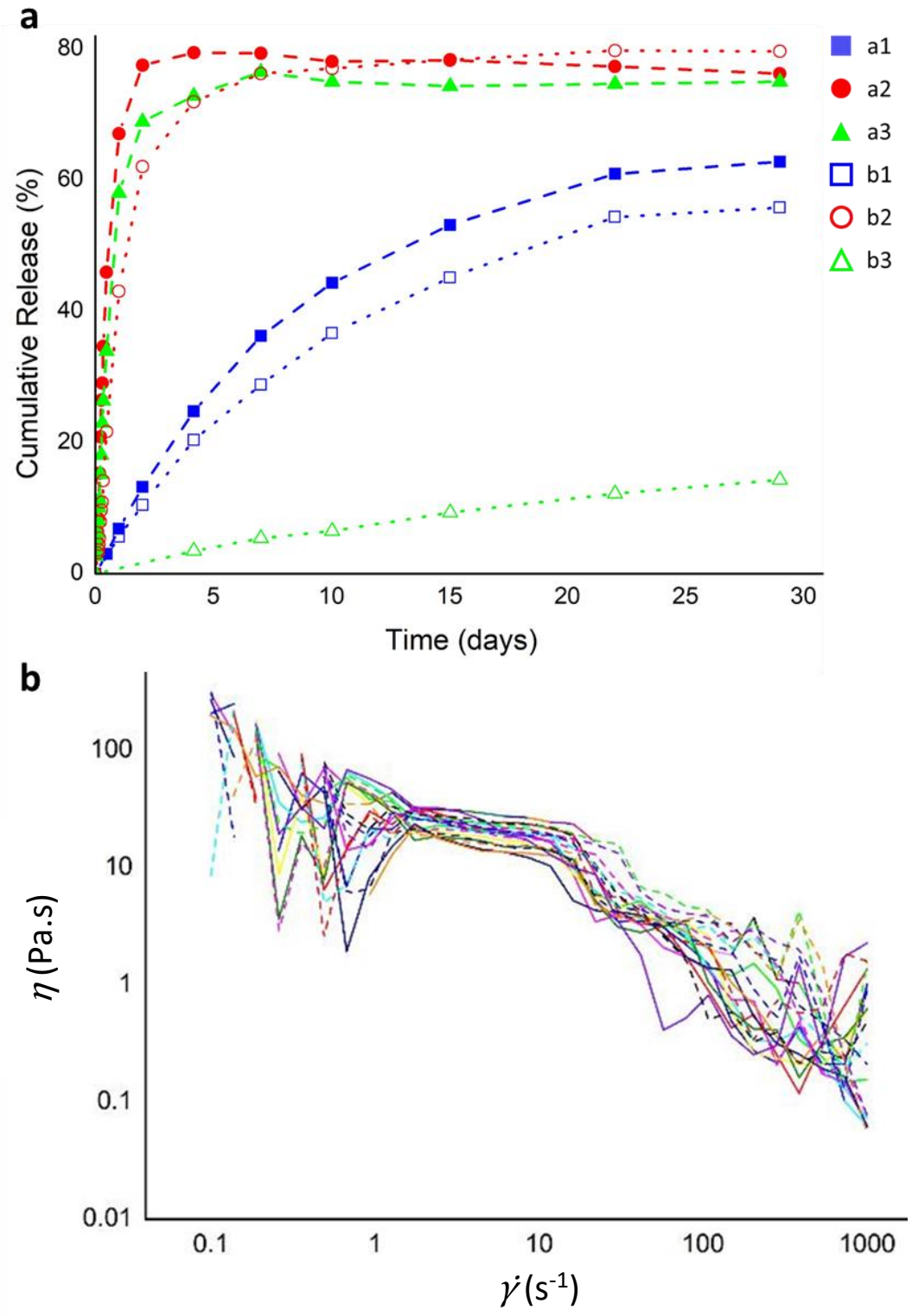



Figure 5.17. **a**) Release profiles of the six tablets produced from the blend containing 40 wt.% BSAg. Profiles a1-3 correspond to tablets from batch a, while b1-3 relate to those from batch b. **b**) Complete rheology profiles of the blend containing 40 wt% BSAg.

Three of the tablets (a2, a3 and b2) gave the same release profile, and could be averaged to give the overall result. However, this would not capture the extent of the inconsistency between the release profiles. Therefore, it could be more thorough to average all six profiles (Figure 5.18).

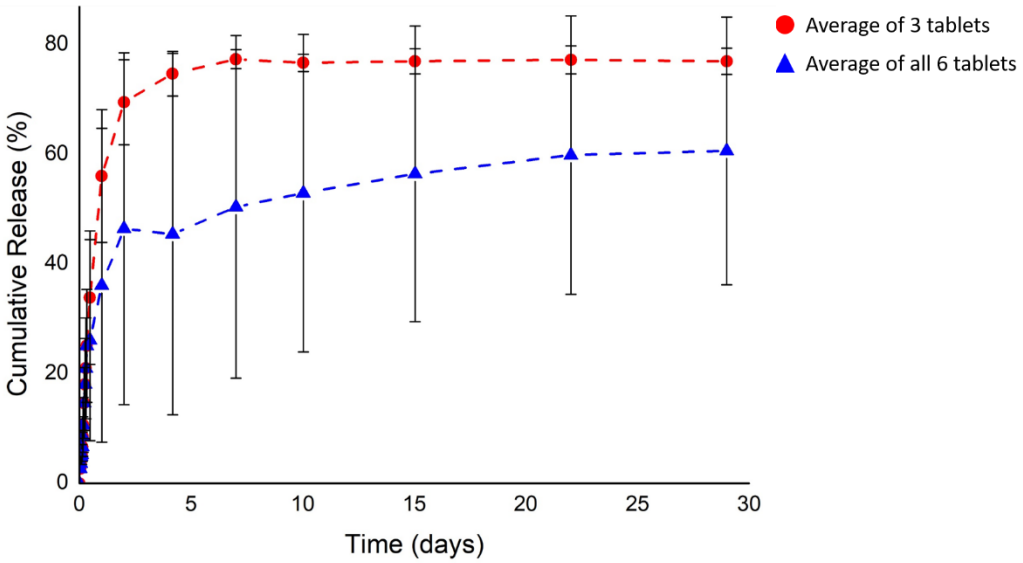



Figure 5.18 Comparison of the averages of the release profiles shown in Figure 5.17a.

In comparison, the release profiles for the four tablets produced from the blend containing 40 wt.% BSAm ($PLGA_{36}$11.25:BSAm40) were more comparable to one another (Figure 5.19a). This could be due to the reduction in particle size; however, the same trend is not apparent in the content assay or rheology data. Each tablet showed accelerated release in the first few days of the study before plateauing at around 50-70% release after 10 days. However, the average of all four profiles still resulted in large uncertainty in the overall release profile for this formulation. This was consistent with the rheology data being unsuitable for Carreau model fitting and the subsequent calculation of $t_{sat}$ and $\eta_{sat}$ (Table 5.5 and Figure 5.19b).

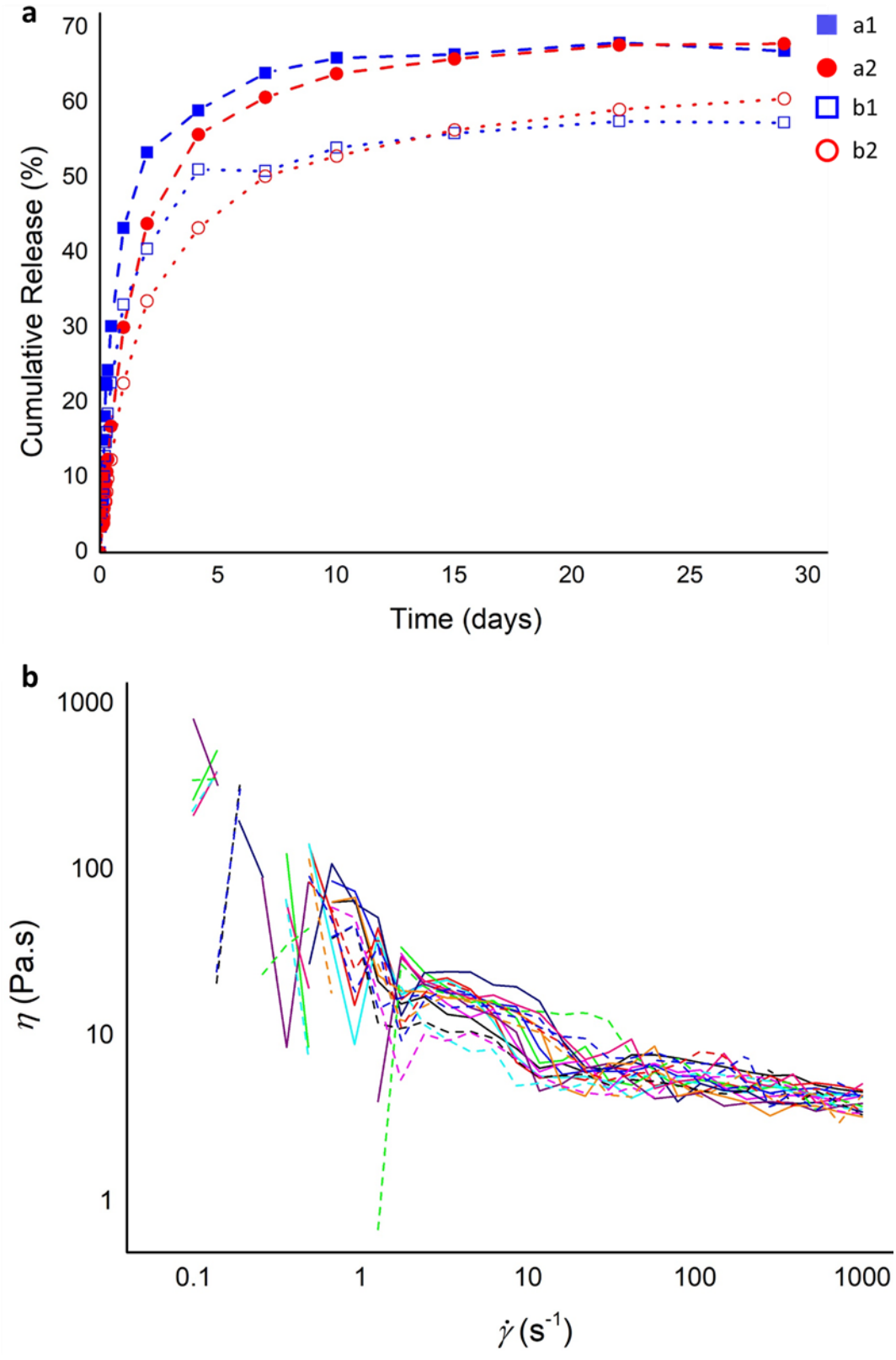



Figure 5.19. **a**) Release profiles of the four tablets produced using the blend containing 40 wt.% BSAm. Profiles a1-2 correspond to tablets from batch a, while b1-2 relate to those from batch b. An average of all four profiles was used for the overall comparison. **b**) Rheology profiles for the blend containing 40 wt.% BSAm.

At lower loadings, it was expected that the samples would show greater homogeneity and this is reflected in the uniformity of the release profiles for the formulation containing 20 wt.% BSAg ($PLGA_{36}15$:BSAg20) (Figure 5.20a). An average of the profiles generated by tablets a1, b1 and b2 was used for the overall comparison while the profile for a2 was excluded from the evaluation. This correlated with the rheology data, where the rheological profiles were reproducible across the two batches suggesting that the formulation consisted of a homogeneous blend of the BSA and the polymers (Figure 5.20b).

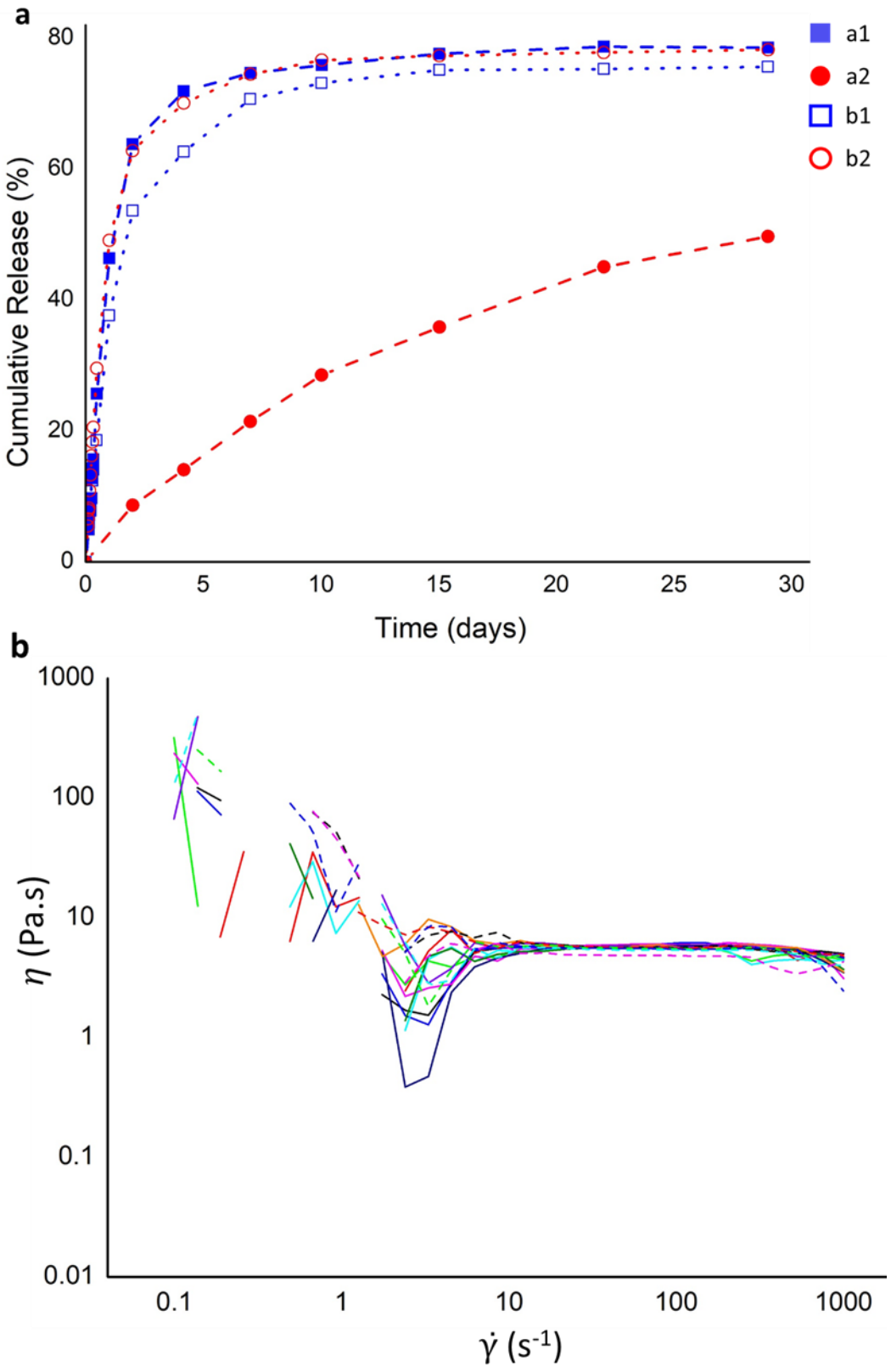



Figure 5.20. **a**) Release profiles of the four tablets produced using the blend containing 20 wt.% BSAg. Profiles a1-2 correspond to tablets from batch a, while b1-2 relate to those from batch b. An average of the profiles from tablets a1, b1 and b2 was used for the overall comparison. **b**) Complete rheology profiles for the blend containing 20 wt.% BSAg.

The release profiles of the tablets produced from the blend containing 20 wt.% BSAm ($PLGA_{36}$15:BSAm30) also only had one anomaly (Figure 5.21a). Hence, the overall profile for this formulation was calculated from an average of the profiles from tablets a1, a2 and b1. Once again, this corroborated with the conclusions drawn from rheology suggesting that the homogeneity of a formulation can be predicted by rheology and be related to its release profile (Figure 5.21b).

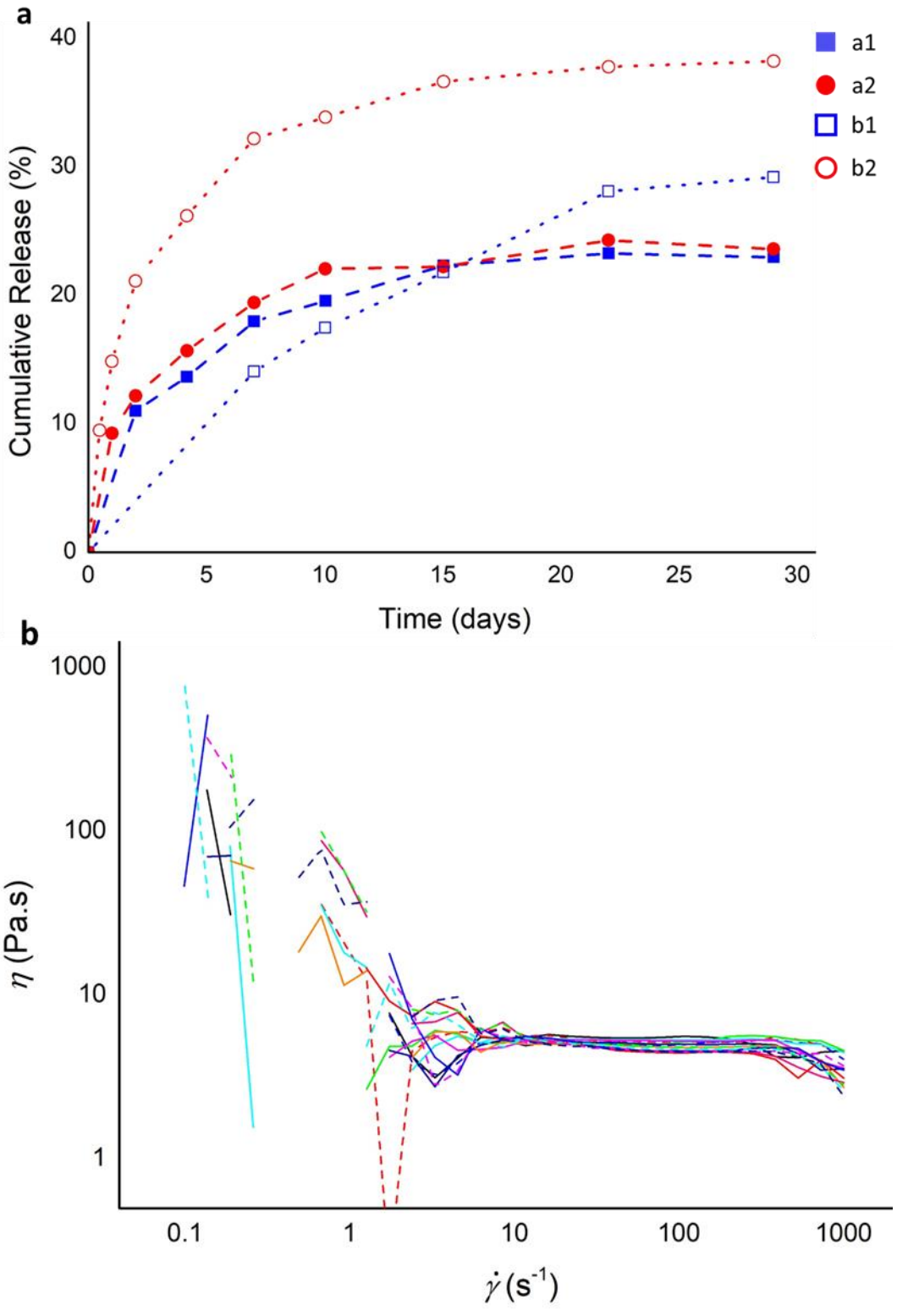



Figure 5.21. **a**) Release profiles of the four tablets produced using the blend containing 20 wt.% BSAm. Profiles a1-2 correspond to tablets from batch a, while b1-2 relate to those from batch b. An average of the profiles from tablets a1, a2 and b1 was used for the overall comparison. **b**) Complete rheology profiles for the blend containing 20 wt.% BSAm.

Increasing the $PLGA_{36}$ content of the formulation to produce a blend containing 20 wt.% BSAm and 30 wt.% $PLGA_{36}$ ($PLGA_{36}$30:BSAm20) resulted in reproducible data from rheology (Figure 5.10b). However, the increased $PLGA_{36}$ content resulted in increased viscosity, which appeared to impede the mixing of the blend, as evidenced by the loading and Raman results (Table 5.6, Table 5.7 and Table 5.8). This seemed to result in an inhomogeneous distribution of BSA as indicated in the release study, where the profiles of the four tablets are dissimilar (Figure 5.22). Due to time constraints, it was not possible to repeat the study with more tablets and therefore the average of the four profiles was used for the overall comparison.

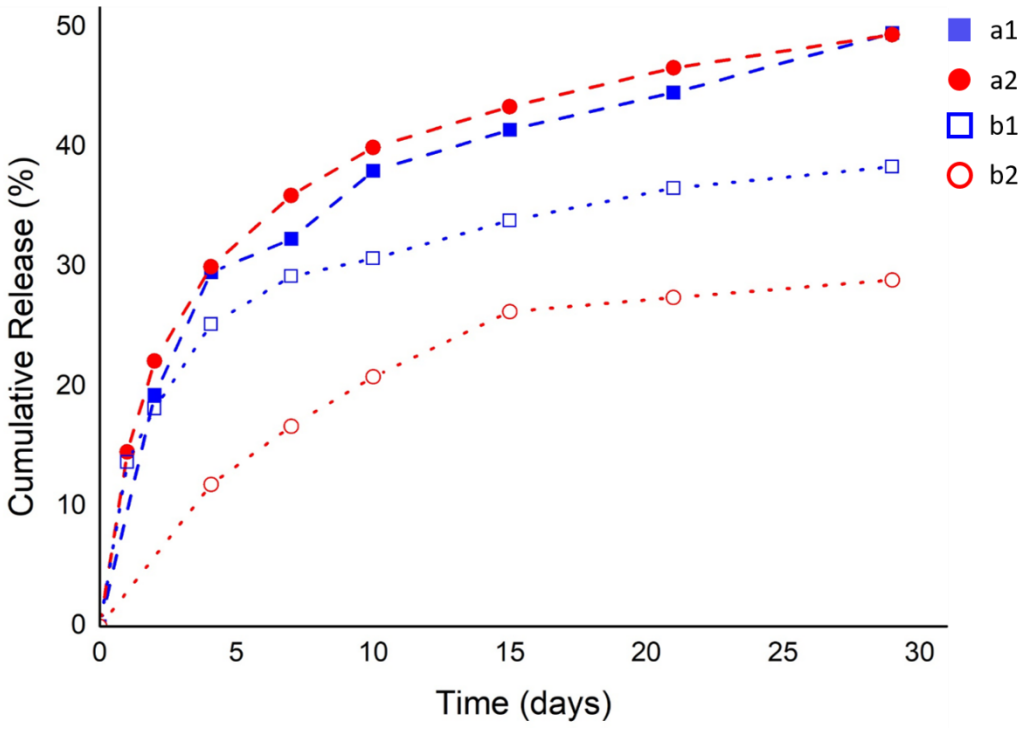
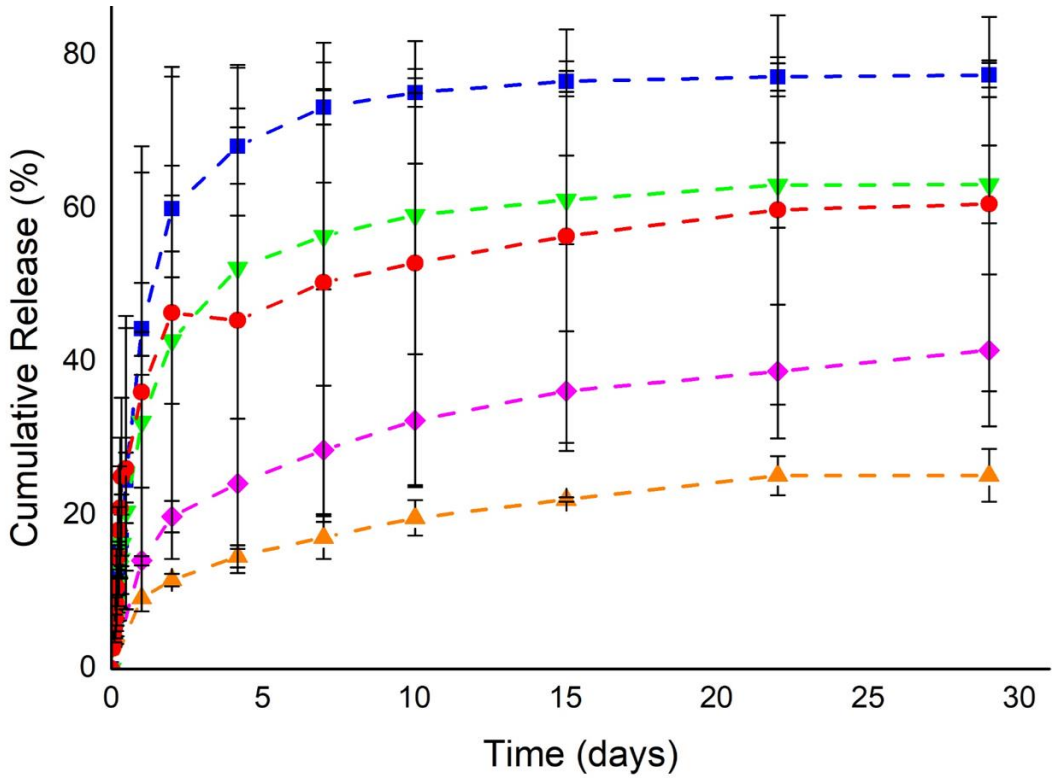



Figure 5.22. Release profiles of the four tablets produced from $PLGA_{36}$30:BSAm20. Profiles a1-2 correspond to tablets from batch a, while b1-2 relate to those from batch b. An average of the profiles from all four tablets was used for the overall comparison.

Although it is not a main focus of this investigation, it is worth mentioning the comparison of the release profiles of the five blends (Figure 5.23). The formulations containing 40 wt.% BSA showed very similar release profiles (Figure 5.23 red circles and green triangles, respectively) in correlation with their comparable rheology profiles. Conversely, the same was not seen for the formulations containing 20 wt.% BSA where $PLGA_{36}$15:BSAg20 (Figure 5.23 blue squares) exhibited a significantly faster rate of release than $PLGA_{36}$15:BSAm20 (Figure 5.23 orange triangles). This could be attributed to the size of the BSA particles, for example, the larger BSA particles (BSAg) are less likely to be encapsulated in the polymer matrix and therefore will be more accessible to the water molecules. In comparison, the smaller BSAm particles could be encapsulated in the polymer matrix and this could inhibit the dissolution of the BSA. For the formulations containing BSAm ($PLGA_{36}$15:BSAm20 and $PLGA_{36}$11.25:BSAm40), increasing the BSA content significantly increases the rate of release from the tablets (Figure 5.23 orange and green triangles) as a result of the increased surface area of BSA with respect to the polymer matrix. Following this argument it makes sense that formulation containing 40 wt.% BSAm released at a faster rate than the one containing 40 wt.% BSAg.




| Symbol | Blend ID | BSA content (wt.%) | Particle size (µm) |
|---|---|---|---|
| ● | $PLGA_{36}$11.25:BSAg40 | 40 | 100 |
| ▼ | $PLGA_{36}$11.25:BSAm40 | 40 | 5 |
| ■ | $PLGA_{36}$15:BSAg20 | 20 | 100 |
| ▲ | $PLGA_{36}$15:BSAm20 | 20 | 5 |
| ◆ | $PLGA_{36}$30:BSAm20 | 20 | 5 |

Figure 5.23. Comparison of the release profiles of the different formulations. Error calculated as ±1 standard deviation from the mean.

Increasing the $PLGA_{36}$ ratio also results in a faster release when $PLGA_{36}$30:BSAm20 (Figure 5.23 pink diamonds) is compared with $PLGA_{36}$15:BSAm20 (Figure 5.23 orange triangles) as expected due to the increased hydrophilicity of the PLGA compared to PLA. However, the real question is whether there was a correlation between the rheological profiles of the formulations and their release. This can be answered by looking at the associated variance in the results (Table 5.9).

Table 5.9. Average RSD values for the full release profile and rheology profile for the five formulations.

| Blend ID | Average RSD | |
|---|---|---|
| | Release | Rheology |
| $PLGA_{36}$11.25:BSAg40 | 13 | 8 |
| $PLGA_{36}$11.25:BSAm40 | 44 | 99 |
| $PLGA_{36}$15:BSAg20 | 9 | 12 |
| $PLGA_{36}$15:BSAm20 | 31 | 206 |
| $PLGA_{36}$30:BSAm20 | 22 | 114 |

In general, where a large variance was observed in the rheological profile of the formulation the release profile also exhibited large variability.

#### 5.6.2.4 Is There a Correlation Between Rheology and Release?

As a general observation, if the formulations can be analysed by rheology, giving reliable, reproducible results then the release profiles over the different batches and tablets are comparable.

For instance, the rheology data of the formulations containing 40 wt.% BSA ($PLGA_{36}$11.25:BSAg40 and $PLGA_{36}$11.25:BSAm40) were unsuitable for Carreau model fitting and the $t_{sat}$ calculation (Table 5.5). In both cases, the release profiles showed inconsistencies between the two batches and multiple tablets (Figure 5.17 and Figure 5.19).

On the other hand, the formulations containing 20 wt.% BSA with 15 wt.% $PLGA_{36}$ ($PLGA_{36}$15:BSAg20 and $PLGA_{36}$15:BSAm20) exhibited reproducible rheology profiles that could be fitted to the Carreau model enabling the calculation of $t_{sat}$ and $\eta_{sat}$ (Figure 5.10b). The release profiles of both formulations were comparable over the two batches, with each formulation having one distinct anomaly, which were discarded from the overall result (Figure 5.20 and Figure 5.21).

However, this was not supported by the content assay (Table 5.6) and the Raman spectroscopy (Table 5.7 and Table 5.8), which suggested that the formulations containing 40 wt.% BSA possessed a more homogeneous distribution of BSA than the

20 wt.% formulations. One possible explanation for the rheological behaviour could be an inhomogeneous distribution of the two polymers due to the presence of BSA, resulting in inconsistent dissolution rates or an effect of the irregular particle shape and size which would be more pronounced at higher loadings of BSA.[250]

The blend with increased $PLGA_{36}$ content ($PLGA_{36}$30:BSAm20) presented an interesting case. The increase in $PLGA_{36}$ content increased the viscosity of the formulation and consequently prevented homogeneous mixing of the drug and the matrix, as determined from the BSA content assay (Table 5.6) and the CLS results from Raman (Table 5.7). This resulted in inconsistent release profiles across the four tablets (Figure 5.22). However, an initial assessment of the rheological data showed it to be reproducible as evidenced by the low RSD value associated with the $\eta_{sat}$ value. Upon closer inspection, it became apparent that despite the reproducibility of the $\eta_{sat}$ value there was actually a large variation throughout the full rheology profile. This could describe the homogeneity of the formulation and would correlate with the large variations observed in the content assay, Raman data and release profiles. Therefore, a comprehensive comparison should be made to fully qualify the quality of the rheology data.

Overall, this suggested that rheology of the formulations as they are being prepared can be used as an indicator of their performance during dissolutions studies. However, the Raman spectroscopy and content assay of the blends show that the 40 wt.% formulations contain a more even distribution of the BSA than the 20 wt.% formulations. This does not mean that rheology cannot provide an insight into the homogeneity of a formulation. For example, the increased presence of the solid BSA could disrupt the polymer miscibility and induce inhomogeneity in the polymer distribution, which would not be detected by the BSA content assay or the Raman spectroscopy.[250]

## 5.7 Summary

The aim of this chapter was to determine whether the rheology of a formulation could be used to predict its performance in an *in vitro* dissolution study. It was expected that a homogeneous formulation would have reproducible release profiles

on a batch-to-batch basis. Therefore, if rheology could assess the homogeneity of a formulation it could be related to its performance in the *in vitro* dissolution studies.

Initially, a selection of polymers were investigated for their suitability as a polymer matrix for the encapsulation of BSA, a model protein based API. Following view cell experiments and rheology measurements a blend of $PLGA_{36}$ and $PLA_{12}$ ($PLGA_{36}$18.75:$PLA_{12}$18.25) was found to be the most suitable.

The $CO_2$ mixing procedure was used to produce five formulations with different BSA loadings, BSA particle size and shape and polymer ratios. All formulations could be ground to yield dry powder samples for rheology and BSA content analysis, and which could be pressed into tablets for the *in vitro* release study.

In comparison with the viscosity of the polymer blend, increasing BSA content increased the viscosity (3 Pa.s, 5 Pa.s and 24 Pa.s for 0, 20 and 40 wt.% BSA respectively, Table 5.5). This was expected as the BSA remained solid during processing and acted as a filler for the formulation. Changing particle size had no effect on the viscosities of the formulations. It was not possible to fit the rheology data of the formulations containing 40 wt.% BSA to the Carreau model or the $t_{sat}$ calculation (Figure 5.10a). On the other hand, the formulations containing 20 wt.% BSA produced typical $\eta$ versus $\dot{\gamma}$ profiles (Figure 5.10b). Increasing the ratio of $PLGA_{36}$ with respect to $PLA_{12}$ resulted in an increase in viscosity (Figure 5.10b). This was unsurprising considering the elevated viscosity of the neat $PLA_{36}$ in comparison with that of the $PLA_{12}$ homopolymer (125 Pa.s and 1.2 Pa.s, respectively, see Chapter 3).

The BSA content of each formulation was determined by GPC and Raman spectroscopy (Table 5.6, Table 5.7 and Table 5.8). The BSA content of the blend with increased $PLGA_{36}$ content was found to be much lower than expected and less uniform across the batches. This could be a direct result of the increased viscosity inhibiting mixing.

An *in vitro* dissolution study was performed to assess the release of BSA from the formulations. The release of BSA from the 40 wt.% blends were found to be non-uniform over the different tablets and batches (Figure 5.17 and Figure 5.19) and this correlated with the divergence observed in the rheology results. By contrast, the

release profiles of the formulations containing 20 wt.% BSA were more consistent coinciding with their reproducible rheology results (Figure 5.20 and Figure 5.21). However, the formulation containing 30 wt.% $PLGA_{36}$ did not exhibit uniform release profiles despite having reproducible $\eta_{sat}$ values (Figure 5.22).

## 5.8 Conclusions

In general, there was a trend between rheology and release. If the rheology of a formulation could be measured and analysed and the viscosity was sufficiently low to promote good mixing of the components then the release profiles should be consistent across the batches. These are preliminary results and more work on a range of formulations should be completed before a definite conclusion can be drawn on whether rheology can assist in formulation development by reducing the need for extensive release studies. For example, the investigation needs to be extended to include different API molecules and to fully investigate the correlation of increased or decreased viscosity on the release profiles. Future work will also investigate the presence or absence of any interactions between the polymers, APIs and $CO_2$.

# Chapter 6

## Summary

## And

## Future Work

## 6.1 Overview

This chapter summarises the key outcomes of this thesis, from the development of a robust and reliable rheology method through to the investigation of the role of rheology for formulation development. An outlook on potential future work is also provided.

## 6.2 Summary

The aim of this thesis was to investigate whether rheology could be used to aid the formulation development process by reducing the number of extensive *in vitro* dissolution studies that usually need to be performed. It was expected that a formulation that can be readily processed would be homogeneous and exhibit batch-to-batch consistency during a release study. Conversely, an inhomogeneous formulation would be expected to show inconsistent release profiles. If rheology could predict the homogeneity of the formulations, the need for multiple *in vitro* release studies could be reduced.

First, a robust and reliable rheology method was developed that was used throughout this thesis to assess the viscosity of the polymers and formulations in the presence of dense phase $CO_2$. Chapter 3 demonstrated that the viscosity of both a semi crystalline polymer, polycaprolactone ($PCL_{112}$) and an amorphous polymer, poly($_{D,L}$-lactic acid) ($PLA_{11}$) could be measured at ambient pressure and elevated temperatures. Directly following this, the samples were exposed to 140 bar of $CO_2$ while the set temperature was maintained. It was discovered that shear was necessary to aid the absorption of $CO_2$ into the polymers. Therefore, the viscosity was analysed at defined time points while the samples were kept under constant shear. This methodology allowed for the calculation of the saturation time ($t_{sat}$), which was the time taken to reach the point where no further viscosity reduction was observed, defined as the saturation viscosity ($\eta_{sat}$). These values were determined by fitting the zero shear viscosities ($\eta_0$), derived from the Carreau model, to an empirical formula.

Next, a method was developed for the analysis of the viscosity at a reduced temperature of 40 °C, suitable for use with formulations containing thermosensitive APIs such as proteins or peptides. Initial studies were performed using $PLA_{11}$; however, because it was supplied as a voluminous powder a pre-melting step at 80 °C was required. Hence, this polymer was unsuitable for use with thermally sensitive APIs and a different $P_{D,L}LA$ ($PLA_{12}$) was sourced, along with a poly($_{D,L}$-lactide-*co*-glycolide) ($PLGA_{36}$). These polymers did not require preheating because they were supplied as granular powders that could be sealed within the measurement cell without heating. Thus, the viscosity was measured directly at 40 °C in the presence of 140 bar of $CO_2$. Again, the viscosity was measured at defined time intervals and the $t_{sat}$ and $\eta_{sat}$ were determined.

The polymers were characterised by GPC, $^1$H NMR and DSC before and after the rheology experiments to confirm that these rheology methods had no detrimental effects on the polymers. No significant changes were observed for the $P_{D,L}LA$s, however, GPC definitively demonstrated that the $PLGA_{36}$ was more susceptible to degradation, especially after exposure to higher temperatures.

The high temperature method developed in Chapter 3 was exploited in Chapter 4 to assess the effect of poly(ethylene glycol) (PEG) on the viscosity of $PLA_{11}$ in combination with dense phase $CO_2$. The effect of the mode by which PEG was introduced was explored, by comparing the rheological properties of PEG/PLA blends with that of PEG-*b*-$P_{D,L}LA$ copolymers. Homopolymers and block copolymers were synthesised via conventional bulk methods and in dense phase $CO_2$ and found to have comparable properties regardless of synthesis method. However, the $CO_2$ purification method proved to be more efficient than the conventional method, with the final polymers having much lower levels of residual monomer and ethanol than those produced via bulk synthesis.

The rheological data showed that PEG and $CO_2$ can dramatically reduce the viscosity of the $PLA_{11}$ and this effect was apparent whether the PEG was added as a blended excipient (PEG/$P_{D,L}LA$ blend) or as a covalently linked entity (PEG-*b*-$P_{D,L}LA$). A further benefit of the presence of PEG was a reduction in $t_{sat}$ from approximately 5 hours for

the $PLA_{11}$ homopolymer down to approximately 2 hours with the addition of 5 wt.% $PEG_5$.

The aim of Chapter 5 was to determine if rheology could be used to predict whether a formulation was suitable for *in vitro* release studies. In order to do this a series of formulations containing BSA were produced. An investigation was performed to identify the most suitable polymer matrix, based on the miscibility of the two polymers and the viscosity of the matrix at processing conditions. It was found that a blend of $PLGA_{36}$ and $PLA_{12}$ ($PLGA_{36}$18.75:$PLA_{12}$81.25) was the most suitable. Five formulations were then produced in duplicate using the $CO_2$ mixing method. These formulations contained two different BSA loadings (20 and 40 wt.%), two different particle sizes of BSA (200 and 5 µm, referred to as BSAg and BSAm respectively) and two different $PLGA_{36}$ to $PLA_{12}$ wt.% ratios (18.75:81.25 and 37.5:62.5). The rheological properties, BSA loading and *in vitro* release of each formulation were then analysed. In general, if a large variance was observed in the rheological profiles of the formulation then the release profile also exhibited large variability (Table 6.1).

Table 6.1. Average RSD values for the full release profile and rheology profile for the five formulations.

| Blend ID | Average RSD (%) | |
|---|---|---|
| | Release | Rheology |
| $PLGA_{36}$11.25:BSAg40 | 13 | 8 |
| $PLGA_{36}$11.25:BSAm40 | 44 | 99 |
| $PLGA_{36}$15:BSAg20 | 9 | 12 |
| $PLGA_{36}$15:BSAm20 | 31 | 206 |
| $PLGA_{36}$30:BSAm20 | 22 | 114 |

For example, a larger distribution was evidenced in the formulations containing 40 wt.% BSA in comparison with the 20 wt.% formulations. This suggested that the 40 wt.% formulations had a less homogeneous distribution of BSA than the 20 wt.% formulations. However, this was not reflected in the content assay or the Raman data, which suggested that the 40 wt.% was more homogeneous than the 20 wt.% formulations. It is possible that the rheology data can predict the homogeneity of the

formulation with respect to the distribution of the two polymers. For example, the increased presence of solid BSA could disrupt the polymer miscibility, reducing the homogeneity of the formulation. This would not be detected by the content assay or the Raman spectroscopy because both of these techniques were specifically used to assess the BSA distribution.

## 6.1 Conclusions

This thesis has successfully demonstrated that the rheological properties of complex systems can be measured in a reproducible, reliable and robust manner at both ambient pressure and in the presence of dense phase $CO_2$. It has also been shown that the viscosity can be measured at temperatures suitable for thermally sensitive APIs. However, the investigation into whether the rheology can be used to determine if a formulation should undergo a release study was inconclusive. Although there was a correlation between formulations exhibiting consistent rheology and release data this did not appear to be related to the BSA distribution or the homogeneity of the formulation. Therefore, there is plenty for scope for further investigation into the relationship between the rheological properties of formulations and their release profiles.

## 6.2 Future Work

In order to draw a definitive conclusion regarding the use of rheology to determine whether formulations are suitable for *in vitro* dissolution testing there are several avenues of investigation that could be followed.

One such avenue is the investigation into the particle size of the components compared to that of the final formulation. This could be investigated using laser diffraction or SEM. This would provide information on how the particles pack during compression, and could explain some of the discrepancies seen in the release profiles. If the particles have a wide size distribution then they will pack closely and upon compression form a more uniform and solid compact. This could also result in inconsistencies in the compact formation, explaining the variability in the release. However, this would not account for the inconsistencies observed in the rheology

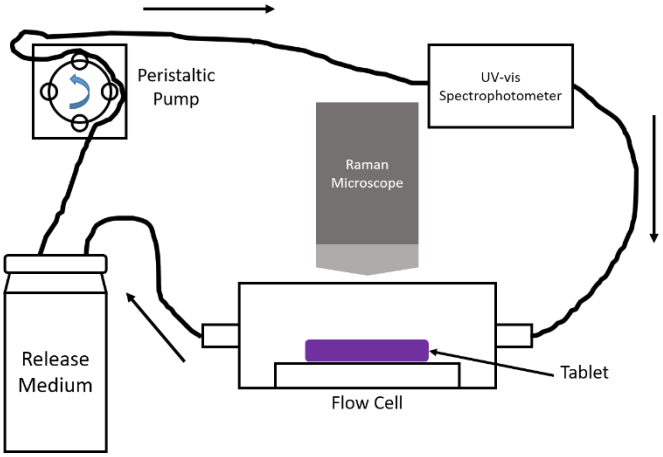
data as the measurements are performed on molten samples where packing is not an issue.

Another avenue of investigation is the determination of interactions between the drug and the polymer that could influence the rheological properties and the release profiles. Preliminary Raman studies on the formulations containing BSA did not exhibit any peak shifts indicating a lack of interactions between the polymer matrix and the API. Therefore, studies should be performed using other APIs. For example, $^{1}H$ NMR showed that aripiprazole, a small molecule API, interacted via hydrogen bonding between the amine group of the aripiprazole and the carbonyl group of the polymer backbone. This could perturb the interaction of $CO_2$ with the polymer backbone diminishing the plasticisation effect. In turn, this could result in elevated viscosity and insufficient mixing leading to inhomogeneous formulations and inconsistent release. In order to assess whether polymer/drug interactions could disrupt the $CO_2$/polymer interactions, analysis of the formulations in $CO_2$ could be performed under high pressure. For example, the University of Nottingham has recently procured a high pressure NMR tube, capable of withstanding pressures up to 1000 bar. There is also the possibility for high pressure FTIR or DSC studies to investigate these tertiary systems.

A brief study was carried out to determine the most promising polymer matrix composition. However, a series of different polymer ratios could also be investigated to evaluate the effect of viscosity on the homogeneity and consistency of the formulations. Alternative polymers could also be investigated.

In this work, the release study was performed on solid tablet forms of the formulations. Although initial Raman data suggested there were no interactions present in the dry tablets, the presence of the release buffer could alter intermolecular interactions. To simultaneously measure changes in the chemistry of the tablet components and the release of an API, a Raman UV-vis flow cell system could be implemented (Scheme 6.1). Here, the Raman spectroscopy could be used to detect changes in the physical and chemical properties of the tablet components whilst the UV-vis spectrometer would detect the release of the API. In this set up, the tablet would be placed in a flow cell positioned directly under the objective of

the Raman microscope. The dissolution medium could then be continuously pumped through the flow cell and the dissolution rate monitored by in line UV-vis spectrophotometry.[251]




Scheme 6.1. Experimental set up of the Raman UV-vis flow cell, where the arrows indicate the direction of flow of the release medium.

Another possibility is to produce microspheres of the formulations rather than tablets and perform the release studies on those. An investigation into the optimisation of the modified PGSS method could be performed exploring the effect of rheological properties on particle formation and subsequent release. As it was not possible to produce microparticles during this work, this could be an interesting continuation of the preliminary data presented in this thesis. For example, will the same trend be seen for the microparticles as was observed for the tablets, where increased variability in the rheology data coincided with increased variability in the release study?

## 6.3 References


(1) Charles E. Carraher, J.; Lagowski, J. J. In *Polymer Chemistry*; Marcel Dekker Inc: U. S. A, 2003; pp 20–60.

(2) Darrin, Q. Global Plastics Production 1917 to 2050 https://www.darrinqualman.com/global-plastics-production/.

(3) The New Plastics Economy Rethinking the future of plastics http://www3.weforum.org/docs/WEF_The_New_Plastics_Economy.pdf (accessed Jul 4, 2018).

(4) Grun, G.-C. Six data visualisations that explain the plastic problem https://www.dw.com/en/six-data-visualizations-that-explain-the-plastic-problem/a-36861883 (accessed Jul 4, 2018).

(5) Geyer, R.; Jambeck, J. R.; Law, K. L. *Science Advances* **2017**, *3* (7), e1700782.

(6) *Nature Communications* **2018**, *9* (1), 2157.

(7) Bioplastics: facts and figures http://docs.european-bioplastics.org/publications/EUBP_Facts_and_figures.pdf (accessed Jul 4, 2018).

(8) Elvers, D.; Song, C. H.; Steinbüchel, A.; Leker, J. *Polymer Reviews* **2016**, *56* (4), 584–606.

(9) Gupta, B.; Revagade, N.; Hilborn, J. *Progress in Polymer Science* **2007**, *32* (4), 455–482.

(10) Hillery, A. M. In *Drug Delivery and Targetting for Pharmacists and Pharmaceutical Scientists*; Hillery, A. M., Lloyd, A. W., Swarbrick, J., Eds.; Taylor & Francis Group, 2001; pp 1–48.

(11) Lee, V. H. L.; Yang, J. J. In *Drug Delivery and Targeting for Pharmacists and Pharmaceutical Scientists*; Hillery, A. M., Lloyd, A. W., Swarbrick, J., Eds.; CRC Press Taylor & Francis Group: Florida, 2001; pp 146–183.

(12) Crommelin, D. J. A.; Hennink, W. E.; Storm, G. In *Drug Delivery and Targeting for Pharmacists and Pharmaceutical Scientists*; Hillery, A. M., Lloyd, A. W., Swarbrick, J., Eds.; CRC Press Taylor & Francis Group: Florida, 2001; pp 118–143.

(13) Lansley, A. B.; Martin, G. P. In *Drug Delivery and Targeting for Pharmacists and*

*Pharmaceutical Scientists*; Hillery, A. M., Lloyd, A. W., Swarbrick, J., Eds.; CRC Press Taylor & Francis Group: Florida, 2001; pp 238–268.

(14) Ibraheem, D.; Elaissari, A.; Fessi, H. *International Journal of Pharmaceutics* **2014**, *477* (1–2), 578–589.

(15) Ullyot, G. E.; Ullyot, B. H.; Slater, L. B. *Bulletin for the History of Chemistry* **2000**, *25* (1), 16–20.

(16) Svedres, E. V. GlaxoSmithKline LLC. US Patent 2793979, 1957.

(17) Holland, S. J.; Tighe, B. J.; Gould, P. L. *Journal of Controlled Release* **1986**, *4* (3), 155–180.

(18) Jeong, B.; Bae, Y. H.; Lee, D. S.; Kim, S. W. *Nature* **1997**, *388* (6645), 860–862.

(19) Renukuntla, J.; Vadlapudi, A. D.; Patel, A.; Boddu, S. H. S.; Mitra, A. K. *International Journal of Pharmaceutics* **2013**, *447* (1–2), 75–93.

(20) Griffith, L. G. *Acta Materialia* **2000**, *48* (1), 263–277.

(21) Nair, L. S.; Laurencin, C. T. *Progress in Polymer Science* **2007**, *32* (8–9), 762–798.

(22) Ikada, Y.; Tsuji, H. *Macromolecular Rapid Communications* **2000**, *21* (3), 117–132.

(23) Hile, D. D.; Amirpour, M. L.; Akgerman, A.; Pishko, M. V. *Journal of Controlled Release* **2000**, *66* (2–3), 177–185.

(24) Sinha, V. R.; Trehan, A. *Journal of Controlled Release* **2003**, *90* (3), 261–280.

(25) Lewis, D. H. In *Biodegradable Polymers as Drug Delivery Systems*; Chasin, M., Langer, R., Eds.; Marcel Dekker INC: New York, 1990; Vol. 45, pp 1–43.

(26) Cocero, M. J.; Martin, A.; Mattea, F.; Varona, S.; Martín, Á.; Mattea, F.; Varona, S. *Journal of Supercritical Fluids* **2009**, *47* (3), 546–555.

(27) Inkinen, S.; Hakkarainen, M.; Albertsson, A. C.; Sodergard, A. *Biomacromolecules* **2011**, *12* (3), 523–532.

(28) Alexis, F. *Polymer International* **2005**, *54* (1), 36–46.

(29) Woodruff, M. A.; Hutmacher, D. W. *Progress in Polymer Science* **2010**, *35* (10), 1217–1256.

(30) Liu, H.; Zhang, J. *Journal of Polymer Science, Part B: Polymer Physics* **2011**, *49* (15), 1051–1083.

(31) Zentner, G. M.; Rathi, R.; Shih, C.; McRea, J. C.; Seo, M. H.; Oh, H.; Rhee, B. G.;

Mestecky, J.; Moldoveanu, Z.; Morgan, M.; Weitman, S. *Journal of Controlled Release* **2001**, *72* (1–3), 203–215.

(32) Okada, H. *Advanced Drug Delivery Reviews* **1997**, *28* (1), 43–70.

(33) Okada, H.; Heya, T.; Igari, Y.; Ogawa, Y.; Toguchi, H.; Shimamoto, T. *International Journal of Pharmaceutics* **1989**, *54* (3), 231–239.

(34) Park, K. *Journal of Controlled Release* **2014**, *190*, 3–8.

(35) Vemmer, M.; Patel, A. V. *Biological Control* **2013**, *67* (3), 380–389.

(36) Williams, H. D.; Trevaskis, N. L.; Charman, S. A.; Shanker, R. M.; Charman, W. N.; Pouton, C. W.; Porter, C. J. H. *Pharmacological Reviews* **2013**, *65* (1), 315–499.

(37) Ho, M. L.; Fu, Y. C.; Wang, G. J.; Chen, H. T.; Chang, J. K.; Tsai, T. H.; Wang, C. K. *J Control Release* **2008**, *128* (2), 142–148.

(38) Wang, H.; Zhao, Y.; Wu, Y.; Hu, Y.; Nan, K.; Nie, G.; Chen, H. *Biomaterials* **2011**, *32* (32), 8281–8290.

(39) Li, Y.-P. P.; Pei, Y.-Y. Y.; Zhang, X.-Y. Y.; Gu, Z.-H. H.; Zhou, Z.-H. H.; Yuan, W.-F. F.; Zhou, J.-J. J.; Zhu, J.-H. H.; Gao, X.-J. J. *Journal of Controlled Release* **2001**, *71* (2), 203–211.

(40) Tomar, L.; Tyagi, C.; Kumar, M.; Kumar, P.; Singh, H.; Choonara, Y. E.; Pillay, V. *International Journal of Nanomedicine* **2013**, *8*, 505–520.

(41) Kang, B. K.; Chon, S. K.; Kim, S. H.; Jeong, S. Y.; Kim, M. S.; Cho, S. H.; Lee, H. B.; Khang, G. *International Journal of Pharmaceutics* **2004**, *286* (1–2), 147–156.

(42) Jeffery, H.; Davis, S. S.; O'Hagan, D. T. *Pharmaceutical Research: An Official Journal of the American Association of Pharmaceutical Scientists*. 1993, pp 362–368.

(43) Ito, F.; Fujimori, H.; Makino, K. *Colloids and Surfaces B: Biointerfaces* **2007**, *54* (2), 173–178.

(44) USP General Chapters: <467> Organic Volatile Impurities http://www.pharmacopeia.cn/v29240/usp29nf24s0_c467.html (accessed Jul 16, 2018).

(45) Caliceti, P.; Veronese, F. M.; Lora, S. *International Journal of Pharmaceutics* **2000**, *211* (1–2), 57–65.

(46) Uchida, T.; Nagareya, N.; Sakakibara, S.; Konishi, Y.; Nakai, A.; Nishikata, M.;

Matsuyama, K.; Yohshida, K. *CHEMICAL & PHARMACEUTICAL BULLETIN* **1997**, *45* (9), 1539–1543.

(47) Arpagaus, C.; Collenberg, A.; Rütti, D.; Assadpour, E.; Jafari, S. M. *International Journal of Pharmaceutics* **2018**, *546* (1–2), 194–214.

(48) Sosnik, A.; Seremeta, K. P. *Advances in Colloid and Interface Science* **2015**, *223*, 40–54.

(49) Walters, R. H.; Bhatnagar, B.; Tchessalov, S.; Izutsu, K.-I.; Tsumoto, K.; Ohtake, S. *Journal of Pharmaceutical Sciences* **2014**, *103* (9), 2673–2695.

(50) Cal, K.; Sollohub, K. *Journal of Pharmaceutical Sciences* **2010**, *99* (2), 575–586.

(51) León-Martínez, F. M.; Méndez-Lagunas, L. L.; Rodríguez-Ramírez, J. *Carbohydrate Polymers* **2010**, *81* (4), 864–870.

(52) Qian, F.; Huang, J.; Hussain, M. A. *Journal of Pharmaceutical Sciences* **2010**, *99* (7), 2941–2947.

(53) Guerrero, S.; Muñíz, E.; Teijón, C.; Olmo, R.; Teijón, J. M.; Blanco, M. D. *Journal of Pharmaceutical Sciences* **2008**, *97* (8), 3153–3169.

(54) Anaya Castro, M. A.; Alric, I.; Brouillet, F.; Peydecastaing, J.; Fullana, S. G.; Durrieu, V. *AAPS PharmSciTech* **2017**, *19* (3), 1124–1132.

(55) Gavini, E.; Chetoni, P.; Cossu, M.; Alvarez, M. G.; Saettone, M. F.; Giunchedi, P. *European Journal of Pharmaceutics and Biopharmaceutics* **2004**, *57* (2), 207–212.

(56) Repka, M. A.; Bandari, S.; Kallakunta, V. R.; Vo, A. Q.; McFall, H.; Pimparade, M. B.; Bhagurkar, A. M. *International Journal of Pharmaceutics* **2018**, *535* (1–2), 68–85.

(57) Crowley, M. M.; Zhang, F.; Repka, M. A.; Thumma, S.; Upadhye, S. B.; Kumar Battu, S.; McGinity, J. W.; Martin, C. *Drug Development and Industrial Pharmacy* **2007**, *33* (9), 909–926.

(58) Shah, S.; Maddineni, S.; Lu, J.; Repka, M. A. *International Journal of Pharmaceutics* **2013**, *453* (1), 233–252.

(59) Aho, J.; Boetker, J. P.; Baldursdottir, S.; Rantanen, J. *International Journal of Pharmaceutics* **2015**, *494* (2), 623–642.

(60) Qi, F.; Wu, J.; Li, H.; Ma, G. *Frontiers of Chemical Science and Engineering* **2018**, 1–14.

(61) Jermain, S. V.; Brough, C.; Williams, R. O. *International Journal of Pharmaceutics* **2018**, *535* (1–2), 379–392.

(62) Sathigari, S. K.; Radhakrishnan, V. K.; Davis, V. A.; Parsons, D. L.; Babu, R. J. *Journal of Pharmaceutical Sciences* **2012**, *101* (9), 3456–3464.

(63) Zhang, J.; Vo, A. Q.; Feng, X.; Bandari, S.; Repka, M. A. *AAPS PharmSciTech* **2018**.

(64) Boetker, J.; Water, J. J.; Aho, J.; Arnfast, L.; Bohr, A.; Rantanen, J. *European Journal of Pharmaceutical Sciences* **2016**, *90*, 47–52.

(65) Vo, A. Q.; Feng, X.; Pimparade, M.; Ye, X.; Kim, D. W.; Martin, S. T.; Repka, M. A. *European Journal of Pharmaceutical Sciences* **2017**, *102*, 71–84.

(66) Pimparade, M. B.; Vo, A.; Maurya, A. S.; Bae, J.; Morott, J. T.; Feng, X.; Kim, D. W.; Kulkarni, V. I.; Tiwari, R.; Vanaja, K.; Murthy, R.; Shivakumar, H. N.; Neupane, D.; Mishra, S. R.; Murthy, S. N.; Repka, M. A. *European Journal of Pharmaceutics and Biopharmaceutics* **2017**, *119*, 81–90.

(67) Cossé, A.; König, C.; Lamprecht, A.; Wagner, K. G. *AAPS PharmSciTech* **2017**, *18* (1), 15–26.

(68) Palem, C. R.; Dudhipala, N. R.; Battu, S. K.; Repka, M. A.; Rao Yamsani, M. *Drug Development and Industrial Pharmacy* **2016**, *42* (3), 473–484.

(69) Albarahmieh, E.; Qi, S.; Craig, D. Q. M. *International Journal of Pharmaceutics* **2016**, *514* (1), 270–281.

(70) Gupta, S. S.; Solanki, N.; Serajuddin, A. T. M. *AAPS PharmSciTech* **2016**, *17* (1), 148–157.

(71) Whitaker, M. J.; Hao, J. Y.; Davies, O. R.; Serhatkulu, G.; Stolnik-Trenkic, S.; Howdle, S. M.; Shakesheff, K. M. *Journal of Controlled Release* **2005**, *101* (1–3), 85–92.

(72) Cowie, J. M. G.; Arrighi, V. In *Polymers: Chemistry and Physiscs of Modern Materials*; CRC Press Taylor & Francis Group, LLC: U. S. A, 2008; pp 321–343.

(73) Charles E. Carraher, J.; Lagowski, J. J. In *Polymer Chemistry*; Marcel Dekker Inc: U. S. A, 2003; pp 527–544.

(74) Jordan, F.; Naylor, A.; Kelly, C. A.; Howdle, S. M.; Lewis, A.; Illum, L. *Journal of Controlled Release* **2010**, *141* (2), 153–160.

(75) Inactive Ingredients http://www.drugs.com/inactive/ (accessed Jun 16, 2016).

(76) U.S. Department of Health and Human Services; Food and Drug Administration. *Guidance for Industry Nonclinical Studies for the Safety Evaluation of Pharmaceutical Excipients*; 2005.

(77) Smith, R. M. *Pure and Applied Chemistry* **1993**, *65* (11), 2397–2403.

(78) Darr, J. A.; Poliakoff, M. *Chemical Reviews* **1999**, *99* (2), 495–542.

(79) Licence, P.; Litchfield, D.; Dellar, M. P.; Poliakoff, M. *Green Chemistry* **2004**, *6* (8), 352–354.

(80) Phase Diagrams https://chem.libretexts.org/Textbook_Maps/General_Chemistry/Map%3A_General_Chemistry_(Petrucci_et_al.)/12%3A_Intermolecular_Forces%3A_Liquids_And_Solids/12.4%3A_Phase_Diagrams (accessed Aug 6, 2018).

(81) Eckert, C. a.; Knutson, B. L.; Debenedetti, P. G. *Nature* **1996**, *383* (6598), 313–318.

(82) Kazarian, S. G. *Polymer Science* **2000**, *42*, 78–101.

(83) DeSimone, J. M. *Science* **2002**, *297* (5582), 799–803.

(84) Nalawade, S. P.; Picchioni, F.; Janssen, L. *Progress in Polymer Science* **2006**, *31* (1), 19–43.

(85) Zosel, K. *Angewandte Chemie International Edition in English* **1978**, *17* (10), 702–709.

(86) Wang, J. S.; Chiu, K. *Journal of Hazardous Materials* **2008**, *158* (2–3), 384–391.

(87) Licence, P.; Ke, J.; Sokolova, M.; Ross, S. K.; Poliakoff, M. *Green Chemistry* **2003**, *5* (2), 99–104.

(88) Yoda, S.; Bratton, D.; Howdle, S. M. *Polymer* **2004**, *45* (23), 7839–7843.

(89) Bratton, D.; Brown, M.; Howdle, S. M. *Chem Commun (Camb)* **2004**, No. 7, 808–809.

(90) Cooper, A. I. *Advanced Materials* **2003**, *15* (13), 1049–1059.

(91) Alessi, P.; Cortesi, A.; Kikic, I.; Vecchione, F. *Journal of Applied Polymer Science* **2003**, *88* (9), 2189–2193.

(92) Reverchon, E.; Cardea, S. *The Journal of Supercritical Fluids* **2007**, *40* (1), 144–152.

(93) Davies, O. R.; Lewis, A. L.; Whitaker, M. J.; Tai, H.; Shakesheff, K. M.; Howdle, S. M. *Advanced Drug Delivery Reviews* **2008**, *60* (3), 373–387.

(94) Reverchon, E.; Antonacci, A. *Journal of Supercritical Fluids* **2007**, *39* (3), 444–452.

(95) Marizza, P.; Keller, S. S.; Mullertz, A.; Boisen, A. *Journal of Controlled Release* **2014**, *173*, 1–9.

(96) Kazarian, S. G.; Vincent, M. F.; Eckert, C. A. *Review of Scientific Instruments* **1996**, *67* (4), 1586–1589.

(97) Shieh, Y. T.; Su, J. H.; Manivannan, G.; Lee, P. H. C.; Sawan, S. P.; Spall, W. D. *Journal of Applied Polymer Science* **1996**, *59* (4), 695–705.

(98) Yeo, S.-D.; Kiran, E. *The Journal of Supercritical Fluids* **2005**, *34* (3), 287–308.

(99) Jung, J.; Perrut, M. *The Journal of Supercritical Fluids* **2001**, *20* (3), 179–219.

(100) Asghari, I.; Esmaeilzadeh, F. *International Journal of Pharmaceutics* **2012**, *433* (1–2), 149–156.

(101) Türk, M.; Bolten, D. *The Journal of Supercritical Fluids* **2010**, *55* (2), 778–785.

(102) Kikic, I.; Vecchione, F. *Current Opinion in Solid State and Materials Science* **2003**, *7* (4–5), 399–405.

(103) Tom, J. W.; Debenedetti, P. G. *Biotechnology Progress* **1991**, *7* (5), 403–411.

(104) Chen, K.; Zhang, X.; Pan, J.; Zhang, W.; Yin, W. *Powder Technology* **2005**, *152* (1–3), 127–132.

(105) Barrett, A.; Dehghani, F.; Foster, N. *Pharmaceutical Research* **2008**, *25* (6), 1274–1289.

(106) Kim, M.-S.; Kim, J.-S.; Park, H. J.; Cho, W. K.; Cha, K.-H.; Hwang, S.-J. *International Journal of Nanomedicine* **2011**, *6*, 2997–3009.

(107) Montes, A.; Kin, N.; Gordillo, M. D.; Pereyra, C.; de la Ossa, E. J. M. *The Journal of Supercritical Fluids* **2014**, *89* (0), 58–67.

(108) Elizondo, E.; Córdoba, A.; Sala, S.; Ventosa, N.; Veciana, J. *The Journal of Supercritical Fluids* **2010**, *53* (1–3), 108–114.

(109) Kang, Y.; Yin, G.; Ouyang, P.; Huang, Z.; Yao, Y.; Liao, X.; Chen, A.; Pu, X. *Journal of Colloid and Interface Science* **2008**, *322* (1), 87–94.

(110) Chen, A.-Z.; Wang, G.-Y.; Wang, S.-B.; Feng, J.-G.; Liu, Y.-G.; Kang, Y.-Q. *Materials* **2012**, *5* (10), 1841–1852.

(111) Naylor, A.; Lewis, A. L.; Ilium, L. *Therapeutic Delivery* **2011**, *2* (12), 1551–1565.

(112) Hao, J. Y.; Whitaker, M. J.; Wong, B.; Serhatkulu, G.; Shakesheff, K. M.; Howdle,

S. M. *Journal of Pharmaceutical Sciences* **2004**, *93* (4), 1083–1090.

(113) Morrison, F. A.; Gubbins, K. F. *Understanding Rheology*; Oxford University Press: New York, 2001.

(114) Barnes; Hutton; Walters; Barnes, H. A.; Hutton, J. F.; Walters, K. *An introduction to rheology*; Elsevier, 1989; Vol. 3.

(115) *Oxford Dictionary of Biochemistry and Molecular Biology*; Cammack, R., Atwood, T., Campbell, P., Parish, H., Smith, A., Vella, F., Stirling, J., Eds.; Oxford University Press, 2006.

(116) Utz, J. Rheometry: Selecting the Right Measuring System - Anton Paar Blog https://blog.anton-paar.com/rheometry-selecting-the-right-measuring-system/ (accessed Jul 19, 2018).

(117) Ferry, J. D. *Viscoelastic properties of polymers*; J. Wiley, 1980.

(118) Goodenow, J.; Orr, R.; Ross, D. Mathematical Models of Water Clocks http://www.nawcc-index.net/Articles/Goodenow-WaterClocks.pdf (accessed Jul 19, 2018).

(119) How to Measure Viscosity https://wiki.anton-paar.com/en/how-to-measure-viscosity/ (accessed Jul 12, 2018).

(120) Mills, A. A. *Source: Notes and Records of the Royal Society of London* **1982**, *37* (1), 35–61.

(121) Viscometer Design and Application Review https://www.engineersedge.com/instrumentation/viscometer_design_and_application_review_9820.htm (accessed Jul 19, 2018).

(122) Piau, J. M.; Bremond, M.; Couette, J. M.; Piau, M. *Rheologica Acta* **1994**, *33* (5), 357–368.

(123) Marcondes, W. A Practical Approach to Rheology and Rheometry http://www.ebah.com.br/content/ABAAAgazIAK/a-practical-approach-to-rheology-and-rheometry-scharamm?part=4 (accessed Jul 19, 2018).

(124) Vlachopoulos, J.; Strutt, D. Polymer processing www.mslab.boun.edu.tr/polymer.doc (accessed Jun 2, 2016).

(125) Elias, H.-G. *An Introduction to Polymer Science*; VCH Verlagsgesellschaft mbH: Germany, 1997.

(126) Reverchon, E.; Adami, R.; Cardea, S.; Della Porta, G. *Journal of Supercritical*

*Fluids* **2009**, *47* (3), 484–492.

(127) Gerhardt, L. J.; Manke, C. W.; Gulari, E. *Journal of Polymer Science Part B: Polymer Physics* **1997**, *35* (3), 523–534.

(128) Royer, J. R.; Gay, Y. J.; Desimone, J. M.; Khan, S. A. *Journal of Polymer Science Part B: Polymer Physics* **2000**, *38* (23), 3168–3180.

(129) Tai, H.; Upton, C. E.; White, L. J.; Pini, R.; Storti, G.; Mazzotti, M.; Shakesheff, K. M.; Howdle, S. M. *Polymer* **2010**, *51* (6), 1425–1431.

(130) Kelly, C. A.; Howdle, S. M.; Shakesheff, K. M.; Jenkins, M. J.; Leeke, G. A. *Journal of Polymer Science Part B: Polymer Physics* **2012**, *50* (19), 1383–1393.

(131) Curia, S.; De Focatiis, D. S. A.; Howdle, S. M. *Polymer* **2015**, *69*, 17–24.

(132) Pepper, K. J.; Masson, T.; De Focatiis, D.; Howdle, S. M. *The Journal of Supercritical Fluids* **2018**, *133* (July 2017), 343–348.

(133) Mertsch, R.; Wolf, B. A. *Macromolecules* **1994**, *27*, 3289–3294.

(134) Xiong, Y.; Kiran, E. *Polymer* **1995**, *36* (25), 4817–4826.

(135) Fleming, O. S.; Kazarian, S. G. In *Supercritical Carbon Dioxide*; Wiley-VCH Verlag GmbH & Co. KGaA, 2006; pp 205–238.

(136) Gourgouillon, D.; Avelino, H. M. N. .; Fareleira, J. M. N. .; Nunes da Ponte, M. *The Journal of Supercritical Fluids* **1998**, *13* (1–3), 177–185.

(137) Nobelen, M.; Hoppe, S.; Fonteix, C.; Pla, F.; Dupire, M.; Jacques, B. *Chemical Engineering Science* **2006**, *61* (16), 5334–5345.

(138) Kelly, C. A.; Murphy, S. H.; Leeke, G. A.; Howdle, S. M.; Shakesheff, K. M.; Jenkins, M. J. *European Polymer Journal* **2013**, *49* (2), 464–470.

(139) Raps, D.; Koppl, T.; de Anda, A. R.; Altstadt, V. *Polymer* **2014**, *55* (6), 1537–1545.

(140) Kelly, C. A.; Naylor, A.; Illum, L.; Shakesheff, K. M.; Howdle, S. M. *Advanced Functional Materials* **2012**, *22* (8), 1684–1691.

(141) Sarode, A. L.; Sandhu, H.; Shah, N.; Malick, W.; Zia, H. *European Journal of Pharmaceutical Sciences* **2013**, *48* (3), 371–384.

(142) Maru, S. M.; de Matas, M.; Kelly, A.; Paradkar, A. *European Journal of Pharmaceutical Sciences* **2011**, *44* (4), 471–478.

(143) Chokshi, R. J.; Sandhu, H. K.; Iyer, R. M.; Shah, N. H.; Malick, A. W.; Zia, H. *Journal of Pharmaceutical Sciences* **2005**, *94* (11), 2463–2474.

(144) Bialleck, S.; Rein, H. *European Journal of Pharmaceutics and Biopharmaceutics* **2011**, *79* (2), 440–448.

(145) Chomcharn, N.; Xanthos, M. *International Journal of Pharmaceutics* **2013**, *450* (1–2), 259–267.

(146) Suwardie, H.; Wang, P.; Todd, D. B.; Panchal, V.; Yang, M.; Gogos, C. G. *European Journal of Pharmaceutics and Biopharmaceutics* **2011**, *78* (3), 506–512.

(147) Tadros, T. F. In *Rheology of Dispersions: Principles and Applications*; Wiley-VCH Verlag GmbH & Co. KGaA: Wokingham, UK, 2010; pp 85–120.

(148) Greenhalgh, D. J.; Williams, A. C.; Timmins, P.; York, P. *Journal of Pharmaceutical Sciences* **1999**, *88* (11), 1182–1190.

(149) Yang, M.; Wang, P.; Suwardie, H.; Gogos, C. *International Journal of Pharmaceutics* **2011**, *403* (1–2), 83–89.

(150) Lyons, J. G.; Devine, D. M.; Kennedy, J. E.; Geever, L. M.; O'Sullivan, P.; Higginbotham, C. L. *European Journal of Pharmaceutics and Biopharmaceutics* **2006**, *64* (1), 75–81.

(151) Avgerinos, T.; Kantiranis, N.; Panagopoulou, A.; Malamataris, S.; Kachrimanis, K.; Nikolakakis, I. *Drug Development and Industrial Pharmacy* **2018**, *44* (2), 338–348.

(152) Andrews, G. P.; Donnelly, L.; Jones, D. S.; Curran, R. M.; Morrow, R. J.; Woolfson, A. D.; Malcolm, R. K. *Biomacromolecules* **2009**, *10* (9), 2427–2435.

(153) Aminabhavi, T. M.; Agnihotri, S. A.; Naidu, B. V. K. *Journal of Applied Polymer Science* **2004**, *94* (5), 2057–2064.

(154) Chauvet, M.; Sauceau, M.; Fages, J. *The Journal of Supercritical Fluids* **2017**, *120*, 408–420.

(155) Lyons, J.; Hallinan, M.; Kennedy, J.; Devine, D.; Geever, L.; Blackie, P.; Higginbotham, C. *International Journal of Pharmaceutics* **2007**, *329* (1–2), 62–71.

(156) Verreck, G.; Decorte, A.; Heymans, K.; Adriaensen, J.; Liu, D.; Tomasko, D.; Arien, A.; Peeters, J.; Van den Mooter, G.; Brewster, M. E. *International Journal of Pharmaceutics* **2006**, *327* (1–2), 45–50.

(157) USP General Chapters: <1088><1092>

http://www.pharmacopeia.cn/v29240/usp29nf24s0_c711.html (accessed Jun 12, 2018).

(158) Wyss, D. H. M.; Larsen, R. J.; Weitz, P. D. A. 2007, pp 68–70.

(159) Material Functions Derived from Oscillatory Tests https://ciks.cbt.nist.gov/~garbocz/SP946/node11.htm (accessed Aug 1, 2018).

(160) Phan-Thien, N.; Rhodes, P. W. T. *Understanding Viscoelasticity*; Stanley, P. H. E., Needs, P. R., Eds.; Springer: Heidelberg, 2013.

(161) Severs, E. T. In *Rheology of Polymers*; Reinhold Publishing Corporation: New York, 1962; pp 22–42.

(162) Willenbacher, N.; Georgieva, K. *Product Design and Engineering*. Wiley-VCH Verlag GmbH & Co: Germany 2013.

(163) Polymer Properties: Polymer Melts https://www.nottingham.ac.uk/~enzddf/polymerengineering/pmwiki/pmwiki.php?n=Main.PolymerMelts (accessed Aug 1, 2018).

(164) Han, C. D. *Rheology in Polymer Processing*; Academic Press Inc: New York, 1976.

(165) Cross, M. M. *Journal of Colloid Science* **1965**, *20* (5), 417–437.

(166) Carreau, P. J. *Transactions of The Society of Rheology (1957-1977)* **1972**, *16* (1), 99–127.

(167) Molecular Weight of PLA with the BI-MwA https://www.brookhaveninstruments.com/library/polymers/molecular-weight-of-pla-with-the-bi-mwa (accessed Jun 16, 2016).

(168) Zhou, X.; Hong, L. *Colloid and Polymer Science* **2013**, *291* (9), 2155–2162.

(169) Poly (ethylene glycol) dibenzylmethylene Terminated Data Sheet http://www.polymersource.com/dataSheet/P5607-EO (PEO).pdf (accessed Jun 16, 2016).

(170) Desai, K. G. H.; Park, H. J. *Drying Technology* **2005**, *23* (7), 1361–1394.

(171) Westover, R. F. *Polymer Engineering and Science* **1961**, *1* (1), 14–20.

(172) Bae, Y. C. *Polymer* **1996**, *37* (14), 3011–3017.

(173) Lee, M.; Park, C. B.; Tzoganakis, C. *Polymer Engineeriaw and Science* **1999**, *39* (1), 99–109.

(174) Royer, J. R.; Gay, Y. J.; M., A.; DeSimone, J. M.; Khan, S. A. *Polymer* **2002**, *43*, 2375–2383.

(175) Calvignac, B.; Rodier, E.; Letourneau, J.-J.; Vitoux, P.; Aymonier, C.; Fages, J. *The Journal of Supercritical Fluids* **2010**, *55* (1), 96–106.

(176) Hrnčič, M. K.; Škerget, M.; Knez, Ž. *The Journal of Supercritical Fluids* **2014**, *95*, 641–668.

(177) Royer, J. R.; DeSimone, J. M.; Khan, S. A. *Journal of Polymer Science: Part B: Polymer Physics* **2001**, *39*, 3055–3066.

(178) Bae, Y. C.; Gulari, E. *Journal of Applied Polymer Science* **1997**, *63* (4), 459–466.

(179) Handge, U. A.; Altstädt, V. *Journal of Rheology* **2012**, *56* (4), 743.

(180) Mark, J.; Ngai, K.; Graessley, W.; Mandelkern, L.; Samulski, E.; Koenig, J.; Wignall, G. In *Physical Properties of Polymers*; Cambridge University Press: Cambridge, 2004; pp 153–208.

(181) Plastics Additives http://www.bpf.co.uk/plastipedia/additives/default.aspx#Intro (accessed Jun 2, 2016).

(182) Li, F.-J.; Tan, L.-C.; Zhang, S.-D.; Zhu, B. *Journal of Applied Polymer Science* **2016**, *133* (4).

(183) Sungsanit, K.; Kao, N.; Bhattacharya, S. N. *Polymer Engineering & Science* **2012**, *52* (1), 108–116.

(184) Toncheva, A.; Mincheva, R.; Kancheva, M.; Manolova, N.; Rashkov, I.; Dubois, P.; Markova, N. *European Polymer Journal* **2016**, *75*, 223–233.

(185) Nazari, T.; Garmabi, H. *Micro & Nano Letters* **2014**, *9* (10), 686–690.

(186) Pillin, I.; Montrelay, N.; Grohens, Y. *Polymer* **2006**, *47* (13), 4676–4682.

(187) Sheth, M.; Kumar, R. A.; Dave, V.; Gross, R. A.; McCarthy, S. P. *Journal of Applied Polymer Science* **1997**, *66* (8), 1495–1505.

(188) Kumar, N.; Ravikumar, M. N. V.; Domb, A. J. *Advanced Drug Delivery Reviews* **2001**, *53* (1), 23–44.

(189) Malmsten, M.; Lindman, B. *Macromolecules* **1992**, *25*, 5440–5445.

(190) Chen, G.; Hoffman, A. S. *Nature* **1995**, *373* (6509), 49–52.

(191) Xiao, R. Z.; Zeng, Z. W.; Zhou, G. L.; Wang, J. J.; Li, F. Z.; Wang, A. M. *International Journal of Nanomedicine* **2010**, *5* (1), 1057–1065.

(192) Hiemstra, C.; Zhong, Z.; Dijkstra, P. J.; Feijen, J. *Macromolecular Symposia* **2005**, *224*, 119–131.

(193) Lucke, A.; Teßmar, J.; Schnell, E.; Schmeer, G.; Göpferich, A. *Biomaterials* **2000**, *21* (23), 2361–2370.

(194) Otsuka, H.; Nagasaki, Y.; Kataoka, K. *Biomacromolecules* **2000**, *1* (1), 39–48.

(195) Rafat, M.; Cléroux, C. A.; Fong, W. G.; Baker, A. N.; Leonard, B. C.; O'Connor, M. D.; Tsilfidis, C. *Biomaterials* **2010**, *31* (12), 3414–3421.

(196) Pulkkinen, M.; Pikkarainen, J.; Wirth, T.; Tarvainen, T.; Haapaaho, V.; Korhonen, H.; Seppala, J.; Jarvinen, K. *European Journal of Pharmaceutics and Biopharmaceutics* **2008**, *70* (1), 66–74.

(197) Han, C. D.; Baek, D. M.; Kim, J. K.; Chu, S. G. *Polymer* **1992**, *33* (2), 294–305.

(198) Jelonek, K.; Li, S.; Wu, X.; Kasperczyk, J.; Marcinkowski, A. *International Journal of Pharmaceutics* **2015**, *485* (1–2), 357–364.

(199) Utracki, L. a; Kamal, M. R. *Polymer Engineering and Science* **1982**, *22* (2), 96–114.

(200) Sadiku-Agboola, O.; Sadiku, E. R.; Adegbola, A. T.; Biotidara, O. F. *Materials Sciences and Applications* **2011**, *02* (01), 30–41.

(201) Wu, D.; Wu, L.; Zhang, M.; Zhao, Y. *Polymer Degradation and Stability* **2008**, *93* (8), 1577–1584.

(202) Avolio, R.; Castaldo, R.; Gentile, G.; Ambrogi, V.; Fiori, S.; Avella, M.; Cocca, M.; Errico, M. E. *European Polymer Journal* **2015**, *66*, 533–542.

(203) Oliaei, E.; Kaffashi, B.; Davoodi, S. *Journal of Applied Polymer Science* **2016**, *133* (15), 1–13.

(204) Xie, M.; Li, H. *European Polymer Journal* **2007**, *43* (8), 3480–3487.

(205) Babaei, A.; Arefazar, A. *Journal of Applied Polymer Science* **2015**, *132* (20), 41969–41977.

(206) Djellali, S.; Sadoun, T.; Haddaoui, N.; Bergeret, A. *Polymer Bulletin* **2015**, *72* (5), 1177–1195.

(207) Liao, H.; Zheng, L.; Hu, Y.; Zha, X.; Xu, X.; Wen, Y.; Tao, G.; Liu, C. *Journal of Applied Polymer Science* **2015**, *132* (24), n/a-n/a.

(208) Zhao, Y.; Huang, H.-X.; Chen, Y.-K. *Polymer Bulletin* **2010**, *64* (3), 291–302.

(209) Wu, D.; Zhang, Y.; Zhang, M.; Zhou, W. *European Polymer Journal* **2008**, *44* (7),

2171–2183.

(210) Lee, M.; Park, C. B.; Tzoganakis, C. *Polymer Engineering and Science* **2004**, *39*, 99–109.

(211) Goddard, A. R.; Pérez-Nieto, S.; Passos, T. M.; Quilty, B.; Carmichael, K.; Irvine, D. J.; Howdle, S. M. *Green Chemistry* **2016**, *18* (17), 4772–4786.

(212) Dag, A.; Durmaz, H.; Kirmizi, V.; Hizal, G.; Tunca, U. *Polymer Chemistry* **2010**, *1* (5), 621–623.

(213) Schwach, G.; Coudane, J.; Engel, R.; Vert, M. *Polymer Bulletin* **1994**, *32* (5–6), 617–623.

(214) Chmura, A. J.; Davidson, M. G.; Frankis, C. J.; Jones, M. D.; Lunn, M. D. *Chemical Communications* **2008**, No. 11, 1293.

(215) Jamshidian, M.; Tehrany, E. A.; Imran, M.; Jacquot, M.; Desobry, S. *Comprehensive Reviews in Food Science and Food Safety* **2010**, *9* (5), 552–571.

(216) Poly(ethylene glycol), MW 7500 (PEG 7500) http://www.polysciences.com/default/polyethylene-glycol-mw-7500 (accessed May 4, 2018).

(217) Dorgan, J. R.; Williams, J. S.; Lewis, D. N. *Journal of Rheology* **1999**, *43* (5), 1141.

(218) Miller-Chou, B. A.; Koenig, J. L. *Progress in Polymer Science (Oxford)* **2003**, *28* (8), 1223–1270.

(219) Berendsen, H. J. C. *A student's guide to data and error analysis*; Cambridge University Press, 2011.

(220) Martin, O.; Avérous, L. *Polymer* **2001**, *42* (14), 6209–6219.

(221) Tai, H.; Mather, M. L.; Howard, D.; Wang, W.; White, L. J.; Crowe, J. A.; Morgan, S. P.; Chandra, A.; Williams, D. J.; Howdle, S. M.; Shakesheff, K. M.; Darr, J.; Layrolle, P.; Buckland, T. *European Cells & Materials* **2007**, *14*, 76–77.

(222) Bates, C. M.; Bates, F. S. *Macromolecules* **2017**, *50* (1), 3–22.

(223) Dealy, J. M.; Larson, R. G. *Structure and rheology of molten polymers : from structure to flow behavior and back again*; Hanser Publishers, 2006.

(224) Marroum, P. J. *Dissolution Technologies* **2014**, *21* (3), 11–16.

(225) Edwards, L. J. *Transactions of the Faraday Society* **1951**, *47* (I), 1191–1210.

(226) In Vitro Dissolution Testing - Solid Oral Dosage Forms https://www.particlesciences.com/news/technical-briefs/2010/in-vitro-

dissolution-testing-for-solid-oral-dosage-forms.html (accessed Jun 12, 2018).

(227) Noyes, A. A.; Whitney, W. R. *Journal of the American Chemical Society* **1897**, *19* (12), 930–934.

(228) Nelson, E. *Journal of the American Pharmaceutical Association (Scientific ed.)* **1957**, *46* (10), 607–614.

(229) Lindenbaum, J.; Mellow, M. H.; Blackstone, M. O.; Butler, V. P. *New England Journal of Medicine* **1971**, *285* (24), 1344–1347.

(230) *Guidance for Industry Dissolution Testing of Immediate Release Solid Oral Dosage Forms*; U.S. Department of Health and Human Services Food and Drug Administration Center for Drug Evaluation and Research (CDER), 1997.

(231) *Guidance for Industry Guidance for Industry Extended Release Oral Dosage Forms: Development, Evaluation, and Application of In Vitro/In Vivo Correlations*; U.S. Department of Health and Human Services Food and Drug Administration Center for Drug Evaluation and Research (CDER), 1997.

(232) *Guidance for Industry Immediate Release Solid Oral Dosage Forms*; Center for Drug Evaluation and Research (CDER), 1995.

(233) *Guidance for Industry SUPAC-MR: Modified Release Solid Oral Dosage Forms Scale-Up and Postapproval Changes: Chemistry, Manufacturing, and Controls; In Vitro Dissolution Testing and In Vivo Bioequivalence Documentation*; U.S. Department of Health and Human Services Food and Drug Administration Center for Drug Evaluation and Research (CDER), 1997.

(234) Wang, Q.; Fotaki, N.; Mao, Y. *Dissolution Technologies* **2009**, *16* (3), 6–12.

(235) Dressman, J. B.; Amidon, G. L.; Reppas, C.; Shah, V. P. *Pharmaceutical research* **1998**, *15* (1), 11–22.

(236) Poly(ethylene glycol), MW 400 http://www.polysciences.com/default/polyethylene-glycol-mw-400 (accessed May 29, 2018).

(237) Poly(ethylene glycol) average Mn 6,000 | Sigma-Aldrich https://www.sigmaaldrich.com/catalog/product/aldrich/81260?lang=en&region=GB (accessed Jun 19, 2018).

(238) Polycaprolactone average Mw ~14,000, average Mn ~10,000 by GPC | Sigma-Aldrich

https://www.sigmaaldrich.com/catalog/product/aldrich/440752?lang=en&region=GB (accessed Jun 19, 2018).

(239) Poly(ethylene glycol) average Mn 400 | Sigma-Aldrich https://www.sigmaaldrich.com/catalog/product/aldrich/202398?lang=en&region=GB (accessed Jun 19, 2018).

(240) spectrumlabs.com. Float-A-Lyzer G2 http://spectrumlabs.com/lit/420x10732x000.pdf (accessed Jul 24, 2018).

(241) Fox Equation http://polymerdatabase.com/polymer physics/Fox.html (accessed May 30, 2018).

(242) Lao, L. L.; Venkatraman, S. S.; Peppas, N. A. *European Journal of Pharmaceutics and Biopharmaceutics* **2008**, *70* (3), 796–803.

(243) Howdle, S. M.; Watson, M. S.; Whitaker, M. J.; Popov, V. K.; Davies, M. C.; Mandel, F. S.; Wang, J. D.; Shakesheff, K. M. *Chemical Communications* **2001**, No. 1, 109–110.

(244) Krieger, I. M.; Dougherty, T. J. *Transactions of the Society of Rheology* **1959**, *3* (1), 137–152.

(245) Li, Y.; Han, C.; Bian, J.; Han, L.; Dong, L.; Gao, G. *Polymer Composites* **2012**, *33* (10), 1719–1727.

(246) Mutel, A. T.; Kamal, M. R. *Polymer Composites* **1984**, *5* (1), 29–35.

(247) Kister, G.; Cassanas, G.; Vert, M. *Polymer* **1998**, *39* (2), 267–273.

(248) Vey, E.; Rodger, C.; Booth, J.; Claybourn, M.; Miller, A. F.; Saiani, A. *Polymer Degradation and Stability* **2011**, *96* (10), 1882–1889.

(249) Lin, V. J. C.; Koenig, J. L. *Biopolymers* **1976**, *15* (1), 203–218.

(250) Fenouillot, F.; Cassagnau, P.; Majesté, J.-C. *Polymer* **2009**, *50* (6), 1333–1350.

(251) Tres, F.; Treacher, K.; Booth, J.; Hughes, L. P.; Wren, S. A. C.; Aylott, J. W.; Burley, J. C. *Molecular Pharmaceutics* **2016**, *13* (3), 1166–1175.

(252) Hao, J. Y.; Whitaker, M. J.; Serhatkulu, G.; Shakesheff, K. M.; Howdle, S. M. *Journal of Materials Chemistry* **2005**, *15* (11), 1148–1153.

(253) Areerat, S.; Nagata, T.; Ohshima, M. *Polymer Engineering & Science* **2002**, *42* (11), 2234–2245.

(1) Charles E. Carraher, J.; Lagowski, J. J. In *Polymer Chemistry*; Marcel Dekker Inc: U. S. A, 2003; pp 20–60.

(2) Darrin, Q. Global Plastics Production 1917 to 2050 https://www.darrinqualman.com/global-plastics-production/.

(3) The New Plastics Economy Rethinking the future of plastics http://www3.weforum.org/docs/WEF_The_New_Plastics_Economy.pdf (accessed Jul 4, 2018).

(4) Grun, G.-C. Six data visualisations that explain the plastic problem https://www.dw.com/en/six-data-visualizations-that-explain-the-plastic-problem/a-36861883 (accessed Jul 4, 2018).

(5) Geyer, R.; Jambeck, J. R.; Law, K. L. *Science Advances* **2017**, *3* (7), e1700782.

(6) *Nature Communications* **2018**, *9* (1), 2157.

(7) Bioplastics: facts and figures http://docs.european-bioplastics.org/publications/EUBP_Facts_and_figures.pdf (accessed Jul 4, 2018).

(8) Elvers, D.; Song, C. H.; Steinbüchel, A.; Leker, J. *Polymer Reviews* **2016**, *56* (4), 584–606.

(9) Gupta, B.; Revagade, N.; Hilborn, J. *Progress in Polymer Science* **2007**, *32* (4), 455–482.

(10) Hillery, A. M. In *Drug Delivery and Targetting for Pharmacists and Pharmaceutical Scientists*; Hillery, A. M., Lloyd, A. W., Swarbrick, J., Eds.; Taylor & Francis Group, 2001; pp 1–48.

(11) Lee, V. H. L.; Yang, J. J. In *Drug Delivery and Targeting for Pharmacists and Pharmaceutical Scientists*; Hillery, A. M., Lloyd, A. W., Swarbrick, J., Eds.; CRC Press Taylor & Francis Group: Florida, 2001; pp 146–183.

(12) Crommelin, D. J. A.; Hennink, W. E.; Storm, G. In *Drug Delivery and Targeting for Pharmacists and Pharmaceutical Scientists*; Hillery, A. M., Lloyd, A. W., Swarbrick, J., Eds.; CRC Press Taylor & Francis Group: Florida, 2001; pp 118–143.

(13) Lansley, A. B.; Martin, G. P. In *Drug Delivery and Targeting for Pharmacists and Pharmaceutical Scientists*; Hillery, A. M., Lloyd, A. W., Swarbrick, J., Eds.; CRC Press Taylor & Francis Group: Florida, 2001; pp 238–268.

(14) Ibraheem, D.; Elaissari, A.; Fessi, H. *International Journal of Pharmaceutics* **2014**, *477* (1–2), 578–589.

(15) Ullyot, G. E.; Ullyot, B. H.; Slater, L. B. *Bulletin for the History of Chemistry* **2000**, *25* (1), 16–20.

(16) Svedres, E. V. GlaxoSmithKline LLC. US Patent 2793979, 1957.

(17) Holland, S. J.; Tighe, B. J.; Gould, P. L. *Journal of Controlled Release* **1986**, *4* (3), 155–180.

(18) Jeong, B.; Bae, Y. H.; Lee, D. S.; Kim, S. W. *Nature* **1997**, *388* (6645), 860–862.

(19) Renukuntla, J.; Vadlapudi, A. D.; Patel, A.; Boddu, S. H. S.; Mitra, A. K. *International Journal of Pharmaceutics* **2013**, *447* (1–2), 75–93.

(20) Griffith, L. G. *Acta Materialia* **2000**, *48* (1), 263–277.

(21) Nair, L. S.; Laurencin, C. T. *Progress in Polymer Science* **2007**, *32* (8–9), 762–798.

(22) Ikada, Y.; Tsuji, H. *Macromolecular Rapid Communications* **2000**, *21* (3), 117–132.

(23) Hile, D. D.; Amirpour, M. L.; Akgerman, A.; Pishko, M. V. *Journal of Controlled Release* **2000**, *66* (2–3), 177–185.

(24) Sinha, V. R.; Trehan, A. *Journal of Controlled Release* **2003**, *90* (3), 261–280.

(25) Lewis, D. H. In *Biodegradable Polymers as Drug Delivery Systems*; Chasin, M., Langer, R., Eds.; Marcel Dekker INC: New York, 1990; Vol. 45, pp 1–43.

(26) Cocero, M. J.; Martin, A.; Mattea, F.; Varona, S.; Martín, Á.; Mattea, F.; Varona, S. *Journal of Supercritical Fluids* **2009**, *47* (3), 546–555.

(27) Inkinen, S.; Hakkarainen, M.; Albertsson, A. C.; Sodergard, A. *Biomacromolecules* **2011**, *12* (3), 523–532.

(28) Alexis, F. *Polymer International* **2005**, *54* (1), 36–46.

(29) Woodruff, M. A.; Hutmacher, D. W. *Progress in Polymer Science* **2010**, *35* (10), 1217–1256.

(30) Liu, H.; Zhang, J. *Journal of Polymer Science, Part B: Polymer Physics* **2011**, *49* (15), 1051–1083.

(31) Zentner, G. M.; Rathi, R.; Shih, C.; McRea, J. C.; Seo, M. H.; Oh, H.; Rhee, B. G.; Mestecky, J.; Moldoveanu, Z.; Morgan, M.; Weitman, S. *Journal of Controlled Release* **2001**, *72* (1–3), 203–215.

(32) Okada, H. *Advanced Drug Delivery Reviews* **1997**, *28* (1), 43–70.

(33) Okada, H.; Heya, T.; Igari, Y.; Ogawa, Y.; Toguchi, H.; Shimamoto, T.

*International Journal of Pharmaceutics* **1989**, *54* (3), 231–239.

(34) Park, K. *Journal of Controlled Release* **2014**, *190*, 3–8.

(35) Vemmer, M.; Patel, A. V. *Biological Control* **2013**, *67* (3), 380–389.

(36) Williams, H. D.; Trevaskis, N. L.; Charman, S. A.; Shanker, R. M.; Charman, W. N.; Pouton, C. W.; Porter, C. J. H. *Pharmacological Reviews* **2013**, *65* (1), 315–499.

(37) Ho, M. L.; Fu, Y. C.; Wang, G. J.; Chen, H. T.; Chang, J. K.; Tsai, T. H.; Wang, C. K. *J Control Release* **2008**, *128* (2), 142–148.

(38) Wang, H.; Zhao, Y.; Wu, Y.; Hu, Y.; Nan, K.; Nie, G.; Chen, H. *Biomaterials* **2011**, *32* (32), 8281–8290.

(39) Li, Y.-P. P.; Pei, Y.-Y. Y.; Zhang, X.-Y. Y.; Gu, Z.-H. H.; Zhou, Z.-H. H.; Yuan, W.-F. F.; Zhou, J.-J. J.; Zhu, J.-H. H.; Gao, X.-J. J. *Journal of Controlled Release* **2001**, *71* (2), 203–211.

(40) Tomar, L.; Tyagi, C.; Kumar, M.; Kumar, P.; Singh, H.; Choonara, Y. E.; Pillay, V. *International Journal of Nanomedicine* **2013**, *8*, 505–520.

(41) Kang, B. K.; Chon, S. K.; Kim, S. H.; Jeong, S. Y.; Kim, M. S.; Cho, S. H.; Lee, H. B.; Khang, G. *International Journal of Pharmaceutics* **2004**, *286* (1–2), 147–156.

(42) Jeffery, H.; Davis, S. S.; O'Hagan, D. T. *Pharmaceutical Research: An Official Journal of the American Association of Pharmaceutical Scientists*. 1993, pp 362–368.

(43) Ito, F.; Fujimori, H.; Makino, K. *Colloids and Surfaces B: Biointerfaces* **2007**, *54* (2), 173–178.

(44) USP General Chapters: <467> Organic Volatile Impurities http://www.pharmacopeia.cn/v29240/usp29nf24s0_c467.html (accessed Jul 16, 2018).

(45) Caliceti, P.; Veronese, F. M.; Lora, S. *International Journal of Pharmaceutics* **2000**, *211* (1–2), 57–65.

(46) Uchida, T.; Nagareya, N.; Sakakibara, S.; Konishi, Y.; Nakai, A.; Nishikata, M.; Matsuyama, K.; Yohshida, K. *CHEMICAL & PHARMACEUTICAL BULLETIN* **1997**, *45* (9), 1539–1543.

(47) Arpagaus, C.; Collenberg, A.; Rütti, D.; Assadpour, E.; Jafari, S. M. *International Journal of Pharmaceutics* **2018**, *546* (1–2), 194–214.

(48) Sosnik, A.; Seremeta, K. P. *Advances in Colloid and Interface Science* **2015**, *223*, 40–54.

(49) Walters, R. H.; Bhatnagar, B.; Tchessalov, S.; Izutsu, K.-I.; Tsumoto, K.; Ohtake, S. *Journal of Pharmaceutical Sciences* **2014**, *103* (9), 2673–2695.

(50) Cal, K.; Sollohub, K. *Journal of Pharmaceutical Sciences* **2010**, *99* (2), 575–586.

(51) León-Martínez, F. M.; Méndez-Lagunas, L. L.; Rodríguez-Ramírez, J. *Carbohydrate Polymers* **2010**, *81* (4), 864–870.

(52) Qian, F.; Huang, J.; Hussain, M. A. *Journal of Pharmaceutical Sciences* **2010**, *99* (7), 2941–2947.

(53) Guerrero, S.; Muñíz, E.; Teijón, C.; Olmo, R.; Teijón, J. M.; Blanco, M. D. *Journal of Pharmaceutical Sciences* **2008**, *97* (8), 3153–3169.

(54) Anaya Castro, M. A.; Alric, I.; Brouillet, F.; Peydecastaing, J.; Fullana, S. G.; Durrieu, V. *AAPS PharmSciTech* **2017**, *19* (3), 1124–1132.

(55) Gavini, E.; Chetoni, P.; Cossu, M.; Alvarez, M. G.; Saettone, M. F.; Giunchedi, P. *European Journal of Pharmaceutics and Biopharmaceutics* **2004**, *57* (2), 207–212.

(56) Repka, M. A.; Bandari, S.; Kallakunta, V. R.; Vo, A. Q.; McFall, H.; Pimparade, M. B.; Bhagurkar, A. M. *International Journal of Pharmaceutics* **2018**, *535* (1–2), 68–85.

(57) Crowley, M. M.; Zhang, F.; Repka, M. A.; Thumma, S.; Upadhye, S. B.; Kumar Battu, S.; McGinity, J. W.; Martin, C. *Drug Development and Industrial Pharmacy* **2007**, *33* (9), 909–926.

(58) Shah, S.; Maddineni, S.; Lu, J.; Repka, M. A. *International Journal of Pharmaceutics* **2013**, *453* (1), 233–252.

(59) Aho, J.; Boetker, J. P.; Baldursdottir, S.; Rantanen, J. *International Journal of Pharmaceutics* **2015**, *494* (2), 623–642.

(60) Qi, F.; Wu, J.; Li, H.; Ma, G. *Frontiers of Chemical Science and Engineering* **2018**, 1–14.

(61) Jermain, S. V.; Brough, C.; Williams, R. O. *International Journal of Pharmaceutics* **2018**, *535* (1–2), 379–392.

(62) Sathigari, S. K.; Radhakrishnan, V. K.; Davis, V. A.; Parsons, D. L.; Babu, R. J. *Journal of Pharmaceutical Sciences* **2012**, *101* (9), 3456–3464.

(63) Zhang, J.; Vo, A. Q.; Feng, X.; Bandari, S.; Repka, M. A. *AAPS PharmSciTech* **2018**.

(64) Boetker, J.; Water, J. J.; Aho, J.; Arnfast, L.; Bohr, A.; Rantanen, J. *European Journal of Pharmaceutical Sciences* **2016**, *90*, 47–52.

(65) Vo, A. Q.; Feng, X.; Pimparade, M.; Ye, X.; Kim, D. W.; Martin, S. T.; Repka, M. A. *European Journal of Pharmaceutical Sciences* **2017**, *102*, 71–84.

(66) Pimparade, M. B.; Vo, A.; Maurya, A. S.; Bae, J.; Morott, J. T.; Feng, X.; Kim, D. W.; Kulkarni, V. I.; Tiwari, R.; Vanaja, K.; Murthy, R.; Shivakumar, H. N.; Neupane, D.; Mishra, S. R.; Murthy, S. N.; Repka, M. A. *European Journal of Pharmaceutics and Biopharmaceutics* **2017**, *119*, 81–90.

(67) Cossé, A.; König, C.; Lamprecht, A.; Wagner, K. G. *AAPS PharmSciTech* **2017**, *18* (1), 15–26.

(68) Palem, C. R.; Dudhipala, N. R.; Battu, S. K.; Repka, M. A.; Rao Yamsani, M. *Drug Development and Industrial Pharmacy* **2016**, *42* (3), 473–484.

(69) Albarahmieh, E.; Qi, S.; Craig, D. Q. M. *International Journal of Pharmaceutics* **2016**, *514* (1), 270–281.

(70) Gupta, S. S.; Solanki, N.; Serajuddin, A. T. M. *AAPS PharmSciTech* **2016**, *17* (1), 148–157.

(71) Whitaker, M. J.; Hao, J. Y.; Davies, O. R.; Serhatkulu, G.; Stolnik-Trenkic, S.; Howdle, S. M.; Shakesheff, K. M. *Journal of Controlled Release* **2005**, *101* (1–3), 85–92.

(72) Cowie, J. M. G.; Arrighi, V. In *Polymers: Chemistry and Physiscs of Modern Materials*; CRC Press Taylor & Francis Group, LLC: U. S. A, 2008; pp 321–343.

(73) Charles E. Carraher, J.; Lagowski, J. J. In *Polymer Chemistry*; Marcel Dekker Inc: U. S. A, 2003; pp 527–544.

(74) Jordan, F.; Naylor, A.; Kelly, C. A.; Howdle, S. M.; Lewis, A.; Illum, L. *Journal of Controlled Release* **2010**, *141* (2), 153–160.

(75) Inactive Ingredients http://www.drugs.com/inactive/ (accessed Jun 16, 2016).

(76) U.S. Department of Health and Human Services; Food and Drug Administration. *Guidance for Industry Nonclinical Studies for the Safety Evaluation of Pharmaceutical Excipients*; 2005.

(77) Smith, R. M. *Pure and Applied Chemistry* **1993**, *65* (11), 2397–2403.

(78) Darr, J. A.; Poliakoff, M. *Chemical Reviews* **1999**, *99* (2), 495–542.

(79) Licence, P.; Litchfield, D.; Dellar, M. P.; Poliakoff, M. *Green Chemistry* **2004**, *6* (8), 352–354.

(80) Phase Diagrams https://chem.libretexts.org/Textbook_Maps/General_Chemistry/Map%3A_General_Chemistry_(Petrucci_et_al.)/12%3A_Intermolecular_Forces%3A_Liquids_And_Solids/12.4%3A_Phase_Diagrams (accessed Aug 6, 2018).

(81) Eckert, C. a.; Knutson, B. L.; Debenedetti, P. G. *Nature* **1996**, *383* (6598), 313–318.

(82) Kazarian, S. G. *Polymer Science* **2000**, *42*, 78–101.

(83) DeSimone, J. M. *Science* **2002**, *297* (5582), 799–803.

(84) Nalawade, S. P.; Picchioni, F.; Janssen, L. *Progress in Polymer Science* **2006**, *31* (1), 19–43.

(85) Zosel, K. *Angewandte Chemie International Edition in English* **1978**, *17* (10), 702–709.

(86) Wang, J. S.; Chiu, K. *Journal of Hazardous Materials* **2008**, *158* (2–3), 384–391.

(87) Licence, P.; Ke, J.; Sokolova, M.; Ross, S. K.; Poliakoff, M. *Green Chemistry* **2003**, *5* (2), 99–104.

(88) Yoda, S.; Bratton, D.; Howdle, S. M. *Polymer* **2004**, *45* (23), 7839–7843.

(89) Bratton, D.; Brown, M.; Howdle, S. M. *Chem Commun (Camb)* **2004**, No. 7, 808–809.

(90) Cooper, A. I. *Advanced Materials* **2003**, *15* (13), 1049–1059.

(91) Alessi, P.; Cortesi, A.; Kikic, I.; Vecchione, F. *Journal of Applied Polymer Science* **2003**, *88* (9), 2189–2193.

(92) Reverchon, E.; Cardea, S. *The Journal of Supercritical Fluids* **2007**, *40* (1), 144–152.

(93) Davies, O. R.; Lewis, A. L.; Whitaker, M. J.; Tai, H.; Shakesheff, K. M.; Howdle, S. M. *Advanced Drug Delivery Reviews* **2008**, *60* (3), 373–387.

(94) Reverchon, E.; Antonacci, A. *Journal of Supercritical Fluids* **2007**, *39* (3), 444–452.

(95) Marizza, P.; Keller, S. S.; Mullertz, A.; Boisen, A. *Journal of Controlled Release* **2014**, *173*, 1–9.

(96) Kazarian, S. G.; Vincent, M. F.; Eckert, C. A. *Review of Scientific Instruments* **1996**, *67* (4), 1586–1589.

(97) Shieh, Y. T.; Su, J. H.; Manivannan, G.; Lee, P. H. C.; Sawan, S. P.; Spall, W. D. *Journal of Applied Polymer Science* **1996**, *59* (4), 695–705.

(98) Yeo, S.-D.; Kiran, E. *The Journal of Supercritical Fluids* **2005**, *34* (3), 287–308.

(99) Jung, J.; Perrut, M. *The Journal of Supercritical Fluids* **2001**, *20* (3), 179–219.

(100) Asghari, I.; Esmaeilzadeh, F. *International Journal of Pharmaceutics* **2012**, *433* (1–2), 149–156.

(101) Türk, M.; Bolten, D. *The Journal of Supercritical Fluids* **2010**, *55* (2), 778–785.

(102) Kikic, I.; Vecchione, F. *Current Opinion in Solid State and Materials Science* **2003**, *7* (4–5), 399–405.

(103) Tom, J. W.; Debenedetti, P. G. *Biotechnology Progress* **1991**, *7* (5), 403–411.

(104) Chen, K.; Zhang, X.; Pan, J.; Zhang, W.; Yin, W. *Powder Technology* **2005**, *152* (1–3), 127–132.

(105) Barrett, A.; Dehghani, F.; Foster, N. *Pharmaceutical Research* **2008**, *25* (6), 1274–1289.

(106) Kim, M.-S.; Kim, J.-S.; Park, H. J.; Cho, W. K.; Cha, K.-H.; Hwang, S.-J. *International Journal of Nanomedicine* **2011**, *6*, 2997–3009.

(107) Montes, A.; Kin, N.; Gordillo, M. D.; Pereyra, C.; de la Ossa, E. J. M. *The Journal of Supercritical Fluids* **2014**, *89* (0), 58–67.

(108) Elizondo, E.; Córdoba, A.; Sala, S.; Ventosa, N.; Veciana, J. *The Journal of Supercritical Fluids* **2010**, *53* (1–3), 108–114.

(109) Kang, Y.; Yin, G.; Ouyang, P.; Huang, Z.; Yao, Y.; Liao, X.; Chen, A.; Pu, X. *Journal of Colloid and Interface Science* **2008**, *322* (1), 87–94.

(110) Chen, A.-Z.; Wang, G.-Y.; Wang, S.-B.; Feng, J.-G.; Liu, Y.-G.; Kang, Y.-Q. *Materials* **2012**, *5* (10), 1841–1852.

(111) Naylor, A.; Lewis, A. L.; Ilium, L. *Therapeutic Delivery* **2011**, *2* (12), 1551–1565.

(112) Hao, J. Y.; Whitaker, M. J.; Wong, B.; Serhatkulu, G.; Shakesheff, K. M.; Howdle, S. M. *Journal of Pharmaceutical Sciences* **2004**, *93* (4), 1083–1090.

(113) Morrison, F. A.; Gubbins, K. F. *Understanding Rheology*; Oxford University Press: New York, 2001.

(114) Barnes; Hutton; Walters; Barnes, H. A.; Hutton, J. F.; Walters, K. *An*

*introduction to rheology*; Elsevier, 1989; Vol. 3.

(115) *Oxford Dictionary of Biochemistry and Molecular Biology*; Cammack, R., Atwood, T., Campbell, P., Parish, H., Smith, A., Vella, F., Stirling, J., Eds.; Oxford University Press, 2006.

(116) Utz, J. Rheometry: Selecting the Right Measuring System - Anton Paar Blog https://blog.anton-paar.com/rheometry-selecting-the-right-measuring-system/ (accessed Jul 19, 2018).

(117) Ferry, J. D. *Viscoelastic properties of polymers*; J. Wiley, 1980.

(118) Goodenow, J.; Orr, R.; Ross, D. Mathematical Models of Water Clocks http://www.nawcc-index.net/Articles/Goodenow-WaterClocks.pdf (accessed Jul 19, 2018).

(119) How to Measure Viscosity https://wiki.anton-paar.com/en/how-to-measure-viscosity/ (accessed Jul 12, 2018).

(120) Mills, A. A. *Source: Notes and Records of the Royal Society of London* **1982**, *37* (1), 35–61.

(121) Viscometer Design and Application Review https://www.engineersedge.com/instrumentation/viscometer_design_and_application_review_9820.htm (accessed Jul 19, 2018).

(122) Piau, J. M.; Bremond, M.; Couette, J. M.; Piau, M. *Rheologica Acta* **1994**, *33* (5), 357–368.

(123) Marcondes, W. A Practical Approach to Rheology and Rheometry http://www.ebah.com.br/content/ABAAAgazIAK/a-practical-approach-to-rheology-and-rheometry-scharamm?part=4 (accessed Jul 19, 2018).

(124) Vlachopoulos, J.; Strutt, D. Polymer processing www.mslab.boun.edu.tr/polymer.doc (accessed Jun 2, 2016).

(125) Elias, H.-G. *An Introduction to Polymer Science*; VCH Verlagsgesellschaft mbH: Germany, 1997.

(126) Reverchon, E.; Adami, R.; Cardea, S.; Della Porta, G. *Journal of Supercritical Fluids* **2009**, *47* (3), 484–492.

(127) Gerhardt, L. J.; Manke, C. W.; Gulari, E. *Journal of Polymer Science Part B: Polymer Physics* **1997**, *35* (3), 523–534.

(128) Royer, J. R.; Gay, Y. J.; Desimone, J. M.; Khan, S. A. *Journal of Polymer Science*

*Part B: Polymer Physics* **2000**, *38* (23), 3168–3180.

(129) Tai, H.; Upton, C. E.; White, L. J.; Pini, R.; Storti, G.; Mazzotti, M.; Shakesheff, K. M.; Howdle, S. M. *Polymer* **2010**, *51* (6), 1425–1431.

(130) Kelly, C. A.; Howdle, S. M.; Shakesheff, K. M.; Jenkins, M. J.; Leeke, G. A. *Journal of Polymer Science Part B: Polymer Physics* **2012**, *50* (19), 1383–1393.

(131) Curia, S.; De Focatiis, D. S. A.; Howdle, S. M. *Polymer* **2015**, *69*, 17–24.

(132) Pepper, K. J.; Masson, T.; De Focatiis, D.; Howdle, S. M. *The Journal of Supercritical Fluids* **2018**, *133* (July 2017), 343–348.

(133) Mertsch, R.; Wolf, B. A. *Macromolecules* **1994**, *27*, 3289–3294.

(134) Xiong, Y.; Kiran, E. *Polymer* **1995**, *36* (25), 4817–4826.

(135) Fleming, O. S.; Kazarian, S. G. In *Supercritical Carbon Dioxide*; Wiley-VCH Verlag GmbH & Co. KGaA, 2006; pp 205–238.

(136) Gourgouillon, D.; Avelino, H. M. N. .; Fareleira, J. M. N. .; Nunes da Ponte, M. *The Journal of Supercritical Fluids* **1998**, *13* (1–3), 177–185.

(137) Nobelen, M.; Hoppe, S.; Fonteix, C.; Pla, F.; Dupire, M.; Jacques, B. *Chemical Engineering Science* **2006**, *61* (16), 5334–5345.

(138) Kelly, C. A.; Murphy, S. H.; Leeke, G. A.; Howdle, S. M.; Shakesheff, K. M.; Jenkins, M. J. *European Polymer Journal* **2013**, *49* (2), 464–470.

(139) Raps, D.; Koppl, T.; de Anda, A. R.; Altstadt, V. *Polymer* **2014**, *55* (6), 1537–1545.

(140) Kelly, C. A.; Naylor, A.; Illum, L.; Shakesheff, K. M.; Howdle, S. M. *Advanced Functional Materials* **2012**, *22* (8), 1684–1691.

(141) Sarode, A. L.; Sandhu, H.; Shah, N.; Malick, W.; Zia, H. *European Journal of Pharmaceutical Sciences* **2013**, *48* (3), 371–384.

(142) Maru, S. M.; de Matas, M.; Kelly, A.; Paradkar, A. *European Journal of Pharmaceutical Sciences* **2011**, *44* (4), 471–478.

(143) Chokshi, R. J.; Sandhu, H. K.; Iyer, R. M.; Shah, N. H.; Malick, A. W.; Zia, H. *Journal of Pharmaceutical Sciences* **2005**, *94* (11), 2463–2474.

(144) Bialleck, S.; Rein, H. *European Journal of Pharmaceutics and Biopharmaceutics* **2011**, *79* (2), 440–448.

(145) Chomcharn, N.; Xanthos, M. *International Journal of Pharmaceutics* **2013**, *450* (1–2), 259–267.

(146) Suwardie, H.; Wang, P.; Todd, D. B.; Panchal, V.; Yang, M.; Gogos, C. G. *European Journal of Pharmaceutics and Biopharmaceutics* **2011**, *78* (3), 506–512.

(147) Tadros, T. F. In *Rheology of Dispersions: Principles and Applications*; Wiley-VCH Verlag GmbH & Co. KGaA: Wokingham, UK, 2010; pp 85–120.

(148) Greenhalgh, D. J.; Williams, A. C.; Timmins, P.; York, P. *Journal of Pharmaceutical Sciences* **1999**, *88* (11), 1182–1190.

(149) Yang, M.; Wang, P.; Suwardie, H.; Gogos, C. *International Journal of Pharmaceutics* **2011**, *403* (1–2), 83–89.

(150) Lyons, J. G.; Devine, D. M.; Kennedy, J. E.; Geever, L. M.; O'Sullivan, P.; Higginbotham, C. L. *European Journal of Pharmaceutics and Biopharmaceutics* **2006**, *64* (1), 75–81.

(151) Avgerinos, T.; Kantiranis, N.; Panagopoulou, A.; Malamataris, S.; Kachrimanis, K.; Nikolakakis, I. *Drug Development and Industrial Pharmacy* **2018**, *44* (2), 338–348.

(152) Andrews, G. P.; Donnelly, L.; Jones, D. S.; Curran, R. M.; Morrow, R. J.; Woolfson, A. D.; Malcolm, R. K. *Biomacromolecules* **2009**, *10* (9), 2427–2435.

(153) Aminabhavi, T. M.; Agnihotri, S. A.; Naidu, B. V. K. *Journal of Applied Polymer Science* **2004**, *94* (5), 2057–2064.

(154) Chauvet, M.; Sauceau, M.; Fages, J. *The Journal of Supercritical Fluids* **2017**, *120*, 408–420.

(155) Lyons, J.; Hallinan, M.; Kennedy, J.; Devine, D.; Geever, L.; Blackie, P.; Higginbotham, C. *International Journal of Pharmaceutics* **2007**, *329* (1–2), 62–71.

(156) Verreck, G.; Decorte, A.; Heymans, K.; Adriaensen, J.; Liu, D.; Tomasko, D.; Arien, A.; Peeters, J.; Van den Mooter, G.; Brewster, M. E. *International Journal of Pharmaceutics* **2006**, *327* (1–2), 45–50.

(157) USP General Chapters: <1088><1092> http://www.pharmacopeia.cn/v29240/usp29nf24s0_c711.html (accessed Jun 12, 2018).

(158) Wyss, D. H. M.; Larsen, R. J.; Weitz, P. D. A. 2007, pp 68–70.

(159) Material Functions Derived from Oscillatory Tests

https://ciks.cbt.nist.gov/~garbocz/SP946/node11.htm (accessed Aug 1, 2018).

(160) Phan-Thien, N.; Rhodes, P. W. T. *Understanding Viscoelasticity*; Stanley, P. H. E., Needs, P. R., Eds.; Springer: Heidelberg, 2013.

(161) Severs, E. T. In *Rheology of Polymers*; Reinhold Publishing Corporation: New York, 1962; pp 22–42.

(162) Willenbacher, N.; Georgieva, K. *Product Design and Engineering*. Wiley-VCH Verlag GmbH & Co: Germany 2013.

(163) Polymer Properties: Polymer Melts https://www.nottingham.ac.uk/~enzddf/polymerengineering/pmwiki/pmwiki.php?n=Main.PolymerMelts (accessed Aug 1, 2018).

(164) Han, C. D. *Rheology in Polymer Processing*; Academic Press Inc: New York, 1976.

(165) Cross, M. M. *Journal of Colloid Science* **1965**, *20* (5), 417–437.

(166) Carreau, P. J. *Transactions of The Society of Rheology (1957-1977)* **1972**, *16* (1), 99–127.

(167) Molecular Weight of PLA with the BI-MwA https://www.brookhaveninstruments.com/library/polymers/molecular-weight-of-pla-with-the-bi-mwa (accessed Jun 16, 2016).

(168) Zhou, X.; Hong, L. *Colloid and Polymer Science* **2013**, *291* (9), 2155–2162.

(169) Poly (ethylene glycol) dibenzylmethylene Terminated Data Sheet http://www.polymersource.com/dataSheet/P5607-EO (PEO).pdf (accessed Jun 16, 2016).

(170) Desai, K. G. H.; Park, H. J. *Drying Technology* **2005**, *23* (7), 1361–1394.

(171) Westover, R. F. *Polymer Engineering and Science* **1961**, *1* (1), 14–20.

(172) Bae, Y. C. *Polymer* **1996**, *37* (14), 3011–3017.

(173) Lee, M.; Park, C. B.; Tzoganakis, C. *Polymer Engineeriaw and Science* **1999**, *39* (1), 99–109.

(174) Royer, J. R.; Gay, Y. J.; M., A.; DeSimone, J. M.; Khan, S. A. *Polymer* **2002**, *43*, 2375–2383.

(175) Calvignac, B.; Rodier, E.; Letourneau, J.-J.; Vitoux, P.; Aymonier, C.; Fages, J. *The Journal of Supercritical Fluids* **2010**, *55* (1), 96–106.

(176) Hrnčič, M. K.; Škerget, M.; Knez, Ž. *The Journal of Supercritical Fluids* **2014**, *95*, 641–668.

(177) Royer, J. R.; DeSimone, J. M.; Khan, S. A. *Journal of Polymer Science: Part B: Polymer Physics* **2001**, *39*, 3055–3066.

(178) Bae, Y. C.; Gulari, E. *Journal of Applied Polymer Science* **1997**, *63* (4), 459–466.

(179) Handge, U. A.; Altstädt, V. *Journal of Rheology* **2012**, *56* (4), 743.

(180) Mark, J.; Ngai, K.; Graessley, W.; Mandelkern, L.; Samulski, E.; Koenig, J.; Wignall, G. In *Physical Properties of Polymers*; Cambridge University Press: Cambridge, 2004; pp 153–208.

(181) Plastics Additives http://www.bpf.co.uk/plastipedia/additives/default.aspx#Intro (accessed Jun 2, 2016).

(182) Li, F.-J.; Tan, L.-C.; Zhang, S.-D.; Zhu, B. *Journal of Applied Polymer Science* **2016**, *133* (4).

(183) Sungsanit, K.; Kao, N.; Bhattacharya, S. N. *Polymer Engineering & Science* **2012**, *52* (1), 108–116.

(184) Toncheva, A.; Mincheva, R.; Kancheva, M.; Manolova, N.; Rashkov, I.; Dubois, P.; Markova, N. *European Polymer Journal* **2016**, *75*, 223–233.

(185) Nazari, T.; Garmabi, H. *Micro & Nano Letters* **2014**, *9* (10), 686–690.

(186) Pillin, I.; Montrelay, N.; Grohens, Y. *Polymer* **2006**, *47* (13), 4676–4682.

(187) Sheth, M.; Kumar, R. A.; Dave, V.; Gross, R. A.; McCarthy, S. P. *Journal of Applied Polymer Science* **1997**, *66* (8), 1495–1505.

(188) Kumar, N.; Ravikumar, M. N. V.; Domb, A. J. *Advanced Drug Delivery Reviews* **2001**, *53* (1), 23–44.

(189) Malmsten, M.; Lindman, B. *Macromolecules* **1992**, *25*, 5440–5445.

(190) Chen, G.; Hoffman, A. S. *Nature* **1995**, *373* (6509), 49–52.

(191) Xiao, R. Z.; Zeng, Z. W.; Zhou, G. L.; Wang, J. J.; Li, F. Z.; Wang, A. M. *International Journal of Nanomedicine* **2010**, *5* (1), 1057–1065.

(192) Hiemstra, C.; Zhong, Z.; Dijkstra, P. J.; Feijen, J. *Macromolecular Symposia* **2005**, *224*, 119–131.

(193) Lucke, A.; Teßmar, J.; Schnell, E.; Schmeer, G.; Göpferich, A. *Biomaterials* **2000**, *21* (23), 2361–2370.

(194) Otsuka, H.; Nagasaki, Y.; Kataoka, K. *Biomacromolecules* **2000**, *1* (1), 39–48.

(195) Rafat, M.; Cléroux, C. A.; Fong, W. G.; Baker, A. N.; Leonard, B. C.; O'Connor, M. D.; Tsilfidis, C. *Biomaterials* **2010**, *31* (12), 3414–3421.

(196) Pulkkinen, M.; Pikkarainen, J.; Wirth, T.; Tarvainen, T.; Haapaaho, V.; Korhonen, H.; Seppala, J.; Jarvinen, K. *European Journal of Pharmaceutics and Biopharmaceutics* **2008**, *70* (1), 66–74.

(197) Han, C. D.; Baek, D. M.; Kim, J. K.; Chu, S. G. *Polymer* **1992**, *33* (2), 294–305.

(198) Jelonek, K.; Li, S.; Wu, X.; Kasperczyk, J.; Marcinkowski, A. *International Journal of Pharmaceutics* **2015**, *485* (1–2), 357–364.

(199) Utracki, L. a; Kamal, M. R. *Polymer Engineering and Science* **1982**, *22* (2), 96–114.

(200) Sadiku-Agboola, O.; Sadiku, E. R.; Adegbola, A. T.; Biotidara, O. F. *Materials Sciences and Applications* **2011**, *02* (01), 30–41.

(201) Wu, D.; Wu, L.; Zhang, M.; Zhao, Y. *Polymer Degradation and Stability* **2008**, *93* (8), 1577–1584.

(202) Avolio, R.; Castaldo, R.; Gentile, G.; Ambrogi, V.; Fiori, S.; Avella, M.; Cocca, M.; Errico, M. E. *European Polymer Journal* **2015**, *66*, 533–542.

(203) Oliaei, E.; Kaffashi, B.; Davoodi, S. *Journal of Applied Polymer Science* **2016**, *133* (15), 1–13.

(204) Xie, M.; Li, H. *European Polymer Journal* **2007**, *43* (8), 3480–3487.

(205) Babaei, A.; Arefazar, A. *Journal of Applied Polymer Science* **2015**, *132* (20), 41969–41977.

(206) Djellali, S.; Sadoun, T.; Haddaoui, N.; Bergeret, A. *Polymer Bulletin* **2015**, *72* (5), 1177–1195.

(207) Liao, H.; Zheng, L.; Hu, Y.; Zha, X.; Xu, X.; Wen, Y.; Tao, G.; Liu, C. *Journal of Applied Polymer Science* **2015**, *132* (24), n/a-n/a.

(208) Zhao, Y.; Huang, H.-X.; Chen, Y.-K. *Polymer Bulletin* **2010**, *64* (3), 291–302.

(209) Wu, D.; Zhang, Y.; Zhang, M.; Zhou, W. *European Polymer Journal* **2008**, *44* (7), 2171–2183.

(210) Lee, M.; Park, C. B.; Tzoganakis, C. *Polymer Engineering and Science* **2004**, *39*, 99–109.

(211) Goddard, A. R.; Pérez-Nieto, S.; Passos, T. M.; Quilty, B.; Carmichael, K.; Irvine,

D. J.; Howdle, S. M. *Green Chemistry* **2016**, *18* (17), 4772–4786.

(212) Dag, A.; Durmaz, H.; Kirmizi, V.; Hizal, G.; Tunca, U. *Polymer Chemistry* **2010**, *1* (5), 621–623.

(213) Schwach, G.; Coudane, J.; Engel, R.; Vert, M. *Polymer Bulletin* **1994**, *32* (5–6), 617–623.

(214) Chmura, A. J.; Davidson, M. G.; Frankis, C. J.; Jones, M. D.; Lunn, M. D. *Chemical Communications* **2008**, No. 11, 1293.

(215) Jamshidian, M.; Tehrany, E. A.; Imran, M.; Jacquot, M.; Desobry, S. *Comprehensive Reviews in Food Science and Food Safety* **2010**, *9* (5), 552–571.

(216) Poly(ethylene glycol), MW 7500 (PEG 7500) http://www.polysciences.com/default/polyethylene-glycol-mw-7500 (accessed May 4, 2018).

(217) Dorgan, J. R.; Williams, J. S.; Lewis, D. N. *Journal of Rheology* **1999**, *43* (5), 1141.

(218) Miller-Chou, B. A.; Koenig, J. L. *Progress in Polymer Science (Oxford)* **2003**, *28* (8), 1223–1270.

(219) Berendsen, H. J. C. *A student's guide to data and error analysis*; Cambridge University Press, 2011.

(220) Martin, O.; Avérous, L. *Polymer* **2001**, *42* (14), 6209–6219.

(221) Tai, H.; Mather, M. L.; Howard, D.; Wang, W.; White, L. J.; Crowe, J. A.; Morgan, S. P.; Chandra, A.; Williams, D. J.; Howdle, S. M.; Shakesheff, K. M.; Darr, J.; Layrolle, P.; Buckland, T. *European Cells & Materials* **2007**, *14*, 76–77.

(222) Bates, C. M.; Bates, F. S. *Macromolecules* **2017**, *50* (1), 3–22.

(223) Dealy, J. M.; Larson, R. G. *Structure and rheology of molten polymers : from structure to flow behavior and back again*; Hanser Publishers, 2006.

(224) Marroum, P. J. *Dissolution Technologies* **2014**, *21* (3), 11–16.

(225) Edwards, L. J. *Transactions of the Faraday Society* **1951**, *47* (I), 1191–1210.

(226) In Vitro Dissolution Testing - Solid Oral Dosage Forms https://www.particlesciences.com/news/technical-briefs/2010/in-vitro-dissolution-testing-for-solid-oral-dosage-forms.html (accessed Jun 12, 2018).

(227) Noyes, A. A.; Whitney, W. R. *Journal of the American Chemical Society* **1897**, *19* (12), 930–934.

(228) Nelson, E. *Journal of the American Pharmaceutical Association (Scientific ed.)*

**1957**, *46* (10), 607–614.

(229) Lindenbaum, J.; Mellow, M. H.; Blackstone, M. O.; Butler, V. P. *New England Journal of Medicine* **1971**, *285* (24), 1344–1347.

(230) *Guidance for Industry Dissolution Testing of Immediate Release Solid Oral Dosage Forms*; U.S. Department of Health and Human Services Food and Drug Administration Center for Drug Evaluation and Research (CDER), 1997.

(231) *Guidance for Industry Guidance for Industry Extended Release Oral Dosage Forms: Development, Evaluation, and Application of In Vitro/In Vivo Correlations*; U.S. Department of Health and Human Services Food and Drug Administration Center for Drug Evaluation and Research (CDER), 1997.

(232) *Guidance for Industry Immediate Release Solid Oral Dosage Forms*; Center for Drug Evaluation and Research (CDER), 1995.

(233) *Guidance for Industry SUPAC-MR: Modified Release Solid Oral Dosage Forms Scale-Up and Postapproval Changes: Chemistry, Manufacturing, and Controls; In Vitro Dissolution Testing and In Vivo Bioequivalence Documentation*; U.S. Department of Health and Human Services Food and Drug Administration Center for Drug Evaluation and Research (CDER), 1997.

(234) Wang, Q.; Fotaki, N.; Mao, Y. *Dissolution Technologies* **2009**, *16* (3), 6–12.

(235) Dressman, J. B.; Amidon, G. L.; Reppas, C.; Shah, V. P. *Pharmaceutical research* **1998**, *15* (1), 11–22.

(236) Poly(ethylene glycol), MW 400 http://www.polysciences.com/default/polyethylene-glycol-mw-400 (accessed May 29, 2018).

(237) Poly(ethylene glycol) average Mn 6,000 | Sigma-Aldrich https://www.sigmaaldrich.com/catalog/product/aldrich/81260?lang=en&region=GB (accessed Jun 19, 2018).

(238) Polycaprolactone average Mw ~14,000, average Mn ~10,000 by GPC | Sigma-Aldrich https://www.sigmaaldrich.com/catalog/product/aldrich/440752?lang=en&region=GB (accessed Jun 19, 2018).

(239) Poly(ethylene glycol) average Mn 400 | Sigma-Aldrich https://www.sigmaaldrich.com/catalog/product/aldrich/202398?lang=en&r

egion=GB (accessed Jun 19, 2018).

(240) spectrumlabs.com. Float-A-Lyzer G2 http://spectrumlabs.com/lit/420x10732x000.pdf (accessed Jul 24, 2018).

(241) Fox Equation http://polymerdatabase.com/polymer physics/Fox.html (accessed May 30, 2018).

(242) Lao, L. L.; Venkatraman, S. S.; Peppas, N. A. *European Journal of Pharmaceutics and Biopharmaceutics* **2008**, *70* (3), 796–803.

(243) Howdle, S. M.; Watson, M. S.; Whitaker, M. J.; Popov, V. K.; Davies, M. C.; Mandel, F. S.; Wang, J. D.; Shakesheff, K. M. *Chemical Communications* **2001**, No. 1, 109–110.

(244) Krieger, I. M.; Dougherty, T. J. *Transactions of the Society of Rheology* **1959**, *3* (1), 137–152.

(245) Li, Y.; Han, C.; Bian, J.; Han, L.; Dong, L.; Gao, G. *Polymer Composites* **2012**, *33* (10), 1719–1727.

(246) Mutel, A. T.; Kamal, M. R. *Polymer Composites* **1984**, *5* (1), 29–35.

(247) Kister, G.; Cassanas, G.; Vert, M. *Polymer* **1998**, *39* (2), 267–273.

(248) Vey, E.; Rodger, C.; Booth, J.; Claybourn, M.; Miller, A. F.; Saiani, A. *Polymer Degradation and Stability* **2011**, *96* (10), 1882–1889.

(249) Lin, V. J. C.; Koenig, J. L. *Biopolymers* **1976**, *15* (1), 203–218.

(250) Fenouillot, F.; Cassagnau, P.; Majesté, J.-C. *Polymer* **2009**, *50* (6), 1333–1350.

(251) Tres, F.; Treacher, K.; Booth, J.; Hughes, L. P.; Wren, S. A. C.; Aylott, J. W.; Burley, J. C. *Molecular Pharmaceutics* **2016**, *13* (3), 1166–1175.

(252) Hao, J. Y.; Whitaker, M. J.; Serhatkulu, G.; Shakesheff, K. M.; Howdle, S. M. *Journal of Materials Chemistry* **2005**, *15* (11), 1148–1153.

(253) Areerat, S.; Nagata, T.; Ohshima, M. *Polymer Engineering & Science* **2002**, *42* (11), 2234–2245.